Division of Advanced Drug Delivery and Tissue Engineering

School of Pharmacy

Crossing Mucosal Barriers for Non-invasive Protein Delivery: a Vitamin B_{12}-mediated Approach

Robyn Fowler, BSc. Hons

Thesis submitted to the University of Nottingham for the degree of Doctor of Philosophy

September 2012

“The breath of wind that moved them was still chilly on this day in May; the flowers gently resisted, curling up with a kind of trembling grace and turning their pale stamens towards the ground. The sun shone through them, revealing a pattern of interlacing, delicate blue veins, visible through the opaque petals; this added something alive to the flower's fragility, to it’s ethereal quality, something almost human, in the way that human can mean frailty and endurance both at the same time. The wind could ruffle these ravishing creations but it couldn't destroy them, or even crush them; they swayed there, dreamily; they seemed ready to fall but held fast to their slim strong branches-...”

Irène Némirovsky

List of publications

Vllasaliu, D., Fowler, R., Garnett, M. *et al*. 2011. Barrier characteristics of epithelial cultures modelling the airway and intestinal mucosa: a comparison. Biochem. Biophys. Res. Comm. 415(4):579-585

Vllasaliu, D., Casettari, L., Fowler, R. *et al*. 2012. Absorption-promoting effects of chitosan in airway and intestinal cell lines: a comparative study. Int. J Pharm. 430(1-2):151-160

Vllasaliu, D., Shubber, S., Fowler, R. *et al*. 2012. Epithelial toxicity of alkylglycoside surfactants. J. Pharm. Sci. Accepted for publication. Sept. 2012.

Fowler, R. Vllasaliu, D., Fernández Trillo, F. *et al*. 2012. Nanoparticle transport across intestinal epithelial cells: pathway switching through bioconjugation. In draft for submission to SMALL. Sept. 2012

Abstract

Mucosal delivery of biotherapeutics as a non-invasive means of delivery could potentially be enhanced using nanoscale therapeutic carriers. However, nanoparticles do not readily cross the mucosal barriers, with the epithelium severely restricting their translocation into the systemic circulation. Translocation of nanocarriers across the mucosae may be improved by employing ligands capable of exploiting receptor-mediated cell uptake processes.

This work explores the potential of vitamin B_{12} transport pathway for mucosal delivery of B_{12}-decorated model nanoparticles and investigates the cell trafficking pathways involved in these processes. Cyanocobalamin (vitamin B_{12}) was chemically modified to produce the α-ω-aminohexylcarbamate B_{12} derivative – as a suitable bioconjugate – which was then conjugated to fluorescent, carboxy-functional nanoparticles (<200 nm). These systems were applied to intestinal Caco-2 monolayers, expressing the relevant proteins involved in B_{12} trafficking and endocytic processes.

Vitamin B_{12}-conjugated nanoparticles demonstrated notably increased cell uptake and transport capacities in Caco-2 monolayers, compared to their unconjugated counterparts. Importantly, the cell uptake of B_{12}-conjugated nanoparticles occurred via a pathway that was different to that used by both soluble B_{12} and unmodified nanoparticles. B_{12}-conjugated nanoparticles circumnavigated the lysosomal compartment and were transported by a route perturbed by caveolae-specific inhibitors, unlike the clathrin-mediated trafficking of soluble vitamin B_{12}. These previously unreported observations are important and have potential implications in the field of bioconjugate and nanocarrier-mediated drug delivery.

Epithelial cell uptake and transport of B_{12}-conjugated nanoparticles was also investigated in airway-derived Calu-3 cells, shown to express the B_{12}-intrinsic factor receptor, cubilin. B_{12}-nanoparticles showed markedly larger cell uptake and transport capacities in Calu-3 layers, with B_{12}-conjugation dramatically influencing the

intracellular trafficking of the particles in a similar way to Caco-2 cells. The B_{12} endocytotic machinery therefore shows potential for delivery of nanocarrier-associated therapeutics across the airways.

Present work also aimed to establish methods for the production of stable nano-sized protein crystals displaying a slow drug release profile, based on evidence that protein therapeutics which are formulated in this manner, offer beneficial drug-delivery properties and can be targeted using biological ligands. Nano- and micron-sized insulin crystals were prepared by an adaptation of the batch crystallisation approach. The crystals were stabilised using a chemical crosslinker, namely β-[Tris(hydroxymethyl) phosphino] propionic acid (THPP). The resulting insulin crystals were generally stable in the absence of crystalisation buffer, displayed a slow-release profile, with the released insulin retaining its biological activity. This study therefore shows that formulating protein bioactives in this form is possible and may provide a promising strategy to develop biotherapeutics with improved drug delivery properties.

Acknowledgements

I wanted to take this rather appropriate opportunity express my deepest thanks and gratitude to all the people who have supported, inspired and helped me throughout my Ph.D.

I especially want to thank my principal supervisor, Dr. Snow Stolnik, for her friendship and guidance during my research and study at Nottingham University. Her perpetual energy and enthusiasm for research and above all her resounding faith in me and my work, kept me going through those tough times. Her light-heartedness and ability to make me laugh became the best remedy for my Ph.D. blues. I will never forget those times in her office when despite our mutual frustrations; we were able to see the funny side of things. I think she'll always remember me as this highly stressed out individual, who liked to use far too many words to explain a very simple concept. We joked and teased many a time over my favourite phrase - "We'll cross that bridge when we come to it."

I wish to thank my fabulous co-supervisors, Professor Cameron Alexander and Dr Martin Garnett for their continuous help and support throughout the Ph.D. and for the conversations that clarified my thinking on the project and on other matters. I thank them not only for their sound advice and guidance over these past four years, but for keeping their doors open for me, even when the time came for reviewing my tedious and long thesis chapters. I wish to extend my thanks and appreciation to my internal assessor Dr Franco Falcone for his expert advice and opinion on the project and for his introduction and training in PCR. His patience, good will and great sense of humour motivated me to complete a key stage of the project and for this I am hugely grateful.

I'd like to express my deepest thanks to my former and current industrial supervisors (UCB); Professor Mike Eaton (ETP nanomedicine), Helen Horsley and Bryan Smith for their meaningful insight into the project and for their welcomed advice and comments

on chemistry aspects and compound synthesis. Thanks also to Adam Hold and Ian Whitcombe at UCB for compound purification and analysis.

Special thanks also to Dr Emma King and Denise Christie from the Advanced Microscopy Unit for all of their help and advice with microscopy prep. Despite being completely rushed off of their feet (most of the time), they would always spare me a few minutes, which was and still is, much appreciated. I was fortunate also, to have the absolute pleasure of working with Luca Casettari (Urbino University, Italy) and Francisco Fernández Trillo (Paco). I owe them my sincere thanks for analysing numerous NMR spectra and for drawing the chemical structure of vitamin B_{12} a countless number of times (without seeming to mind too much) and perhaps most importantly, for ensuring the safety of others whilst I re-enacted (rather abysmally) the role of a chemist.

I'd like to acknowledge Nottingham University's best senior lab technician and personal friend, Christy Grainger-Boultby for her expert advice and assistance on instruments, laboratory protocols and for ensuring the department's safety at all times. All my lab buddies in the depths and dungeons of the Boots Science building made it an extraordinary and insanely fun place to work. In particular, I would like to thank Jennie Lord for her friendship and banter over the past three years. Everyone else, including {*an endless list of names of all the wonderful people in BSB *smile**}, who truly inspired me in research and life through our often long liaises in the lab and office. Thanks.

My warmest heart-felt love and thanks go out to my colleague, partner and best friend, Driton Vllasaliu. With him, I share exceptionally fond memories and experiences. Professionally, I thank him for his training, knowledge and expertise in the lab and personally, I thank him for just being him and for eating his vegetables. Long may we continue to laugh, learn and to achieve together!

My sincerest gratitude and upmost respect goes to my family and friends for their never-ending love and encouragement throughout my life; this intermittent chapter

would have certainly been impossible without them. I am hugely indebted to my father, Tony Fowler, for his continued guidance, love and reassurance. He certainly instilled the belief in me that “hard work pays off” and this enabled me to excel in my studies (both at DAHS and in Durham). I know how hard he worked to support and provide for us, giving me the best upbringing anyone could wish for. He always had extreme faith in my abilities and has wholeheartedly supported me in all my endeavours and if I had one wish, it’s that I have made him half as proud of me, as I am of him. My mother, Pauline Fowler has always been a shoulder to lean on, an ear to listen and a heart to comfort - in other words, a perfect mum. Her wise words on current affairs, matters of the heart or just simply culinary conundrums, are always appreciated. Her supreme artistic talent and eye for colour and design gives her a certain edge - that makes her truly special to all who know and love her.

Mum and Dad - A massive thank you to you both. You are my everything.

Table of Contents

List of Figures

List of Tables

Abbreviations

$	Dollar
%	Percentage
℃	Degree centigrade
µg	Micrograms
µl	Microliter
µm	Micrometer
µM	Micromolar
Å	Angstrom
aa	Amino acid
AIC	Air-interface culture
Am	Amnionless
ANOVA	Analysis of variance
Asp	Aspartic acid
ATCC	American Type Culture Collection
BCA	Biopharmaceutics Classification System
bp	Base pair
BSA	Bovine Serum Albumin
C-CPE	Clostridium perfringens enterotoxin
CDI	1,1'-carbonyldiimidazole
cDNA	Complementary Deoxyribonucleic acid
cDNA	Complementary DNA
CDT	1,1'-carbonyldi(1,2,4-triazole)
CFTR	Cystic fibrosis transmembrane conductance regulator
Ch-T-B	Cholera Toxin B-subunit
Cm/s	Centimetre per second
cm^2	Centimetre squared
CO_2	Carbon dioxide
CoA	Coenzyme A
COOH	Carboxylic acid group
COSY	Correlation spectroscopy
CPD	Critical point dryer
CPP	Cell penetrating peptide
Da	Dalton
DABCO	1,4-diazabicyclo[2.2.2]octane
DAPI	4',6-diamidino-2-phenylindole
DBTC	Di(1-benzotriazolyl) carbonate
DLS	Dynamic Light Scattering
DMEM	Dulbecco's Modified Eagle's medium
DMSO	Dimethylsulphoxide
dNTP	Deoxyribonucleotide triphosphate
ECACC	European Collection of Cell Cultures
EDAC	1-ethyl-3-[3-dimethylaminopropyl]carbodiimide
EDTA	Ethylene diamine tetraacetic acid
ELP	Elastin-like polypeptide
EMEM	Essential Minimum Eagle's medium
ESI-MS	Electrospray-ionisation mass spectrometry
FAE	Follicle Associated Epithelia
FBS	Foetal Bovine Serum
FcRn	Neonatal Fc receptor
FD	FITC-dextran
FD10	FITC-dextran 10kDa
FD150	FITC-dextran 150kDa
FD20	FITC-dextran 20kDa
FD4	FITC-dextran 4kDa
FD40	FITC-dextran 40kDa

FD70	FITC-dextran 70kDa
FDA	Food & Drug Administration
FITC	Fluorescein isothiocyanate
fmole	femtomole
FR	Folate receptor
GAG	Glycosaminoglycan
G-CSF	Granulocyte-colony stimulating factor
gDNA	Genomic DNA
GI	Gastrointestinal
GIT	Gastrointestinal Tract
GLP-1	Glucagon-like peptide-1
Gly	Glycine
GPI	Glycosylphosphatidylinisotol
GTP	Guanosine 5'-Triphosphate
HBSS	Hank's balanced salt solution
HC	Haptocorrin
HEPES	4-(2-hydroxethyl)-1-piperazineethanesulfonic acid
HIV	Human immunodeficiency virus
HPLC	High Performance Liquid Chromatography
IF	Intrinsic factor
IFN-β	Interferon-β
Ig	Immunoglobulin
IgG	Immunoglobulin G
IM	Intramuscular
IV	Intravenous
JAM	Junction Adhesion Molecule
kDa	Kilodalton
LAMP-1	Lysosomal associated membrane protein-1
LCC	Liquid covered culture
LDH	Lactate Dehydrogenase
Leu	Leucine
LHRH	Luteinising hormone releasing factor
Lys	Lysine
m^2	Meter squared
MALDI	Matrix-assisted laser desorption/ionisation
MDCK	Madin Darby-canine kidney
MES	2(NMorpholino)ethanesulfonic acid
MHC	Major Histocompatibility Complex
ml	Milliliter
mM	Milimolar
mRNA	Messenger RNA
mRNA	Messenger RNA
MTS	3-(4,5-dimethylthiazol-2-yl)-5(3-carboxymethonyphenol)-2-(4-sulfophenyl)-2H-tetrazolium
MV	Medium voltage
MW	Molecular weight
NAC	N-acetyl cysteine
NADPH	nicotinamide adenine dinucleotide phosphate (reduced)
NCBI	National Center for Biotechnology Information
NEAA	Non essential amino acids
NHS	N-hydroxysuccinimide
nm	nanometer
NMR	Nuclear Magnetic Resonance
NOESY	Nuclear Overhauser effect spectroscopy
NPs	Nanoparticles
OH	Hydroxyl group

P_{app}	Apparent Permeability Coefficient
PBS	Phosphate Buffered Saline
PCR	Polymerase Chain Reaction
PEG	Polyethylene Glycol
PES	Phenazine ethosulfate
PFA	Paraformaldehyde
PhRMA	Pharmaceutical Research and Manufacturers of America
PLA	Poly(lactic-acid)
PLGA	Poly(lactic-*co*glycolic) acid
PS	Polystyrene
PVC	Poly-(vinyl chloride)
R&D	Research and Development
RES	Reticuloendothelial system
Rf	Retention Factor
rHUIF	Recombinant human intrinsic factor
RME	Receptor-mediated endocytosis
RNA	Ribonucleic Acid
SC	Subcutaneous
sCT	Salmon calcitonin
SEM	Scanning Electron Microscopy
siRNA	Small interfering RNA
TAT	Transactivator of transcription
TC	Transcobalamin
TCA	Tricarboxylic acid
TCII-R	Transcobalamin II receptor
TEA	Triethylamine
TEER	Transepithelial Electrical Resistance
TEM	Transmission Electron microscopy
TFA	Trifluoroacetic acid
THPP	β-[Tris(hydroxymethyl)phosphino] propionic acid
TJ	Tight Junction
TLC	Thin Layer Column Chromatography
TMC	N-trimethyl chitosan chloride
TNF	Tumor Necrosis Factor
TOCSY	Total Correlation spectroscopy
TOF-MS	Time-of-flight Mass spectrometry
US	United States
UV	Ultra Violet
v/v	Volume per volume
VB_{12} or B_{12}	Vitamin B_{12}, cobalamin
w/v	Weight per volume
w/w	Weight per weight
WGA	Wheat germ agglutinin
YO	Yellow Orange
Zn	Zinc
Zn^{2+}	Zinc cation
ZO-1	Zonula Occludens-1
α	alpha
β	Beta
ω	omega
Ω	Ohm

Chapter 1: Delivery of protein therapeutics across mucosal surfaces

1.1 The rationale behind mucosal protein delivery

There is an increasing demand for non-invasive methods for the delivery of protein pharmaceuticals, which has emanated from the overwhelming growth of biotechnology. In 2009, over 12 billion U.S dollars were invested in biologics/biotechnology research and development (R&D), representing a 26% share in the total R&D expenditure [1]. Furthermore, a recent report by the Pharmaceutical Research and Manufacturers of America (PhRMA) states that in 2011 there were 901 biologicals in development, targeting more than 100 diseases [2]. A significant proportion of these are therapeutics based on different proteins, with monoclonal antibodies becoming increasingly popular (Figure 1.1).

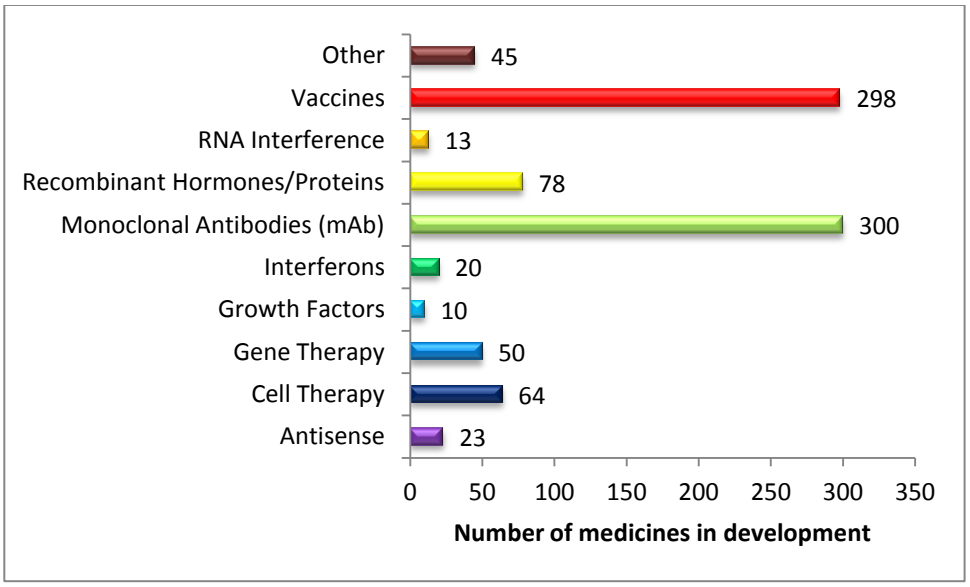

Figure 1.1. Number of 'biologics' in development (by product category) 2011. Adapted from a report by PhRMA [1].

Despite considerable interest in protein and peptide therapies (and biologicals in general) the development of non-invasive delivery systems for this drug category remains a huge challenge. This challenge is due to the physicochemical properties of this class of therapeutics, including large molecular size, susceptibility to enzymatic degradation, short plasma half-life, immunogenicity, and the tendency to undergo

aggregation, adsorption and denaturation [3-5]. Oral administration of drugs in general is desirable due to the obvious advantage of patient acceptability. However, there are several physiological barriers that limit the oral bioavailability of protein and peptide drugs, such as the pH across the GI tract (pH 1~8), digestive enzymes, intestinal flora, and the epithelial barrier. Consequently, the bioavailability of most peptides and proteins following oral administration is less than 1% [6].

The choice of drug delivery system undoubtedly requires an in-depth understanding of the physicochemical characteristics, the pharmacology and the intended clinical application of any chosen therapeutic. In view of the aforementioned problems, protein drugs are predominantly administered parenterally. However, disadvantages associated with the parenteral route, include patient discomfort (a barrier influencing patient compliance), high cost and the requirement for administration by a healthcare professional. This necessitates research into alternative ways of administering this class of therapeutics. From the drug delivery perspective, the ideal goal is to develop a preferentially oral delivery system for biological therapeutics that would achieve therapeutically relevant systemic bioavailability, with controlled release being an added advantage for a prolonged therapeutic effect. Many biologicals are very potent e.g. growth factors such as fibroblast growth factor [7], vascular endothelial growth factor [8] and bone morphogenic proteins [9]. Localised delivery may also be necessary in these cases since high systemic levels of these factors are required to achieve the local effect in the target tissues and this often leads to systemic toxicity.

Research into identification of non-invasive administration routes is intensifying. Although major breakthroughs in the form of popular products on the market are still not apparent, some commercial progress has been made in the past several years. Examples of non-parenteral delivery technologies, their associated companies and therapeutic proteins/peptides under development are listed in Table 1.1.

<table>
<tr><th>Delivery Pathway</th><th>Buccal</th><th>Nasal</th><th>Pulmonary</th><th>Oral</th></tr>
<tr><td rowspan="4">Technologies (associated companies)</td><td>Rapidmist™ (Generex)</td><td>CPE-215® (CPEX Pharmaceuticals) Thiomers (ThioMatrix)</td><td>Promaxx (Baxter Healthcare Corporation)</td><td>Eligen® (Emisphere) Spheromers™ and PIN™ (Spherics)</td></tr>
<tr><td rowspan="3">Thiomers (ThioMatrix)</td><td rowspan="3">Intravail® (Aegis Therapeutics)</td><td>Technosphere® (MannKind Corporation)</td><td>LPM™ (DOR Biopharma)</td></tr>
<tr><td>MicroDose Electronic dry powder inhaler (MicroDose Therapeutx)</td><td rowspan="2">Polymer/Bioadhesive platform (CoreMed, Inc.)</td></tr>
<tr><td>Polymer/Bioadhesive platform (CoreMed, Inc)</td></tr>
<tr><td rowspan="6">Therapeutic proteins in research (associated companies)</td><td rowspan="6"></td><td>Insulin (CPEX Pharmaceutics, Inc.)</td><td rowspan="6">Insulin, GLP-1 (MannKind Corporation)</td><td>Insulin (Oramed)</td></tr>
<tr><td>Insulin, Glucagon-like-peptide-1 (GLP-1) (MDRNA)</td><td>Salmon calcitonin, heparin, GLP-1, Insulin, (Emisphere)</td></tr>
<tr><td>Insulin, PTH, and desmopressin (Unigene)</td><td>Salmon calcitonin (Unigene/Tarsa therapeutics)</td></tr>
<tr><td>Cyclosporin (APT Pharmaceuticals, Inc)</td><td rowspan="2">Insulin (Diabetology, Ltd.)</td></tr>
<tr><td rowspan="2">GLP-1 (Amylin)</td></tr>
<tr><td>Nodlin, Nodexen (NOD Pharmaceuticals, Inc.)</td></tr>
<tr><td rowspan="5">Marketed products (therapeutic protein, associated companies)</td><td rowspan="5">Oral-lyn™ (India) (Generax)</td><td rowspan="2">Miacalcin (calcitonin, Novartis)</td><td rowspan="5">None known</td><td>Minirin (Ferring)</td></tr>
<tr><td>Leuprolide (DOR Biopharma)</td></tr>
<tr><td>Minirin (desmopressin, Ferring)</td><td rowspan="3">Nocutil (Gebro Pharma)</td></tr>
<tr><td>Suprecur (Sanofi-Aventis)</td></tr>
<tr><td>Fortical® (Unigene)</td></tr>
</table>

Table 1.1. Delivery technologies and marketed/researched therapeutic proteins. Table sourced and modified from [10, 11] (Colour-coding denotes preclinical, phase I, phase II, phase III, and discontinued).

Some of the potential benefits offered by the mucosal route for drug delivery include high surface area for absorption (e.g. intestinal and pulmonary routes), rapid absorption (nasal, pulmonary, sublingual, vaginal routes) and avoidance of first pass (hepatic) metabolism. However, as will be discussed in the later sections of this

chapter, mucosal administration presents unique challenges for the delivery of 'fragile' macromolecules such as protein therapeutics.

1.2 Possible routes for mucosal protein delivery

1.2.1 Oral Route

For biological drugs to be absorbed through the gastrointestinal (GI) tract, they must be protected from proteolytic enzymes and traverse the epithelial barrier, passing into the bloodstream. In addition, the high acidity in the gastrointestinal environment causes protein denaturation prior to absorption [12, 13]. The severity of the biological barriers of the GI tract to macromolecular drug absorption is highlighted by an *in vivo* study on the oral absorption of native insulin in a murine model, which revealed bioavailabilities of less than 1% [14]. This low level of bioavailability means that development of unassisted oral delivery formulations is not economically viable with the current knowledge and technology, especially when considering the considerably higher cost of raw material associated with biologics compared to small chemical entities.

Considering the physiological barriers to oral absorption of biologics in general, even if the therapeutic has sufficient stability and resilience to enzymatic degradation to survive transit through the stomach and into the intestines, it is then faced with a number of further barriers (Figure 1.2). The drug must first dissolve in the contents of the intestinal lumen (if it is not already in solution), before passing through a mucus layer, protecting the surface of the epithelial cells. The epithelial cell layer represents the next barrier stage. The therapeutic must cross the epithelial cells on its way to the capillaries. The lipid-based plasma membrane of epithelial cells makes penetration of hydrophilic macromolecules (e.g. protein therapeutics) into the circulation by partitioning and diffusion almost impossible. The epithelial cell barrier is particularly effective in limiting the absorption of proteins due its appearance as an almost continuous sheet, owing to the close intercellular distance of adjacent epithelial cells due to epithelial tight junctions (TJs). The small pore diameter of the TJs restricts the intercellular passage of molecules larger than 1000 Da [15, 16].

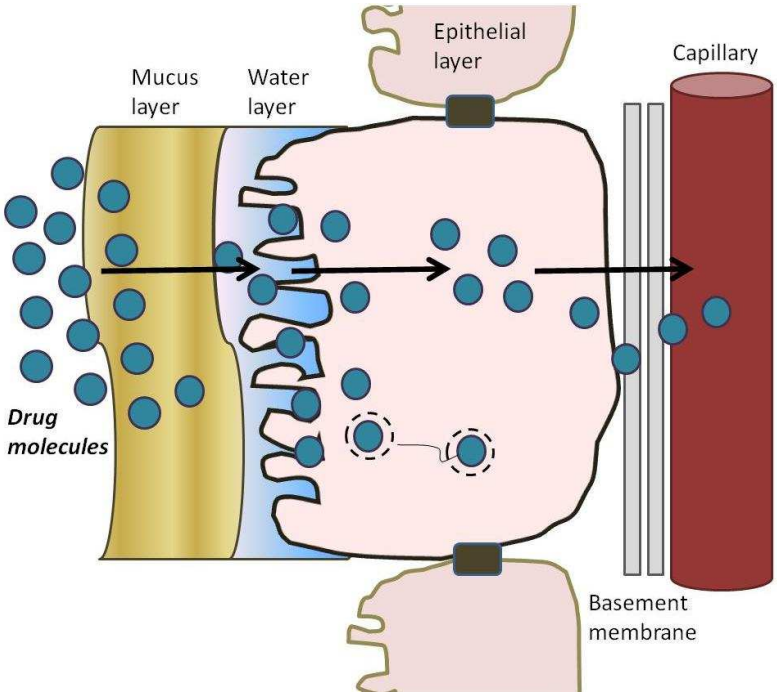

Figure 1.2. Drug absorption barriers in the intestine. Adapted from [17].

A few protein drug candidates intended for oral administration are showing promise in the development pipeline. For example, Glucagon-like peptide-1 (GLP-1, a gut hormone that stimulates insulin secretion for treatment of diabetes), is currently undergoing phase I clinical trials. Capsulin™ oral anti-diabetic (OAD) - an insulin product (by Diabetology) for treatment of type 2 diabetes mellitus is currently in phase II. It incorporates absorption enhancers and exhibits a reported bioequivalence of 6-10% relative to injected insulin [18].

1.2.2 Pulmonary route

From a physiological perspective, the respiratory system can be categorised according to the conducting regions, consisting of the air-transmitting passages of the nose, nasopharynx, larynx, trachea, bronchi and bronchioles [19], and respiratory regions (where gaseous exchange occurs) comprising of alveolar ducts and saccules. The anatomical structure of the conducting airways subtly changes with the restriction in diameter of the respiratory tubes [20], with the pseudostratified, columnar and ciliated epithelium with goblet cells and submucosal glands transitioning into a flattened squamous organisation devoid of goblet cells or glands. These structural airway features are presented schematically in Figure 1.3.

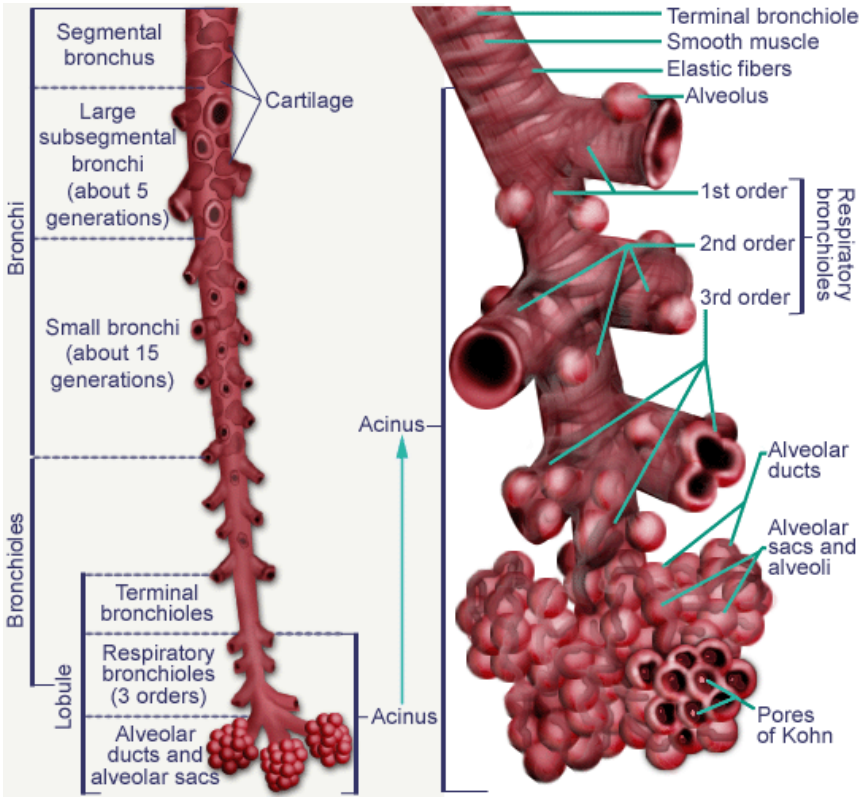

Figure 1.3. Subdivisions and Structure of Intrapulmonary Airways. Taken from [21].

The large surface area of the lung (approximately 140 m^2) for drug absorption [22] makes pulmonary delivery an attractive non-invasive option. Furthermore, first-pass metabolism is bypassed with this route and enzymatic activity has been reported as negligible [12]. The epithelial cells of the alveoli are very thin, hence the barrier to systemic drug absorption is potentially low. It is therefore unsurprising that pulmonary drug delivery is an exciting and emerging field for new pharmaceutical agents, with recent data estimating that the global pulmonary drug delivery technologies market may reach US$37.7 billion by 2015 [23].

Aerosol-based formulations offer a number of advantages, including more rapid absorption into the systemic circulation (this may be especially important for drugs where fast onset of action is critical), higher bioavailability than with other non-invasive modes of administration [24], minimal systemic side effects and preferred alternatives to injections. In light of these benefits, the pharmaceutical industry is investing major resources in aerosol drug delivery and biotechnology, including research in particle engineering, dispersion technology, dry powder formulations and drug delivery device design [25]. The commercial interest in developing inhaled insulin formulations

remains ever popular despite the withdrawal of Exubera® (inhaled insulin product, marketed by Pfizer) in 2007. This is exemplified by the efforts of Mannkind to develop their ultra rapid-acting inhaled insulin therapy (Afrezza™), which is in late stage clinical trial. Despite its advantages, drug delivery via the pulmonary route is influenced by factors such as lung disease, smoking and exercise [22], and this should be taken into account when offering treatment via this route to the patient.

1.2.3 Other mucosal routes for systemic delivery of protein therapeutics

The nasal route offers another attractive option for non-invasive protein delivery. The nasal mucosa is equipped with a robust epithelial cell layer and sub-epithelial vascularisation [12]. As *per* pulmonary delivery, nasal delivery avoids first pass metabolism [26] and experiences lower enzymatic activity in comparison to that found in the GI tract and liver [27] and importantly, provides ease of self-administration. There are however several limitations, including the rapid mucociliary clearance of foreign particulates (which might be problematic for protein delivery [28]), the sensitivity of the nasal cavity to changes in pH and the presence of nasal secretions [29]. Finally, the low molecular weight cut-off for the nasal route (approximately 1000 Da), similar to other mucosal surfaces, necessitates the use of permeation enhancers which may trigger irritation to the nasal mucosa and permit access for pathogens and other harmful substances [27].

The **buccal** administration route can also be exploited due to a good surface area for absorption and the highly vascularised supporting tissue. Despite avoidance of first pass metabolism by the liver, the presence of saliva acts as an additional barrier to drug transport, through its physiological role in the defence against foreign agents [30].

Less common routes for transmucosal protein delivery are via the rectal [31], vaginal [32] and ocular [33] mucosal surfaces. **Rectal** delivery enables direct protein absorption by the lymphatic system, thereby circumventing the problems of liver degradation [22]. The disadvantages associated with this approach include longer transit/dissolution times in the colon milieu, bacterial activity and interference from

faecal matter [5]. Low and variable extents of absorption associated with the **ocular** and **vaginal** routes, even in the presence of absorption enhancers, and localised adverse reactions mean that both these routes show little promise for protein delivery [12, 22]. Low bioavailabilities prevail with the former route as a consequence of local irritation to the eye and subsequent tear production [34].

1.3 The epithelial cell barrier: challenge at mucosal surfaces

1.3.1 Pathways for macromolecular transport

Small, amphipathic molecules readily internalise and exit from epithelial cells without a specific transport system by having the ability to partition in and out of lipid bilayer membranes (apical and basolateral) (Figure 1.4A). The transport of smaller hydrophilic macromolecules is limited largely to the paracellular route (i.e. between adjacent cells; Figure 1.4B). Larger macromolecules and nano-sized particles may be transported across the cells *via* transcytosis, through a series of tightly regulated vesicular structures involving highly complex signalling pathways, which control and restrict their passage into and out of the circulation (Figure 1.4C) [35, 36].

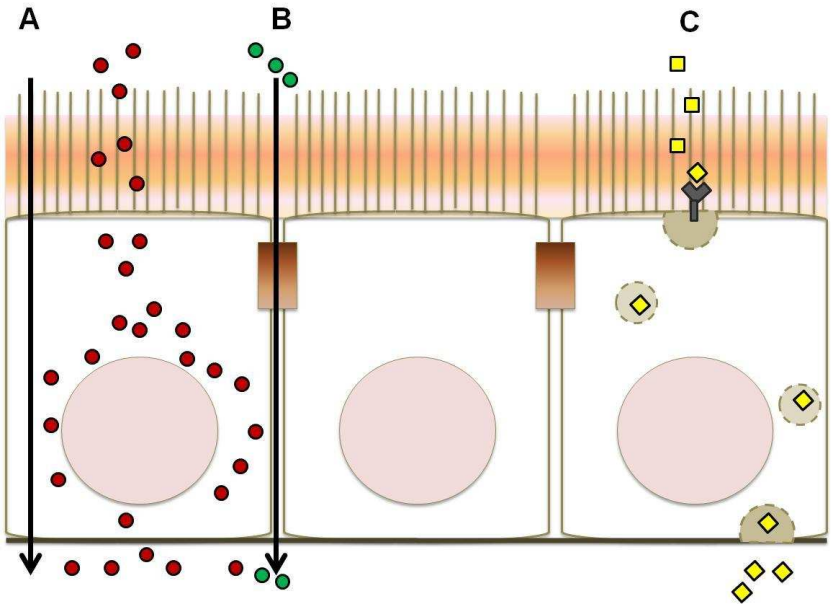

Figure 1.4. Possible pathways for translocation of molecules and nanoparticles across the mucosal surfaces.

A) Trancellular route, applicable to small, lipophilic molecules, B) Paracellular (between cells) route, relevant to relatively small, hydrophilic macromolecules, and C) Transcytosis (which may be receptor mediated), through which large macromolecules and nanoparticles can potentially traverse the mucosal surfaces.

1.3.2 Physiological barriers to mucosal absorption

Effective systemic delivery of protein therapeutics following mucosal administration faces a number of physiological barriers. These barriers are represented schematically in Figure 1.5. In addition to the epithelial cell layer barrier, drug absorption is also affected by mucus [37] and the mucociliary clearance mechanism. For example, mucociliary clearance alone is capable of clearing 50% of an administered nasal spray dose from the ciliated respiratory mucosa in less than 20 minutes [38].

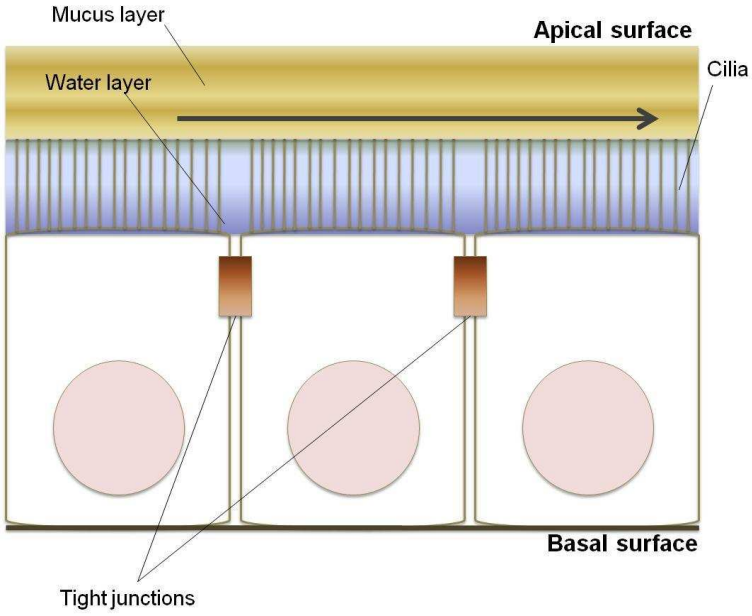

Figure 1.5. Physiological barriers to mucosal drug absorption.

In mucosal surfaces such as nasal bronchial and intestinal, epithelial cells are interconnected by tight junctions. Cells are covered by a thick mucus layer, which is normally secreted by goblet cells (not shown). Cilia beat in a synchronised fashion, resulting in unidirectional movement of mucus (represented by the grey arrow). This mucociliary clearance mechanism clears the mucus-trapped material (which may include administered drugs) from the mucosal surfaces in the nose and lung and acts as a lubricant in the gastrointestinal tract.

Proteolytic enzyme action may limit the availability of peptide and protein therapeutics in their active form at the mucosal surface [39]. However, the physicochemical properties of plasma membranes of epithelial cells and the close proximity of adjacent cells, which is enabled by the existence of epithelial TJs, present the most severe

barriers to macromolecular drug absorption. These barriers are discussed in detail below.

1.3.3 Intercellular tight junctions

The intercellular TJs surround the intestinal epithelial cells in a belt-like manner at the apical cellular borders. They form a paracellular seal between the lateral membranes of adjacent epithelial cells and act as both a structural “barrier” and a strict regulator of the paracellular movement of water, ions, neutral molecules and inflammatory cells [40-42]. The TJs also limit the diffusion of proteins and lipids between the apical and basolateral domains of the plasma membrane [43] and recruit cytoskeletal and signalling molecules involved in cell polarity, growth, differentiation and apoptosis [44].

On ultrathin section electron micrographs, TJs are viewed as a series of fusion points between the outer leaflets of the membrane of adjacent cells [45]. Freeze-fracture replica electron micrographs depict the TJs as a continuous anastomotic network of filaments on the protoplasmic face of the plasma membrane, with complementary grooves on the exoplasmic face [45]. These lateral contacts, define the extent of paracellular permeability [46, 47], which in turn is directly proportional to the number and density of tight junctional strands. Furthermore, it appears that the degree of permeability is related to the physiological role of the underlying tissue, with intestinal epithelial cells displaying higher permeability compared with airway epithelial cells and cells derived from the gall bladder [48, 49].

The TJs themselves are comprised of various cortical and integral proteins. Of the former, at least 16 different molecules have been discovered [45]. While some of these proteins serve as scaffolds linking the integral proteins of the TJ to the actin cytoskeleton, others serve as cross linkers of transmembrane junctional proteins. Many proteins also play key roles in vesicular trafficking through their association to kinases and Ras. At the TJ, three integral proteins are found: occludin, claudins and JAM (junction adhesion molecule), as well as cytoplasmic plaque proteins, including zonula occludens-1/2/3, cingulin and 7H6 [45]. Both the occludins and the claudins

consist of four transmembrane regions and two extracellular domains and interact with complementary molecules on adjacent cells leading to the creation of critical adhesion points [50]. These proteins comprise the backbone of the TJ strands. On the other hand, cytoplasmic plaque proteins are thought to link claudin and occludin to the actin cytoskeleton through PDZ (acronym for post synaptic density protein (PSD95), Drosophila disc large tumor suppressor (Dlg1), and zonula occludens-1 protein (ZO-1)) domains. They cross-link the transmembrane junction proteins and play an important role in cell signalling and vesicular trafficking [44]. JAM is a glycosylated 43 kDa protein with three distinct domains: an extracellular region of 215 amino acids that contains two variable type Ig domains, a single transmembrane domain, and a short intracellular tail (45 aa) that displays a classical type II PDZ binding motif [51].

From the drug delivery perspective, TJs present a significant barrier towards mucosal delivery of biomolecular therapeutics such as proteins. This is expected in view of the fact that the dimensions of the paracellular space lie between ~20-50 Å and therefore larger solutes with a molecular radius within this range and greater are restricted to alternative routes of transmucosal transport (i.e. are inevitably excluded from the paracellular route) [52, 53].

1.3.4 Gastrointestinal barriers

The GI tract provides a variety of physiological and morphological barriers against protein or peptide delivery, including: (i) proteolytic enzymes in the gut lumen (e.g. pepsin, trypsin, chymotrypsin), (ii) proteolytic enzymes at the brush border membrane (endopeptidases), (iii) the mucus layer, (iv) the bacterial gut flora and (v) the epithelial cell lining itself. The histological architecture of the gut mucosa is therefore designed specifically to selectively prevent the uptake of particulate matter from the environment.

Mucus-covered enterocytes represent the largest population of cells in the mucosa of the small intestine (ca. 90%) [54]. They are arranged as a single cell monolayer at the

GI surface and serve to control the absorption of nutrients, electrolytes and fluids and function as barrier to the environment. Immunological surveillance occurring at the surface of the GI tract [55], presents a further barrier to the delivery of biomacromolecules.

Highly specialised enterocytes situated in the intestinal tissue, the membranous microfold (M) cells, gather antigens and macromolecules from the GI surface. Morphologically, crypt-derived M cells [56] differ from absorptive enterocytes by possessing immature microvillus and glycocalyx structures, apical microfolds, increased intracellular vacuolisation and absence of mucus. Absorptive enterocytes and M cells constitute the follicle associated epithelia (FAE) of the Peyer's patch. The FAE collectively shuttles colloidal (particulate) antigens, small bacteria and viruses via a transcytotic mechanism to lymphoid micro-compartments, which are in close proximity to their casing epithelia [55]. The Peyer's patches themselves are described as oval aggregates (assembled from solitary lymphoid nodules) situated in the antimesometrial gut wall (ileum) [57]. From a drug delivery perspective, the physiological role of the Peyer's patches (including the transport mechanism) is thought to be important for the delivery of nano-sized colloidal carriers.

In the 1960s and 1970s, extensive research was conducted to decipher the nature of the enzymatic barrier in the intestines [58-61], with research initially focusing on its role in nutrient absorption. The hydrolysis of peptides and proteins occurs at different sites; either luminally, at the brush border, or intracellularly. Protein digestion is initiated in the gastric juice by a family of aspartic proteinases, commonly known as pepsins, which are most active at pH 2-3, but become inactive at a pH of above 5. The mixture of peptides resulting from the partial digestion of proteins in the stomach by pepsins will then be acted upon by pancreatic proteases upon reaching the duodenum and beyond. Such proteases include trypsin, α-chymotrypsin, elastase, and carboxypeptidase A. These proteases act in concert to cleave the majority of the internal peptide linkages and have an optimum pH of about 8.

1.3.5 The mucus barrier

The presence of mucus lining the mucosal surfaces is crucial for protection from invasion by foreign agents such as bacteria, viruses, allergens and irritants. Mucus also displays lubricating properties, important in assisting in daily functions such as eye movement and the passage of food through the digestive tract [11]. The mucus gel is largely composed of linear, glycosylated mucin fibres entwined in a dense network [62, 63], enabling particle entrapment and further hindrance of movement through the dense gel layer [64, 65]. The rate of diffusion through the mucus layer is thought to be affected by the relative size of the permeant, the effective mesh size of the mucus gel and interactions between the permeant and the components of mucus [66].

Contrary to the initial belief that the mucus barrier prevents mucosal uptake of large molecules primarily by hindering their diffusion, it is now known that most proteins, including large antibodies diffuse relatively easily through mucus [67]. This is thought to be because the mesh size (approximately 1 μm) of mucin fibres within mucus is much larger than most proteins, as demonstrated by an interesting study conducted by Saltzman and co-workers [68]. However, there is a body of evidence to suggest that human mucus largely prevents the movement of nanoparticles [69-71], which is an important consideration when designing a carrier-based therapeutic formulation for mucosal delivery.

Various attempts have been made to enhance nanoparticle transport across the mucus layer – a popular approach being attachment of polyethylene glycol (PEG) to the nanoparticle surface [69, 72]. In a study by Wang *et al*. [72], an alteration of the surface charge of negatively charged polystyrene particles (220 nm diameter) towards a more neutral charge, as a consequence of modification by short-chain length PEG, resulted in enhanced diffusion across cervicovaginal mucus. Furthermore, a reduction of PEG coating density on the surface of particles decreased the rate of particle transport, leading the authors to conclude that particle transport through mucus could

potentially be improved by the presence of a net neutral surface (to avoid binding to mucus) and a small radius to present entanglement with the mucin network. In a separate study reporting diffusion in cervical mucus, Cu *et al*. [73] examined the effect of immobilisation of different molecular weight PEG (2, 5 and 10 kDa) onto the surface of poly(lactic-*co*glycolic) acid (PLGA) nanoparticles (170 nm diameter). Surface modification with PEG enhanced the diffusion of particles (by 3- to 10-fold compared to unmodified particles), with the extent of increase in diffusion being dependent on the molecular weight of PEG and the coating density. A study by Lai *et al*. [69] also demonstrated that relatively large (500 nm and 200 nm) PEGylated nanoparticles can rapidly penetrate human mucus, with an effective diffusion coefficient only 4- and 6-fold lower than that for the same particles in water. Comparatively, the diffusion coefficient of uncoated particles of equivalent size was 2,400- to 40,000-fold lower in mucus than in water.

1.4 Enhancing mucosal protein delivery: commonly investigated strategies

Various approaches have been explored with the view to improve mucosal absorption and the subsequent bioavailability of protein therapeutics (Figure 1.6). These include the use of delivery systems that prolong the duration of drug contact with the mucosal surface (mucoadhesive polymers) [74, 75] (Figure 1.6A), chemical agents that increase membrane fluidity and/or disrupt cell membranes (e.g. surfactants) [76-78] (Figure 1.6B) and compounds that promote a transient opening of the epithelial TJs [79, 80] (Figure 1.6C). Receptor-mediated transcytotic pathways (Figure 1.6D) have also been exploited for the mucosal delivery of protein therapeutics (reviewed in section 1.4.3). Furthermore, chemicals that reduce mucus viscosity (mucolytics) [81-84], those that improve the stability of the administered protein drug, e.g. proteolytic enzyme inhibitors [85, 86], and agents which trigger dissociation of protein aggregates (e.g. cyclodextrins) [87] have also been investigated.

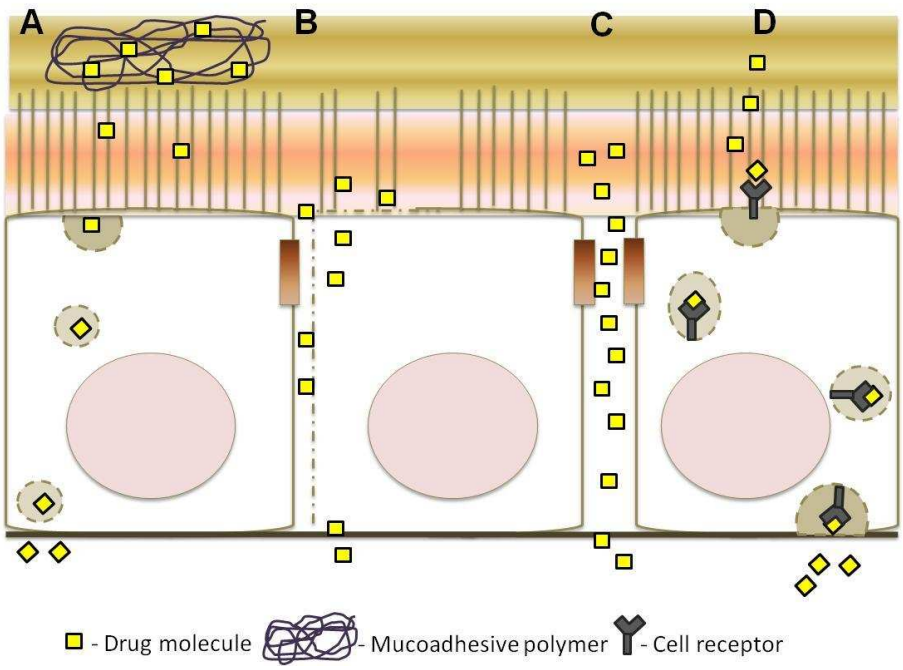

Figure 1.6. Visited strategies for improved mucosal absorption of protein therapeutics.

A) Mucoadhesive polymers prolonging the residence time of the complexed protein drug at the mucosal surface, B) Surface-active permeability enhancers compromising cell membrane integrity, whereby otherwise membrane-impermeable protein drug crosses the epithelial barrier, C) TJ opening where the paracellular space is increased, improving the paracellular access of protein molecules, and D) Exploiting epithelial transcytotic mechanisms by conjugating the drug (or a drug carrier nanoparticulate system) to a ligand (not shown) that is transported transepithelially via thisroute.

1.4.1 Surfactants and tight junction modulating absorption enhancers

A range of ionic and non-ionic surfactants have been explored for their potential as mucosal absorption enhancers [88-90]. However, many investigations have revealed that the use of surfactants as permeability enhancers is associated with cell toxicity, frequently observed in the form of cell membrane damage, altered cell morphology [88, 91, 92] and mucociliary arrest [93], which fundamentally flaws their application.

The biodegradable, biocompatible, compound chitosan (deacetylated form of chitin) is by far the most extensively studied polymeric absorption enhancer [94, 95]. Chitsosan has been approved for use in wound dressings and for dietary applications the USA by the FDA and by comparable institutions in several other countries. Its capacity to enhance macromolecule absorption across the mucosae has been demonstrated in numerous studies, both *in vitro* [80, 96] and *in vivo* [97-99]. Chitosan displays mildly

basic properties and requires acidic conditions to transform it into the positively charged, water-soluble form. Therefore, at neutral or physiological pH most chitosan molecules will lose their charge and precipitate from solution [100], which is a problem from the drug delivery perspective. To overcome this problem, chitosan derivatives such as *N*-trimethyl chitosan chloride (TMC) and PEGylated chitosan have been synthesised in an attempt to improve its solubility at neutral pH. Both these derivatives demonstrate absorption enhancing properties: in an aqueous solution, in the 1.5–2.5% concentration range, TMC was found to markedly increase the permeability of peptide drugs (buserelin and porcine insulin) across Caco-2 monolayers at pH 7.4 [96]. Although PEGylation notably improves the aqueous solubility of chitosan at neutral pH, this derivative still required mildly acidic conditions for a permeability promoting effect [79].

Different compounds with an ability to bind calcium so to reduce its extracellular levels, have been investigated for their potential to enhance the mucosal absorption of macromolecules *via* the paracellular route. This is due to early studies showing that depletion of extracellular calcium induces opening of the epithelial TJs [48, 101], thereby increasing paracellular permeability [48, 102-105]. Despite these studies, the conditions under which calcium reduction sufficiently modulates the epithelial barrier to result in meaningful improvements in mucosal drug absorption are unclear. In this respect, recent work from our group by Vllasaliu *et al*. [106] revealed that apical calcium removal produces only a modest effect on the tight junctions, whilst basolateral calcium exhaustion leads to a notably larger effect on the epithelial barrier. This is important from the drug delivery perspective as removal of calcium on the basal (as opposed to the luminal) side of the epithelium is probably unrealistic, hence rendering this approach inefficient for enhancing mucosal delivery of macromolecules.

Some of the more recent studies have employed relatively novel experimental approaches, such as RNA interference, to identify and exploit TJ targets for paracellular drug delivery. For example, Dutzar *et al.* [107] evaluated the effects of

siRNA knockdown of different TJ proteins (different claudins, JAM-1 and occludin) in assays establishing the effect on the epithelial barrier. The work reported that knockdown of claudin 4 inhibited TJ formation and produced a significant decrease in transepithelial electrical resistance (TEER) and an increase in FD4 permeability. Combination knockdowns between claudin 4 and occludin or JAM-1 were found to produce synergistic effects.

1.4.2 Bioadhesive polymers

The use of bioadhesive polymers as a means of delivering therapeutic agents to the gastrointestinal tract has attracted considerable attention in recent decades [108, 109]. Bioadhesive oral drug delivery systems are based on the concept that an interaction will occur between the mucus and the bioadhesive material (usually polymer) included in the drug formulation. This strategy offers advantages such as site specific drug delivery and prolonged residence time at the mucosal surface for improved absorption and bioavailability [110, 111]. With such systems, an improvement in oral bioavailability is often noticed as a direct consequence of more opportunity for the therapeutic to interact closely with the absorption site [112, 113]. The ability to retain an oral delivery system at the target location over a prolonged duration also potentially enables treatment of local conditions and may permit sustained systemic absorption [114, 115]. Despite extensive research on bioadhesive polymer systems, the phenomenon of bioadhesion is not yet entirely understood [116]. The term *bioadhesion* is defined as adhesion to a biological surface (i.e. mucus, mucosal surface or cell membranes). The scenario in which the polymeric system interacts with the mucus coating only is referred to as *mucoadhesion* [117].

The complex interactions between bioadhesive polymers and mucus are governed largely by the intrinsic properties of the concerned polymer and the surrounding physiological environment [118]. Physiologically, the gastrointestinal mucosa is composed of high MW glycoproteins underlying a continuous adherent blanket of mucin [119]. The consistency of the mucin gel is affected by the glycoprotein concentration. The mucin glycoproteins are rich with fucose and sialic acid groups at

their terminal ends housing a net negative charge in the acidic environment. The thickness of the mucin layer ranges between 50 and 500 μm in the stomach to 15–150 μm in the colon. The variation in thickness is attributed to the steady state equilibrium between the mucus secretions and its erosion *via* mechanical and enzymatic degradation.

The vast majority of bioadhesive drug delivery systems are based on hydrophilic hydrogel polymers and are designed primarily for buccal or sublingual applications [120]. The use of these hydrophilic polymers for GIT delivery would result in untimely hydration upon contact with the stomach contents, before developing interactions with the mucosal surface. A bioadhesive system for gastric delivery requires a rapid interaction with the mucosal surface, which must be sufficiently strong to resist the propulsion forces of the stomach wall. The system must remain effective irrespective of continuous production of mucus by the gastric mucosa to replenish the mucus that is lost through peristaltic contractions, as well as dilution of the stomach contents. Hydrophilic bioadhesive polymers often lose adhesiveness upon hydration, therefore, in order to prolong the adhesion, controlled hydration and/or formation of a firm gel network are desirable attributes [121]. The environmental pH is another important factor influencing the success of a bioadhesive system, as shown by recent studies indicating that the bioadhesiveness of polymers with ionisable groups, such as polyacrylic acid, is affected by surrounding pH [122]. As with the other classes of absorption enhancers, bioadhesive polymers/systems must be biocompatible and not trigger local tissue irritation or long-term toxicity. Other desirable characteristics of a bioadhesive dosage form include high drug loading and complete drug release.

1.4.3 Encapsulation systems

Minimisation of drug degradation and loss, prevention of harmful side-effects of the therapeutic, optimal drug bioavailability and site specific absorption are important requirements for some therapeutics. These attributes can potentially be achieved by encapsulating the therapeutic within ‘carriers’. Various such carrier systems are under development, ranging from nano- and micro-particles made of insoluble or

biodegradable natural and synthetic polymers, to liposomes and micelles. These carriers can be tailored to suit the therapeutic need or route of administration. Researchers have endeavoured to produce (singularly or in combination) bio-degradable, stimuli-reactive (e.g. pH- or temperature-sensitive) and target responsive systems, which anchor the drug-loaded system to the site of interest. These targeted systems can be further classified into passive and active targeting strategies. The former is best exemplified in the case of the preferential accumulation of chemotherapeutic agents in solid tumors as a result of the enhanced vascular permeability of tumor tissues compared with healthy tissue [123]. Active targeting involves the surface functionalisation of drug encapulated systems with ligands that are selectively recognised by receptors on the surface of the cells of interest. Since ligand–receptor interactions can be highly selective, this could allow a more precise targeting of the site of interest.

Colloidal drug encapsulation systems such as micelles, vesicle and liquid crystal dispersions, as well as nanoparticle dispersions consisting of small particles of 10–400 nm in diameter, have attracted considerable attention in recent years. In the late 1960s, micelles became popular as drug carriers owing to their easily controllable properties and good pharmacological characteristics [124, 125]. Micelles formed from hydrated amphiphiles consist of an inner core of assembled hydrophobic segments capable of solubilising lipophilic substances and an outer hydrophilic corona serving as a stabilising interface between the hydrophobic core and the external aqueous environment [126]. Depending on the delivery purpose, one can select the size, charge, and surface properties of these carriers simply via the addition of new ingredients to the mixture of amphiphilic substances before micelle preparation and/or by variation of the preparation method [127]. Micelles as drug carriers potentially offer many advantages. Drug bioavailability is potentially enhanced by the ability of micelles to physically entrap the sparingly soluble pharmaceutical and delivering it to the desired site of action at concentrations that can exceed its intrinsic water solubility. Furthermore, the drug is potentially protected as its contact with inactivating species, such as enzymes present in biological fluids, is minimised [128-130]. By far, the most

important feature of micellar delivery systems distinguishing them from other particulate drug carriers, is their small size (~10 to 30 nm) and the narrow size distribution [131].

Liposome carriers, which are capable of entrapping lipid-soluble drugs in the lipid bilayer and water-soluble drugs in the aqueous core [132], are another popular drug encapsulating strategy. Routine preparations are carried out under relatively mild conditions, thereby minimising drug denaturation during encapsulation. However, a significant disadvantage arises from their susceptibility to degradation by intestinal phospholipases and sensitivity to intestinal detergents (e.g. bile salts). Consequently, this degradation will trigger the premature release of the liposome-entrapped drug in the GI fluid [133, 134]. Other colloidal formulations, including emulsions and microemulsions, are effective in the oral administration of drugs with inadequate solubility in biological fluids [135, 136]. Microemulsions (oil/water) are bicontinuous systems composed of a continuous water phase containing nanometer-sized oil droplets, separated by a surfactant/co-surfactant-rich interfacial region [127]. Compared to emulsions, these offer several additional advantages, such as ease of preparation and good thermodynamic stability [136]. However, administration of microemulsions has triggered unwanted effects *in vivo*, especially formulations based on castor oil, wherein renal dysfunction, hypertension, and hepatotoxicity have been reported [127, 137].

More recently, nanoparticle-based encapsulation systems ranging in size from ~15 to 150 nm [138, 139] such as nanospheres [54] and nanocapsules [140, 141], hydrogels [4, 142, 143] and drug-coated silica particles have become popular. In terms of polymers investigated in nanocarrier formulations for oral drug delivery, there is a broad range of materials used for this application, including poly(alkylcyanoacrylates) [141] and terpolymers of methyl methacrylate, 2-hydroxyethylmethacrylate, and *n*-butylacrylate [144]. The reader is referred to additional references for a more comprehensive review of these systems [145-149].

1.4.4 Ligand-receptor mediated drug delivery

Biological processes of receptor-mediated cellular uptake and transport have become attractive in the field of drug/gene delivery in the past several years. These processes can potentially be exploited for designing site-specific delivery systems. Ligand-mediated active targeting has emerged as a novel paradigm in targeting either vascular compartment (first-order), cellular (second-order), or intracellular (third-order) levels [150]. Some of the drug carrier systems described above can potentially be used as cargo units for the site-specific presentation and delivery of various bioactives using biorelevant ligands, including antibodies, polypeptides, oligosaccharides (carbohydrates), viral proteins, fusogenic residues, and molecules of endogenous origin. Of particular relevance in this thesis, is the use of ligand-functionalised nanoparticulate systems (as carriers of therapeutics) for transmucosal delivery of biotherapeutics. The biological transport systems targeted by these appropriately formulated drug delivery systems are diverse and include carbohydrate (lectin) receptors, Fc receptors, complement receptors, interleukin receptors, lipoprotein receptors, transferrin receptors, scavenger receptors, receptors/epitopes expressed on tumor cells, and cell adhesion receptors.

1.5 Crossing the epithelium via the transcytotic route: cellular uptake and trafficking of protein therapeutics

1.5.1 Endocytosis in epithelial cells

Mucosal drug absorption via the transcellular route is wholly dependent on overcoming the plasma membrane barrier at the epithelial cell surface. Generally speaking, clathrin- or caveolin-mediated endocytosis, macropinocytosis and phagocytosis are all extensively described endocytic mechanisms which play an important role in the uptake of macromolecules [151]. Moreover, alternative, clathrin- and caveolin-independent pathways have also been implicated in the cellular uptake of material [152]. A schematic representation of these endocytic pathways is presented in Figure 1.7. From a systemic mucosal drug delivery perspective, the therapeutic must be both effectively internalised *via* epithelial cells and sufficiently transported and released at the basolateral side.

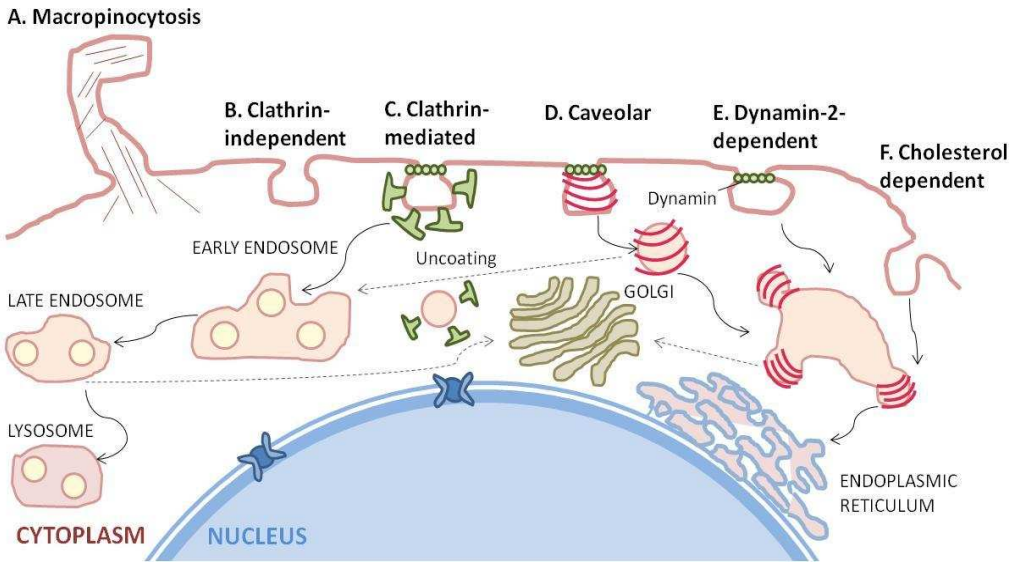

Figure 1.7. A schematic representation of cell endocytosis pathways.

Large particles can internalise via phagocytosis, whereas fluid uptake occurs by macropinocytosis (A). Phagocytosis and Macropinocytosis events often result in the formation of larger vesicles.Cargoes can also be endocytosed by mechanisms which are independent (B, F) of the coat protein clathrin (C) and the fission GTPase, dynamin (D, E). Most internalised cargoes are delivered to the early endosome through vesicular (clathrin- or caveolin-coated vesicles) intermediates derived from the plasma membrane. Some pathways may first traffic to intermediate compartments, such as the caveosome before reaching the early endosome. Adapted from [153].

1.5.1.1 Clathrin-mediated endocytosis

Clathrin-mediated endocytosis, which is responsible for the internalisation of nutrients, pathogens, antigens, growth factors and receptors, is the most extensively characterised mechanism for the entry of molecules into cells. Detailed progression of the entire process has been explicitly detailed in a number of reviews [154, 155]. In short, integral membrane proteins (e.g. activated receptors) bind to cytosolic adaptors, which then form links to the clathrin lattice. Accessory proteins, such as the GTPase dynamin, play a crucial role in the process of endocytosis, e.g. through initiating clathrin polymerisation or inducing membrane curvature. Furthermore, both adaptors and accessory proteins have the capacity to bind PtdIns(4,5)*P*2, a phospholipid concentrated at sites of clathrin-mediated endocytosis [156-159]. Important roles for actin have also been demonstrated in the process of clathrin-mediated endocytosis [160]. Lastly, the nascent coated vesicle is severed from the plasma membrane through a fission reaction thought to be mediated by dynamin [161].

1.5.1.2 Clathrin-independent endocytosis

Clathrin-independent endocytosis can be further sub-divided into dynamin-dependent and dynamin-independent processes [152]. Of the former, caveolae-mediated endocytosis is perhaps the most extensively characterised. Caveolae are inverted omega-shaped invaginations with a maximal diameter of 50-100 nm, connected to the plasma membrane or plasmalemma by a neck-like structure, which provides spatial continuity with the extracellular environment [162]. The principal component, which is also a crucial functional element, is a protein called caveolin [163]. Cholesterol is another essential component of caveolae and is required to maintain structural integrity; caveolae disappear in cells that are depleted of cholesterol [164]. Functioning as both intracellular and transcellular transport systems, caveolae appear to deliver their cargo either to endosomes or across the cell to opposite cell membrane surface [165]. This transcytosis process is thought to occur by one of two mechanisms - *either* caveolae could either pinch off from the plasma membrane, travel across the cell and fuse with the opposite surface, *or*, they may transiently fuse with each other producing channels through which material passes [35]. In contrast to the classical clathrin-dependent pathway, there is evidence that caveolar internalisation avoids lysosomes and hence the degradation of engulfed material [166]. The ability to distinguish the caveolae-mediated pathway from both clathrin-mediated and pinocytosis routes using cholesterol depleting agents such as filipin, nystatin, or methyl-cyclodextrin gives researches an important tool to characterise biological mechanisms of cell internalisation and transport (discussed in more detail in Chapter 5 of this thesis).

1.5.2 Cellular uptake and transport of cargo across epithelial cells

Poor absorption of macromolecular drugs across the mucosal surfaces in part result from the low rate of endocytotic activity occurring at the apical plasma membrane of epithelial cells, which can be further attributed to the important physiological role of the epithelium, which selectively filters and discriminates foreign substances in order to protect cells and organs from the external milieu [167]. This is best exemplified in

polarised cells where a higher rate of endocytosis operates at the basolateral plasma membrane (several-fold higher) than at the apical plasma membrane [168, 169].

However, polarised epithelial cells demonstrate some capacity to internalise macromolecules from both apical and basolateral plasma membrane domains [170]. Researchers commonly employ Madin-Darby Canine Kidney (MDCK) cells to study membrane trafficking in polarised epithelial cells [171], where endocytosis has been found to occur by both clathrin-dependent and clathrin-independent mechanisms [172]. Following cellular internalisation (from both apical and basolateral membranes), fluid-phase markers (cargo) have been shown to enter distinct populations of apical early endosomes and basolateral early endosomes [173, 174]. The fate of this material is entirely dependent on the cell sorting machinery, with a proportion of apically internalised fluid thought to either recycle or transcytose, and the remainder delivered to a shared population of late endosomes and lysosomes [170]. This becomes an important focus in later sections of this thesis.

1.5.2.1 IgG/FcRn pathway

Immunoglobulin G (IgG) is actively transferred from mother to offspring, conferring short-term passive immunity [175, 176]. In addition, IgG has been shown to traverse a number of mucosal surfaces in man – a process that is important in immune surveillance and host defense at mucosal surfaces [177]. IgG is transported by the neonatal Fc receptor (FcRn) [178, 179], which undergoes transcytosis in both apical-to-basolateral and basolateral-to-apical directions [180]. Briefly, IgG either binds to FcRn at the apical surface of the cells or is internalised by fluid phase endocytosis, encountering FcRn in the apical early endosome. Thereafter, IgG/FcRn is either delivered to the apical recycling endosomes or to the common recycling endosomes. Within the recycling endosomes, IgG/FcRn is sorted into coated vesicles that could serve as exocytic carriers to the basolateral cell surface [180].

The IgG/FcRn transport pathway could potentially be exploited for mucosal delivery of biotherapeutics (for a systemic effect) as this system is functional in several organs and tissues, including the lung [181] and intestine [182]. The expression of the FcRn receptor in the lung presumably results from the differentiation of mesenchymal stem cells (common progenitors) in early development. Previous studies investigating pulmonary absorption of therapeutic proteins (erythropoietin and follicle-stimulating hormone) through the FcRn pathway in non-human primates showed promising results [183, 184]. Furthermore, Bitonti *et al.* [185] demonstrated a dose-dependent absorption of protein therapeutics following pulmonary administration in healthy male volunteers. A recent publication from our group by Vllasaliu *et al*. [186] evaluated the IgG/FcRn pathway for mucosal delivery of nanoparticles as therapeutic carriers across airway Calu-3 cells, documenting a potential for Fc-modified nanoparticles to 'shuttle' a model therapeutic antibody fragment across the airway mucosa.

1.5.2.2 Folate-mediated pathway

Folic acid is a vitamin necessary for one-carbon transfer reactions in several metabolic pathways. Because folic acid is essential for the biosynthesis of nucleotide bases, the vitamin is consumed in vast quantities by proliferating cells [187]. Normal cells transport physiological folates across the plasma membrane using either the reduced folate carrier or the glycosylphosphatidylinisotol (GPI)-anchored folate receptor (FR). The former is found in the majority of cells and constitutes the primary pathway responsible for the physiological uptake of folates. The latter is primarily found on polarised epithelial cells and activated macrophages [188, 189] and preferentially binds and internalises oxidised folates via receptor-mediated endocytosis [190]. FR is over-expressed in cancer cells, making it an obvious target for ligand- and antibody-directed cancer therapeutics [191]. FR is capable of transporting both folic acid and a variety of different folate-linked cargos (i.e. imaging agents, proteins, liposomes, chemotherapeutics, nanoparticles, etc.) [192]. Following FR binding at the cell surface, folate conjugates are internalised via receptor-mediated endocytosis [193-195].

Receptor-mediated uptake of folate-drug conjugates proceeds through a series of stages, commencing with conjugate binding to cell surface FR and ending with the release of a portion of the therapeutic entity into the cytoplasm. Following membrane invagination and internalisation to form an endocytic vesicle, acidification of the endosomal compartment to pH 5 results in release of some (but not all) folate conjugates from their receptor [196, 197]. Subsequent trafficking of the acidic endosome to a recycling intracellular region then allows separation of membrane-bound FR from released conjugates/free drug [192]. Released folate conjugates are thought to be able to circumnavigate the endosome via an unknown mechanism, resulting in drug deposition in the cytoplasm. In contrast, membrane-bound-FRs largely recycle back to the cell surface, allowing for delivery of additional folate-linked drugs into the cell. Moreover, it has been observed that relatively few folate conjugates enter lysosomes for destruction [198], which has important implications for delivery of sensitive drugs.

There have been conflicting reports on the mechanism of endocytosis and subsequent trafficking of GPI-anchored FR [199, 200], with early studies disputing internalisation via the clathrin-mediated pathway [201] and postulating that the receptor is organised into submicron domains at the cell surface. These studies also claimed that the GPI-anchor was responsible for mediating receptor clustering in association with caveolae [199]. Further investigations revealed that the multimerisation of the GPI-anchored FR does not occur in caveolae but instead remains diffuse across the cytoplasm pending folate binding [200]. Later studies indicated that the GPI-anchor organises the FRs into “lipid-rafts” or receptor-rich complexes at the plasma membrane. These submicron domains (<70 nm in diameter) were found devoid of caveolae but rich in sphingolipid and cholesterol [202, 203].

In terms of exploiting folate mediated pathway for mucosal delivery, a recent study by Moradi *et al*. [204] investigated the internalisation of folate decorated nanoparticles in airway Calu-3 cells. More specifically, the study determined the effects of surface

folate-ligand distribution pattern (ligand clustering and density) on the extent of internalisation. The model particulate system consisted of polystyrene nanoparticles, surface-decorated *via* the adsorption of ovalbumin with conjugated folate ligand. The authors demonstrated that increasing overall ligand density on the nanoparticle surface resulted in increased nanoparticle internalisation, up to a saturation point. Surface ligand density was also shown to affect the cellular uptake pathway, with a switch from predominantly clathrin to predominantly caveolae-mediated route as the ligand density was increased. The study also inferred that surface clustering of the folate ligand enhanced cellular internalisation of nanoparticles, relative to its dispersed surface distribution.

1.5.2.3 Vitamin B_{12}-mediated pathway

Like folate, the consumption of vitamin B_{12} (B_{12}; cobalamin) is vital for the survival of all living cells and although bacteria naturally produce vitamin B_{12}, all other species must acquire it through their diet [205]. The cobalamin family comprises molecules with a central cobalt atom, surrounded by a tetrapyrrole ring similar to chlorophyll or porphyrin. The core of vitamin B_{12} is often referred to as a corrinoid or corrin ring [206]. The cobalt atom is additionally attached to a nucleotide (5,6'-di-methylbenzimidazole ribonucleotide) and another group, which dictates its nomenclature (Figure 1.8). Attachment of cyanide as a sixth ligand produces cyanocobalamin (vitamin B_{12}). An attached hydroxyl group yields hydroxycobalamin (vitamin B_{12}a), which is also the dietary form. There are two predominantly active forms of B_{12}: methylocobalamin and adenosylcobalamin, which adopt essential roles in intracellular metabolism. Methionine synthase uses methylcobalamin to produce the amino acid methionine from homocysteine, and methylmalonyl-CoA mutase uses adenosylcobalamin as a cofactor to produce succinyl CoA, which is important in the tricarboxylic acid (TCA) cycle [207]. Mammals have evolved a complex uptake pathway for B_{12} involving a series of transport proteins [207-209]. In this thesis, the uptake pathway is covered in considerable depth. However, the distinct roles of the transport proteins are discussed only superficially. Amongst the cobalamin binding proteins, transcobalamin II (TCII) and intrinsic factor (IF) are probably the most physiologically important [206]. The

reader is referred to recent reviews by Banerjee *et al*. [207] and Randaccio *et al*. [210] for a more in depth discussion of these transport proteins.

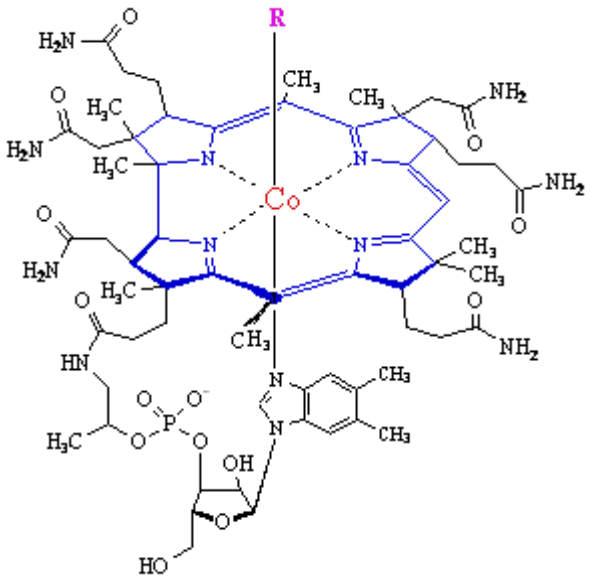

Figure 1.8. Chemical structure of vitamin B_{12}. Taken from [211].

Cyanocobalamin is moderately soluble in water at room temperature (12 g/L) and also in lower alcohols and phenol. It is, however, insoluble in acetone, ether and chloroform. B_{12} is neutral in water and is stable within the pH range of 4-7. The molecular weight of B_{12} is 1355.4 g/mol and its empirical formula reads $C_{63}H_{88}N_{14}O_{14}PCo$ [212]. Several functional groups are readily available for modification on B_{12}. Of importance, however, only a few modification sites maintain the recognition needed to utilise the biological B_{12} uptake pathway for oral delivery [205] (See Chapter 4 for further details).

The absorption of B_{12} in humans is complex (Figure 1.9) [213, 214]. Upon ingestion, B_{12} is initially released from the food by the action of peptic enzymes and the acidic environment of the GI system [215]. This is then followed by binding to and transport by two glycoproteins, haptocorrin (HC; also sometimes referred to as cobalophilin, R binder and transcobalamin I) and IF [208]. HC is the first protein to bind to B_{12}, in the saliva and gastric secretions, and has a high affinity for B_{12} under acidic conditions (pH < 3) thus protecting B_{12} from acid hydrolysis. The HC:B_{12} complex travels from the stomach to the duodenum, where the higher pH decreases the affinity of HC for B_{12}

[216]. Following its release from HC (which is subsequently enzymatically digested), B_{12} binds to IF – a 43.4 kDa glycosylated protein secreted from the pancreas and gastric mucosa [208]. IF facilitates transport across the intestinal enterocyte, which occurs by receptor-mediated endocytosis, *via* the apically located IF-B_{12} receptor, cubilin [217]. Cubilin works synergistically with amnionless, an anchoring protein to transport B_{12} [215]. Cathepsin L degrades IF within the lysosomes of the enterocytes [218]. A fraction of vitamin B_{12} will inevitably pass into the circulation by passively diffusing through the ileum [219]. 2-4 hrs following ingestion, B_{12} transcytoses across the enterocytes, appearing in the blood plasma bound to transcobalamin II (TCII). Holo-TCII is internalised by the TCII-receptor (TCII-R) situated on the basolateral side of metabolically active cells [220]**.** Another receptor, megalin can reabsorb holo-TCII from primary urine. Thus, TCII-R and megalin receptors act in concert to ensure widespread delivery and maximal use of B_{12} in the body.

The exploitation of B_{12} cell transport route for drug delivery purposes undoubtedly requires knowledge of the binding between B_{12} and its various transport proteins and the resulting receptor recognition, cell uptake and trafficking of B_{12} bioconjugated pharmaceuticals. These phenomena have implications for formulation design and drug delivery. The potential of the vitamin B_{12} pathway for mucosal delivery of nanoparticles as potential carriers of biotherapeutics is central to this thesis and will be explored in Chapters 4-7.

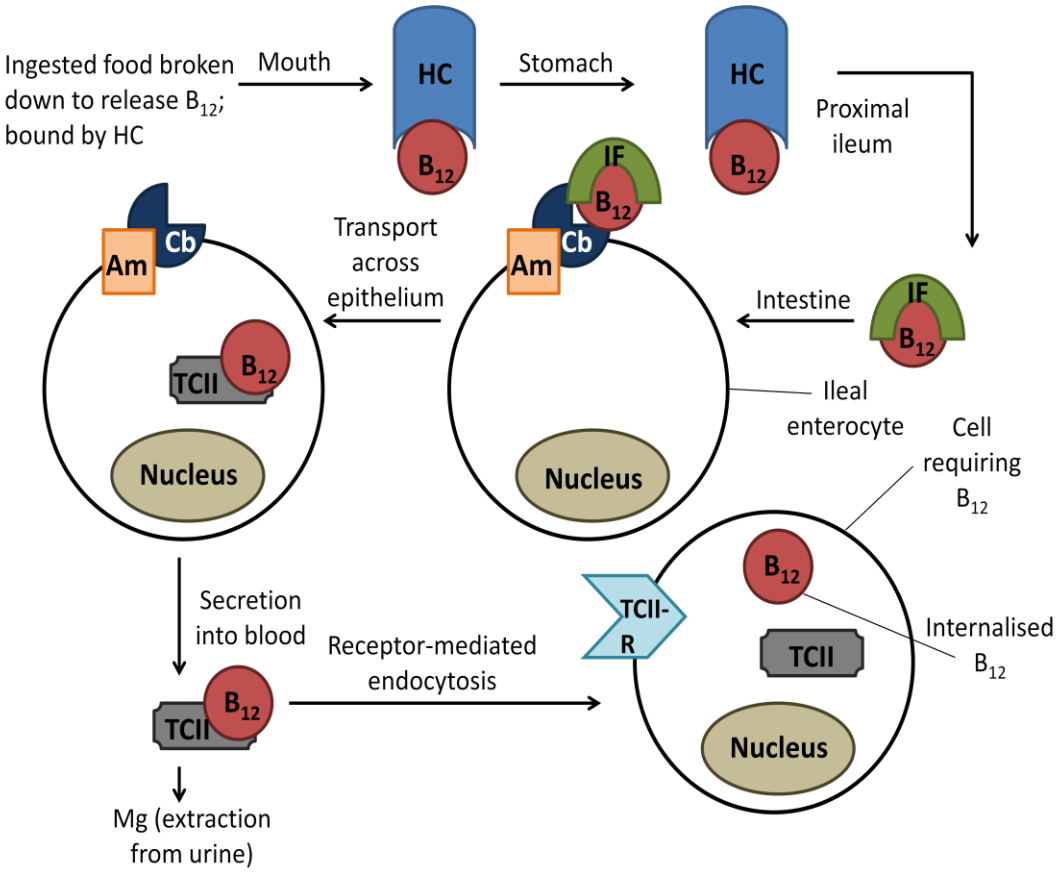

Figure 1.9. Cellular uptake of B_{12} from dietary sources.

The uptake capacity of B_{12} is ~2.5 µg per day for an adult human [221]. HC: Haptocorrin; IF: Intrinsic factor; Am: Amnionless; Cb: Cubilin receptor; Mg: Megalin; TCII: Transcobalamin II; TCII-R: Transcobalamin II receptor. Adapted from [205].

1.5.3 Exploiting transcytotic systems for mucosal delivery: general considerations

Although efforts have been made to identify cargo, uncover numerous cellular pathways and delineate the possible mechanisms involved, many issues remain unaddressed in attempts to successfully exploit the self-functioning cell machinery for therapeutic delivery. Firstly, the choice of the *in vitro* model(s) to study transcytosis is of paramount significance. The use of *in vitro* cell models to investigate transcytosis has many advantages over *in vivo* systems. Animal variability is eliminated, as is the perplexing issue of cargo being either modified or engulfed by cell types other than the one under study. Furthermore, *in vitro* systems can be manipulated in ways not possible *in vivo*, enabling one to measure the effects of different variables (e.g., temperatures, pharmacological agents, etc.) with greater accuracy and precision and

to uncover the molecular mechanisms of transcytosis. These advantages however, are compensated by the loss of *in vivo* context (e.g. the role of the extracellular matrix and the influence of other cell types). In view of this, one should employ a degree of caution when extrapolating *in vitro* results to the *in vivo* situation and when comparing results obtained from the two systems. To this end, researchers should also be wary of findings obtained from cancerous cell lines, which is especially relevant in the case of transcytotic systems, whereby over-expression of receptors and other transporters may give the misguided impression of high levels of transcytotic activity and hence drug delivery, when in reality this activity may be of a therapeutically limited capacity. Another important consideration is the functioning of the biological process of transcytosis in health and disease. Evidence of dysfunctional transcytosis in some disease states has recently emerged, with recent studies implicating abnormal enterocyte transcytosis in the early etio-pathogenesis of Crohn's disease [222].

Currently, drug delivery via the biological cell uptake/transport is restricted by an overall lack of understanding in the complex cell sorting processes involved at the molecular level. Our understanding of how the cell is effectively able to discriminate between cargo destined for transcytosis *versus* degradation in the lysosomes remains poor. In peripheral endothelial cells, apparently separate entry points dictate different fates; internalisation *via* coated pits sends cargo to the endocytic pathway, whereas caveolae-mediated internalisation will ensure a transcytotic fate [35]. In epithelial cells, the transcytotic pathway is a recognised branch of the endocytic pathway, but the destination and the point at which the transcytotic cargo is sorted away from the remainder of the internalised material remains a mystery. And although in some cases signals have been identified in distinct regions of molecules, governing their sub-cellular fate, the precise means of recognition is not fully understood. In enterocytes, megalin recycles to the plasma membrane from endosomes after internalisation and dissociation from its transcytotic cargo. But by contrast, in the thyroid, the same membrane receptor escorts thyroglobulin across the cell [35]. Whilst researchers have been able to pinpoint alternative navigation routes for megalin which appear to be cell

or tissue dependent, the crucial signals which drive it along these different itineraries remain unidentified.

Another unsolved mystery is how the cell discriminates cargo for transcytosis and cargo intended for its own use. Transcytosis is not the only pathway that molecules take to a specific plasma membrane domain and the mechanisms which regulate vesicular transport are highly complex. Knowledge of the binding between a ligand and its various carrier proteins and receptors is essential if the system is to be successfully exploited in drug delivery.

1.5.4 Nanoparticle-mediated delivery of protein therapeutics

The pharmacokinetics and biodistribution of drugs can be tailored to the therapeutic need through the selection of an appropriate drug delivery system [223]. Maintaining constant localised drug delivery to a target site exerts a greater therapeutic effect with potentially lower systemic drug levels than alternative dosing methods. Therapeutic molecules, including proteins, can be encapsulated inside carrier systems composed of materials such as polymers and lipids. As discussed in the earlier sections of this chapter, this encapsulation may protect the therapeutic and provide controlled drug release.

The following attributes are desirable for nanoparticles used for drug delivery: a particle core, a biocompatible protective layer, and a linker molecular layer for bioactivity [224]. The linker layer comprises reactive groups at both ends, permitting attachment of the linker to the core and to the bioactive molecules. Conjugation of functional groups can enhance biocompatibility, increase circulation times, and ensue selective targeting of nanoparticles. Hydrophilic polymers, such as PEG, are often coated onto the surface of nanoparticles to minimise their uptake by the reticuloendothelial system (RES) and thus increase the circulation time of administrated nanoparticle-linked drugs. This is important as nano-scale drug carriers administrated systemically have been shown to be taken up primarily by the RES

through the phagocytotic pathway [225, 226]. Liposomes coated with PEG display longer circulation times after intravenous administration in mice [227].

For nanoparticle-mediated drug delivery, size ranges of 10 to 200 nm are typically employed. The small size allows nanoparticles to penetrate tissues, especially tumors with a high level of specificity [228], improving the targeted delivery of drug. Table 1.2 broadly summarises the types of nanoparticles developed so far for enhancing drug delivery.

Particle Class	Materials	Size	Toxicity	Application
liposomes	lipid mixtures	30-200 nm	low	drug/gene delivery
dendrimers	branched polymers	5-50 nm	depends on cell type	drug/gene delivery
polymer carriers	polylactic acid, polysaccharides, poly(cyano)acrylates, poly(lactide-co-glycolide)	50-2000 nm	low	drug/gene delivery
magnetic nanoparticles	Iron oxide	100-200 nm	low	diagnosis/drug delivery
gold nanoparticles	chlorauric acid, sodium citrate	30 nm - 1.6 µm	low	drug delivery

Table 1.2. Applications of nanoparticles in Drug/gene delivery [224].

From a pharmaceutical perspective, polymeric nanoparticles are of great interest owing to their potential resilience in the GI tract and the protection provided for encapsulated drugs. By incorporating various polymeric materials within or on the nanoparticle surface, the physicochemical properties (e.g. hydrophobicity and surface charge) can be modulated to improve behavioural characteristics in the physiological environment. The targeting of nanoparticles, bioadhesive properties and cellular uptake can be greatly enhanced and the drug release properties tailored to suit the therapeutic need [229]. In modifying the surface of the nanoparticle by adsorption or chemical grafting with molecules such as PEG, poloxamers and bioactive components (e.g. lectins and invasins), they are further protected from the harsh gastrointestinal environment and this further helps to enhance their transmucosal transport [230-232].

In terms of the types of materials employed to formulate nano-scale therapeutic carriers, biodegradable and biocompatible PLGA is perhaps the most widely used material for synthesising nanoparticles for sustainable drug release [233-236]. PLGA

is non-toxic and displays a good sustained release profile (through diffusion and by the degradation of the nanoparticles) [237, 238]. PLGA undergoes hydrolysis following administration, forming biocompatible and metabolisable moieties such as lactic acid and glycolic acid, which are later removed from the body by the citric acid cycle [239]. These nanoparticles are generally made by emulsion solvent evaporation or by solvent displacement techniques [240].

The surface properties of nanoparticles have important implications for their *in vivo* fate, including nanoparticle-cell interaction, in addition to drug release properties [241]. In view of this, alteration of the surface properties of nanoparticles becomes critical to targeted drug delivery [242], with surface conjugation or coating of ligands that specifically bind to target cells or tissues, being a common approach. The choice of such ligands depends on the desired application of the delivery system, with antibodies [243], folate [244, 245] and peptides [246] commonly explored for targeted drug delivery in cancer therapy.

Considering the use of nano-carriers for systemic drug delivery following oral administration, considerable efforts have been made to improve nanoparticle formulation and uptake through the intestinal mucosa. However, some important questions remain: is it possible for nanoparticles to reach the systemic circulation in sufficient number to induce the desired pharmacological response? The majority of studies conducted for drug delivery research purposes, generate assumptions from data based on *in vitro* cell transport studies or from animal models: can we afford to ascertain nanoparticle behaviours and drug release properties from these and extrapolate this to valid predictions in man? With focus on nanoparticle transport across the gut mucosa, researchers must first of all appreciate that two types of intestinal cells are concerned with the uptake and transport of particulate matter: the enterocytes and the M cells. Despite comprising the majority of cells in the gastrointestinal tract, the enterocytes possess a low endocytic activity. It is generally agreed that particles are mostly transcytosed in the FAE [247-249] and because M

cells are capable of transporting a wide range of materials, it seems logical to expand on efforts to exploit these cells in drug delivery.

Particle transport by M cells is predominantly transcellular and energy-requiring [250]. Following their uptake by M cells, nanoparticles below 1 µm are delivered to the basal side [251], while particles larger than 5 µm become trapped in Peyer's patches [252]. Particles below 1 µm and more desirably below 200 nm are likely to be optimal for M cell uptake [247, 253]. Of further interest is the relationship between nanoparticle surface charge and its subsequent interaction with M cells. Of note, Jung *et al*. [254] report that absorption through M cells is optimised with the use of hydrophobic, negatively charged nanoparticles.

The chemical stability of nanoparticles is essential for biodegradability and subsequent release of the encapsulated drug [255]. Undoubtedly, colloidal stability is also important as a number of biological processes are affected by nanoparticle size. In this regard, PEG coated nanoparticles offer greater colloidal stability, together with diminished immunogenicity, resulting from reduced adsorption of plasma proteins onto the polymer surface [256, 257]. Whilst researchers have speculated over which polymer(s) would be most efficient for nanoparticle oral delivery, there is a problematic lack of comparative studies. However, it is generally agreed that the smaller the size, the better the uptake regarding both enterocytes and M cells.

1.5.5 Lectin-mediated transcellular protein delivery

Lectins are proteins or glycoproteins of plant, bacterial or vertebrate origin that specifically recognise and bind to polysaccharide or glycoconjugate moieties [258]. In particular, plant lectins (e.g. tomato lectin [259]) are a popular choice for oral drug delivery because of their non-toxic properties, tendency to bind to sugar moieties of glycocalyx expressed on the intestinal epithelial cells and their intrinsic resistance to digestion in the gastrointestinal tract [258]. A study carried out by Russell-Jones *et al*. [260] explored the effect of particle size, lectin ligand density and inhibitors on the uptake of lectin-coated nanoparticles by epithelial cells for oral drug delivery

applications. The degree of uptake was most influenced by the density of lectin on the particle, which when increased from 2 times to 8 times, resulted in a linear increase in the uptake of material. In another study [261], tomato lectin-conjugated nanoparticles were found to efficiently penetrate the mucus gel and were transported across epithelial cells. However, a severe limitation of tomato lectin arises from its apparent cross-reactivity with N-acetylglucosamine in the mucus layer, resulting in a reduced amount of tomato lectin conjugates available for epithelial cell surface binding [262].

1.6. Protein crystals for the delivery of biopharmaceuticals

The concept for drug crystal formulations has been around for decades, especially in the case of small therapeutic molecules. The main advantages of crystal preparations include better handling, stability, and varied dissolution characteristics, which allow better control over bioavailability [263]. Moreover, the possibility of chemical degradation is extensively minimised in crystalline *versus* amorphous or soluble forms. However, rapid advances made in the development of crystal formulations for small molecular therapeutics are not yet been matched by those of protein crystals. It is, nevertheless, envisaged that at least some of desirable traits observed for small molecule therapeutic crystals, could one day be mirrored for some protein formulations, including protection of the integrity and biological/biochemical function of the therapeutic agent, sustained release, improved bioavailability and abolishment of repetitive dosing regimens [263].

1.6.1 An Introduction to crystallisation

Protein crystals are solids comprised of an ordered packing of molecular units into defined lattice space groups and are formed from the same processes as small molecule crystals [263]. In crystalline form, proteins adopt a more energetically favourable state (3-6 kcal greater than in solution) [264]. The dimensions of protein crystals are usually smaller than non-biologic crystals and thus, are restricted to a ‘terminal’ size [265]. The intrinsic stability of protein crystals is governed by hydrophobic interactions, H-bonds and salt bridges between or within proteins. Fewer

and weaker intermolecular interactions undoubtedly means that they are more fragile than non-biologic crystals [265]. Water (solvent) molecules reside within the protein crystal structure, as well as loosely associated in channels within the crystal lattice around the protein molecules. This moisture is thought to be important for maintaining the hydrated configuration of proteins [263, 266].

Generally, theories based on the nucleation dynamics and crystal growth kinetics of small molecule crystals can be applied to macromolecular crystals [267, 268]. In this regard, the processes of crystal nucleation and growth depend on both the solubility and the supersaturation of the protein in its environment. Initiation of crystal formation is thus dependent on both the supersaturated chemical potential of the molecule and its chemical potential in the saturated solution [263]. Thus, to grow a crystal from solution, the solute molecules must be brought into a thermodynamically unstable state. Figure 1.10 shows a phase diagram used in crystallisation literature. The parameter represented on the x-axis can be temperature, pH or another variable which influences the solubility of the protein. In the under-saturated region, crystals will not form or grow. Above the saturation limit, the solution is supersaturated. Supersaturation is further divided into the higher labile region, which promotes spontaneous nucleation and the lower metastable region, which is closer to the saturation limit and therefore growth of existing nuclei may occur, whereas nucleation is impossible (but these conditions will permit crystal growth). When a solution is supersaturated, the thermodynamics of the system drive the exclusion of solute molecules from the solution, resulting in the net accumulation of the solid state. The control of this process leads to formation of crystals from the solute. It must be noted that the nucleation of protein crystals generally requires a high degree of super saturation (2-10 times that of saturation) [269]. Indeed, too high saturation is likely to cause random precipitation.

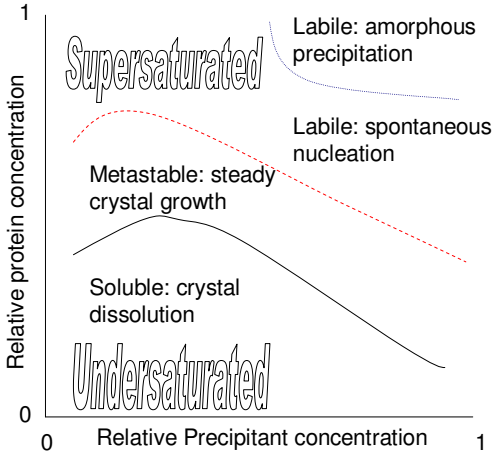

Figure 1. 10. Solubility phase diagram used for the crystallisation of proteins, shown here as a function of precipitant concentration. Adapted from [263].

1.6.2 Protein crystallisation techniques

Small scale protein crystal production methods include slow vapour diffusion of the solvent over a miniature reservoir (hanging and sitting drop method), direct mixing of protein solution with a strong precipitant (batch method) and dialysis of the protein-electrolyte solution [270]. Supersaturation of the system can also be achieved by changing the temperature of the solution [271, 272]. Despite the necessity for supersaturated conditions for protein crystal growth, growing conditions must be carefully monitored to prevent rampant growth and resultant defects in the crystals. Metastable supersaturated conditions are often employed with the view to avoid this unwanted outcome. In this process, crystal seeds are used as nuclei, which then promote further growth. Homogeneous methods employ crystal seeds of the same protein (usually spontaneous nucleation in a bulk fluid) and heterogeneous techniques whereby seeds of a different nature are used (typically crystals of another protein bearing structural similarities to the one being grown).

In practice, a well studied example in the field of protein crystal drug delivery is insulin. Amorphous insulin formulations are by and large fast acting, but insulin crystals can be formulated and fine-tuned to display slow and medium release properties. Slow-acting insulin formulations are usually crystallised with Zn^{2+} [273]. Variations in the experimental conditions (i.e. amount of co-precipitated zinc, temperature, pH, and

addition of protamine) have led to many formulations of varying action profiles [273]. Importantly, bovine and porcine insulin formulations have been shown to display different action properties, compared to human insulin [274]. *In vivo*, the crystalline forms of insulin have proved efficient in allowing prolonged therapeutic action following delivery. However, *in vitro*, crystalline suspensions of insulin were found to be only two times more stable than amorphous insulin (small therapeutic molecules typically achieve an order of magnitude higher stability) [275].

1.6.3 Drug Nanocrystals as therapeutic agents

Drug delivery systems based on crystallisation approaches are becoming increasingly popular. In one such example, Pechenov *et al*. [276], developed and characterised injectable controlled release systems comprising α-amylase crystals. Their findings indicated that protein crystals could be incorporated into *in situ* formable gels with changes in crystal morphology allowing modulation of the protein release profiles. In another such study by Kraft and co-workers [277], the authors evaluated nanobudesonide (nanocrystal budesonide) for nebulisation in patients with steroid-responsive pulmonary disease. The crystals (75-300 nm size range) were found to possess more favourable release properties than the traditionally prepared formulations (Pulmicort Respules). Ostrander *et al*. [278] compared the effectiveness of a concentrated NanoCrystal™ colloidal dispersion of beclomethasone dipropionate (mean particle size of 164 nm) with commercialised Vanceril and demonstrated a greater potential for drug delivery to the conductive airways of the lung in both quantity as well as percent of emitted dose. Moschwitzer *et al*. [279] developed hydrocortisone acetate nanocrystals using a high pressure homogenisation technique. Evaluation of crystal size by Photon Correlation Spectroscopy (PCS) revealed an average size of 716 nm ± 64 nm and *in vitro* dissolution tests showed improved drug release for pellets containing the drug nanocrystals. Govardhan *et al*. [280], produced nanocrystals of human growth hormone coated with a monomolecular layer of positively charged poly(arginine), which the authors claimed produced a highly efficient means of extending the half-life of therapeutic proteins.

Crystal formation has also proved a successful method for the delivery of vaccines. The progress towards subunit vaccines has been limited by their poor immunogenicity and limited stability. To enhance the immune response, subunit vaccines require improved adjuvants and delivery vehicles [281]. A crystalline vaccine formulation of human serum albumin showed a 10-fold increase in antibody titer for highly cross-linked crystals and a 30-fold increase for lightly-cross-linked crystals [281]. In another study by Murdan *et al*. [282], diphtheria toxoid was crystallised to form protein-coated micro-crystals to improve the thermal stability of the vaccine. The diphtheria toxoid was crystallised in the presence of L-glutamine and produced crystals in the region of 10 µm. The crystalline formulation produced was shown not to result in any change in antibody response to the toxoid.

Promising crystal drug candidates are those that have sufficient physical robustness outside of their crystallisation buffer. Alas, this is seldom the case, with fragile protein crystals 'melting' or dissolving when removed from their supersaturated crystallisation medium. Furthermore, crystals often lose their stability through mechanical processing e.g. by stirring, shaking or pipetting. To an extent, this can be remedied either by cross-linking fragile forms of protein crystals with reversible cross-linking agents [283, 284] or by co-precipitation of the protein with biocompatible multivalent ions like Zn^{2+} [273]. The former strategy becomes a subject of investigation in the final chapter of this thesis.

1.7 Conclusion

Research into non-invasive protein delivery has continued to evolve over the past decade, although extensive research and development is still needed to produce strategies which are feasible for commercialisation. The universal aim of mucosal delivery strategies involves the design of formulations (likely to be based on multi-component systems) that exhibit no toxicity upon repeated administration, preserve the biological function of the therapeutic molecule, achieving adequate bioavailability, with acceptable production costs and can be tailored to a range of protein drugs. Commonly visited strategies so far have included the use of absorption enhancers,

mucoadhesive excipients and attempts to exploit epithelial transcytotic mechanisms, with or without the use of drug delivery systems based on nanoparticulate carriers. Novel approaches in tackling the mucosal barrier for drug delivery purposes continue to provide hope that in the not too distant future, non-invasive administration of protein drugs will be an option for the patient.

1.8 Project Preview

This chapter has reviewed the current situation in the field of non-invasive delivery of protein therapeutics, discussing some of the challenges and pitfalls faced by researchers. The work presented in this thesis is predominantly based on investigating the potential of the vitamin B_{12} biological transport pathway for the mucosal delivery of nanoparticles as biotherapeutic carriers. Work initially focuses on assessing the suitability of Caco-2 cells, as a commonly used model of the intestinal mucosa, as a system to study the vitamin B_{12} transport pathway. The synthesis and characterisation of the α-ω-aminohexylcarbamate derivative of B_{12}, together with its attachment to carboxy functionalised synthetic polymer nanoparticles (50-200 nm scale) will be described. This is followed by investigation of the intracellular trafficking and transport behaviour of these nanoparticles in Caco-2 (as well as airway Calu-3 cells), which is the central aim of the thesis. The final chapter describes the design and characterisation of 'stabilised' micro- and nano- crystals, which show promise for the development of a suitable oral delivery platform for protein bioactives.

1.9 References

1. PhRMA, *PhRMA Annual Member Survey*. 2011, The Pharmaceutical Research and Manufacturers of America: Washington, U.S.
2. PhRMA, *Biotechnology Medicines in Development*, in *Medicines in Development*. 2011, The Pharmaceutical Research and Manufacturers of America: Washington, U.S.
3. Saffran, M., et al., *Insulin and the gastrointestinal tract.* J Control Release, 1997. **46**(1-2): p. 89-98.
4. Saffran, M., et al., *A new approach to the oral administration of insulin and other peptide drugs.* Science, 1986. **233**(4768): p. 1081-4.
5. Fix, J.A., *Oral controlled release technology for peptides: status and future prospects.* Pharm Res, 1996. **13**(12): p. 1760-4.
6. Mahato, R.I., et al., *Emerging trends in oral delivery of peptide and protein drugs.* Crit Rev Ther Drug Carrier Syst, 2003. **20**(2-3): p. 153-214.
7. Laham, R.J., et al., *Local perivascular delivery of basic fibroblast growth factor in patients undergoing coronary bypass surgery: results of a phase I randomized, double-blind, placebo-controlled trial.* Circulation, 1999. **100**(18): p. 1865-71.
8. Cleland, J.L., et al., *Development of poly-(D,L-lactide--coglycolide) microsphere formulations containing recombinant human vascular endothelial growth factor to promote local angiogenesis.* J Control Release, 2001. **72**(1-3): p. 13-24.
9. Kirker-Head, C.A., *Potential applications and delivery strategies for bone morphogenetic proteins.* Adv Drug Deliv Rev, 2000. **43**(1): p. 65-92.
10. Moeller, E.H. and L. Jorgensen, *Alternative routes of administration for systemic delivery of protein pharmaceuticals.* Drug Discovery Today: Technologies, 2008. **5, No. 2–3**
11. Vllasaliu, D., *In Vitro Investigation into Strategies for Mucosal Delivery of Proteins*, in *Pharmacy*. 2010, University of Nottingham.
12. Peppas, N.A. and D.A. Carr, *Impact of Absorption and Transport on Intelligent Therapeutics and Nano-scale Delivery of Protein Therapeutic Agents.* Chem Eng Sci, 2009. **64**(22): p. 4553-4565.
13. Guggi, D., A.H. Krauland, and A. Bernkop-Schnurch, *Systemic peptide delivery via the stomach: in vivo evaluation of an oral dosage form for salmon calcitonin.* J Control Release, 2003. **92**(1-2): p. 125-35.
14. Perakslis, E., A. Tuesca, and A. Lowman, *Complexation hydrogels for oral protein delivery: an in vitro assessment of the insulin transport-enhancing effects following dissolution in simulated digestive fluids.* J Biomater Sci Polym Ed, 2007. **18**(12): p. 1475-90.
15. Illum, L., *Transport of drugs from the nasal cavity to the central nervous system.* Eur J Pharm Sci, 2000. **11**(1): p. 1-18.
16. Stolnik, S. and K. Shakesheff, *Formulations for delivery of therapeutic proteins.* Biotechnol Lett, 2009. **31**(1): p. 1-11.
17. Soltero, R. and N. Ekwuribe, *Oral delivery of protein and peptide drugs.* Innovations in Pharmaceutical technology, 2001. **1**: p.106-110
18. Diabetology. *Capsulin™ OAD (oral anti-diabetic)* [cited 24/01/2012]; Available from: http://www.diabetology.co.uk/capsulinoad.htm.
19. Itoh, H., M. Nishino, and H. Hatabu, *Architecture of the lung: morphology and function.* J Thorac Imaging, 2004. **19**(4): p. 221-7.
20. Weibel, E.R. and D.M. Gomez, *Architecture of the human lung. Use of quantitative methods establishes fundamental relations between size and number of lung structures.* Science, 1962. **137**(3530): p. 577-85.
21. Martin, J. *Pulmonary Ventilation*. McGill Molson Medical Informatics 2008 [cited 2012 27/01/2012]; Available from: http://alexandria.healthlibrary.ca/documents/notes/bom/unit_2/L-16%20Pulmonary%20Ventilation.xml.
22. Owens, D.R., B. Zinman, and G. Bolli, *Alternative routes of insulin delivery.* Diabet Med, 2003. **20**(11): p. 886-98.

23. Jose, S. *Global pulmonary drug delivery technologies market is projected to reach US$37.7 Billion by 2015, According to New Report by Global Industry Analysts*. 2010 [cited 2012 27/1/2012].
24. Smola, M., T. Vandamme, and A. Sokolowski, *Nanocarriers as pulmonary drug delivery systems to treat and to diagnose respiratory and non respiratory diseases.* Int J Nanomedicine, 2008. **3**(1): p. 1-19.
25. Cawley, M. *Pulmonary Drug Delivery: An Update for the Respiratory Care Practitioner* 2011 [cited 27/01/2012].
26. Turker, S., E. Onur, and Y. Ozer, *Nasal route and drug delivery systems.* Pharm World Sci, 2004. **26**(3): p. 137-42.
27. Ugwoke, M.I., N. Verbeke, and R. Kinget, *The biopharmaceutical aspects of nasal mucoadhesive drug delivery.* J Pharm Pharmacol, 2001. **53**(1): p. 3-21.
28. Kissel, T. and U. Werner, *Nasal delivery of peptides: an in vitro cell culture model for the investigation of transport and metabolism in human nasal epithelium.* J Control Release, 1998. **53**(1-3): p. 195-203.
29. Arora, P., S. Sharma, and S. Garg, *Permeability issues in nasal drug delivery.* Drug Discov Today, 2002. **7**(18): p. 967-75.
30. Nicolazzo, J.A., B.L. Reed, and B.C. Finnin, *Buccal penetration enhancers--how do they really work?* J Control Release, 2005. **105**(1-2): p. 1-15.
31. Uchida, T., et al., *Rectal Delivery of Insulin Using a Bioadhesive Hydrogel Preparation Containing Lauric Acid as an Enhancer in Rats.* Pharmacy and Pharmacology Communications, 1999. **5**: p. 523-527.
32. Richardson, J.L., L. Illum, and N.W. Thomas, *Vaginal absorption of insulin in the rat: effect of penetration enhancers on insulin uptake and mucosal histology.* Pharm Res, 1992. **9**(7): p. 878-83.
33. Harris, D., J. Liaw, and J.R. Robinson, *Routes of delivery: Case studies: (7) Ocular delivery of peptide and protein drugs.* Advanced Drug Delivery Reviews, 1992. **8**(2-3): p. 331-339.
34. Sinha, V.R. and A. Trehan, *Biodegradable microspheres for protein delivery.* J Control Release, 2003. **90**(3): p. 261-80.
35. Tuma, P.L. and A.L. Hubbard, *Transcytosis: crossing cellular barriers.* Physiol Rev, 2003. **83**(3): p. 871-932.
36. Mostov, K., T. Su, and M. ter Beest, *Polarized epithelial membrane traffic: conservation and plasticity.* Nat Cell Biol, 2003. **5**(4): p. 287-93.
37. Mrsny, R.J., *Lessons from nature: "Pathogen-Mimetic" systems for mucosal nano-medicines.* Adv Drug Deliv Rev, 2009. **61**(2): p. 172-92.
38. Merkus, F.W., et al., *Nasal mucociliary clearance as a factor in nasal drug delivery.* Adv Drug Deliv Rev, 1998. **29**(1-2): p. 13-38.
39. Park, K., I.C. Kwon, and K. Park, *Oral protein delivery: Current status and future prospect.* Reactive & Functional Polymers, 2011. **71**: p. 280-287.
40. Anderson, J.M. and C.M. Van Itallie, *Tight junctions and the molecular basis for regulation of paracellular permeability.* Am J Physiol, 1995. **269**(4 Pt 1): p. G467-75.
41. Madara, J.L., *Loosening tight junctions. Lessons from the intestine.* J Clin Invest, 1989. **83**(4): p. 1089-94.
42. Godfrey, R.W., *Human airway epithelial tight junctions.* Microsc Res Tech, 1997. **38**(5): p. 488-99.
43. Stevenson, B.R. and B.H. Keon, *The tight junction: morphology to molecules.* Annu Rev Cell Dev Biol, 1998. **14**: p. 89-109.
44. Tsukita, S., M. Furuse, and M. Itoh, *Multifunctional strands in tight junctions.* Nat Rev Mol Cell Biol, 2001. **2**(4): p. 285-93.
45. Gonzalez-Mariscal, L., et al., *Tight junction proteins.* Prog Biophys Mol Biol, 2003. **81**(1): p. 1-44.
46. Claude, P., *Morphological factors influencing transepithelial permeability: a model for the resistance of the zonula occludens.* J Membr Biol, 1978. **39**(2-3): p. 219-32.
47. Madara, J.L. and K. Dharmsathaphorn, *Occluding junction structure-function relationships in a cultured epithelial monolayer.* J Cell Biol, 1985. **101**(6): p. 2124-33.

48. Ma, T.Y., et al., *Mechanism of extracellular calcium regulation of intestinal epithelial tight junction permeability: role of cytoskeletal involvement.* Microsc Res Tech, 2000. **51**(2): p. 156-68.
49. Vllasaliu, D., et al., *Barrier characteristics of epithelial cultures modelling the airway and intestinal mucosa: a comparison.* Biochem Biophys Res Commun. **415**(4): p. 579-85.
50. Chen-Quay, S.C., et al., *Identification of tight junction modulating lipids.* J Pharm Sci, 2009. **98**(2): p. 606-19.
51. Martin-Padura, I., et al., *Junctional adhesion molecule, a novel member of the immunoglobulin superfamily that distributes at intercellular junctions and modulates monocyte transmigration.* J Cell Biol, 1998. **142**(1): p. 117-27.
52. Madara, J.L., *Regulation of the movement of solutes across tight junctions.* Annu Rev Physiol, 1998. **60**: p. 143-59.
53. Rubas, W., et al., *Flux measurements across Caco-2 monolayers may predict transport in human large intestinal tissue.* J Pharm Sci, 1996. **85**(2): p. 165-9.
54. Jung, T., et al., *Biodegradable nanoparticles for oral delivery of peptides: is there a role for polymers to affect mucosal uptake?* Eur J Pharm Biopharm, 2000. **50**(1): p. 147-60.
55. Sanderson, I.R. and W.A. Walker, *Uptake and transport of macromolecules by the intestine: possible role in clinical disorders (an update).* Gastroenterology, 1993. **104**(2): p. 622-39.
56. Gebert, A., H.J. Rothkotter, and R. Pabst, *M cells in Peyer's patches of the intestine.* Int Rev Cytol, 1996. **167**: p. 91-159.
57. Jani, P., et al., *The uptake and translocation of latex nanospheres and microspheres after oral administration to rats.* J Pharm Pharmacol, 1989. **41**(12): p. 809-12.
58. Matthews, D.M., *Intestinal absorption of peptides.* Physiol Rev, 1975. **55**(4): p. 537-608.
59. Gardner, M.L., *Intestinal assimilation of intact peptides and proteins from the diet--a neglected field?* Biol Rev Camb Philos Soc, 1984. **59**(3): p. 289-331.
60. Lee, V.H. and A. Yamamoto, *Penetration and enzymatic barriers to peptide and protein absorption.* Advanced Drug Delivery Reviews, 1989. **4**(2): p. 171–207.
61. Matthews, D.M. and J.W. Payne, *Transmembrane transport of small peptides.* Curr. Top. Membr. Transport. , 1980. **14**: p. 331-425.
62. Bansil, R. and B.S. Turner, *Mucin structure, aggregation, physiological functions and biomedical applications.* Current Opinion in Colloid & Interface Science, 2006. **11**: p. 164-170.
63. Thornton, D.J. and J.K. Sheehan, *From mucins to mucus: toward a more coherent understanding of this essential barrier.* Proc Am Thorac Soc, 2004. **1**(1): p. 54-61.
64. Lafitte, G., K. Thuresson, and O. Soderman, *Mixtures of mucin and oppositely charged surfactant aggregates with varying charge density. Phase behavior, association, and dynamics.* Langmuir, 2005. **21**(16): p. 7097-104.
65. Albanese, C.T., et al., *Role of intestinal mucus in transepithelial passage of bacteria across the intact ileum in vitro.* Surgery, 1994. **116**(1): p. 76-82.
66. Khanvilkar, K., M.D. Donovan, and D.R. Flanagan, *Drug transfer through mucus.* Adv Drug Deliv Rev, 2001. **48**(2-3): p. 173-93.
67. Cu, Y. and W.M. Saltzman, *Drug delivery: Stealth particles give mucus the slip.* Nat Mater, 2009. **8**(1): p. 11-3.
68. Saltzman, W.M., et al., *Antibody diffusion in human cervical mucus.* Biophys J, 1994. **66**(2 Pt 1): p. 508-15.
69. Lai, S.K., et al., *Rapid transport of large polymeric nanoparticles in fresh undiluted human mucus.* Proc Natl Acad Sci U S A, 2007. **104**(5): p. 1482-7.
70. Braeckmans, K., et al., *Three-dimensional fluorescence recovery after photobleaching with the confocal scanning laser microscope.* Biophys J, 2003. **85**(4): p. 2240-52.
71. Olmsted, S.S., et al., *Diffusion of macromolecules and virus-like particles in human cervical mucus.* Biophys J, 2001. **81**(4): p. 1930-7.

72. Wang, Y.Y., et al., *Addressing the PEG mucoadhesivity paradox to engineer nanoparticles that "slip" through the human mucus barrier.* Angew Chem Int Ed Engl, 2008. **47**(50): p. 9726-9.
73. Cu, Y. and W.M. Saltzman, *Controlled surface modification with poly(ethylene)glycol enhances diffusion of PLGA nanoparticles in human cervical mucus.* Mol Pharm, 2009. **6**(1): p. 173-81.
74. Bernkop-Schnurch, A., et al., *Thiomers: potential excipients for non-invasive peptide delivery systems.* Eur J Pharm Biopharm, 2004. **58**(2): p. 253-63.
75. Leitner, V.M., D. Guggi, and A. Bernkop-Schnurch, *Thiomers in noninvasive polypeptide delivery: in vitro and in vivo characterization of a polycarbophil-cysteine/glutathione gel formulation for human growth hormone.* J Pharm Sci, 2004. **93**(7): p. 1682-91.
76. Ahsan, F., et al., *Enhanced bioavailability of calcitonin formulated with alkylglycosides following nasal and ocular administration in rats.* Pharm Res, 2001. **18**(12): p. 1742-6.
77. Arnold, J., et al., *Nasal administration of low molecular weight heparin.* J Pharm Sci, 2002. **91**(7): p. 1707-14.
78. Arnold, J.J., et al., *Correlation of tetradecylmaltoside induced increases in nasal peptide drug delivery with morphological changes in nasal epithelial cells.* J Pharm Sci, 2004. **93**(9): p. 2205-13.
79. Casettari, L., et al., *Effect of PEGylation on the Toxicity and Permeability Enhancement of Chitosan.* Biomacromolecules, 2010. **11**(11): p. 2854-2865
80. Vllasaliu, D., et al., *Tight junction modulation by chitosan nanoparticles: comparison with chitosan solution.* Int J Pharm. **400**(1-2): p. 183-93.
81. Takatsuka, S., et al., *Absorption enhancement of poorly absorbed hydrophilic compounds from various mucosal sites by combination of mucolytic agent and non-ionic surfactant.* Int J Pharm, 2007. **338**(1-2): p. 87-93.
82. Matsuyama, T., et al., *Influence of fillers in powder formulations containing N-acetyl-L-cysteine on nasal peptide absorption.* J Control Release, 2007. **120**(1-2): p. 88-94.
83. Matsuyama, T., et al., *Improved nasal absorption of salmon calcitonin by powdery formulation with N-acetyl-L-cysteine as a mucolytic agent.* J Control Release, 2006. **115**(2): p. 183-8.
84. Bernkop-Schnurch, A., C. Valenta, and S.M. Daee, *Peroral polypeptide delivery. A comparative in vitro study of mucolytic agents.* Arzneimittelforschung, 1999. **49**(9): p. 799-803.
85. Bernkop-Schnurch, A., H. Zarti, and G.F. Walker, *Thiolation of polycarbophil enhances its inhibition of intestinal brush border membrane bound aminopeptidase N.* J Pharm Sci, 2001. **90**(11): p. 1907-14.
86. Bernkop-Schnurch, A., *The use of inhibitory agents to overcome the enzymatic barrier to perorally administered therapeutic peptides and proteins.* J Control Release, 1998. **52**(1-2): p. 1-16.
87. Loftsson, T. and M.E. Brewster, *Pharmaceutical applications of cyclodextrins. 1. Drug solubilization and stabilization.* J Pharm Sci, 1996. **85**(10): p. 1017-25.
88. Anderberg, E.K., C. Nystrom, and P. Artursson, *Epithelial transport of drugs in cell culture. VII: Effects of pharmaceutical surfactant excipients and bile acids on transepithelial permeability in monolayers of human intestinal epithelial (Caco-2) cells.* J Pharm Sci, 1992. **81**(9): p. 879-87.
89. Fix, J.A., et al., *Acylcarnitines: drug absorption-enhancing agents in the gastrointestinal tract.* Am J Physiol, 1986. **251**(3 Pt 1): p. G332-40.
90. Hochman, J.H., J.A. Fix, and E.L. LeCluyse, *In vitro and in vivo analysis of the mechanism of absorption enhancement by palmitoylcarnitine.* J Pharmacol Exp Ther, 1994. **269**(2): p. 813-22.
91. Swenson, E.S., W.B. Milisen, and W. Curatolo, *Intestinal permeability enhancement: structure-activity and structure-toxicity relationships for nonylphenoxypolyoxyethylene surfactant permeability enhancers.* Pharm Res, 1994. **11**(10): p. 1501-4.
92. Duizer, E., et al., *Absorption enhancement, structural changes in tight junctions and cytotoxicity caused by palmitoyl carnitine in Caco-2 and IEC-18 cells.* J Pharmacol Exp Ther, 1998. **287**(1): p. 395-402.

93. Braga, P.C., et al., *Topical tolerability of salmon calcitonin assessed by mucociliary transport velocity investigation.* Arzneimittelforschung, 1990. **40**(8): p. 938-41.
94. Dodane, V. and V.D. Vilivalam, *Pharmaceutical applications of chitosan.* Pharmaceutical Science and Technology Today 1998. **1**: p. 246–253.
95. Muzzarelli, R.A.A., *Chitosan-based dietary foods.* Carbohydrate Polymers, 1996. **29**: p. 309-316.
96. Kotze´, A.F., et al., *Chitosans for enhanced delivery of therapeutic peptides across intestinal epithelia: in vitro evaluation in Caco-2 cell monolayers.* Int. J. Pharmaceutics, 1997. **159**: p. 243-253.
97. Luessen, H.L., et al., *Mucoadhesive polymers in peroral peptide drug delivery. VI. Carbomer and chitosan improve the intestinal absorption of the peptide drug buserelin in vivo.* Pharm Res, 1996. **13**(11): p. 1668-72.
98. Zhang, Y.J., et al., *Permeation-enhancing effects of chitosan formulations on recombinant hirudin-2 by nasal delivery in vitro and in vivo.* Acta Pharmacol Sin, 2005. **26**(11): p. 1402-8.
99. Sinswat, P. and P. Tengamnuay, *Enhancing effect of chitosan on nasal absorption of salmon calcitonin in rats: comparison with hydroxypropyl- and dimethyl-beta-cyclodextrins.* Int J Pharm, 2003. **257**(1-2): p. 15-22.
100. van der Lubben, I.M., et al., *Chitosan and its derivatives in mucosal drug and vaccine delivery.* Eur J Pharm Sci, 2001. **14**(3): p. 201-7.
101. Citi, S., *Protein kinase inhibitors prevent junction dissociation induced by low extracellular calcium in MDCK epithelial cells.* J Cell Biol, 1992. **117**(1): p. 169-78.
102. Cereijido, M., et al., *Polarized monolayers formed by epithelial cells on a permeable and translucent support.* J Cell Biol, 1978. **77**(3): p. 853-80.
103. Martinez-Palomo, A., et al., *Experimental modulation of occluding junctions in a cultured transporting epithelium.* J Cell Biol, 1980. **87**(3 Pt 1): p. 736-45.
104. Tomita, M., M. Hayashi, and S. Awazu, *Absorption-enhancing mechanism of sodium caprate and decanoylcarnitine in Caco-2 cells.* J Pharmacol Exp Ther, 1995. **272**(2): p. 739-43.
105. Raiman, J., et al., *Effects of various absorption enhancers on transport of clodronate through Caco-2 cells.* Int J Pharm, 2003. **261**(1-2): p. 129-36.
106. Vllasaliu, D., et al., *Evaluation of calcium depletion as a strategy for enhancement of mucosal absorption of macromolecules.* Biochem Biophys Res Commun. **418**(1): p. 128-33.
107. B. Dutzar, L.C., and S.C. Chen. *siRNA knockdown of claudin expression inhibits tight junction formation and induces loss of differentiation in respiratory epithelia*. in *The 2004 AAPS National Biotechnology Conference*. 2003. Boston, U.S.A. Abstract.
108. Lee, J.W., J.H. Park, and J.R. Robinson, *Bioadhesive-based dosage forms: the next generation.* J Pharm Sci, 2000. **89**(7): p. 850-66.
109. Longer, M.A., H.S. Ch'ng, and J.R. Robinson, *Bioadhesive polymers as platforms for oral controlled drug delivery III: oral delivery of chlorothiazide using a bioadhesive polymer.* J Pharm Sci, 1985. **74**(4): p. 406-11.
110. Jiménez-castellanos, M.R., Z. Hussein, and C.T. Rhodes, *Mucoadhesive Drug Delivery Systems.* Drug Dev. Ind. Pharm., 1993. **19** p. 143-194.
111. Junginger, H.E., *Bioadhesive Polymer Systems for Peptide Delivery.* Acta Pharm. Technol, 1990. **36**: p. 110-126.
112. Woodley, J., *Bioadhesion: new possibilities for drug administration?* Clin Pharmacokinet, 2001. **40**(2): p. 77-84.
113. Bernkop-Schnurch, A. and G. Walker, *Multifunctional matrices for oral peptide delivery.* Crit Rev Ther Drug Carrier Syst, 2001. **18**(5): p. 459-501.
114. Jones, D.S., A.D. Woolfson, and A.F. Brown, *Viscoelastic properties of bioadhesive, chlorhexidine-containing semi-solids for topical application to the oropharynx.* Pharm Res, 1998. **15**(7): p. 1131-6.
115. Chourasia, M.K. and S.K. Jain, *Pharmaceutical approaches to colon targeted drug delivery systems.* J Pharm Pharm Sci, 2003. **6**(1): p. 33-66.

116. Bredenberg, S. and C. Nystrom, *In-vitro evaluation of bioadhesion in particulate systems and possible improvement using interactive mixtures.* J Pharm Pharmacol, 2003. **55**(2): p. 169-77.
117. Smart, J.D., *The basics and underlying mechanisms of mucoadhesion.* Adv Drug Deliv Rev, 2005. **57**(11): p. 1556-68.
118. Sigurdsson, H.H., T. Loftsson, and C.M. Lehr, *Assessment of mucoadhesion by a resonant mirror biosensor.* Int J Pharm, 2006. **325**(1-2): p. 75-81.
119. ATUMA, C., *Gastrointestinal Mucosal Protective Mechanisms: Mudolatory Effects of Heliobacter pyroli on the Gastric Mucus Gel Barrier and Mucosal Blood Flow in vivo*, in *Faculty of medicine*. 2000, Acta Universitatis Upsaliensis.: Uppsala. p. 60.
120. Shojaei, A.H., *Buccal mucosa as a route for systemic drug delivery: a review.* J Pharm Pharm Sci, 1998. **1**(1): p. 15-30.
121. Mortazavi, S.A. and J.D. Smart, *An In Vitro Method for Assessing the Duration of Mucoadhesion* J. Controlled Release, 1994. **31**: p. 207–212.
122. Hu, M. and X. Li, *Oral Bioavailability: Basic Principles, Advanced Concepts, and Applications*. Drug Discovery and development, ed. B. Wang. 2011, Canada: Wiley & Sons.
123. Drummond, D.C., et al., *Optimizing liposomes for delivery of chemotherapeutic agents to solid tumors.* Pharmacol Rev, 1999. **51**(4): p. 691-743.
124. Yokoyama, M., et al., *Preparation of micelle-forming polymer-drug conjugates.* Bioconjug Chem, 1992. **3**(4): p. 295-301.
125. Wiedmann, T.S. and L. Kamel, *Examination of the solubilization of drugs by bile salt micelles.* J Pharm Sci, 2002. **91**(8): p. 1743-64.
126. Kataoka, K., et al., *Block copolymer micelles as vehicles for drug delivery.* J. Controlled Release, 1993. **24**: p. 119-132.
127. Francis, M.F., M. Cristea, and F.M. Winnik, *Polymeric micelles for oral drug delivery: Why and how*.* Pure Appl. Chem., 2004. **76**(7-8): p. 1321–1335.
128. Yokoyama, M., et al., *Characterization and anticancer activity of the micelle-forming polymeric anticancer drug adriamycin-conjugated poly(ethylene glycol)-poly(aspartic acid) block copolymer.* Cancer Res, 1990. **50**(6): p. 1693-700.
129. Lee, V.H. and A. Yamamoto, *Penetration and enzymatic barriers to peptide and protein absorption.* Advanced Drug Delivery Reviews, 1990. **4**(2): p. 171–207.
130. Torchilin, V.P., *Structure and design of polymeric surfactant-based drug delivery systems.* J Control Release, 2001. **73**(2-3): p. 137-72.
131. Florence, A.T. and N. Hussain, *Transcytosis of nanoparticle and dendrimer delivery systems: evolving vistas.* Adv Drug Deliv Rev, 2001. **50 Suppl 1**: p. S69-89.
132. Sharma, A. and U.S. Sharma, *Liposomes in drug delivery: progress and limitations.* Int. J. Pharmaceutics, 1997. **154**: p. 123-140.
133. Okada, J., S. Cohen, and R. Langer, *In vitro evaluation of polymerized liposomes as an oral drug delivery system.* Pharm Res, 1995. **12**: p. 576-582.
134. Deshmukh, D.S., W.D. Bear, and H. Brockerhoff, *Can intact liposomes be absorbed in the gut?* Life Sci., 1980. **28**: p. 239-242.
135. Toorisaka, E., et al., *Hypoglycemic effect of surfactant-coated insulin solubilized in a novel solid-in-oil-in-water (S/O/W) emulsion.* Int J Pharm, 2003. **252**(1-2): p. 271-4.
136. Itoh, K., et al., *Improvement of physicochemical properties of N-4472. Part II: characterization of N-4472 microemulsion and the enhanced oral absorption.* Int J Pharm, 2002. **246**(1-2): p. 75-83.
137. Uchida, M., et al., *Involvement of nitric oxide from nerves on diarrhea induced by castor oil in rats.* Jpn J Pharmacol, 2000. **82**(2): p. 168-70.
138. Couvreur, P. and F. Puisieux, *Nano- and microparti- cles for the delivery of polypeptides and proteins.* Adv. Drug Del. Rev, 1993. **10**: p. 141-162.
139. Sakuma, S., M. Hayashi, and M. Akashi, *Design of nanoparticles composed of graft copolymers for oral peptide delivery.* Adv Drug Deliv Rev, 2001. **47**(1): p. 21-37.

140. Damge, C., et al., *New approach for oral administration of insulin with polyalkylcyanoacrylate nanocapsules as drug carrier.* Diabetes, 1988. **37**(2): p. 246-51.
141. Sai, P., et al., *Prophylactic oral administration of metabolically active insulin entrapped in isobutylcyanoacrylate nanocapsules reduces the incidence of diabetes in nonobese diabetic mice.* J Autoimmun, 1996. **9**(6): p. 713-22.
142. Edman, P., B. Ekman, and I. Sjoholm, *Immobilization of proteins in microspheres of biodegradable polyacryldextran.* J Pharm Sci, 1980. **69**(7): p. 838-42.
143. Andrianov, A.K. and L.G. Payne, *Polymeric carriers for oral uptake of microparticulates.* Adv Drug Deliv Rev, 1998. **34**(2-3): p. 155-170.
144. Kukan, M., et al., *Disposition of lypophilized (methylmethacrylate-14C, 2-hydroxyethylmethacrylate, butylacrylate) nanoparticles in rats and their effect on zoxazolamine paralysis time.* Pharmazie, 1991. **46**(1): p. 37-9.
145. Kreuter, J., *Peroral administration of nanoparticles.* Adv. Drug Del. Rev., 1991. **7**: p. 71-86.
146. Fasano, A., *Innovative strategies for the oral delivery of drugs and peptides.* Trends Biotechnol, 1998. **16**(4): p. 152-7.
147. Gershanik, T. and S. Benita, *Self-dispersing lipid formulations for improving oral absorption of lipophilic drugs.* Eur J Pharm. Biopharm, 2000. **50**: p. 179-188.
148. Leuner, C. and J. Dressman, *Improving drug solubility for oral delivery using solid dispersions.* Eur J Pharm Biopharm, 2000. **50**(1): p. 47-60.
149. Vasir, J.K., K. Tambwekar, and S. Garg, *Bioadhesive microspheres as a controlled drug delivery system.* Int. J. Pharmaceutics, 2003. **255**: p. 13-32.
150. Vyas, S.P., A. Singh, and V. Sihorkar, *Ligand-receptor-mediated drug delivery: an emerging paradigm in cellular drug targeting.* Crit Rev Ther Drug Carrier Syst, 2001. **18**(1): p. 1-76.
151. Le Roy, C. and J.L. Wrana, *Clathrin- and non-clathrin-mediated endocytic regulation of cell signalling.* Nat Rev Mol Cell Biol, 2005. **6**(2): p. 112-26.
152. Mayor, S. and R.E. Pagano, *Pathways of clathrin-independent endocytosis.* Nat Rev Mol Cell Biol, 2007. **8**(8): p. 603-12.
153. Marsh, M. and A. Helenius, *Virus entry: open sesame.* Cell, 2006. **124**(4): p. 729-40.
154. Benmerah, A. and C. Lamaze, *Clathrin-coated pits: vive la difference?* Traffic, 2007. **8**(8): p. 970-82.
155. Rappoport, J.Z., S.M. Simon, and A. Benmerah, *Understanding living clathrin-coated pits.* Traffic, 2004. **5**(5): p. 327-37.
156. Ford, M.G., et al., *Curvature of clathrin-coated pits driven by epsin.* Nature, 2002. **419**(6905): p. 361-6.
157. Ford, M.G., et al., *Simultaneous binding of PtdIns(4,5)P2 and clathrin by AP180 in the nucleation of clathrin lattices on membranes.* Science, 2001. **291**(5506): p. 1051-5.
158. Beck, K.A. and J.H. Keen, *Interaction of phosphoinositide cycle intermediates with the plasma membrane-associated clathrin assembly protein AP-2.* J Biol Chem, 1991. **266**(7): p. 4442-7.
159. Zoncu, R., et al., *Loss of endocytic clathrin-coated pits upon acute depletion of phosphatidylinositol 4,5-bisphosphate.* Proc Natl Acad Sci U S A, 2007. **104**(10): p. 3793-8.
160. Rappoport, J.Z., *Focusing on clathrin-mediated endocytosis.* Biochem J, 2008. **412**(3): p. 415-23.
161. Takei, K., et al., *Tubular membrane invaginations coated by dynamin rings are induced by GTP-gamma S in nerve terminals.* Nature, 1995. **374**(6518): p. 186-90.
162. Gumbleton, M., A.G. Abulrob, and L. Campbell, *Caveolae: an alternative membrane transport compartment.* Pharm Res, 2000. **17**(9): p. 1035-48.
163. Rothberg, K.G., et al., *Caveolin, a protein component of caveolae membrane coats.* Cell, 1992. **68**(4): p. 673-82.

164. Rodrigues, G.J., et al., *Caveolae dysfunction contributes to impaired relaxation induced by nitric oxide donor in aorta from renal hypertensive rats.* J Pharmacol Exp Ther, 2007. **323**(3): p. 831-7.
165. Schnitzer, J.E., et al., *Filipin-sensitive caveolae-mediated transport in endothelium: reduced transcytosis, scavenger endocytosis, and capillary permeability of select macromolecules.* J Cell Biol, 1994. **127**(5): p. 1217-32.
166. Bathori, G., L. Cervenak, and I. Karadi, *Caveolae--an alternative endocytotic pathway for targeted drug delivery.* Crit Rev Ther Drug Carrier Syst, 2004. **21**(2): p. 67-95.
167. Harush-Frenkel, O., et al., *Surface charge of nanoparticles determines their endocytic and transcytotic pathway in polarized MDCK cells.* Biomacromolecules, 2008. **9**(2): p. 435-43.
168. von Bonsdorff, C.H., S.D. Fuller, and K. Simons, *Apical and basolateral endocytosis in Madin-Darby canine kidney (MDCK) cells grown on nitrocellulose filters.* EMBO J, 1985. **4**(11): p. 2781-92.
169. Naim, H.Y., et al., *Apical and basolateral coated pits of MDCK cells differ in their rates of maturation into coated vesicles, but not in the ability to distinguish between mutant hemagglutinin proteins with different internalization signals.* J Cell Biol, 1995. **129**(5): p. 1241-50.
170. Bomsel, M., et al., *Endocytosis in filter-grown Madin-Darby canine kidney cells.* J Cell Biol, 1989. **109**(6 Pt 2): p. 3243-58.
171. Apodaca, G., *Endocytic traffic in polarized epithelial cells: role of the actin and microtubule cytoskeleton.* Traffic, 2001. **2**(3): p. 149-59.
172. Eker, P., et al., *Selective regulation of apical endocytosis in polarized Madin-Darby canine kidney cells by mastoparan and cAMP.* J Biol Chem, 1994. **269**(28): p. 18607-15.
173. Bucci, C., et al., *Rab5a is a common component of the apical and basolateral endocytic machinery in polarized epithelial cells.* Proc Natl Acad Sci U S A, 1994. **91**(11): p. 5061-5.
174. Leung, S.M., W.G. Ruiz, and G. Apodaca, *Sorting of membrane and fluid at the apical pole of polarized Madin-Darby canine kidney cells.* Mol Biol Cell, 2000. **11**(6): p. 2131-50.
175. Morphis, L.G. and D. Gitlin, *Maturation of the maternofoetal transport system for human gamma-globulin in the mouse.* Nature, 1970. **228**(5271): p. 573.
176. Brambell, F.W., *The transmission of immunity from mother to young and the catabolism of immunoglobulins.* Lancet, 1966. **2**(7473): p. 1087-93.
177. Dickinson, B.L., et al., *Bidirectional FcRn-dependent IgG transport in a polarized human intestinal epithelial cell line.* J Clin Invest, 1999. **104**(7): p. 903-11.
178. Simister, N.E. and A.R. Rees, *Isolation and characterization of an Fc receptor from neonatal rat small intestine.* Eur J Immunol, 1985. **15**(7): p. 733-8.
179. Simister, N.E. and K.E. Mostov, *An Fc receptor structurally related to MHC class I antigens.* Nature, 1989. **337**(6203): p. 184-7.
180. Rojas, R. and G. Apodaca, *Immunoglobulin transport across polarized epithelial cells.* Nat Rev Mol Cell Biol, 2002. **3**(12): p. 944-55.
181. Spiekermann, G.M., et al., *Receptor-mediated immunoglobulin G transport across mucosal barriers in adult life: functional expression of FcRn in the mammalian lung.* J Exp Med, 2002. **196**(3): p. 303-10.
182. Israel, E.J., et al., *Expression of the neonatal Fc receptor, FcRn, on human intestinal epithelial cells.* Immunology, 1997. **92**(1): p. 69-74.
183. Bitonti, A.J., et al., *Pulmonary delivery of an erythropoietin Fc fusion protein in non-human primates through an immunoglobulin transport pathway.* Proc Natl Acad Sci U S A, 2004. **101**(26): p. 9763-8.
184. Low, S.C., et al., *Oral and pulmonary delivery of FSH-Fc fusion proteins via neonatal Fc receptor-mediated transcytosis.* Hum Reprod, 2005. **20**(7): p. 1805-13.
185. Bitonti, A.J. and J.A. Dumont, *Pulmonary administration of therapeutic proteins using an immunoglobulin transport pathway.* Adv Drug Deliv Rev, 2006. **58**(9-10): p. 1106-18.

186. Vllasaliu, D., et al., *Fc-mediated transport of nanoparticles across airway epithelial cell layers.* J Control Release, 2012. **158**(3): p. 479-86.
187. Lu, Y. and P.S. Low, *Folate-mediated delivery of macromolecular anticancer therapeutic agents.* Adv Drug Deliv Rev, 2002. **54**(5): p. 675-93.
188. Nakashima-Matsushita, N., et al., *Selective expression of folate receptor beta and its possible role in methotrexate transport in synovial macrophages from patients with rheumatoid arthritis.* Arthritis Rheum, 1999. **42**(8): p. 1609-16.
189. Turk, M.J., et al., *Folate-targeted imaging of activated macrophages in rats with adjuvant-induced arthritis.* Arthritis Rheum, 2002. **46**(7): p. 1947-55.
190. Antony, A.C., *The biological chemistry of folate receptors.* Blood, 1992. **79**(11): p. 2807-20.
191. Gruner, B.A. and S.D. Weitman, *The folate receptor as a potential therapeutic anticancer target.* Invest New Drugs, 1998. **16**(3): p. 205-19.
192. Hilgenbrink, A.R. and P.S. Low, *Folate receptor-mediated drug targeting: from therapeutics to diagnostics.* J Pharm Sci, 2005. **94**(10): p. 2135-46.
193. Kamen, B.A. and A. Capdevila, *Receptor-mediated folate accumulation is regulated by the cellular folate content.* Proc Natl Acad Sci U S A, 1986. **83**(16): p. 5983-7.
194. Antony, A.C., et al., *Studies of the role of a particulate folate-binding protein in the uptake of 5-methyltetrahydrofolate by cultured human KB cells.* J Biol Chem, 1985. **260**(28): p. 14911-7.
195. Leamon, C.P. and P.S. Low, *Delivery of macromolecules into living cells: a method that exploits folate receptor endocytosis.* Proc Natl Acad Sci U S A, 1991. **88**(13): p. 5572-6.
196. Wileman, T., C. Harding, and P. Stahl, *Receptor-mediated endocytosis.* Biochem J, 1985. **232**(1): p. 1-14.
197. Lee, R.J., S. Wang, and P.S. Low, *Measurement of endosome pH following folate receptor-mediated endocytosis.* Biochim Biophys Acta, 1996. **1312**(3): p. 237-42.
198. Turek, J.J., C.P. Leamon, and P.S. Low, *Endocytosis of folate-protein conjugates: ultrastructural localization in KB cells.* J Cell Sci, 1993. **106 (Pt 1)**: p. 423-30.
199. Rothberg, K.G., et al., *Cholesterol controls the clustering of the glycophospholipid-anchored membrane receptor for 5-methyltetrahydrofolate.* J Cell Biol, 1990. **111**(6 Pt 2): p. 2931-8.
200. Mayor, S., K.G. Rothberg, and F.R. Maxfield, *Sequestration of GPI-anchored proteins in caveolae triggered by cross-linking.* Science, 1994. **264**(5167): p. 1948-51.
201. Rothberg, K.G., et al., *The glycophospholipid-linked folate receptor internalizes folate without entering the clathrin-coated pit endocytic pathway.* J Cell Biol, 1990. **110**(3): p. 637-49.
202. Wu, M., et al., *Clustering of GPI-anchored folate receptor independent of both cross-linking and association with caveolin.* J Membr Biol, 1997. **159**(2): p. 137-47.
203. Varma, R. and S. Mayor, *GPI-anchored proteins are organized in submicron domains at the cell surface.* Nature, 1998. **394**(6695): p. 798-801.
204. Moradi, E., et al., *Ligand density and clustering effects on endocytosis of folate modified nanoparticles.* RSC Adv., 2012. **2**: p. 3025-3033.
205. Clardy, S.M., et al., *Vitamin B12 in drug delivery: breaking through the barriers to a B12 bioconjugate pharmaceutical.* Expert Opin Drug Deliv. **8**(1): p. 127-40.
206. Markle, H.V., *Cobalamin.* Critical Reviews in Clinical Laboratory Sciences, 1996. **33**(4): p. 247-356.
207. Banerjee, R., C. Gherasim, and D. Padovani, *The tinker, tailor, soldier in intracellular B12 trafficking.* Curr Opin Chem Biol, 2009. **13**(4): p. 484-91.
208. Banerjee, R., *Intrinsic factor, haptocorrin and their receptors*. Chemistry and biochemistry of B12, ed. D. Alpers and G. Russell-Jones. 1999, New York: John Wiley & Sons. 411-440.

209. Banerjee, R., ed. *Chemistry and biochemistry of B12*. Transcobalamin II., ed. S. Rothenberg, E. Quadros, and A. Regec. 1999, John Wiley & Sons: New York. 441-473.
210. Randaccio, L., et al., *Vitamin B12: unique metalorganic compounds and the most complex vitamins.* Molecules. **15**(5): p. 3228-59.
211. Bristol, U.o. [cited; Available from: http://www.chm.bris.ac.uk/motm/vitaminb12/structure.html.
212. Wilson, S., Reinhard, K.S., Gao, X., *Drug delivery and targeting with vitamin B12 conjugates*. 2007, New York University: United States.
213. Weir, D.G. and J.M. Scott, *Cobalamins Physiology, Dietary Sources and Requirements*, in *Encyclopedia of human nutrition*, S.M.J.a.C. B., Editor. 1999. p. 394-401.
214. Shils, M.E., Olson J.A, Shike M., & Ross A.C. , ed. *Modern Nutrition in Health and Disease*. 1999, Williams and Wilkins: Baltimore, USA.
215. Coudroy, G., et al., *Contribution of cubilin and amnionless to processing and membrane targeting of cubilin-amnionless complex.* J Am Soc Nephrol, 2005. **16**(8): p. 2330-7.
216. Morkbak, A.L., J.F. Pedersen, and E. Nexo, *Glycosylation independent measurement of the cobalamin binding protein haptocorrin.* Clin Chim Acta, 2005. **356**(1-2): p. 184-90.
217. Andersen, C.B., et al., *Structural basis for receptor recognition of vitamin-B(12)-intrinsic factor complexes.* Nature. **464**(7287): p. 445-8.
218. Okuda, K., *Discovery of Vitamin B12 in the liver and its absorption factor in the stomach: A historical review.* J Gastroenterol Hepatol., 1999. **14**: p. 301-308.
219. Andres E, L.N., Noel E, Kaltenbach G, Ben Abdelgheni M, Perrin AE, Noblet-Dick M, Maloisel F, Schlienger JL, Blickle JF *Vitamin B12 (cobalamin) deficiency in elderly patients.* CMAJ, 2004. **171**: p. 251-259.
220. Seetharam, B., *Receptor-mediated endocytosis of Cobalamin (Vitamin B12).* Annu. Rev. Nutr, 1999. **19**: p. 173-195.
221. Carkeet, C., et al., *Human vitamin B12 absorption measurement by accelerator mass spectrometry using specifically labeled (14)C-cobalamin.* Proc Natl Acad Sci U S A, 2006. **103**(15): p. 5694-9.
222. Pravda, J., *Crohn's disease: evidence for involvement of unregulated transcytosis in disease etio-pathogenesis.* World J Gastroenterol. 2011. **17**(11): p. 1416-26.
223. Allen, T.M. and P.R. Cullis, *Drug delivery systems: entering the mainstream.* Science, 2004. **303**(5665): p. 1818-22.
224. Jin, S. and K. Ye, *Nanoparticle-mediated drug delivery and gene therapy.* Biotechnol Prog, 2007. **23**(1): p. 32-41.
225. Brigger, I., C. Dubernet, and P. Couvreur, *Nanoparticles in cancer therapy and diagnosis.* Adv Drug Deliv Rev, 2002. **54**(5): p. 631-51.
226. Otsuka, H., Y. Nagasaki, and K. Kataoka, *PEGylated nanoparticles for biological and pharmaceutical applications.* Adv Drug Deliv Rev, 2003. **55**(3): p. 403-19.
227. Blume, G. and G. Cevc, *Liposomes for the sustained drug release in vivo.* Biochim Biophys Acta, 1990. **1029**(1): p. 91-7.
228. Cuenca, A.G., et al., *Emerging implications of nanotechnology on cancer diagnostics and therapeutics.* Cancer, 2006. **107**(3): p. 459-66.
229. Galindo-Rodriguez, S.A., Allemann, E, Fessi, H, and Doelker, E., *Polymeric nanoparticles for oral delivery of drugs and vaccines: a critical evaluation of in vivo studies.* Crit. Rev. Ther. Drug Carr. Syst., 2005. **22**: p. 419-464.
230. Lowe, P.G., and Temple, C.S, , *Calcitonin and insulin in isobutylcyanoacrylate nanocapsules: protection against proteases and effect on intestinal absorption in rats.* J. Pharm. Pharmacol. , 1994. **46**: p. 547-552.
231. Mathiowitz, E., Jacob, J.S, Jong, Y.S, Carino, G.P, Chickering, D.E, Chaturvedi, P, Santos, C.A, Vijayaraghavan, K, Montgomery, S, Bassett, M and Morrell, C., *Biologically erodable microspheres as potential oral delivery systems.* Nature, 1997. **386**: p. 410-414.

232. Tobio, M., Gref, R., Sanchez, A., Langer, R., Alonso, M.J., *Stealth PLA-PEG nanoparticles as protein carriers for nasal administration.* Pharm. Res., 1998. **15**: p. 270-275.
233. Blanco, M.D., et al., *5-Fluorouracil-loaded microspheres prepared by spray-drying poly(D,L-lactide) and poly(lactide-co-glycolide) polymers: characterization and drug release.* J Microencapsul, 2005. **22**(6): p. 671-82.
234. Kilic, A.C., et al., *Preparation and characterization of PLGA nanospheres for the targeted delivery of NR2B-specific antisense oligonucleotides to the NMDA receptors in the brain.* J Microencapsul, 2005. **22**(6): p. 633-41.
235. Olivier, J.C., *Drug transport to brain with targeted nanoparticles.* NeuroRx, 2005. **2**(1): p. 108-19.
236. Eley, J.G., V.D. Pujari, and J. McLane, *Poly (lactide-co-glycolide) nanoparticles containing coumarin-6 for suppository delivery: in vitro release profile and in vivo tissue distribution.* Drug Deliv, 2004. **11**(4): p. 255-61.
237. Panyam, J., et al., *Rapid endo-lysosomal escape of poly(DL-lactide-co-glycolide) nanoparticles: implications for drug and gene delivery.* FASEB J, 2002. **16**(10): p. 1217-26.
238. Lupi, A., et al., *Biodegradable microspheres for prolidase delivery to human cultured fibroblasts.* J Pharm Pharmacol, 2004. **56**(5): p. 597-603.
239. Panyam, J. and V. Labhasetwar, *Biodegradable nanoparticles for drug and gene delivery to cells and tissue.* Adv Drug Deliv Rev, 2003. **55**(3): p. 329-47.
240. Jain, R.A., *The manufacturing techniques of various drug loaded biodegradable poly(lactide-co-glycolide) (PLGA) devices.* Biomaterials, 2000. **21**(23): p. 2475-90.
241. Labhasetwar, V., *Nanotechnology for drug and gene therapy: the importance of understanding molecular mechanisms of delivery.* Curr Opin Biotechnol, 2005. **16**(6): p. 674-80.
242. Sahoo, S.K., W. Ma, and V. Labhasetwar, *Efficacy of transferrin-conjugated paclitaxel-loaded nanoparticles in a murine model of prostate cancer.* Int J Cancer, 2004. **112**(2): p. 335-40.
243. Kirpotin, D.B., et al., *Antibody targeting of long-circulating lipidic nanoparticles does not increase tumor localization but does increase internalization in animal models.* Cancer Res, 2006. **66**(13): p. 6732-40.
244. Hattori, Y., M. Sakaguchi, and Y. Maitani, *Folate-linked lipid-based nanoparticles deliver a NFkappaB decoy into activated murine macrophage-like RAW264.7 cells.* Biol Pharm Bull, 2006. **29**(7): p. 1516-20.
245. Hattori, Y. and Y. Maitani, *Enhanced in vitro DNA transfection efficiency by novel folate-linked nanoparticles in human prostate cancer and oral cancer.* J Control Release, 2004. **97**(1): p. 173-83.
246. Shiku, H., et al., *Development of a cancer vaccine: peptides, proteins, and DNA.* Cancer Chemother Pharmacol, 2000. **46 Suppl**: p. S77-82.
247. Jani, P., Halbert, G.W., Langridge, J., Florence, A.T., *Nanoparticle uptake by the rat gastrointestinal mucosa: quantitation and particle size dependency. .* J. Pharm. Pharmacol., 1990. **42**: p. 821-826.
248. Lavelle, E.C., Sharif, S., Thomas, N.W., Holland, J., Davis, S.S, *The importance of gastrointestinal uptake of particles in the design of oral delivery systems.* Adv Drug Deliv Rev, 1995. **18**: p. 5-22.
249. O'Hagan, D.T., *Intestinal translocation of particulates - implications for drug and antigen delivery.* Adv Drug Deliv Rev, 1990. **5**: p. 265-285.
250. Brayden, D.J., Jepson, M.A., Baird, A.W., *Keynote review: intestinal Peyer's patch M cells and oral vaccine targeting.* Drug Discov. Today, 2005. **10**: p. 1145-1157.
251. Clark, M.A., Blair, H., Liang, L., Brey, R.N., Brayden, D., Hirst, B.H., *Targeting polymerised liposome vaccine carriers to intestinal M cells.* Vaccine, 2001. **20**: p. 208-217.
252. des Rieux, A., Fievez, V, Garinot, M, Schneider, Y-J, and Preat, V., *Nanoparticles as potential oral delivery systems of proteins and vaccines: A mechanistic approach.* Journal of Controlled Release, 2006. **116**: p. 1-27.
253. des Rieux, A., Ragnarsson, E.G.E., Gullberg, E., Preat, V., Schneider, Y.J., Artursson, P., *Transport of nanoparticles across an in vitro model of the*

human intestinal follicle associated epithelium. Eur. J. Pharm. Sci., 2005. **25**: p. 455-465.
254. Jung, T., Kamm, W., Breitenbach, A., Kaiserling, E., Xiao, J.X., Kissel, T., *Biodegradable nanoparticles for oral delivery of peptides: is there a role for polymers to affect mucosal uptake?* Eur. J. Pharm. Biopharm. , 2000. **50**: p. 147-160.
255. Florence, A.T., *Nanoparticle uptake by the oral route: fulfilling its potential?* Drug. Discov. Today. Technol. , 2005. **2**: p. 75-81.
256. Sagnella, S. and K. Mai-Ngam, *Chitosan based surfactant polymers designed to improve blood compatibility on biomaterials.* Colloids and Surfaces B-Biointerfaces, 2005. **42**(2): p. 147-155.
257. Amiji, M.M., *Synthesis of anionic poly(ethylene glycol) derivative for chitosan surface modification in blood-contacting applications.* Carbohydrate Polymers, 1997. **32**(3-4): p. 193-199.
258. Lehr, C.M., *Bioadhesion technologies for the delivery of peptide and protein drugs to the gastrointestinal tract.* Crit Rev Ther Drug Carrier Syst, 1994. **11**(2-3): p. 119-60.
259. Kilpatrick, D.C., et al., *Tomato lectin resists digestion in the mammalian alimentary canal and binds to intestinal villi without deleterious effects.* FEBS Lett, 1985. **185**(2): p. 299-305.
260. Russell-Jones, G.J., H. Veitch, and L. Arthur, *Lectin-mediated transport of nanoparticles across Caco-2 and OK cells.* Int J Pharm, 1999. **190**(2): p. 165-74.
261. Hussain, N., P.U. Jani, and A.T. Florence, *Enhanced oral uptake of tomato lectin-conjugated nanoparticles in the rat.* Pharm Res, 1997. **14**(5): p. 613-8.
262. Lehr, C.M., et al., *Bioadhesion by means of specific binding of tomato lectin.* Pharm Res, 1992. **9**(4): p. 547-53.
263. Jen, A. and H.P. Merkle, *Diamonds in the rough: protein crystals from a formulation perspective.* Pharm Res, 2001. **18**(11): p. 1483-8.
264. Drenth, J. and C. Hass, *Protein crystals and their stability.* J. Crystal growth, 1992. **122**: p. 107-109.
265. McPherson, A., *Crystallisation of Biological Macromolecules*. 1999, Cold Spring Harbor: Cold Spring Harbour Laboratory Press.
266. Frey, M., *Water structure associated with proteins and its role in crystallization.* Acta Crystallogr D Biol Crystallogr, 1994. **50**(Pt 4): p. 663-6.
267. Feigelson, R.S., *The relevance of small molecule crystal growth theories and techniques to the growth of biological macromolecules.* J. Crystal growth, 1988. **90**: p. 1-13.
268. Wiencek, J.M., *New strategies for protein crystal growth.* Annu Rev Biomed Eng, 1999. **1**: p. 505-34.
269. Mikol, V. and R. Giege, *The physical chemistry of protein crystallization*. Crystallization of nucleic acids and proteins: a practical appraoch, ed. A. Ducruix and R. Giege. 1992, New York: Oxford University Press.
270. Ducruix, A. and R. Giege, *Methods of crystallization*. Crystallization of Nucleic Acids and Proteins: A practical Approach, ed. A. Ducruix and R. Giege. 1992, New York: Oxford University Press.
271. Luft, J.R., D.M. Rak, and D.G. DeTitta, *Microbatch macromolecular crystallization on a thermal gradient.* J. Crystal growth, 1999. **196**: p. 447-449.
272. Schall, C.A., et al., *Application of temperature control strategies to the growth of hen egg-white lysozyme crystals.* J. Crystal. Growth, 1996. **165**: p. 299-307.
273. Brange, J. and L. Langkjaer, *Insulin formulation and delivery.* Pharm Biotechnol, 1997. **10**: p. 343-409.
274. Hildebrandt, P., et al., *The subcutaneous absorption of human and bovine ultralente insulin formulations.* Diabet Med, 1985. **2**(5): p. 355-9.
275. Brange, J. and L. Langkjoer, *Insulin structure and stability.* Pharm Biotechnol, 1993. **5**: p. 315-50.
276. Pechenov, S., et al., *Injectable controlled release formulations incorporating protein crystals.* J Control Release, 2004. **96**(1): p. 149-58.
277. Kraft, W.K., et al., *The pharmacokinetics of nebulized nanocrystal budesonide suspension in healthy volunteers.* J. Clin. Pharmacol., 2004. **44**(1): p. 67-72.

278. Ostrander, K.D., H.W. Bosch, and D.M. Bondanza, *An in-vitro assessment of a NanoCrystal beclomethasone dipropionate colloidal dispersion via ultrasonic nebulization.* Eur J Pharm Biopharm, 1999. **48**(3): p. 207-15.
279. Moschwitzer, J. and R.H. Muller, *New method for the effective production of ultrafine drug nanocrystals.* J Nanosci Nanotechnol, 2006. **6**(9-10): p. 3145-53.
280. Govardhan, C., et al., *Novel long-acting crystal formulation of human growth hormone.* Pharm Res, 2005. **22**(9): p. 1461-70.
281. St Clair, N., et al., *Cross-linked protein crystals for vaccine delivery.* Proc Natl Acad Sci U S A, 1999. **96**(17): p. 9469-74.
282. Murdan, S., et al., *Immobilisation of vaccines onto micro-crystals for enhanced thermal stability.* Int J Pharm, 2005. **296**(1-2): p. 117-21.
283. Govardhan, C.P., *Crosslinking of enzymes for improved stability and performance.* Curr Opin Biotechnol, 1999. **10**(4): p. 331-5.
284. Ayala, M., et al., *Cross-linked crystals of chloroperoxidase.* Biochem Biophys Res Commun, 2002. **295**(4): p. 828-31.

Chapter 2: Materials and general methods

2.1 Materials

2.1.1 Cells, culture media, media components and cell solutions

Caco-2 and NIH 3T3 cells were obtained from the European Collection of Cell Cultures (ECACC) and used at passages 45-60 and 35-50, respectively. Calu-3 were obtained from the American Type Culture Collection (ATCC) and used between passages 20-30. Essential Minimum Eagle's Medium (EMEM) medium, Dulbecco's Modified Eagles Medium (DMEM), Hanks Balanced Salt Solution (HBSS) with sodium bicarbonate and without phenol red, 2.5% Trypsin/EDTA solution, Antibiotic/Antimycotic solution (containing penicillin, streptomycin and amphotericin), L-glutamine, sodium pyruvate and Foetal Bovine Serum (FBS, non-USA origin) were all obtained from Sigma-Aldrich (UK). Phosphate buffered saline (PBS) tablets were purchased from Oxoid (UK). Cell media (EMEM and DMEM) were supplemented with penicillin, streptomycin and amphotericin at final concentrations of 100 units/ml, 0.1 mg/ml and 0.25 µg/ml, respectively, and FBS at a final concentration of 10% v/v. For Caco-2 and NIH 3T3 cell culture, both EMEM and DMEM were further supplemented with L-glutamine and non-essential amino acids (NEAA, Fisher Scientific, UK). For Calu-3 culture, EMEM was also supplemented with sodium pyruvate (1mM) and L-glutamine. Hereafter, supplemented media are referred to as cell media, DMEM, or EMEM. Dimethylsulphoxide (DMSO, used as cryopreservant), 4-(2-hydroxyethyl)-1-piperazineethanesulfonic acid (HEPES), Hoechst 33342, 1,4-diazabicyclo[2.2.2]octane (DABCO) and 2 (NMorpholino)ethanesulfonic acid (MES) were all obtained from Sigma-Aldrich (UK).

2.1.2 Plasticware and glassware

Polystyrene transwell® permeable supports, referred to in this thesis as 'filters' or 'transwells', of 12 mm diameter, 0.4 µm pore size (with a surface area of 1.1 cm^2) were obtained from Corning Life Sciences (Holland). Cell culture flasks (75 cm^2,

canted neck with vented caps), 96-well polystyrene microplates (black or clear, non-cell culture treated) and sterile pipettes, used routinely for the maintenance of cells, were also purchased from Corning Life Sciences (Holland). Clear, tissue culture treated 96-well plates, black 96-well microplates (used for fluorescence measurement) and sterile cryovials (1 ml capacity) were supplied by Nunc. Sterile centrifuge tubes (of 15 ml and 50 ml volume capacity) were purchased from Greiner (USA) and sterile universals (5 ml and 30 ml volume capacity) were obtained from Sterilin (UK). Freezing container ('Mr Frosty'), providing a controlled cooling rate of 1°C per minute, was purchased from Nalgene® Labware (USA). Haemocytometer (Improved Neubauer, to British Standard 748) was purchased from Scientific Laboratory Supplies (SLS, UK).

2.1.3 Cell toxicity assay reagents

3-(4,5-dimethylthiazol-2-yl)-5(3-carboxymethonyphenol)-2-(4-sulfophenyl)-2H-tetrazolium-(MTS) reagent (commercially known as 'CellTiter 96 AQueous One Solution Cell Proliferation Assay') was purchased from Promega (UK). Lactate Dehydrogenase (LDH) assay kit (known commercially as '*In Vitro* Toxicology Assay Kit, TOX7') was purchased from Sigma-Aldrich (UK). The BCA protein assay kit was obtained from Novagen® (UK).

2.1.4 Antibodies

Mouse, anti-human Zonula Occludens-1 (ZO-1, TJ protein) was purchased from Zymed (part of Invitrogen, USA). Rabbit, anti-human lysosomal associated membrane protein 1 (LAMP1); goat, anti-mouse FITC-IgG and goat, anti-rabbit FITC-IgG were purchased from Sigma-Aldrich (UK). Rabbit, anti-human cubilin antibody (polyclonal IgG); rabbit, anti-human caveolin-1 (polyclonal IgG); rabbit, anti-human transcobalamin II (TCII); goat, anti-rabbit FITC-IgG and goat anti-rabbit rhodamine-IgG were purchased from Santa Cruz (USA). Alexa-fluor® 594 labelled goat anti-mouse antibody was purchased from Invitrogen.

2.1.5 Chemicals

FITC-labelled dextrans ('FDs') of approximate average MW of 4 kDa ('FD4'), 10 kDa ('FD10'), 20 kDa ('FD20'), 40 kDa ('FD40'), 70 kDa ('FD70') and 150 kDa ('FD150'), FITC-labelled insulin (FITC-insulin), ethylene diamine tetraacetic acid (EDTA), paraformaldehyde, osmium tetroxide, Triton X-100, Bovine Serum Albumin (BSA), glutaraldehyde and 1,4-Diazabicyclo-octane (DABCO, UV mountant) were all obtained from Sigma-Aldrich (UK). DAPI (4',6-diamidino-2-phenylindole) with antifade mounting media (commercially known as Slowfade-Gold®) and Lysotracker™ Green were obtained from Invitrogen. Fluorescent polystyrene carboxy-modified nanoparticles (YO, Fluoresbrite®) of 50, 100 and 200 nm nominal diameter were supplied by Polysciences Europe GmbH (Germany). Solid 1,1'-carbonyldiimidazole (CDI), anhydrous dimethyl sulfoxide, cyanocobalamin and N-hydroxy-succinimide (NHS) were purchased from Acros® (Belgium). 1,6-hexanediamine, ethyl acetate and acetone were obtained from Fisher Scientific (UK). 1-ethyl-3-[3-Dimethylaminopropyl]carbodiimide (EDAC) was purchased from Calbiochem (UK). Insulin from bovine pancreas was purchased from Sigma-Aldrich (UK). THPP (ß-[Tris(hydroxymethyl) phosphino] propionic acid (betaine) (THPP) was obtained from Fisher Scientific. All water was obtained from an ELGA purification system (resistivity 15 MV cm^{-3}, Maxima USF ELGA, UK). All other chemicals and materials unless otherwise stated, were purchased from Sigma-Aldrich (UK) or Fisher Scientific.

2.2 Methods

2.2.1 Maintenance of cells

2.2.1.1 Maintenance of cells in culture flasks

All cell lines were routinely cultured in 75 cm^2 flasks at 5% CO_2, 95% relative humidity and 37°C until confluence (in this work confluence was considered as approximately 75-95% coverage of the flask surface by cells). Cell culture medium was replaced every other day by aspirating the old culture media from the flasks, followed by the addition of 12-14 ml of fresh media, pre-warmed to 37°C. Cell growth was monitored

regularly by viewing the cells under an optical microscope. Once confluent, cells were passaged using the following procedure: culture medium was removed (aspirated) from the flask and cells washed with PBS (6 ml, pre-warmed to 37℃), which was added to the flask and the flask gently swirled. Fresh PBS was used to remove any dead cells remaining in the flask and traces of media; it was important to perform this step prior to the addition of trypsin/EDTA solution to cells since FBS present in the cell culture media inhibits the action of trypsin. PBS was then aspirated and replaced with 2.5-3 ml of pre-warmed (37℃) 2.5% trypsin/EDTA solution. The flask was gently swirled to ensure that trypsin/EDTA solution covered the cells and then transferred to the incubator at 37℃. The flask was observed at regular intervals for cell detachment from the tissue culture flask plastic. The period of incubation with trypsin/EDTA solution was dependent on the cell line and the extent of confluence. Generally, for NIH 3T3 and Caco-2 cells an incubation period of approximately 15 min was sufficient for complete cell detachment from the flask plastic. On the other hand, Calu-3 cells required no less than 20 min incubation with trypsin/EDTA for complete detachment. Following cell detachment, approximately 9 ml of pre-warmed (37℃) culture medium was added to the flasks in order to dilute the cell suspension and deactivate trypsin (different media were used for each cell line, as will be described later). The resulting cell suspension was transferred to a sterile centrifuge tube and the cells centrifuged (pelleted) at 13,000 rpm for 5 min. Trypsin-containing supernatant was aspirated and pre-warmed culture medium (37℃, 5-10 ml) added to the cell pellet to create a cell suspension. A proportion of the resulting cell suspension was transferred to a new flask (containing pre-warmed culture medium appropriate for the cell line) for further culturing. Split ratios between 1:3 and 1:5 were normally used for Calu-3 cells, while higher ratios between 1:6 and 1:10 were typically used for both NIH 3T3 and Caco-2 cells. Although both Caco-2 and Calu-3 cells were cultured in EMEM, media components were varied in order to achieve optimal cell growth in each respective cell line. Mouse NIH 3T3 fibroblasts were cultured in DMEM. Culture media were supplemented with various components as described above (section 2.1.1).

2.2.1.2 Frozen storage of cells

Cells were cultured to confluence and then detached from the flask as described previously (section 2.2.1.1). Following centrifugation of the cell suspension, the supernatant was aspirated, and the cell pellet re-suspended in 1 ml of complete culture medium containing sterile DMSO. The concentration of DMSO used was 5% v/v for Calu-3 and Caco-2 cells and 7.5% v/v for NIH 3T3 cells. The cell suspension was added to a sterile cryovial (clearly labelled with the cell type, passage number, user name and date), which was placed into a freezing container ('Mr Frosty') in a -80°C freezer for a gradual, controlled temperature decrease. Cells were stored at –80°C for up to 4 weeks. Thereafter, cells were transferred into a liquid nitrogen cell storage tank. Note that cells from a single confluent monolayer in one 75 cm^2 tissue culture flask were transferred and stored frozen in a single cryovial; multiple flasks of cells were routinely detached and transferred into the equivalent number or sterile cryovials for frozen storage.

2.2.1.3 Cell revival

Cryovials containing frozen cells were removed from the liquid nitrogen-containing storage tank and thawed by placing the cryovial in the incubator at 37°C for approximately 5 min. DMSO-containing medium was removed by transferring the cell suspension into a centrifuge tube containing approximately 8 ml of warm (37°C) culture medium, centrifuging the resulting suspension at 13,000 rpm for 5 min and aspirating the supernatant. The cell pellet was thereafter suspended in approximately 5 ml of culture medium and transferred into a 75 cm^2 flask containing approximately 10 ml of fresh, warmed (37°C) culture medium. Note that cells from one cryovial were revived and transferred into one tissue culture flask.

2.2.1.4 Culture of cells on transwells

2.2.1.4.1 Calu-3 cells

Calu-3 cells were cultured to confluence in 75 cm^2 flasks at 5% CO_2 and 37°C. Cells were then detached from the flasks using the method described above (2.2.1.1).

Transwell® filters were incubated with EMEM (250 µl and 1.5 ml on the apical and basolateral chambers, respectively) at 37°C for approximately 15 min prior to the addition of cells. This was performed in order to coat the surface of the filter plastic with proteins present in the culture medium (serum), to encourage cell attachment to plastic. It should be noted that polystyrene transwell® filters were used for all experiments in this thesis, as opposed to polycarbonate filters due to better attachment by cells. Cells were counted using a haemocytometer and the volume of the cell suspension containing the required number of cells was calculated. These volumes were subsequently added to the donor compartments of the transwells. The number of cells added ('seeding density') was 10^5 per 1.1 cm^2 of the Transwell® filter area. The apical chamber volume was made up to 500 µl by adding warmed EMEM. After seeding on filters, cells were maintained at 5% CO_2, 37°C with EMEM. Following initial seeding on filters, Calu-3 cells can be cultured in two different ways:, cells can either be continuously exposed to the culture medium on both apical and basolateral sides (0.5 ml and 1.5 ml, respectively), i.e. cells grown using liquid-covered culture (LCC); or cells can be cultured on transwells with medium (0.5 ml) present in the basolateral chamber only. The latter culture condition is known as air-interfaced culture (AIC). In this thesis, LCC conditions were employed for all experiments. Calu-3 cells were typically cultured on filters for 21 days prior to their use in experiments as confluent and polarised cell layers. Hereafter, the term ‘polarised’ is used to define fully differentiated, filter-cultured cell layers.

2.2.1.4.2 Caco-2 cells

Caco-2 cells were seeded on filters in a similar way to Calu-3 cells, except that a density of $2x10^5$ cells/cm^2 was used. Caco-2 cells were cultured using LCC conditions, with EMEM as the culture medium and were routinely grown on filters for 21-23 days (with culture medium replaced every other day) prior to their use in experiments as confluent, polarised cell monolayers.

2.2.2 Measurement of TEER

Transepithelial electrical resistance (TEER) is a convenient, reliable and non-destructive method to monitor the growth of epithelial tissue cultures *in vitro*, evaluate cell layer integrity and determine the presence and the tightness of the cellular tight junctions (TJs) [1]. Formally a measure of resistance to ion flux across an epithelial layer, it further enables the measurement of changes in paracellular ion flux linked to tight junctional disruption [2] and can also be employed as an indirect measure of cell toxicity [2, 3]. TEER can be conveniently measured using a portable ohmmeter (EVOM, World Precision Instruments), comprising a set of "chopstick" electrodes as illustrated in Figure 2.1. The chopstick electrodes were firstly pre-sterilised by immersing in absolute ethanol for approximately 30 min prior to their use. The electrodes were then washed with PBS and carefully placed in the culture medium bathing the cell layers; the shorter electrode was submerged in the medium present in the apical chamber, while the longer electrode was placed in the basal medium. The resulting readings were recorded and are expressed in this thesis as the mean of 5 separate measurements (unless otherwise stated) ± standard deviation.

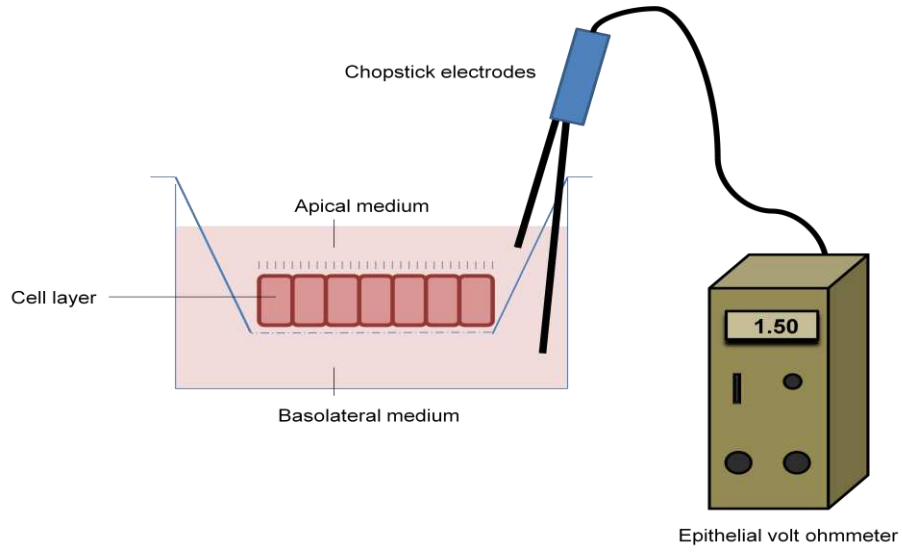

Figure 2. 1. Schematic representation of TEER measurement using an epithelial volt ohmmeter.

For simply monitoring cell growth, TEER was measured in the culture medium. TEER was measured following the incubation of cells with the culture medium on both sides

(apical and basolateral) after the cells were allowed to equilibrate for at least 30 min. Routinely, following TEER measurement, the culture medium was replaced to prevent any damage that may result from leakage of ions from the electrodes.

During the initial culture of Caco-2 and Calu-3 cells on filters, TEER was measured every other day, starting from day 5 to 21 of culture. This routine was continued until the TEER development profile was found to be reproducible. In order to prevent unnecessary damage to the cell layers during the measurement process (predominantly from leakage of ions from the electrodes), TEER was subsequently only measured prior to the use of cell layers in experiments in order to verify cell layer intactness and TJ formation. TEER values reported in this thesis take into account the area of the cell layer (assumed to amount to the area of the transwell® filter) and are expressed as $\Omega.cm^2$. In addition, electrical resistance across the cell-free transwell® filters (background resistance) was also measured on every batch of transwell® filters used in the experiments. This value typically ranged between 100 and 115 $\Omega.cm^2$ and was subtracted from the measured cell layer TEER in all experiments [4].

Only polarised cell layers exhibiting TEER of 500 $\Omega.cm^2$ (for Calu-3) and 800 $\Omega.cm^2$ (for Caco-2) or above were included in the cell uptake and transport experiments detailed in this thesis.

The experiments were conducted in HBSS in all cases, which was buffered at pH 6.0 (with 10 mM MES) or pH 7.4 (using 25 mM HEPES), depending on the nature of the sample applied. Prior to the application of test samples to cells, the culture medium was removed, cells washed with PBS and HBSS (warmed to 37°C; pH 7.4) added to both sides of the cell layers. Cells were equilibrated in HBSS (i.e. incubated at 37°C, 5% CO_2) for approximately 45 min, following which initial TEER measurements were conducted. After the 3 hour transport period, the test sample was removed from the apical chamber and following a repeated wash step with PBS (3 times), the HBSS was replaced on both the apical and basolateral sides, after which a final TEER

measurement was made to verify that cell layer integrity was maintained throughout the course of the experiment. In the case of application of a test compound (i.e. for toxicity assessment), HBSS was then removed from the apical side of the cell layers and replaced with the test samples (previously warmed to 37°C). Unless otherwise stated, cells were incubated with the samples for 3 hours, with TEER measurements made every 30 min following sample application in the presence of the tested samples in HBSS. The samples were removed from the cells 3 hours post-application and cells washed with PBS (3 times). Culture medium (appropriate for the cell line, see section 2.2.1.1) was then added to the cell layers and cells incubated with the culture medium overnight. In order to determine whether the effect of the tested samples on TEER was reversible, TEER was measured (in culture medium) 24 hours (the following day) after test sample application.

2.2.3 FITC-dextran (FD) permeability measurements

An alternative method to assess monolayer integrity is to study the transport of a hydrophilic marker molecule representative of a model drug that is passively transported through the cell layer, either transcellularly or paracellularly [4]. In these studies, fluorescein isothiocyanate (FITC)–labelled dextrans (FDs) of varying MWs were used as macromolecular markers, modelling hydrophilic, large MW protein drugs. The availability of FDs in different MWs and as fluorescently labelled (enabling a relatively simple quantification) makes these molecules highly appropriate for use in experiments investigating macromolecular permeability across epithelial cell layers. As detailed in the previous section, TEER measurements were conducted prior to the permeability experiments in order to ensure that the cell layers were confluent and intact. TEER was also assessed after the experiment to verify that the cell 'barrier' was maintained throughout the course of the permeability studies. As previously discussed, only cell layers exhibiting TEER ≥500 $\Omega.cm^2$ (Calu-3) and ≥ 800 $\Omega.cm^2$ (Caco-2) (i.e. 'confluent cell layers') were deemed suitable for FD permeability experiments. Unless otherwise indicated in subsequent chapters, permeability experiments were conducted as follows. Culture medium was removed from the cell

layers and cells washed with warm (37℃) PBS. Buffered HBSS (with 25mM HEPES, pH 7.4) was then added to the apical (0.5 ml) and basolateral (1.5 ml) chambers of the Transwell® system. Cells were incubated (at 37℃/5% CO_2) with HBSS for approximately 45 min for the purpose of equilibration. TEER was then measured in order to confirm the 'confluence' and the intactness of the cell layers, following which HBSS was removed from the apical side. FDs were dissolved in HBSS (500 µg/ml) and were then applied to the apical side of the cells (donor compartment of the transwells). FD permeability was determined by sampling (100 µl) the basolateral solution at regular time intervals (every 30 min over 3 hours). The sampled solutions were immediately replaced with an equivalent volume of the transport medium (HBSS). Between sampling times, cells were incubated at 37℃/5% CO_2. Sampled solutions were transferred into a black 96-well plate, which was then covered with aluminium foil to protect from light. Sample solution fluorescence (485 nm excitation, 535 nm emission) was then determined using an MFX microtiter plate fluorometer (Dynex Technologies, USA). Transported FD in the basolateral solutions was quantified by converting the fluorescence readings into FD concentrations and ultimately amounts, through construction of calibration curves. The fluorescence intensity of progressively diluted FD solutions of known FD concentrations was measured. At least three such calibration curves were established; the mean values were then calculated and used for FD quantification in each experiment. In this thesis, all FD permeability data is expressed as the apparent permeability coefficient (P_{app}), calculated using the following equation:

$$P_{app} = \left(\frac{\Delta Q}{\Delta t}\right) \times \left(\frac{1}{A \times C_0}\right)$$

Where:

- P_{app} is the apparent permeability in cm s^{-1}
- $\frac{\Delta Q}{\Delta t}$ is the permeability rate [amount FD (µg) traversing the cell layers over time (s)].

This was determined by plotting the amount of transported solute over time and

calculating the gradient of the straight-line (i.e. steady state) portion (typically transport over time points 30 min – 3 h) of the resulting curve (and conversion into seconds)

• A is the diffusion area of the layer (cm^2), and

• C_0 is the initial FD concentration (500 µg/ml)

2.2.4 Cell toxicity studies

2.2.4.1 Background information

The MTS assay uses a colorimetric method to determine the number of viable cells in proliferation or cytotoxicity assays. This method can be used to replace the classic ^{3}H-thymidine incorporation assay. The one solution assay system contains a novel tetrazolium compound 3-(4,5-dimethylthiazol-2-yl)-5-(3-carboxymethoxyphenyl)- 2-(4-sulfophenyl)-2Htetrazolium (inner salt), MTS, and an electron-coupling reagent, (phenazine ethosulfate, PES). PES combines with MTS and confers enhanced chemical stability and allows the formation of a stable solution. The principle of the assay is that the MTS tetrazolium compound is reduced in cells into a coloured formazan compound which is soluble in tissue culture media. This conversion occurs via the production of NADPH/NADH by dehydrogenase enzymes, present in metabolically active cells [5].

The Lactate dehydrogenase (LDH) assay (first described by Legrand *et al.* [1, 6]) is another cytotoxicity analysis that can be used alongside the MTS assay. Lactate dehydrogenase (LDH) is a soluble cytosolic enzyme that is released into the culture medium following loss of membrane integrity resulting from cell death. LDH activity, therefore, can be used as an indicator of cell membrane integrity and serves as a general means to assess both cell viability and cytotoxicity resulting from chemical compounds or environmental toxic factors [7]. The numerous commercially available kits measure LDH activity present in the culture medium using a coupled two-step reaction. In the first step, LDH catalyses the reduction of NAD^+ to NADH and H^+ by oxidation of lactate to pyruvate. In the second step of the reaction, diaphorase uses the newly-formed NADH and H^+ to catalyze the reduction of a tetrazolium salt (INT) to highly-coloured formazan which absorbs strongly at 490-520 nm. The relative

cytotoxicity caused by the test agent can be standardised against a series of controls (as described in Chapter 8).

2.2.4.2 MTS Cell metabolic activity assay

The MTS assay was performed on Caco-2 cells unless otherwise stated. In all experiments, cells were seeded on 96-well plates (sterile, cell culture treated) at a density of 10^4 cells per well and incubated at 37℃/5%CO_2 for 24 hours, unless otherwise stated. This seeding density was chosen (optimised), based on previous observations made within our group as it produced an absorbance value within the linear range of the assay, as recommended by the manufacturer. The culture medium was aspirated and replaced with test sample solutions (at different concentrations), dissolved in HBSS (at pH 7.4). Cells incubated with HBSS (at the same pH as the test samples) were used as the negative control, whereas cells incubated with Triton X-100 (0.2% v/v in HBSS at pH identical to that of the test samples) were used as the positive control. Samples were previously warmed and applied to cells at 37℃. Following the application of the samples, cells were incubated at 37℃/5%CO_2 for 2 hours. Sample solutions were then aspirated and cells washed with PBS. 100 µl of culture medium (at 37℃) was added onto each well, followed by 20 µl of the MTS reagent. Cells were incubated with the combined culture medium/MTS reagent for 2-3 hours, following which absorbance (492 nm) was measured using a Dynex absorbance microplate reader (Dynex Technologies, USA). The relative cell metabolic activity (%) was calculated using the following equation:

$$\text{Relative Metabolic Activity (\%)} = \frac{(\text{Abs}_\text{s} - \text{Abs}_\text{Tx})}{(\text{Abs}_\text{HBSS} - \text{Abs}_\text{Tx})}$$

Where:

- Abs_s is the absorbance with the tested samples
- Abs_{Tx} is the absorbance with Triton X-100
- Abs_{HBSS} is the absorbance with HBSS

2.2.4.3 LDH assay

The LDH assay was performed to test the membrane toxicity of different compounds on Caco-2 cells. Cells were seeded on 96-well plates (sterile, cell culture treated) at 10^4 cells per well and cultured for 24 hours (unless otherwise stated) before the assay. Culture medium was removed and cells washed with PBS. Test compounds of different concentrations dissolved in HBSS (pH 7.4, at 37℃) were then applied. Triton X-100 (0.2% v/v in HBSS) was used as the positive control (assuming it caused complete LDH release), whereas HBSS (pH 7.4) was used as the negative control. Cells were incubated with samples and controls for 2 hours, after which 50 µl of the solutions were removed from each well and transferred to a new 96-well plate. 100 µl of the LDH reagent was added to the samples and the plate was incubated at room temperature for 30 min. After this period, absorbance (490 nm) was measured using the Dynex absorbance microplate reader. LDH release was calculated as the percentage relative to the controls, using the following equation:

$$\text{Relative LDH release } (\%) = \frac{(\text{Abs}_\text{s} - \text{Abs}_\text{HBSS})}{(\text{Abs}_\text{Tx} - \text{Abs}_\text{HBSS})}$$

Where:

- Abs_s is the absorbance obtained with the tested samples
- Abs_HBSS is the absorbance with HBSS
- Abs_Tx is the absorbance with Triton X-100

2.2.5 Cell imaging and labelling

2.2.5.1 Scanning Electron Microscopy (SEM)

Filter-cultured confluent Caco-2 and Calu-3 cell layers were fixed by replacing the culture medium with 1:1 mixture of culture medium and fixing solution, which comprised 2.5% v/v glutaraldehyde in 0.1 M sodium cacodylate buffer (pH 7.2) on both apical and basolateral sides of the transwells. Following an incubation interval of

5 min, this solution was removed and replaced with 100% of the fixing solution on the apical side only and incubated for a further 30 min. The fixing solution was then removed and the cell samples washed three times with 0.1M phosphate/cacodylate buffer. The samples were then post-fixed and stained with 1% w/v osmium tetroxide in distilled water by incubation at room temperature for 60 min. Osmium tetroxide solution was then removed and samples dehydrated in a graded series of ethanol in water (5 x 1 min in distilled water; 2 x 5 min in 50% ethanol, 2 x 5 min in 70% ethanol, 2 x 5 min in 90% ethanol, 3 x 10 min in 100% ethanol). Samples were dried using a critical point dryer (CPD). This technique has been shown to give rise to significantly fewer dehydration artifacts compared with other dehydration methods. Following the CPD process, the samples were removed and mounted on aluminium stubs with adhesive double-sided carbon tape. The samples were gold coated for 3 minutes under an argon atmosphere in a Blazers Union SCD030 sputter coater unit (Blazers Ltd, UK). The CPD, mounting and coating of the samples was carried out by the Advanced Microscopy unit (School of Biomedical Sciences) at the University of Nottingham. Coated samples were examined with a JEOL 6060LV (JEOL, Welwyn, UK) variable pressure scanning electron microscope operating at an accelerating voltage of 10 kV. Image analysis was carried out using the in-built SEM control user interface software (version 6.57) and digital imaging system.

2.2.5.2 Transmission Electron Microscopy (TEM)

Filter-cultured confluent Caco-2 and Calu-3 layers were fixed with 4% paraformaldehyde and then washed with 0.1 M phosphate/cacodylate buffer. Cells were post fixed with 1% aqueous osmium tetroxide for 30 mins, followed by extensive washing (5x1 min) with distilled water. Samples were then dehydrated in a graded ethanol series by washing the cells for 5 min (twice) with 50% ethanol, followed by 70% ethanol, followed by 90% ethanol and then finally with 3x10 min washes with 100% ethanol. Finally, two 5 min washes were performed with 100% dried acetone. Cell samples were then infiltrated with resin for a duration of 30 minutes in 1:3 resin:acetone mix, 1 hour in 1:1 resin:acetone mix and 3x1 hour incubations in pure

resin. Samples were embedded in the resin and left in the embedding oven for 48 hours at 60°C. Once the resin block polymerised, the substrate was removed from the cells by immersing the block in liquid nitrogen and snapping the substrate from the block. The block was then embedded in a microcentrifuge tube containing fresh resin and was polymerised as before, enclosing the cell layer in a resin block. The layer was cut out of the block by sawing either side of it to give a disc of resin with the layer running through the middle. The disc was cut in half to form 2 semi-circles, which were stuck onto the top of a blank resin block (using Araldite® epoxy resin). The Araldite® was left to set for 1 hour. Ultrathin sections were cut using a cryoultramicrotome (Leica EM, UC6/FC6, Milton Keynes, UK) and viewed by TEM (Jeol JEM 1010 Electron Microscope, Japan). Note that the late stages of sample preparation for TEM were performed by the Advanced Microscopy Unit group, School of Biomedical Sciences, University of Nottingham.

2.2.5.3 Lysotracker™ staining and LAMP1 immunostaining

To enable the assessment of intracellular nanoparticle fate in filter-cultured cells, two complementary techniques were selected: the use of Lysotracker™ probe to identify active lysosomal compartments [8], and immunostaining for lysosomal associated membrane protein (LAMP1) - a heavily glycosylated lysosomal membrane protein, thought to play an important role in protecting the lysosomal membrane from proteolytic enzymes within the lysosomes [9, 10]. Because the protein is ubiquitously expressed, its antibody was used in this case to identify localised or clustered regions, likely to be representative of lysosomal structures. Caco-2 and Calu-3 cell layers were cultured in the manner described in section 2.2.1.4. Lysotracker™ Green DND-26 (Invitrogen) was diluted (according to the manufacturer's instructions) in HBSS and nanoparticles (unmodified and B_{12}-conjugated) were suspended in this solution to achieve a final incubation concentration of 250 µg/ml. The IF-B_{12}-nanoparticle complexes were prepared as described in Chapter 5. As detailed in section 2.2.2, TEER measurements were conducted prior to the nanoparticle trafficking experiments in order to ensure that the cells were confluent and the cell layer intact. As previously discussed, only cell layers exhibiting TEER ≥500 $\Omega.cm^2$ (Calu-3) and ≥ 800 $\Omega.cm^2$

(Caco-2) (i.e. 'confluent cell layers') were deemed suitable for these studies. Culture medium was removed from the cell layers and cells washed with warm (37℃) PBS. Buffered HBSS (with 25 mM HEPES, pH 7.4) was then added to the apical (0.5 ml) and basolateral (1.5 ml) chambers of the transwell® system. Cells were incubated (at 37℃/5% CO_2) with HBSS for approximately 45 min for the purpose of equilibration. The lysotracker-containing nanoparticle suspensions (0.5 ml) were applied to the apical side of the cell monolayers and incubated at 37˚C for 2 hrs. Following a series of wash steps with PBS and fixation with 4% paraformaldehyde (PFA), 300 µl of Hoechst dye solution (100 µg/ml) was added to the samples (for nuclei staining) and incubated at room temperature for 5 min. The Hoechst solution was then removed and the cells were washed 4 times with PBS. Transwell® filters (containing cells) were then excised and mounted (using DABCO mounting medium) on glass slides for confocal imaging. Cells were imaged using a Leica TCS SP2 system mounted on a Leica DMIRE2 inverted microscope.

Although imaging was conducted using a sequential scanning mode where cross emission between different fluorophores is minimised, a control set of experiments were conducted to verify that the imaged pattern did not result from fluorophore cross emission between the Lysotracker™ marker and fluorescent nanoparticles. In these experiments cells were treated with either the Lysotracker™ probe or the YO nanoparticles (Table 2.1), followed by imaging using the optimised sequential scan settings. Cell samples incubated with the Lysotracker™ probe were imaged using nanoparticle scan settings (529 nm/546 nm, ex/em) and cells treated with nanoparticles were visualised using Lysotracker™ settings (504 nm/511 nm).

Cell treatment with			
	Lysotracker™ Green DND-26 (Lysosomal marker)	**Unlabelled (non-fluorescent) 50 nm NPs**	**YO 50 nm NPs**
Experiment			
A. Scanning for Lysotracker™		+	+
B. Scanning for YO 50 nm NPs	+	+	
C. Scanning for Lysotracker™			+
D. Scanning for YO 50 nm NPs	+		
E. Scanning for Lysotracker™	+	+	

Table 2. 1. Experimental set-up for control Lysosomal studies using Lysotracker™ Green DND-26 (Exc. 504/ Em. 511 nm) with unmodified NPs (50 nm, Exc. 529/Em. 546 nm) in Caco-2 monolayers.

where '+' denotes 'present' in each sample. For experiments A-B, cells were incubated with either YO fluorescent NPs and unlabelled (non-fluorescent) particles or with the Lysotracker™ probe and unlabelled NPs. For experiments C-E, cells were incubated only with YO fluorescent NPs/unlabelled NPs or the Lysotracker™ probe.

For anti-LAMP 1 immunostaining studies, nanoparticles (unmodified and B_{12}-conjugated) were applied (in HEPES-buffered HBSS) to the apical side and the cells incubated at 37°C over 2 hrs. Following aspiration of the nanoparticle suspensions, the cells were fixed with 4% PFA. The cells were then permeabilised with 0.2% Triton X-100 over 10 min and after another wash step, incubated in PBS/1% BSA at 4°C for 1 hr before the addition of anti-LAMP1 (lysosomal associated membrane protein-1) antibody (Sigma-Aldrich, UK), diluted 1:50 in PBS/1% BSA for 30 min. The cells were washed with PBS and incubated with the secondary antibody (goat, anti-rabbit IgG-FITC, Sigma-Aldrich) diluted 1:100 (in 1% BSA/PBS) for another 30 min (whilst protecting from light). Staining for cell nuclei and confocal microscopy were conducted as described above.

2.2.5.4 Zonula Occludens (ZO-1) TJ staining

Confluent, filter-cultured cell layers (Caco-2 and Calu-3) were fixed in paraformaldehyde for approximately 10 min at room temperature. Cells were then washed with PBS and permeabilised by incubating with Triton X-100 (0.2% v/v in PBS) for approximately 10 min. Cells were then washed with PBS, followed by the application of 1% BSA/PBS for approximately 1 hour. Thereafter, BSA/PBS solution was aspirated and replaced with mouse, anti-human ZO-1 (primary) antibody, diluted

in 1% BSA/PBS to a final concentration of 10 µg/ml. The cell samples were incubated with the primary antibody for 45 min. The primary antibody solution was then removed and cells washed with PBS (5 times). Alexa fluor® 594-labelled goat, anti-mouse (secondary) antibody, diluted according to manufacturer's instructions in 1% BSA/PBS was then applied to the cells for 30 min. The secondary antibody solution was then aspirated and cells washed with PBS extensively. 300 µl of Hoechst 33342 (100 µg/ml) was added to the samples (for nuclei staining) and incubated at room temperature for 5 min. The Hoechst solution was then removed and the cells were washed 4 times with PBS. Transwell® filters (containing cells) were then excised and mounted using 1,4-diazabicyclo[2.2.2]octane (DABCO) (1% diluted in 9:1 glycerol:PBS) on glass slides for confocal imaging, using the system described above.

2.2.5.5 Clathrin and Caveolin-1 staining

Filter-confluent Caco-2 and Calu-3 cells were fixed with 4% paraformaldehyde (PFA) (diluted in PBS) for 10 min at room temperature. The cells were permeabilised via the addition of 0.2% v/v Triton X-100 for 10 min. The cells were washed with PBS, before incubation with 1% BSA/PBS (for 1hr). The primary antibody rabbit, anti-human caveolin-1 (Santa Cruz Biotechnology, Inc.) was diluted 1:50 with 1% BSA/PBS and incubated with the cells for 30 min. For clathrin immunostaining, the primary antibody (rabbit, anti-clathrin (Abcam, UK)) was diluted 1:200 in 1% BSA/PBS. The cells were washed 3 times with PBS and incubated with the secondary antibody (goat, anti-rabbit IgG-rhodamine and goat, anti-rabbit IgG-FITC for caveolin-1 and clathrin, respectively) diluted 1:100 (in 1% BSA/PBS) for another 30 min. The control cell layers were incubated with the appropriate secondary antibody only. Following extensive washes with PBS, the cell nuclei were stained with Hoechst 33342 (100 µg/ml), the cells washed and the filter membrane excised from the insert. Cells were mounted on a slide using DABCO mounting medium and covered with a glass cover slip. Confocal imaging was carried out as detailed in sections above.

2.2.6 Molecular Biology techniques

2.2.6.1 cDNA synthesis

2.2.6.1.1 Isolation of mRNA from cells

The commercially available µMACS™ kit (Miltenyi Biotec, UK) was used to extract and reverse transcribe mRNA from filter-cultured Caco-2 and Calu-3 cells on day 7 (Caco-2 only), day 14 (Caco-2 only) and day 21 of Transwell® culture. This single-step method captures mRNA magnetically with oligo-dT magnetic beads. Before beginning, all surfaces were cleaned with RNaseZAP™ solution. The cells were harvested and resuspended in 1 ml of lysis buffer (high salt buffer containing 1% SDS) per 10^7 cells. The cells were lysed completely by applying shear stress with vigorous vortexing for 3-5 min. The resulting lysate was passed through a lysate column by centrifugation at 14000 rpm in a desktop centrifuge for 3 min and mixed with oligo dT magnetic microbeads (50 µg/ml cell lysate), which bind to the mRNA. For mRNA isolation, the magnetically labelled mRNA contained in the lysate was applied to the MACSµ column in the magnetic field of the thermoMACS™ separator. The column was prepared by rinsing with 100 µl of lysis/binding buffer and allowed to pass through. The column was rinsed twice with 200 µl lysis buffer and washed four times with 100 µl low salt wash buffer containing NaCl, Tris-HCl and EDTA. The purpose of this step was to ensure complete removal of proteins and DNA from the lysate. The µMACS column was rinsed with lysis buffer before applying the lysate.

2.2.6.1.2 cDNA synthesis

Continuing from above (2.2.6.1.1), with mRNA remaining in the MACSµ column. 20 µl of the enzyme mix containing the reverse transcriptase and dNTPs was applied on the column matrix and incubated at 42°C for 1 hour. To prevent evaporation, sealing solution (1 µl) was applied at the top of the column matrix. The column was then rinsed twice with 100 µl of equilibration/wash buffer. 20 µl of cDNA release solution was then applied (for 10 min at 42°C). The newly synthesised cDNA was eluted with 50 µl of cDNA elution buffer. Note, that 50 µl of sscDNA was collected per tube of which 20 µl was collected and pooled for primer optimisation.

2.2.6.2 Polymerase chain reaction (PCR)

2.2.6.2.1 PCR Primer design

Oligonucleotides for PCR amplification were designed using Primer-blast on the NCBI website. This program generates primer pair sequences based on a series of input criteria including intron exclusion and exon spanning regions, enabling differentiation between genomic DNA and complementary DNA (cDNA) of interest. Two different sets of PCR primers were used for human cubilin in Calu-3 and Caco-2 cells respectively. For Calu-3 work, HsCUBN_FOR and HsCUBN_REV primer pairs were employed (Table 2.2) and were designed from human cubilin sequence, National Center for Biotechnology Information (NCBI) Reference Sequence NM_001081.3. For caco-2 work, primer pairs HsCubilin_FOR and HsCubilin_REV were used (NCBI Reference Sequence NM_001081.3). PCR primers for human CD320; HsCD320_FOR and HsCD320_REV were designed from human CD320 sequence, NCBI Reference Sequence NM_016579.3. Finally, PCR primers for human caveolin-1: HsCAV1_FOR and HsCAV2_REV, with NCBI Reference Sequences: NM_001172897.1 NM_001172896.1, NM_001172895.1, NM_001753.4 were designed and synthesised by Sigma-Aldrich. For verification of specificity (i.e. primers specific within the human genome) and assessment of amplification of known splice variants, all primers were blasted against the human genomic and reference mRNA sequences.

Primer	5'- 3' sequence	Expected size (bp)
HsCD320_FOR **HsCD320_REV**	CACCCACCAAGTTCCAGTGCCG GTTCCACAGCCGAGCTCGTCG	cDNA 343/gDNA 1,285
HsCAV-1_FOR **HsCAV-1_REV**	GAGCGAGAAGCAAGTGTACGA ACAGACGGTGTTGGACGTAGAT	cDNA 362/gDNA *
HsCubilin_FOR **HsCubilin_REV**	ACTCTTACCTGCCAACCAACCTGGGAGG AGCAGACCCCGTAAGAAACACCAA	cDNA 201/gDNA 594
HsCUBN_FOR **HsCUBN_REV**	TCCGGCAGACATTGGGGCCT TCCGTGACCCTGCGGTGAGT	cDNA 602/gDNA 292-4170

Table 2.2. Oligonucleotide primer sequences for TCIIR, Caveolin-1 and cubilin expression analysis.

PCR primers designed for human TCIIR (CD320), human Caveolin-1 (CAV-1), and human cubilin (Cubilin/CUBN) shown with respective cDNA and genomic DNA sizes. The resulting amplified PCR product was the size of the cDNA.* denotes primers are specific for cDNA amplification (no target on genomic DNA).

2.2.6.2.2 Sample preparation

Standard 2x PCR ready-to-use Master Mix (ReddyMix™, ABgene®), containing the following components: 1.25 units Thermoprime plus DNA polymerase, 75 mM Tris-HCl (pH 8.8 at 25°C), 20 mM Ammonium sulphate, 1.5 mM $MgCl_2$, 0.01% (w/v) Tween 20, 0.2 mM (each of) dATP, dCTP, dGTP and dTTP, was used in PCR experiments. The ReddyMix™ PCR Master Mix is formulated with a red dye and precipitant for direct loading of PCR products onto agarose gels for electrophoresis. The final PCR reaction mixture consisted of 10 µl PCR Master-Mix, 1 µl each of forward and reverse primers

for the gene of interest (5 µM each final concentration), 1 µl DNA template (extracted cDNA of filter-cultured Caco-2 and Calu-3 cells) and 7 µl nuclease free water (Roche, UK), making a final volume of 20 µl per micro tube. The master mix prepared for CD320 samples comprised a hot start enzyme. The final reaction mixture (per tube) here consisted of 7.5 µl of GoTaq® Hot Start Green Master Mix, 2x (Promega), 5.25 µl nuclease free water, 1.5 µl each of CD320 forward and reverse primers (5 µM final concentration) and 0.75 µl DNA template. GoTaq® Hot Start Polymerase is supplied in 2X Green GoTaq® Reaction Buffer (pH 8.5), 400µM dATP, 400µM dGTP, 400µM dCTP, 400µM dTTP and 4mM $MgCl_2$. Green GoTaq® Reaction Buffer is a proprietary buffer containing a compound that increases sample density, and yellow and blue dyes, which function as loading dyes when reaction products are analysed by agarose gel electrophoresis.

2.2.6.2.3 PCR cycles

PCR amplification of calu-3 cDNA for human cubilin was performed using the following sequential cycles: initial heating at 94°C for 5 min, 94 for 30 sec, annealing at 60°C for 45 sec, extension at 72°C for 90 sec, and this cycling repeated 34 times, followed by a final extension at 72°C for 5 min to ensure completion of all strands. A similar PCR programme was followed for human CD320, human cubilin (for Caco-2 cDNA only) and human caveolin-1 with both Caco-2 and Calu-3 cDNA templates, but with annealing steps at 58°C. Reactions were carried out in a PTC-200 Peltier Thermal Cycler (MJ Research, UK). The reaction mixes were incubated at 4°C prior to DNA agarose gel electrophoresis.

2.2.6.2.4 DNA Agarose Gel electrophoresis

Agarose gels were prepared using a well-established protocol, developed by the group and adapted from Sambrook *et al*. [12]. Briefly, 1% (w/v) agarose gels were prepared using analytical grade agarose (Promega, UK) in 0.5X TBE buffer (1 M Tris-HCl; 1 M Boric Acid; 0.05 M EDTA; pH 8.0) with the addition of ethidium bromide (10 µg/ml). 8 µl (0.8 µg) of TriDye 100 bp DNA Ladder (New England Biolabs) was loaded per gel lane (2 lanes per gel on either side of DNA samples). The DNA samples were loaded (15-20 µl per gel lane) and the gels were run in 0.5X TBE buffer and

electrophoresis was performed using a horizontal gel apparatus (Fisher Scientific, UK) at 100-110 V. DNA fragments were visualised on a UV transilluminator with Gene Genius Bio imaging software (UVP, USA).

2.2.7 Statistical Analysis

Statistical comparisons (for a maximum of two data sets in any given comparison) were performed by Student's t-test generated using Microsoft Excel (2007). Values of $p<0.05$ were considered statistically significant. One way analysis of variance (ANOVA) followed by Bonferroni post-hoc test was applied for comparison of group means of three or more groups. P values of < 0.05 were considered statistically significant. *, **, *** and **** indicate $p<0.05$, $p<0.01$, $p<0.001$ and $p<0.0001$, respectively.

2.3 References

1. Vllasaliu, D., *In vitro investigation into strategies for mucosal delivery of proteins*, in *School of pharmacy*. 2010, University of Nottingham: Nottingham Ph.D Thesis.
2. Velarde, G., et al., *Use of transepithelial electrical resistance in the study of pentachlorophenol toxicity.* Toxicol In Vitro, 1999. **13**(4-5): p. 723-7.
3. Narai, A., S. Arai, and M. Shimizu, *Rapid decrease in transepithelial electrical resistance of human intestinal Caco-2 cell monolayers by cytotoxic membrane perturbents.* Toxicol In Vitro, 1997. **11**(4): p. 347-54.
4. Wise, C., ed. *Methods in Molecular Biology*. Epithelial Cell Culture Protocols. Vol. 188. 2002, Humana Press, Inc.: Totowa, NJ.
5. Scott, B. *CellTiter 96® AQueous One Solution Cell Proliferation Assay From Promega*. 2007 [cited; Available from: http://www.biocompare.co.uk/Articles/ProductReview/837/CellTiter-96-AQueous-One-Solution-Cell-Proliferation-Assay-From-Promega.html.
6. Legrand, C., et al., *Lactate dehydrogenase (LDH) activity of the cultured eukaryotic cells as marker of the number of dead cells in the medium [corrected].* J Biotechnol, 1992. **25**(3): p. 231-43.
7. Unknown, A. *LDH Cytotoxicity Assay Kit* [cited; Available from: http://www.caymanchem.com/app/template/Product.vm/catalog/10008882.
8. Molecular Probes, M. *LysoTracker™ and LysoSensor™ Probes*. 1999 [cited.
9. Chen, J.W., et al., *Isolation and sequencing of a cDNA clone encoding lysosomal membrane glycoprotein mouse LAMP1. Sequence similarity to proteins bearing onco-differentiation antigens.* J Biol Chem, 1988. **263**(18): p. 8754-8.
10. Granger, B.L., et al., *Characterization and cloning of lgp110, a lysosomal membrane glycoprotein from mouse and rat cells.* J Biol Chem, 1990. **265**(20): p. 12036-43.

Chapter 3: Characterisation of the Caco-2 intestinal model

3.1 Introduction

Mucosal drug absorption has been extensively investigated *in vitro* with the aim of understanding, and potentially predicting, drug absorption and bioavailability *in vivo*. This requires the use of mucosal tissue models, either based on excised mucosal tissues, three dimensional models based on multiple cell types or epithelial cell layers of primary and cancerous cell lines (Figure 3.1). Each of these systems is associated with its advantages and disadvantages. For example, although the *in vivo* tissue characteristics are most closely represented by an excised tissue of interest (usually from animals with similar tissue characteristics to humans), this model undoubtedly requires animal sacrifice and suffers from limited viability of the tissue *ex vivo*.

Models based on polarised epithelial cell monolayers are extensively used as suitable *in vitro* alternatives to animal work in the early phase drug development process. In this respect, the Caco-2 cell line is commonly used to produce such a monolayer model of the intestinal epithelium. Apart from offering reduced operational costs and potentially reducing animal usage [1], *in vitro* cell systems can be manipulated in ways that would be impossible *in vivo*, enabling studies on the effects of different variables (e.g. temperature and pharmacological agents), which is particularly useful for investigating the mechanisms of drug absorption. A significant amount of knowledge related to drug transport mechanisms has been obtained from studies in various epithelial cell cultures and these models are routinely used as a screening tool in the pharmaceutical industry for the prediction of intestinal drug absorption [2]. This is due to a reasonably acceptable correlation between passive drug transport through the epithelial cell monolayers and that observed across the human intestine *in vivo* [3-5]. The importance and credibility of the data obtained from drug transport experiments on epithelial cell monolayers is reflected in the fact that both the FDA and the European Medicines Agency [6] recommend the use of monolayers of suitable epithelial cells for classifying the permeability of drug compounds and for monitoring

drug-drug interactions. From the pharmaceutical industry perspective, *in vitro* monolayer systems are useful in early phases of drug development and are central to the process of the Biopharmaceutics Classification System (BCS), serving to identify promising drug candidates, which are then subject to more rigorous (qualitative) *in vivo* investigations. However, homogenous epithelial cell cultures lack the structural complexity and variability found *in vivo* and for this reason it is important to be cautious when extrapolating *in vitro* cell model results to the *in vivo* situation and to compare results obtained from the two systems.

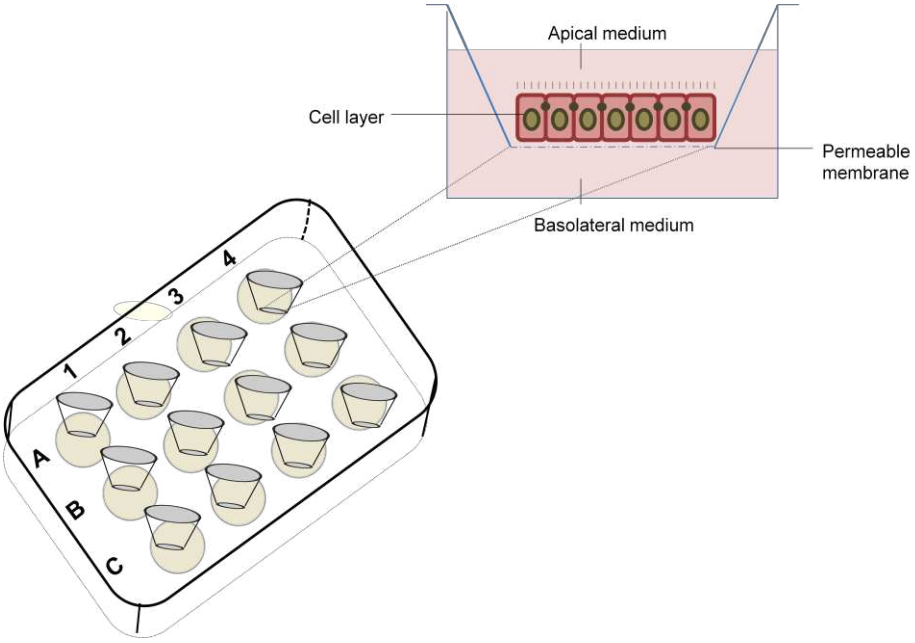

Figure 3.1. Schematic representation of the Transwell® system: cells cultured on permeable supports.

Reproducing the features of the mucosal tissue *in vivo* is an obvious consideration for the establishment of a successful epithelial cell layer model. In this respect, selecting the appropriate cell line expressing relevant morphological features, transporters and enzymes which reflect the tissue of interest is of paramount importance. Once an adequate cell line is chosen, culture conditions may require optimisation. This includes parameters such as seeding density (on permeable supports), time to differentiation, and growth medium. In the process of culturing epithelial cells as mucosal tissue models (as polarised monolayers on permeable supports), measurement of transepithelial electrical resistance (TEER) is routinely employed as an indication of

cell confluence, tight junction formation and cell layer integrity [7] and is also used as an indirect measure of cell toxicity [8, 9].

Colorectal carcinoma-derived Caco-2 cells, when differentiated, resemble enterocytes lining the small intestine [10, 11]. These cells express tight junctions, microvilli, a great number of relevant enzymes and transporters and evidence from extensive research with this cell line has generally demonstrated a good correlation between the *in vitro* permeability and the *in vivo* drug absorption [3].

The work detailed in this chapter assessed the suitability of Caco-2 cell monolayers as a model for the vitamin B_{12} transport system, laying the foundations for subsequent work (Chapters 4-7) investigating the use of the vitamin B_{12} transport pathway for the transmucosal delivery of nanoparticulate carriers. Additionally, the Caco-2 cell line used in this work was also validated as an epithelial barrier that is suitable to study macromolecular absorption (by determining cell morphology and testing the permeability of model macromolecules). This was considered important as, although this cell line has been thoroughly characterised as an intestinal model [12-15], Caco-2 cells are a diverse line consisting of subpopulations that may vary in terms of the extent of differentiation, which are further influenced by culture conditions, time in culture, and batch to batch differences [16-18]. Consequently, large inter-laboratory differences in characteristics exist and therefore it is crucial that the specific batch of cells is independently assessed. With respect to establishing the appropriateness of the Caco-2 model to study the vitamin B_{12} transport system, work was conducted to determine gene expression and immunohistochemical analyses for the key proteins involved in the internalisation and transport of vitamin B_{12} *in vivo,* including the B_{12}-IF receptor, cubilin; the secondary receptor, transcobalamin II receptor (TCIIR), and the TCII carrier protein.

3.2 Methods

3.2.1 TEER profile

Caco-2 cells were cultured on flasks until confluence. Cells were detached from the flasks, seeded on Transwell® permeable supports, following the methods detailed

previously (section 2.2.1). TEER measurements were conducted (in the manner described in section 2.2.2) every 2 or 3 days, starting from day 2 to day 30 of culture.

3.2.2 Morphological characterisation

Caco-2 cells were cultured on permeable supports to form polarised monolayers, as detailed in section 2.2.1. Cells were imaged on day 21 of culture as confluent and polarised monolayers (as judged by TEER measurements). SEM, TEM, and Zonula Occludens-1 (ZO-1) staining were performed according to methods described in section 2.2.5.

3.2.3 Barrier property of Caco-2 monolayers

3.2.3.1 Permeability of varying molecular weight FITC-labelled dextrans

FITC-dextrans (FD) of varying molar mass were used as model macromolecules. The permeability experiments were conducted at 37 ℃ or 4 ℃. Culture medium was initially replaced with warmed (37 ℃) HBSS (transport medium). Cell monolayers were allowed to equilibrate in HBSS for approximately 15 min prior to TEER measurements, which were conducted in order to confirm cell layer intactness and selection of those with appropriate values (sections 2.2.2 and 2.2.3). Prior to application of FDs, cells were equilibrated in HBSS (pre-warmed to 37 ℃ or cooled to 4 ℃) for approximately 45 min. HBSS was then removed from the apical side and replaced with FD solutions, comprising of FD4, FD10, FD20, FD40, FD70 or FD150 dissolved in HBSS (4 ˚C or 37 °C) at 500 µg/ml. Cells were either placed in the incubator at 37 ˚C or in the fridge at 4 ˚C in between sampling intervals. FD permeability was determined as detailed in section 2.2.3.

3.2.3.2 Dynamic light scattering characterisation of FITC-labelled dextrans

The mean hydrodynamic diameter of FDs was determined by Dynamic Light Scattering (DLS) using a Viskotec 802 system. FD4, FD10, FD20, FD40, FD70 and FD150 were dissolved in HBSS at 1 mg/ml (at pH 7.4) to replicate the conditions in which the FDs were applied to cells and were analysed using the default programme setting, wherein the optimal intensity count was 300 k counts and the temperature was 25 ℃. An average of 10 readings per sample were taken. Omnisize software was

used to calculate the size data. The experimental values obtained were plotted against the nominal diameters provided the FD's supplier, Sigma-Aldrich.

3.2.3.3 Insulin translocation across Caco-2 monolayers

Caco-2 cells were cultured on filters as before and used as polarised monolayers. Permeability experiments commenced after replacement of the culture medium with HBSS and equilibration in HBSS (for approximately 30 min). Stock solutions of FITC-insulin dissolved in HBSS (at pH 6.0) at a concentration of 160 µg/ml, were prepared on the day of the permeability experiment. FITC-insulin solution was applied to the apical side of the cells at a final concentration of 80 µg/ml (in HBSS, pH 6.0) and its transport across the cell layers was determined by sampling the basolateral solution (100 µl) at regular time intervals. The sampled volumes from the basolateral chamber were replaced with fresh HBSS. FITC-Insulin transport was quantified by fluorescence measurements (485 nm excitation, 535 nm emission), with reference to a pre-constructed calibration curve of fluorescence intensity against concentration. The known concentration was converted into the amount and data is expressed as apparent permeability coefficient (P_{app}), as well as in micrograms (µg) transported over time.

3.2.3.4 Nanoparticle (NP) transport across Caco-2 monolayers

Caco-2 cells were cultured on filters in the manner described previously (section 2.2.1). Cell monolayers were equilibrated in HBSS for approximately 45 min. TEER was measured just before the addition of nanoparticles; Caco-2 monolayers with a TEER ≥800 $\Omega.cm^2$ were included in the experiment. Carboxy-modified, fluorescent (yellow-orange) polystyrene nanoparticles (Fluoresbrite®) of 50 nm, 100 and 200 nm nominal diameter, were diluted in HBSS (to a final concentration of 400 µg/ml) and applied to the apical side of the cell layers. Apical-to-basolateral translocation was measured by sampling the basolateral solution (100 µl) at 30 min intervals for 3 hours, with an initial sampling point after 15 min. The extent of NP translocation across the cell layers was determined by measuring the fluorescence (529 nm excitation, 546 nm emission) of the basolateral solutions and converting the values obtained into concentrations and through pre-constructed calibration curves (based on the same

principle as for FITC-Insulin quantitation). NP transport across the cell layers is expressed as amount in micrograms over time.

3.2.5 Validation of Caco-2 monolayers as a model for vitamin B_{12} transport

3.2.5.1 Immunohistochemical analysis of cubilin and TCII

Filter-cultured Caco-2 cells were selected for immunostaining experiments on day 21 of culture. The culture medium was removed and cells incubated with HBSS for 45 min, followed by measurement of TEER. The cell monolayers were then fixed with 4% paraformaldehyde (diluted in PBS) for 10 min at room temperature. For TCII samples, an additional permeabilisation step was conducted via the addition of 0.2% (v/v) Triton X-100 for 10 min. Cells were washed with PBS, before incubation with 1% BSA/PBS (for 1hr). The primary antibodies for cubilin and TCII (cubilin H-300; Transcobalamin II H-260; both rabbit, anti-human; Santa Cruz Biotechnology, Inc.) were diluted 1:50 with 1% BSA/PBS and incubated with the cells for 30 min. The cells were washed 3 times with PBS and incubated with the secondary antibody (goat, anti-rabbit IgG-rhodamine) diluted 1:100 (in 1% BSA/PBS) for another 30 min. The control cell layers were incubated with the secondary antibody only. Following a final wash step, the cell nuclei were stained with Hoechst 33342 (0.1mg/ml), cells washed and the filter membrane excised from the insert. Cells were mounted on a slide using 1,4-diazabicyclo[2.2.2]octane (DABCO) (1%, diluted in 9:1 glycerol:PBS) and covered with a glass cover slip. Confocal imaging was carried out using a Leica SP2 CLSM confocal microscope.

3.2.5.2 mRNA expression of cubilin and Transcobalamin II receptor

mRNA was isolated from filter-cultured Caco-2 on day 7, day 14 and day 21 of culture on Transwell® inserts, using the method described in section 2.2.6.1.1. cDNA was synthesised using the protocol described in section 2.2.6.1.2. A conventional PCR was performed on the PTC-200 Thermal Cycler to amplify the cDNA, which was then visualised using gel electrophoresis (section 2.2.6.2). The expected size of the amplified cDNA fragments was 201 bp for cubilin and 343bp for CD320 (encoding

Transcobalamin II receptor). The reader is referred to section 2.2.6.2.1 for primer details.

3.3 Results and discussion

3.3.1 TEER profile

TEER is a convenient, reliable and non-destructive method to monitor the growth of epithelial tissue cultures *in vitro*, evaluate cell layer integrity and indicate the presence of the cellular tight junctions (TJs) [7] (Chapter 2, section 2.2.2 contains further details). Figure 3.2 shows the TEER profile over time in culture for Caco-2 cells grown on permeable supports. Cells exhibited a continuous and steady increase in TEER, which reached up to 2250 Ωcm^2 (on day 21 of culture). TEER values then progressively decreased from day 21 to day 30 of culture (cells displayed lower values of ~1430 Ωcm^2 at the terminal measurement point), presumably as a result of altered cell morphology, changes in TJ distribution and loss of single cell layer organisation. Reported TEER values in the literature for Caco-2 monolayers vary considerably from 150-400 Ωcm^2 [19], up to >2000Ωcm^2 [20, 21], and this variability is thought to arise from differences in the culture conditions employed (e.g. culture medium or permeable supports used), passage number and also owing to the fact that different subpopulations of Caco-2 cell cultures exist, which may vary in terms of degree of differentiation [16].

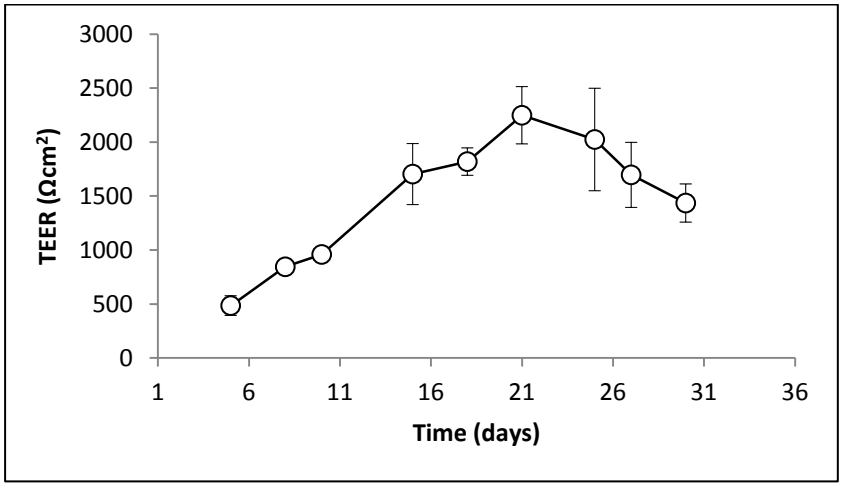

Figure 3. 2. TEER profile of Caco-2 cells cultured on permeable inserts.

TEER is expressed as the measured resistance per area (cm^2) of the cell layer. Background TEER due to the filter was subtracted from the reported TEER values. Data presented as the mean ± SD (n=5).

3.3.2 Morphological characterisation of Caco-2 cells

3.3.2.1 Electron microscopy

SEM micrographs (Figure 3.3a) reveal that Caco-2 cells cultured on permeable supports form a closely packed layer of cells, with distinct, heavily folded cell-cell boundaries (indicated within white boxes). Furthermore, structures likely representing microvilli on the cell surface are clearly apparent. TEM micrographs (Figure 3.3b) depict two adjacent Caco-2 cells inter-connected by a TJ (Tj). The intercellular TJs provide a structural barrier against paracellular permeation [22, 23], thus maintaining the restrictive barrier of the mucosae. As is shown in the figure, TJs typically encircle the epithelial cells in a belt-like manner at the apical cellular borders [24]. Other cellular structures, including the cell nuclei (Nu), mitochondria (Mc) and microvilli (Mv) are also clearly apparent, consistent with reports from other groups [25, 26].

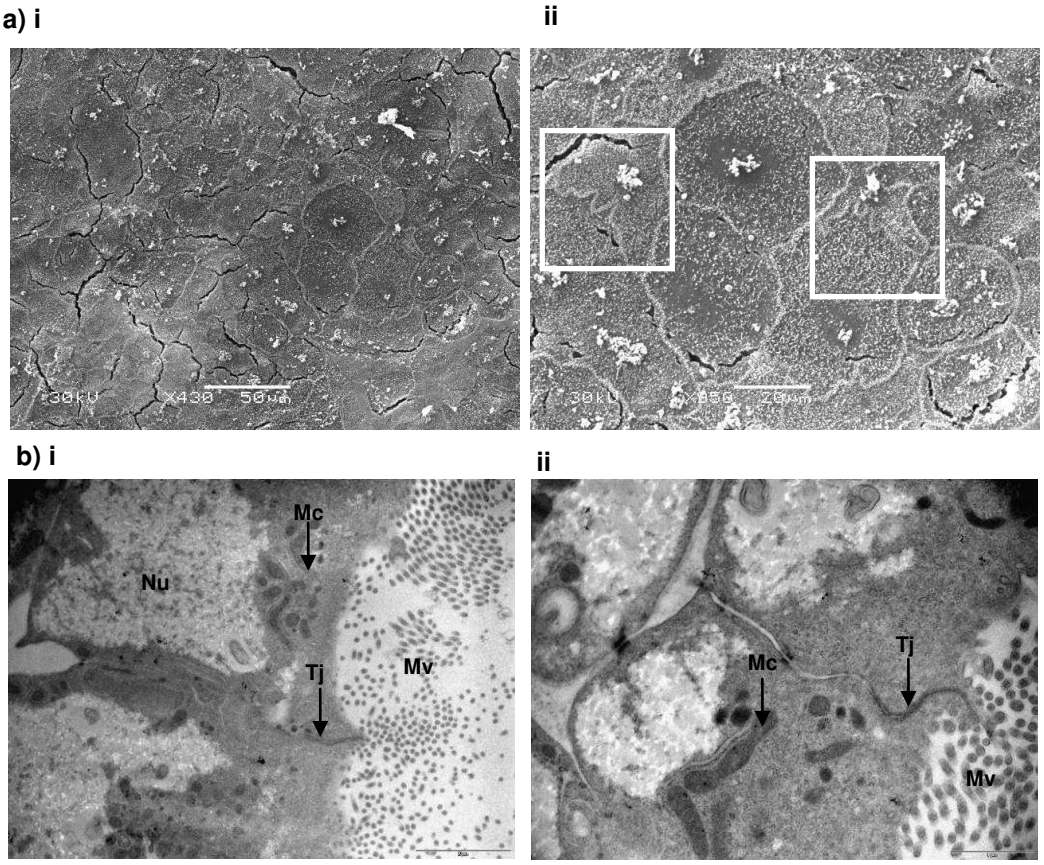

Figure 3. 3. Morphological characterisation of the Caco-2 monolayer model.

a) SEM micrographs, with the expanded region of Caco-2 monolayer; (i) showing cell-cell boundaries and magnified image (ii) depicting convoluted cell-cell boundaries (white boxes) and microvilli. The observed cracks are believed to be artifacts resulting from sample processing for imaging. b) TEM micrographs of filter cultured Caco-2 cells depicting adjacent Caco-2 cells interconnected by a tight junction (Tj) (i) and a magnified region of two cells (ii) depicting a tight junctional boundary (Tj) and other cellular structures including cell nucleus (Nu), mitochondria (Mc) and microvilli (Mv). Scale bars representing 2 µm (bi) and 1 µm (bii).

3.3.2.2 Zonula-Occludens-1 (ZO-1) staining

Immunofluorescence staining of polarised Caco-2 cells with an antibody to ZO-1 protein, a structural and functional component of TJs, revealed the distribution of this protein as continuous circumcellular 'rings' at cell-cell contacts (Figure 3.4). The images clearly highlight a relatively convoluted organisation of the cell-cell boundaries. This observation (which was reproducible) is important, as the obvious consequence of tight junction organisation in this manner is a large surface area of the paracellular space. Interestingly, similar ZO-1 organisation in Caco-2 cells was also observed by Man *et al*. [27], Lindmark *et al*. [28] and Dickman *et al*. [29], though the authors of these studies did not discuss the importance of this observation.

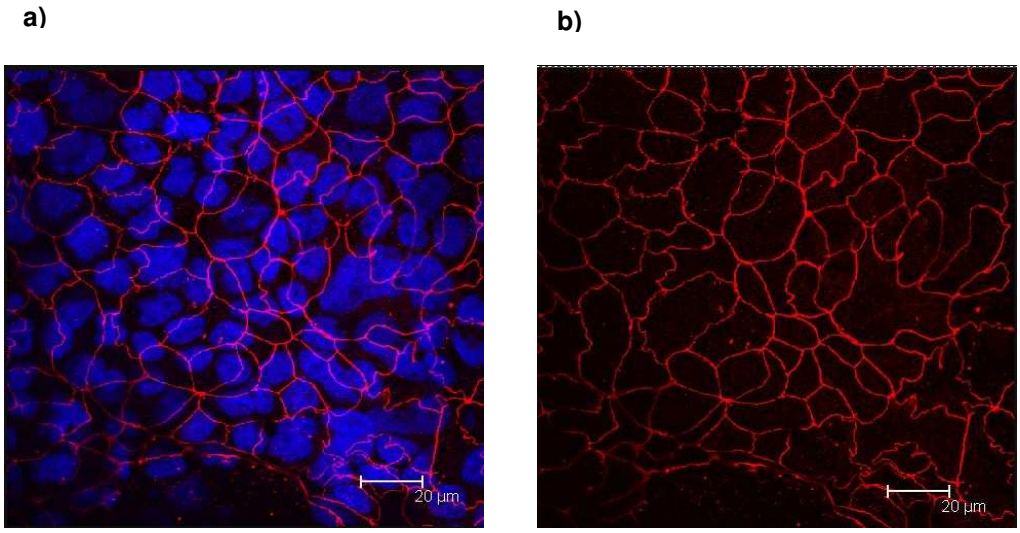

Figure 3. 4. Staining of polarised Caco-2 cells for Zonula Occludens-1 (ZO-1) TJ protein.

a) Overlay image of Caco-2 monolayer showing DAPI-labelled cell nuclei and ZO-1 distribution (Alexa fluor®594-labelled, anti-mouse IgG, and mouse, anti-human ZO-1), b) Red channel showing ZO-1 distribution (Alexa fluor®594-labelled goat, anti-mouse IgG, and mouse, anti-human ZO-1).

3.3.3 Barrier properties of Caco-2 cell layers

3.3.3.1 Permeability of varying Mw FITC-dextrans

As detailed in Chapter 2 (section 2.2.3), epithelial monolayer integrity is often assessed by measuring the transport of a hydrophilic marker molecule (frequently used a macromolecular drug models) that is passively transported through the cell layer, paracellularly [30]. In these studies, fluorescein isothiocyanate (FITC)–labelled dextrans (FDs) of varying molecular weights (MWs) were used as macromolecular markers, modelling hydrophilic, large MW protein drugs. Figure 3.5 shows the permeability, expressed as the apparent permeability coefficient (P_{app}) (Section 2.2.3), of FITC-dextran of varying molecular mass across polarised Caco-2 monolayers. The permeability was tested under normal cell culture conditions (37 ºC) and at 4 ºC (where energy requiring transcellular transport processes are inhibited and passive transport through the paracellular route is not significantly affected). Up to a certain molecular mass, macromolecules preferentially traverse the epithelium via the paracellular route (the macromolecule is accommodated by the paracellular corridor), with active transport processes (such as pinocytosis) likely to be involved to a lesser extent.

The data in Figure 3.5 shows a pattern of decreased transepithelial permeability with increasing solute molecular mass from 4 kDa (FD4) to 150 kDa (FD150). In this respect, P_{app} decreased from 227×10^{-9} to 14.1×10^{-9} cm/s across the range of FDs tested. The trend of reduced solute permeability with increasing molecular mass indicates that the Caco-2 cell monolayer model used in this work forms a functional epithelial barrier capable of discriminating between hydrophilic compounds depending on their size. This property is typical for polarised epithelial cells that are used as mucosal tissue models [14, 20, 31, 32]. Indeed, the pattern of reduced absorption (indicating decreasing permeability) with an increase in molecular mass of the permeant is observed *in vivo*, which is reflected by a decreased absorption as the molecular weight of the permeant (or therapeutic) increases. For example, Miyamoto *et al.* [33] reported an exponential decrease in the bioavailability of FDs with

increasing MW from 4.3 to 167 kDa following nasal administration in rats, even when co-administered with a TJ-opening absorption enhancer, poly-$_L$-arginine.

It is interesting to note that at 37 ºC the difference in permeability between FD4 ($227x10^{-9}$ cm/s) and FD10 ($222x10^{-9}$ cm/s) was not statistically significant, despite the considerable difference in molecular mass (4 kDa *versus* 10 kDa). The permeability of FD20 was approximately 2-fold lower than that of FD10 ($101x10^{-9}$ cm/s *versus* $222x10^{-9}$) and an increase in molar mass from 40 kDa to 70 kDa induced a 5-fold reduction in FD permeability (from $89.7x10^{-9}$ to $16.7x10^{-9}$ cm/s for FD40 and FD70, respectively). Further work assessing FD permeability at 4 ºC (whereby any observed permeability predominantly occurs passively) was conducted to determine the contribution of the paracellular route to the overall transport. FD permeability was significantly reduced at 4 ºC, as compared to that at 37 ºC, a finding that is in agreement with a previously-reported study [34]. Comparing FD4 permeability at both temperatures, the data reveals a reduction in permeability at 4 ºC that amounted to 2.5-fold. For FDs in the middle of the tested molecular weight range, the extent of the suppression of permeability was higher and amounted to 4.3-, 6-, and 7.2-fold for FD10, FD20 and FD40, respectively. These results hence indicate that the contribution of the paracellular route towards the overall permeability across Caco-2 monolayers is the largest for FD4 and then decreases as the molecular weight of the solute increases (from FD10 to FD40). The pattern of change in FD permeability with molecular weight hence indicates that there is a shift from approximately equal transcellular and paracellular contribution to overall transport with FD4 to predominantly transcellular route with larger dextrans such as FD20 and FD40. Note that although the difference in permeability between 37 ºC and 4 ºC for larger dextrans (FD70 and FD150) was not statistically significant, this is thought to result from the very low level of permeability at both temperatures.

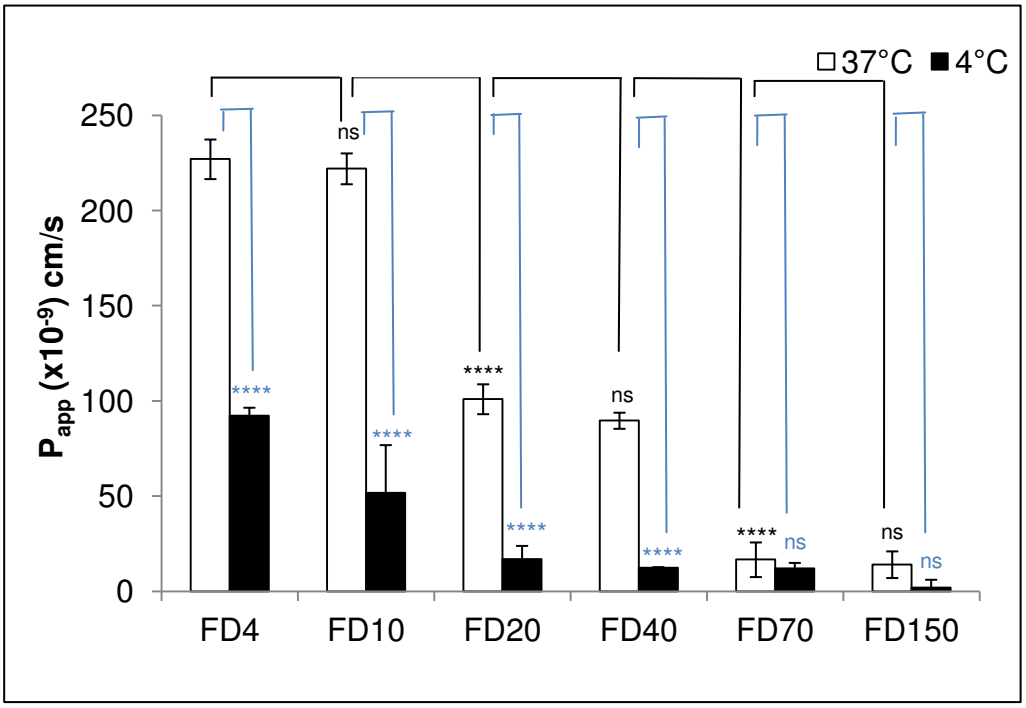

Figure 3. 5. Permeability of model permeants, FITC-dextrans of varying molecular weights) across Caco-2 monolayers.

FITC-dextrans of molecular weight: 4 kDa (FD4), 10 kDa (FD10), 20 kDa (FD20), 40kDa (FD40), 70 kDa (FD70) and 150 kDa (FD150) Permeability experiment was conducted at 37 ºC and at 4 ºC. Permeability was expressed as apparent permeability coefficient (P_{app}) and data presented as the mean ± SD (n=4). Statistical comparisons at 37°C (black) shown for FD10 vs. FD4, FD20 vs. FD10, FD40 vs. FD20, FD70 vs. FD40, FD150 vs. FD70. Statistical comparisons at 37°C vs. 4°C (shown in blue) for each molecular weight FD.

3.3.3.2 Dynamic light scattering study on different Mw dextrans: relating diameter with routes of transport

Figure 3.6a shows DLS data for a series of FITC-dextrans used in the permeability study above. For the purpose of comparison, nominal radii information provided by the supplier (Sigma Aldrich) has been included. The results reveal a directly proportional relationship between the dynamic radii of the dextran and its molecular weight (plotted as a logarithmic scale), with the exception of FD150 (150kDa) where measurements show a larger standard deviation, possibly due to aggregation in solution. Obtaining data on the hydrodynamic radius of each dextran enables further interpretation of the permeability data. Plotting the P_{app} values against the molecular weight of FDs (data from figure 3.5) again highlights the extent to which permeability depends on the

molecular weight of the permeant (Figure 3.6b). Considering the molecular size (hydrodynamic radii determined by DLS), the overall contribution of the paracellular route is the largest with the smallest dextran of 3.6 nm (hydrodynamic radius: 1.8 nm), FD4, as suggested by the low reduction in permeability at 4 ℃. The involvement of the paracellular pathway gradually decreases as solute molecular size (hydrodynamic radius) increases to 11.2 nm (FD40). The data hence indicates that the tight junctions of polarised Caco-2 monolayer model used in this work display some restriction in permeability of solutes of around 3.6 nm in diameter, though this barrier in permeability is notably higher for solutes larger than 5.4 nm (FD10-FD40). Again, FD70 and FD150 do not follow these trends, presumably due to the sensitivity of fluorescence quantitation at very low concentration levels (low permeability).

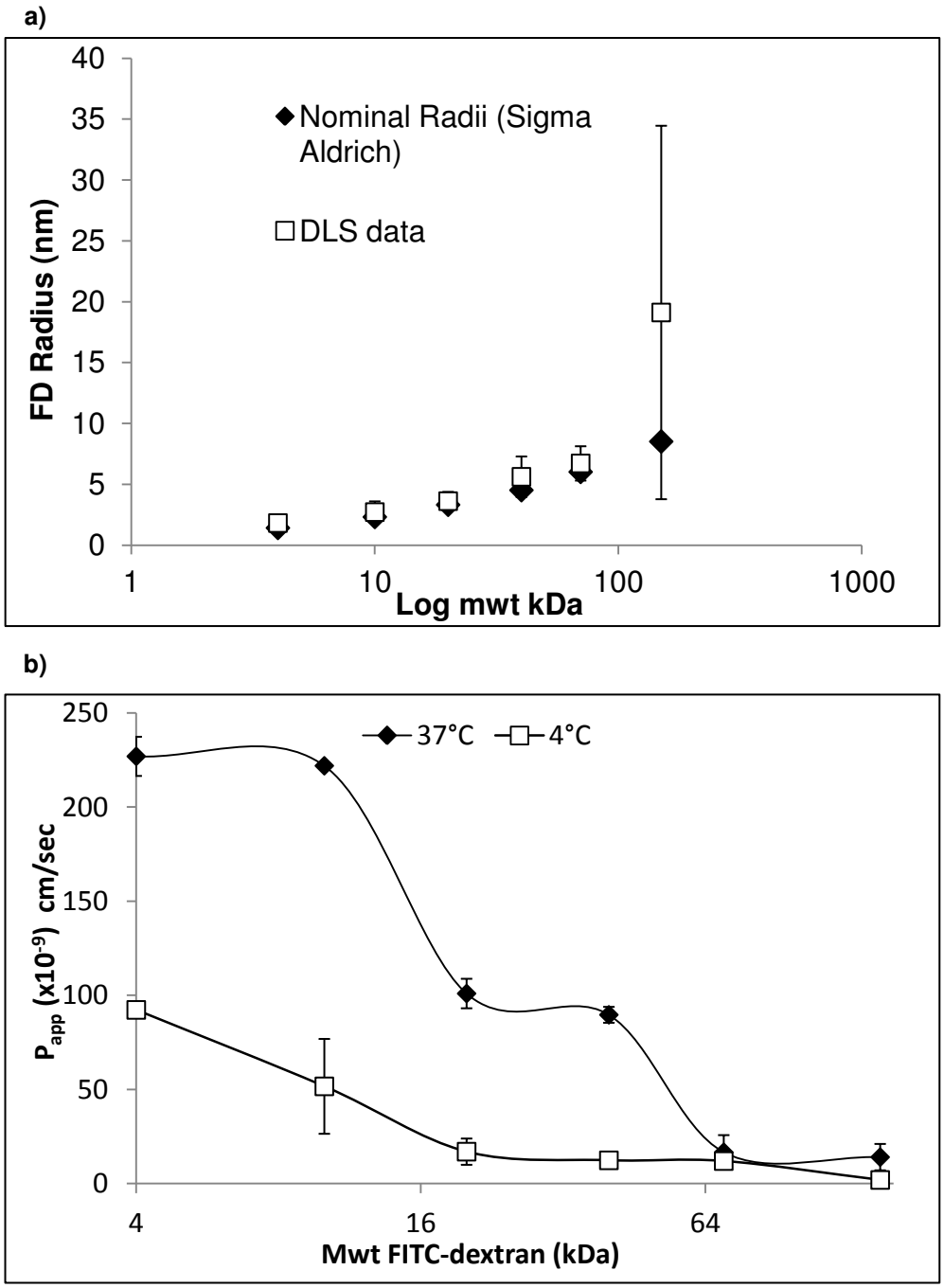

Figure 3. 6. Relationship between FDs molecular weight and particle size with permeability in Caco-2 monolayers.

a) DLS measurements of FD4, 10, 20, 40, 70 and 150 (KDa), b) P_{app} data for FD4, 10, 20, 40, 70 and 150(KDa) at 37°C and 4°C, plotted against a logarithmic scale of the molecular weight of each FD. Data expressed as mean ± SD (n=4).

3.3.3.3 Insulin translocation across Caco-2 monolayers

In an attempt to confirm that the Caco-2 monolayers used in this study also exhibit a barrier to the permeability of a therapeutic peptide, the permeability of FITC-insulin across the polarised cells was investigated as a 'model' protein used in this field. The data in Figure 3.7 shows a linear transport profile of FITC-insulin over time, with a steady increase from 0.4-5.9 µg in the basal chamber after 3 hrs (calculated P_{app} value amounted to $1.34x10^{-6}$ cm/s), which is similar to the value reported by Sadeghi *et al*. [35], where cumulative insulin transport was reported to be reach around 7.5 µg over 4 hrs in Caco-2 monolayers.

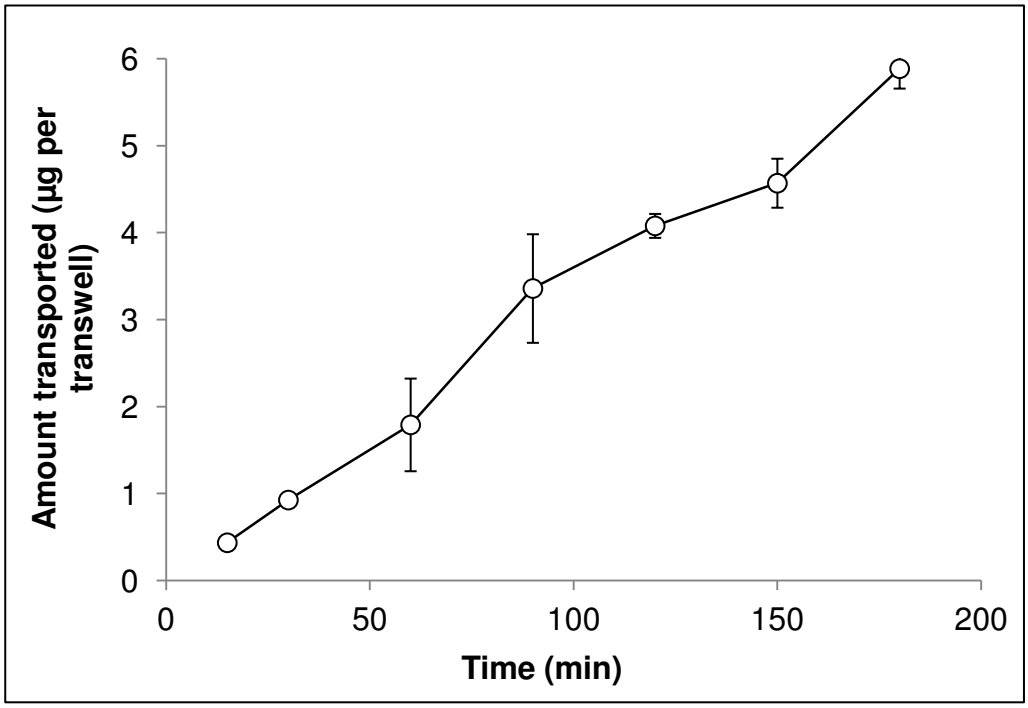

Figure 3. 7. Translocation of FITC-insulin across Caco-2 monolayers over 3 hours. Data presented as the mean ± SD (n=4).

Due to the similarity in molecular weight, it is tempting to compare the permeability of FITC-insulin with FD4. This would highlight a higher permeability of FITC-insulin relative to FD4 (P_{app} $1.34x10^{-6}$ cm/s *versus* $2.27x10^{-7}$). However, it must be noted that this comparison in permeability between insulin and FD4 may not be wholly appropriate considering the difference in molecular structure of the two compounds. In this respect, insulin is a globular molecule existing in aqueous environment as a mixture of dimers, tetramers, and hexamers in equilibrium [36], with the hexameric

conformation having a hydrodynamic radius of 2.8 nm [37]. On the other hand, FD4 has a linear geometry with a hydrodynamic radius of 1.8 nm.

3.3.3.4 Nanoparticle transport across Caco-2 monolayers

In addition to testing the permeability of hydrophilic macromolecules and a model therapeutic protein, the movement of nanoparticles across Caco-2 monolayers was also assessed. This work was conducted to provide an initial indication of the extent of the barrier presented by Caco-2 monolayers to nanoparticle translocation since nanoparticle-mediated drug delivery is central to this thesis (as will be shown in subsequent chapters). Transmucosal transport of nano-scale materials is potentially beneficial to the field of drug delivery [38-43] due to their potential to act as therapeutic carriers and their ability to enhance drug delivery by providing protection of the therapeutic, controlled release, and/or altering drug clearance. Apical-to-basolateral movement of negatively charged polystyrene nanoparticles (nominal diameters of 50,100 and 200 nm) across Caco-2 cells is depicted in Figure 3.8. Nanoparticle transport across the cell monolayers amounted to <1% of the applied amount over 3 hours, highlighting the efficiency of the epithelial barrier towards the movement of nanoparticulates. The cumulative amount of nanoparticles traversing the cell monolayers reached between 1.2-2.2 µg (depending on nanoparticle size), which is similar to an earlier observation reported by Vllasaliu *et al.* [44] in bronchial Calu-3 cells, where 1.25 µg of negatively charged polystyrene nanoparticles traversed the cell layers. Rates of transport are somewhat similar for all nanoparticle sizes, though there are small differences in the transported amount at the terminal time point, where the amount of transported 100 nm particles reached the highest value of 2.2 µg, compared to 50 nm and 200 nm particles (1.2 µg and 1.5 µg, respectively). Note that the uptake and translocation of nanoparticles across Caco-2 monolayers (together with the associated biological mechanisms involved in these processes) is studied in detail in the later sections of this thesis.

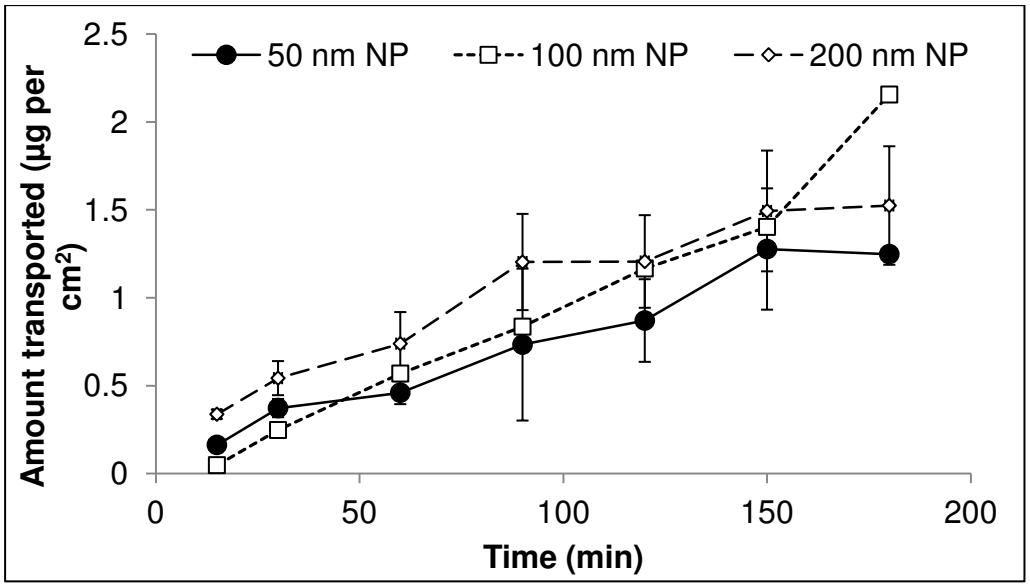

Figure 3. 8. Translocation of nanoparticles of 50 and 100 nm NPs across Caco-2 cell monolayers.

Nanoparticles (fluorescently-labelled, carboxy-modified polystyrene of 50 nm, 100nm and 200 nm nominal diameter) were applied at 400 µg/ml. Nanoparticle translocation expressed as amount of nanoparticles transported to the basolateral chamber. Data presented as the mean ± SD (n=3).

3.3.4 Validation of Caco-2 monolayers as a model for B_{12} transport

3.3.4.1 Staining for cubilin and TC II

Following appropriate morphological and barrier characterisation of Caco-2 (intestinal) model used in this thesis, subsequent work was conducted to confirm its suitability as a model to study the vitamin B_{12} uptake/transport pathway. Initial work determined whether the Caco-2 cultures expressed the appropriate structural components involved in vitamin B_{12} uptake and transport. In this respect, the expression of the vitamin B_{12} cell surface receptor, cubilin [45-47], was tested. Confocal micrographs of polarised Caco-2 monolayers, immunostained on day 21 of culture, indicate expression of the cubilin receptor (Figure 3.9a i), as suggested by the presence of red fluorescence signal (associated with the secondary antibody directed to primary, anti-cubilin antibody) at the periphery of adjacent cells. By contrast, in the control sample (Figure 3.9a ii) where the treatment with the primary, anti-cubilin antibody was omitted, secondary antibody-associated fluorescence was not observed, almost eliminating the possibility of an experimental artefact (false fluorescence signal) resulting from non-specific antibody binding.

Cubilin is just one component of the cell machinery responsible for trafficking of vitamin B_{12}. Therefore, in addition to confirming cubilin expression, further work was conducted to determine whether polarised and differentiated Caco-2 cells express another relevant component of the transport pathway. Immunostaining for TCII, a key protein involved in the binding and transport of vitamin B_{12} out of the enterocytes *in vivo* [1], indicated its presence in Caco-2 cells (Figure 3.9b i). Furthermore, its distribution was not confined to single regions of the cell but was found throughout the entire cytoplasm, consistent with its function of binding to vitamin B_{12} upon exit from the lysosomes for transport out of the cell. In the control sample treated only with the secondary antibody fluorescence was not observed (Figure 3.9b ii), hence minimising the possibility of non-specific secondary antibody binding. It should be noted that immunostaining of the TCII receptor, which permits the active internalisation of vitamin B_{12} in the absence of intrinsic factor *in vivo*, was not carried out due to the lack of commercially-available primary antibodies at the time of study.

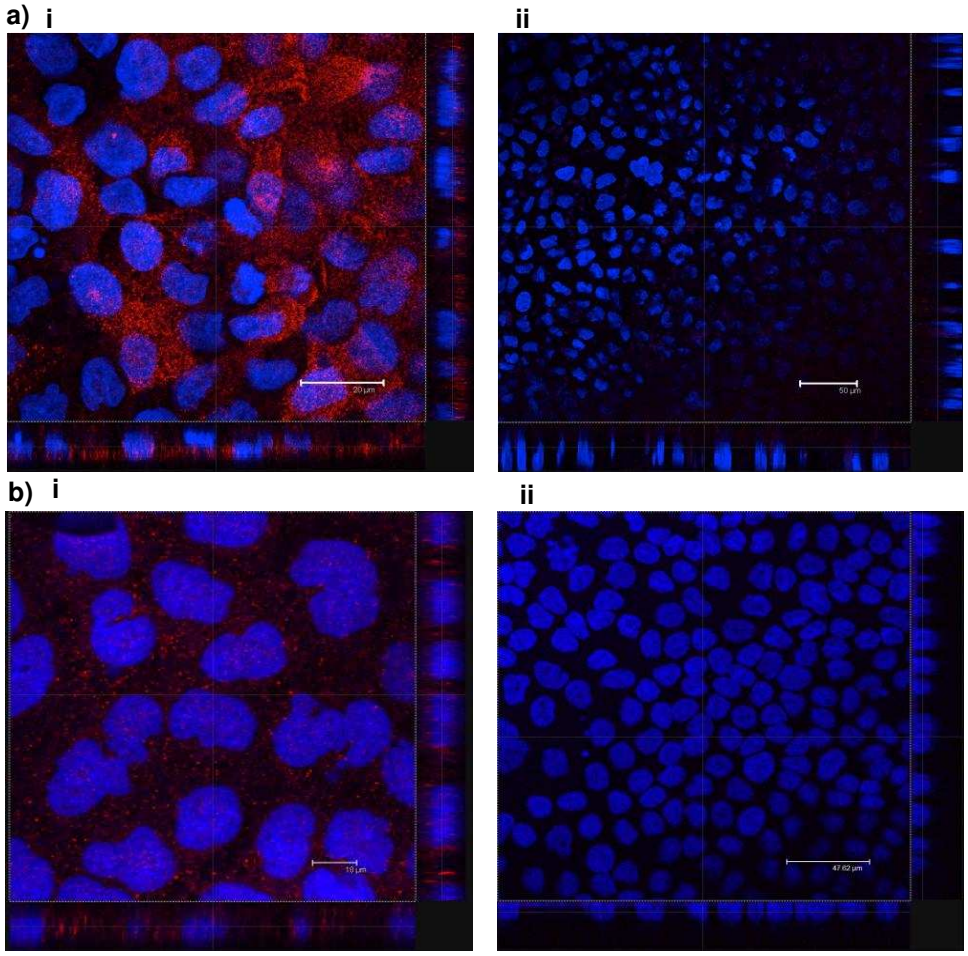

Figure 3. 9. Expression of cubilin (vitamin B_{12}-IF receptor) and transcobalamin II (TCII) by immunohistochemistry in polarised Caco-2 monolayers on day 21 of culture.

a) Expression of cubilin receptor by treatment of cells with anti-human cubilin H-300 followed by goat, anti-rabbit IgG-Rhodamine (i) and control where cells were treated only with the secondary, goat, anti-rabbit IgG-Rhodamine (ii). b) Expression of TCII, shown by treating cells with anti-human TCII H-260, followed by goat, anti-rabbit IgG-Rhodamine (i), and control monolayer, incubated with goat, anti-rabbit IgG-Rhodamine only (ii). Scale bar sizes represent 20, 50, 10 and 48 µm for ai, aii, bi and bii, respectively.

3.3.4.2 mRNA expression of cubilin and Transcobalamin II receptor in Caco-2 monolayers

Caco-2 cells monolayers were analysed using RT-PCR and gel electrophoresis to determine mRNA expression of cubilin and CD320 (transcobalamin II receptor). mRNA expression analysis was conducted following culture of Caco-2 cells on permeable supports for 7, 14 and 21 days. This was done with the view of establishing whether the expression of these components at the mRNA level in Caco-2 cells occurs at earlier time points (day 7 and 14) than the usually used culture period for cell

differentiation (21 days, routinely used in this work). Figure 3.10 reveals expression of both cubilin (A) and CD320 (B) in Caco-2 cells on day 7, 14 and 21 (cDNA amplification products of 201 and 343 bp, respectively). Other non-specific bands were detected (day 7 and 14 for cubilin), depicting smaller fragments which may result from primer-cross reactivity, as a consequence of lower levels of cDNA template present in these samples, or primer adducts (e.g. primer dimers). Analysis of CD320 mRNA reveals a secondary fragment (~260bp) in addition to the band detected at 343 bp (Figure 3.10B) possibly resulting from an alternatively spliced transcript variant encoding a different isoform.

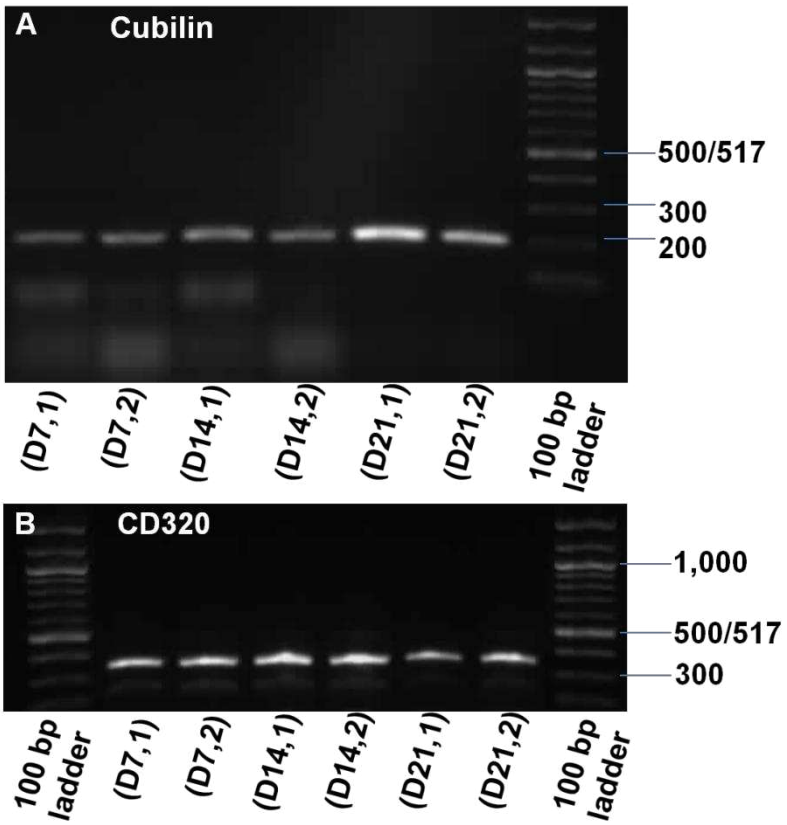

Figure 3. 10. Expression of cubilin (A) and CD320 (B) mRNA in Caco-2 cell monolayers analysed on day 7 (D7), day 14 (D14) and day 21 (D21) of culture (n=2).

As cubilin, the TCII receptor and the TCII carrier proteins are vital facilitators for a functional vitamin B_{12} transport pathway. Therefore, the findings confirming the expression of these components at mRNA level (Figure 3.10) were essential for the

validation of the Caco-2 cell line for further work on the vitamin B_{12} pathway. The expression of cubilin in Caco-2 cells has previously been shown, prompting investigations assessing the possibility of exploiting the vitamin B_{12} transport pathway for drug delivery purposes in this cell line [48-52]. However, whilst some authors have speculated over the expression of TCII receptor on the apical surface of Caco-2 cells [53], this work sought to provide further evidence for expression as a rationale behind receptor-mediated vitamin B_{12} uptake and transport in the absence of IF. Aforementioned, owing to the unavailability of antibodies for the TCII receptor, immunohistochemical analyses could not be used to show expression at the protein level. Instead, gene expression by PCR was used to verify that mRNA transcripts for CD320 exist in Caco-2 cells. Although the expression of the TCII receptor at the mRNA level does not guarantee downstream protein expression, later sections of this thesis show transport of vitamin B_{12} in the absence of IF (Chapter 6) – findings that indicate its presence in Caco-2 cells. Moreover, confirmation of expression of the TCII carrier protein, whose biological function is to transport vitamin B_{12} out of the basolateral membrane following its internalisation by the TCII receptor, also provides some indication that Caco-2 cells express the TCII receptor.

The data therefore confirmed that, following an appropriate culture method, the Caco-2 cells employed in this work have the ability to form polarised monolayers that present a molecular weight-dependent barrier to macromolecular permeability. Although this is a generally reported finding with Caco-2 cells, conducting this work was considered important due to inter-laboratory variabilities generally observed with the Caco-2 cell line. Furthermore, confirming the presence of cellular components involved in absorption and transport of vitamin B_{12} was necessary and an essential prerequisite for the validation of the Caco-2 cell line as an *in vitro* model for studying vitamin B_{12} mediated drug delivery.

3.4 Conclusion

The work detailed in this chapter characterises the Caco-2 cell monolayer model in

terms of its barrier integrity, morphology and determined the appropriateness of its use as a system to study nanoparticle delivery via the vitamin B_{12} pathway. Following appropriate culture (on permeable supports; for a defined time period) intestinal Caco-2 cells were shown to form polarised monolayers, express tight junctions and present a barrier to the permeability of macromolecules, with the extent of this barrier dictated by the molecular weight of the macromolecular solute. Polarised Caco-2 cell monolayers were further shown to restrict apical-to-basolateral translocation of nanoparticles of 50, 100 and 200 nm in size. In establishing whether the Caco-2 model used in this work constitutes a suitable system to investigate the vitamin B_{12} pathway for drug delivery purposes, cells were tested for the expression of specific cell components involved in vitamin B_{12} absorption in enterocytes. In this respect, immunohistochemical and gene expression analyses revealed that Caco-2 cells express the essential constituents of the vitamin B_{12} trafficking pathway, including cubilin, TCII carrier protein and TCII receptor. This work therefore confirmed that the monolayer model based on Caco-2 cells provides an adequate system to study drug delivery strategies exploiting the vitamin B_{12} trafficking pathway, as is explored in subsequent chapters of this thesis.

3.5 References

1. Tuma, P.L. and A.L. Hubbard, *Transcytosis: crossing cellular barriers.* Physiol Rev, 2003. **83**(3): p. 871-932.
2. Tavelin, S., et al., *Applications of epithelial cell culture in studies of drug transport.* Methods Mol Biol, 2002. **188**: p. 233-72.
3. Artursson, P. and J. Karlsson, *Correlation between oral drug absorption in humans and apparent drug permeability coefficients in human intestinal epithelial (Caco-2) cells.* Biochem Biophys Res Commun, 1991. **175**(3): p. 880-5.
4. Tavelin, S., et al., *A conditionally immortalized epithelial cell line for studies of intestinal drug transport.* J Pharmacol Exp Ther, 1999. **290**(3): p. 1212-21.
5. Irvine, J.D., et al., *MDCK (Madin-Darby canine kidney) cells: A tool for membrane permeability screening.* J Pharm Sci, 1999. **88**(1): p. 28-33.
6. Bock, U., et al. *Validation of the Caco-2 cell monolayer system for determining the permeability of drug substances according to the Biopharmaceutics Classification System (BCS)* [cited 2009 25/11/2009]; Available from: http://www.acrossbarriers.de/uploads/media/FCT02-I-0305_BCS.pdf.
7. Vllasaliu, D., *In vitro investigation into strategies for mucosal delivery of proteins*, in *School of pharmacy*. 2010, University of Nottingham: Nottingham.
8. Narai, A., S. Arai, and M. Shimizu, *Rapid decrease in transepithelial electrical resistance of human intestinal Caco-2 cell monolayers by cytotoxic membrane perturbents.* Toxicol In Vitro, 1997. **11**(4): p. 347-54.
9. Velarde, G., et al., *Use of transepithelial electrical resistance in the study of pentachlorophenol toxicity.* Toxicol In Vitro, 1999. **13**(4-5): p. 723-7.
10. Pinto, M., S. Robine-leon, and M.D. Appay, *Enterocyte-like differentiation and polarization of the human colon carcinoma cell line Caco-2 in culture.* Biol. Cell., 1983. **47**: p. 323-330.
11. Hidalgo, I.J., T.J. Raub, and R.T. Borchardt, *Characterization of the human colon carcinoma cell line (Caco-2) as a model system for intestinal epithelial permeability.* Gastroenterology, 1989. **96**(3): p. 736-49.
12. Artursson, P. and R.T. Borchardt, *Intestinal drug absorption and metabolism in cell cultures: Caco-2 and beyond.* Pharm Res, 1997. **14**(12): p. 1655-8.
13. Gres, M.C., et al., *Correlation between oral drug absorption in humans, and apparent drug permeability in TC-7 cells, a human epithelial intestinal cell line: comparison with the parental Caco-2 cell line.* Pharm Res, 1998. **15**(5): p. 726-33.
14. Mathia, N.R., et al., *Permeability characteristics of calu-3 human bronchial epithelial cells: in vitro-in vivo correlation to predict lung absorption in rats.* J Drug Target, 2002. **10**(1): p. 31-40.
15. Foster, K.A., et al., *Characterization of the Calu-3 cell line as a tool to screen pulmonary drug delivery.* Int J Pharm, 2000. **208**(1-2): p. 1-11.
16. Volpe, D.A., *Variability in Caco-2 and MDCK cell-based intestinal permeability assays.* J Pharm Sci, 2008. **97**(2): p. 712-25.
17. Herold, G., et al., *Morphology of CaCo-2 cells varies in different cell batches.* In Vitro Cell Dev Biol Anim, 1994. **30A**(5): p. 289-91.
18. Walter, E. and T. Kissel, *Heterogeneity in the human intestinal cell line Caco-2 leads to differences in transepithelial transport.* Eur J Pharm Sci, 1995. **3**: p. 215-230.
19. Yee, S., *In vitro permeability across Caco-2 cells (colonic) can predict in vivo (small intestinal) absorption in man--fact or myth.* Pharm Res, 1997. **14**(6): p. 763-6.
20. Vllasaliu, D., et al., *Barrier characteristics of epithelial cultures modelling the airway and intestinal mucosa: a comparison.* Biochem Biophys Res Commun, 2011. **415**(4): p. 579-85.
21. Chirayath, M.V., et al., *Vitamin D increases tight-junction conductance and paracellular Ca2+ transport in Caco-2 cell cultures.* Am J Physiol, 1998. **274**(2 Pt 1): p. G389-96.

22. Claude, P., *Morphological factors influencing transepithelial permeability: a model for the resistance of the zonula occludens.* J Membr Biol, 1978. **39**(2-3): p. 219-32.
23. Madara, J.L. and K. Dharmsathaphorn, *Occluding junction structure-function relationships in a cultured epithelial monolayer.* J Cell Biol, 1985. **101**(6): p. 2124-33.
24. Ma, T.Y., et al., *Mechanism of extracellular calcium regulation of intestinal epithelial tight junction permeability: role of cytoskeletal involvement.* Microsc Res Tech, 2000. **51**(2): p. 156-68.
25. Aspenstrom-Fagerlund, B., et al., *Fatty acids increase paracellular absorption of aluminium across Caco-2 cell monolayers.* Chem Biol Interact, 2009. **181**(2): p. 272-8.
26. Brisson, L., et al., *Alpha-tocopheryl acetate is absorbed and hydrolyzed by Caco-2 cells comparative studies with alpha-tocopherol.* Chem Phys Lipids, 2008. **154**(1): p. 33-7.
27. Man, A.L., et al., *Macrophage migration inhibitory factor plays a role in the regulation of microfold (M) cell-mediated transport in the gut.* J Immunol, 2008. **181**(8): p. 5673-80.
28. Lindmark, T., Y. Kimura, and P. Artursson, *Absorption enhancement through intracellular regulation of tight junction permeability by medium chain fatty acids in Caco-2 cells.* J Pharmacol Exp Ther, 1998. **284**(1): p. 362-9.
29. Dickman, K.G., et al., *Rotavirus alters paracellular permeability and energy metabolism in Caco-2 cells.* Am J Physiol Gastrointest Liver Physiol, 2000. **279**(4): p. G757-66.
30. Wise, C., ed. *Methods in Molecular Biology*. Epithelial Cell Culture Protocols. Vol. 188. 2002, Humana Press, Inc.: Totowa, NJ.
31. Leonard, M., et al., *Evaluation of the Caco-2 monolayer as a model epithelium for iontophoretic transport.* Pharm Res, 2000. **17**(10): p. 1181-8.
32. Grainger, C.I., et al., *Culture of Calu-3 cells at the air interface provides a representative model of the airway epithelial barrier.* Pharm Res, 2006. **23**(7): p. 1482-90.
33. Miyamoto, M., et al., *Effect of poly-L-arginine on the nasal absorption of FITC-dextran of different molecular weights and recombinant human granulocyte colony-stimulating factor (rhG-CSF) in rats.* Int J Pharm, 2001. **226**(1-2): p. 127-38.
34. Matsukawa, Y., et al., *Size-dependent dextran transport across rat alveolar epithelial cell monolayers.* J Pharm Sci, 1997. **86**(3): p. 305-9.
35. Sadeghi, A.M., et al., *Permeation enhancer effect of chitosan and chitosan derivatives: comparison of formulations as soluble polymers and nanoparticulate systems on insulin absorption in Caco-2 cells.* Eur J Pharm Biopharm, 2008. **70**(1): p. 270-8.
36. Yu, C.M., S. Mun, and N.H. Wang, *Phenomena of insulin peak fronting in size exclusion chromatography and strategies to reduce fronting.* J Chromatogr A, 2008. **1192**(1): p. 121-9.
37. Malvern. *Protein solutions in research and development*. 2010 [cited 2010 03/01/2010]; Available from: http://www.malvern.com/LabEng/industry/protein/protein_solutions.htm.
38. Carino, G.P., J.S. Jacob, and E. Mathiowitz, *Nanosphere based oral insulin delivery.* J Control Release, 2000. **65**(1-2): p. 261-9.
39. Jani, P., et al., *The uptake and translocation of latex nanospheres and microspheres after oral administration to rats.* J Pharm Pharmacol, 1989. **41**(12): p. 809-12.
40. Jung, T., et al., *Biodegradable nanoparticles for oral delivery of peptides: is there a role for polymers to affect mucosal uptake?* Eur J Pharm Biopharm, 2000. **50**(1): p. 147-60.
41. Vila, A., et al., *Design of biodegradable particles for protein delivery.* J Control Release, 2002. **78**(1-3): p. 15-24.
42. Brooking, J., S.S. Davis, and L. Illum, *Transport of nanoparticles across the rat nasal mucosa.* J Drug Target, 2001. **9**(4): p. 267-79.

43. de la Fuente, M., et al., *Nanoparticles as protein and gene carriers to mucosal surfaces.* Nanomedicine (Lond), 2008. **3**(6): p. 845-57.
44. Vllasaliu, D., et al., *Fc-mediated transport of nanoparticles across airway epithelial cell layers.* J Control Release. **158**(3): p. 479-86.
45. Seetharam, B., et al., *Identification of rat yolk sac target protein of teratogenic antibodies, gp280, as intrinsic factor-cobalamin receptor.* J Clin Invest, 1997. **99**(10): p. 2317-22.
46. Verroust, P.J. and E.I. Christensen, *Megalin and cubilin--the story of two multipurpose receptors unfolds.* Nephrol Dial Transplant, 2002. **17**(11): p. 1867-71.
47. Kozyraki, R., et al., *The intrinsic factor-vitamin B12 receptor, cubilin, is a high-affinity apolipoprotein A-I receptor facilitating endocytosis of high-density lipoprotein.* Nat Med, 1999. **5**(6): p. 656-61.
48. Chalasani, K.B., et al., *Effective oral delivery of insulin in animal models using vitamin B12-coated dextran nanoparticles.* J Control Release, 2007. **122**(2): p. 141-50.
49. Chalasani, K.B., et al., *A novel vitamin B12-nanosphere conjugate carrier system for peroral delivery of insulin.* J Control Release, 2007. **117**(3): p. 421-9.
50. Dix, C.J., et al., *The transport of vitamin B12 through polarized monolayers of Caco-2 cells.* Gastroenterology, 1990. **98**(5 Pt 1): p. 1272-9.
51. Russell-Jones, G.J., L. Arthur, and H. Walker, *Vitamin B12-mediated transport of nanoparticles across Caco-2 cells.* Int J Pharm, 1999. **179**(2): p. 247-55.
52. Russell-Jones, G.J., S.W. Westwood, and A.D. Habberfield, *Vitamin B12 mediated oral delivery systems for granulocyte-colony stimulating factor and erythropoietin.* Bioconjug Chem, 1995. **6**(4): p. 459-65.
53. Bose, S., et al., *Bipolar functional expression of transcobalamin II receptor in human intestinal epithelial Caco-2 cells.* J Biol Chem, 1997. **272**(6): p. 3538-43.

Chapter 4: The synthesis, characterisation and drug delivery application of the α-ω-aminohexylcarbamate derivative of Vitamin B_{12}

4.1 Introduction

The vitamin B_{12} (B_{12}) uptake system offers potential for enhancing the uptake of orally administered proteins, peptides and immunogens [1]. The oral delivery of large biological macromolecules is often impeded by the epithelial cell barrier and in the case of protein biologics, by proteolysis within the gastrointestinal tract. Efforts to enhance oral delivery have focused on ligands conjugated to the pharmaceutically active component and capable of exploiting specific receptor-mediated endocytosis (RME) to provide absorption. Assumptions are made that a ligand of choice will not affect the therapeutic activity of the drug following conjugation and that this complex will be internalised by the cells by RME mechanisms and subsequently transported across. It is also assumedthat the conjugation does not jeopardise the ligand-receptor interaction. Taking all this into consideration, it may be feasible to exploit these endocytic pathways for the import and transport of protein therapeutics across epithelial cells. In addition, oral delivery systems should provide protection to the pharmaceutically active component, the task typically given to the carriers/vectors encapsulating the bioactives. The B_{12} RME mechanism is an extensively studied system for the oral delivery of peptides and proteins, with uptake of B_{12} reported at ~ 1.4 µg per intestinal passage and multiple dosing achievable at 2-3 times per hour [2]. This chapter focuses on some of the details of B_{12} chemistry in the development of B_{12}-bioconjugates and nanocarriers and the importance for recognition of modified B_{12} by transport proteins. These have implications for B_{12}-conjugate uptake and transport across cells and utility in drug delivery.

4.1.1 Bioactivities of B_{12} conjugates

Early work employed B_{12} as a ligand (attachment *via* spacers to part of B_{12}), to aid in the internalisation of protein macromolecules. Russell-Jones and co-workers have shown that this system is capable of transporting luteinising hormone releasing factor

(LHRH)-analogues [3], granulocyte colony stimulating factor (G-CSF), erythropoietin, α-interferon [4, 5] and the LHRH antagonist Antide [2]. Reports claim that the *e*-monoacid conjugates possess 10-fold higher affinity for intrinsic factor (IF) and for Transcobalamin II (TCII) than the alternative *b*- and *d*-monoacids [6, 7]. Table 4.1 lists the peptide/protein B_{12} conjugates which have been reported in the literature. More recent work in the field has focused on both *in vitro* and *in vivo* studies of intestinal uptake of B_{12}-conjugated nanoparticles, with the aim of delivering much larger protein therapeutics such as insulin or G-CSF and to enhance the overall uptake capacity. If B_{12} is covalently coupled to a nanoparticle, which in turn entraps and protects a number of protein therapeutic molecules, this could permit effective delivery, *via* physiological B_{12} uptake and transport processes.

Molecule (direct conjugation and encapsulate insulin delivery)	**Size (kDa)**	**Conjugation site**	**Linker (coupling agent)[§]**	**Use**	**Year/Ref**
Direct Conjugation					
BS albumin	66.0	Phosphate	Phosphate-amine (EDAC)	NA	1971 [8]
YG-globulin	150.0	Phosphate	Phosphate-amine (EDAC)	NA	1971 [8]
HS albumin	66.0	*e*-acid	GABA (EDAC)	Antibody response	1979 [9]
IFN-con	22.0	Ribose-5'-OH	Glutaroyl (CDI)	24-28% activity*	1994 [10]
G-CSF	19.6	*e*-acid	Disulphide (SPDP)	61-66% activity[‡]	1995 [5]
			Amide (EDAC)	29-85% activity[‡]	
			Hydrazide (EDAC)	ND-100% activity[‡]	
EPO	34.0	*e*-acid	Amide (EDAC)	ND-34% activity[‡]	1995 [5]
			hydrazide (EDAC)	17-22% activity[‡]	
ANTIDE-1	1.6	*e*-acid	EGS (EDAC)	ND	1995 [3]
			Amide (EDAC)	30% IF recognition	
			Disulphide (SPDP)	65% IF recognition	
			Hindered thiol (SMPT)	54% IF recognition	
			Thioester (NHS ester of iodoacetic acid)	81% IF recognition	
			Transglutamase cleavable tetrapeptide (EDAC)	60% IF recognition	
ANTIDE-3	1.6	*e*-acid	EGS (EDAC)	ND	1995 [3]
			Amide (EDAC)	ND	
			Disulphide (2-iminothiolane)	ND	
			Hindered thiol (SMPT)	37% IF recognition	
			Thioester (NHS ester of iodoacetic acid)	65% IF recognition	
			Transglutamase cleavable tetrapeptide (EDAC)	48% IF recognition	
LHRH	1.2	*e*-acid	Amide (DCC/NHS)	45% absorbed	2000 [11]
DP3	0.9	*e*-acid	Amide (EDAC)	23% absorbed	2000 [11]
			hexyl (EDAC)	42% absorbed	
Insulin	5.7	Ribose-5'-OH	Amide (CDI, CDT)	26% drop in glucose	2007 [12]
Encapsulate insulin delivery					
B_{12}-coated dextran nano-particles	5.7	Ribose-5'-OH	Amide (CDI)	70-75% drop in plasma glucose	2007 [13]

Table 4. 1. B_{12}-protein/peptide bioconjugates (directly conjugated and encapsulate insulin delivery) reported in the literature.

Modified from [14]. *compared with native IFN-con; ‡compared with unconjugated G-CSF and EPO; [§]linker chosen on basis of yield/activity; ND:not determined; BS, HS: Bovine and human serum; IFN-con: Consensus interferon; G-CSF: Granulocyte-colony stimulating factor; EPO: erythropoietin; ANTIDE: N-Ac-D-Na(2)D, D-Phe (pCl), D-Pal(3)ser, Lys(Nic), D-Lys(Nic), Leu,Lys(IPr), Pro, D-Ala-NH2; LHRH: Lutenizing hormone-releasing hormone; DP3:Octapeptide (Glu-Ala-Ser-Ala-Ser-Tyr-Ser-Ala); GABA: y ami no butyric acid; EDAC: l-ethyl-3-(3-dimethylaminopropyl)carbodiimide; CDI: 1,1'-carbonyldiimidazole; SPDP: N-succinimidyl 3-(2-pyridyldithiio)-propionateJ; SMPT: 4-[(Succinimidyloxy)-carbonyl]-α-(2-pyridyldithio)toluene; NHS: N-hydroxysuccinimide; DCC: N,N'-dicyclohexylcarbodiimide; CDT: 1,1'-carbonyl-di-(1,2,4-triazole)T; EGS: Ethylene glycol bis(succinimidylsuccinate).

In order to exploit the B_{12} transport pathway for drug delivery, it is essential to understand the specific intracellular events occurring within enterocytes following RME of IF-B_{12}. However, the models describing the early phases of the B_{12} absorption pathway, including recognition by IF are incomplete [11]. Early studies implied that, with the exception of substitutions at the Co-β position (cyanide in native B_{12}), any other substitutions of the molecule jeopardise its recognition by IF [15, 16]. On the contrary, some groups report that IF binds more effectively to B_{12} conjugates [17]. In this regard, the solvent accessible surface of B_{12} is considered critical when designing B_{12}-based bioconjugates [14]. The solvent accessibility of TCII to B_{12} is around 6.5% (~80 $Å^2$). For IF, this exposure is even higher, at ~13% (~163 $Å^2$), with haptocorrin (HC) least accessible at 3.2% (~40 $Å^2$) [14, 18]. Undoubtedly, this exposure has significant implications when designing a B_{12}-conjugate, affecting binding to the transport proteins. B_{12} and the therapeutic molecule of interest can *either* be coupled directly together; can be held apart by 'spacer' units, *or* B_{12} can be conjugated to carriers, effectively entrapping the drug. Sites available for modification on B_{12} include the peripheral amides, hydroxyl groups, the cobalt (III) ion and the phosphate moiety [14]. However, it is important to note that not all of these modifications will retain biological recognition by the B_{12} transport proteins, thus rendering them ineffective as methods of attachment. It has been shown that successful modifications with B_{12} can occur at four major sites (Figure 4.1): i) through the 5'-hydroxy group of the ribose moiety of the α-tail [12], ii) through the 2'-hydroxy group of the ribose moiety of the α-tail [19], iii) to the peripheral corrin ring *e*-propionamide [20], and iv) to the cobalt cation [21].

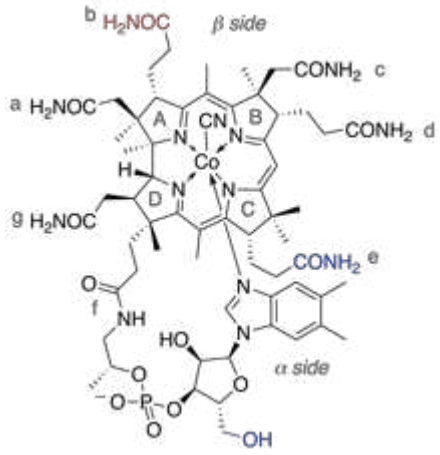

Figure 4. 1. Structure of vitamin B_{12} and potential conjugation sites.

The central cobalt atom is six-coordinated, with equatorial positions occupied by nitrogen atoms of corrin macrocycle. Corrin ring incorporates seven amide side chains, three acetamides (a,c,g) and four propionamides (b,d,e,f). Four pyrrole rings indicated by A,B,C, and D. Groups highlighted in blue have been used for conjugates that maintain binding to HC, TCII and IF. The portion highlighted red, namely the b-propionamide, has been used on conversion to the carboxylic acid, for HC-specific targeting [14].

Importantly, although much more information has been obtained in recent years on the nature of the binding between B_{12} and its transport proteins [22, 23], currently, very little is known about the effect of modifying B_{12} and its subsequent interaction with these proteins, on receptor binding. In 2010, a landmark paper by Anderson *et al*. [24], presented the structure of cubilin$_{(5\text{-}8)}$-IF-B_{12}. This report shed light on the (then) unknown interaction of the IF-B_{12} complex with cubilin (Figure 4.2), which provided new insights into the inevitable influence of B_{12}-conjugation on receptor binding. In addition, the results pointed to sites for directed mutagenesis of IF, facilitating the use of IF as a delivery agent [14]. As apparent in Figure 4.2, IF–B_{12} binds with high affinity to a region encompassed by four ($CUB_{5–8}$) of the 27 CUB domains in cubilin [25].

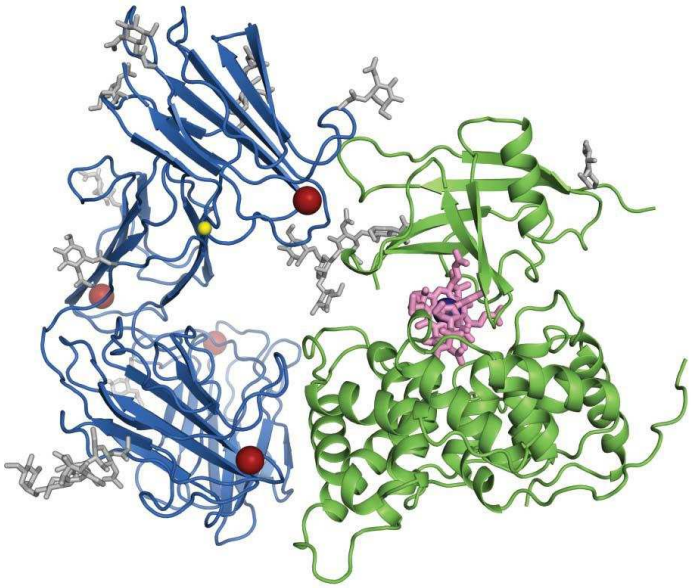

Figure 4. 2. Crystal structure of the Cubilin(5–8)-IF-B12 complex (PDB accession 3KQ4). $Cubilin_{(5–8)}$ is coloured in blue, IF is in green. Calcium ions are shown as red spheres and glycosylations as grey sticks. B_{12} and the cobalt atom are coloured pink and blue, respectively [24].

4.1.2 Chemistries for bioconjugation

McEwan's group (1999) [26] activated the ribose-5'-hydroxyl group of vitamin B_{12} via 1,1'-carbonyldiimidazole (CDI), 1,1'-carbonyldi(1,2,4-triazole) (CDT), or di(1-benzotriazolyl) carbonate (DBTC), and then reacted nucleophiles (aminoalkanes, diaminoalkanes and alkane diacid dihydrides) to attach the desired spacer (Figure 4.3).

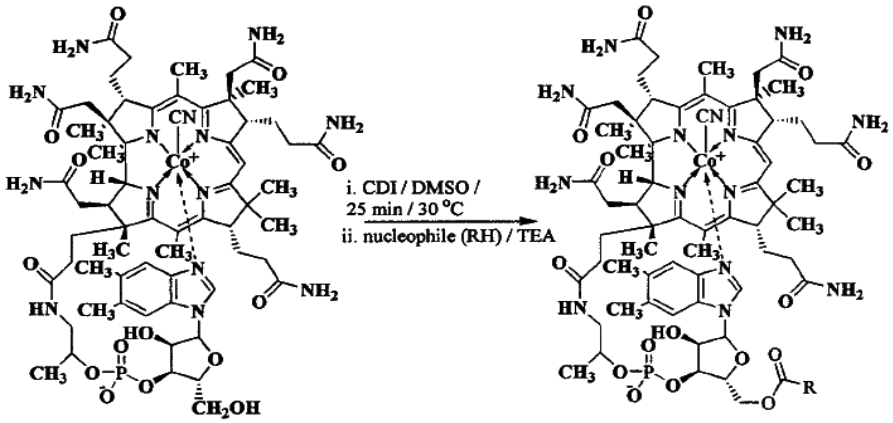

Figure 4. 3. Derivatisation of the ribose-5'-hydroxyl group of vitamin B_{12}.

Their work examined the binding affinity of the 5' carbamate derivatives for HC (which the authors refer to as 'non-IF') and IF and also the uptake of nanoparticles

conjugated to these derivatives by Caco-2 cells. The ribose-5'-carbamate derivatives were shown to possess similar binding affinity for IF as that of the *e*-monocarboxylic acid of B_{12}. Interestingly, the affinity for HC was similar to cyanocobalamin or even higher for some of the smaller derivatives. The data revealed that model polystyrene nanoparticles can be coupled to the ribose 5'-carbamate adipic dihydrazide B_{12} derivative and undergo higher levels of transport in Caco-2 cells compared to unmodified particles.

Other chemistries investigated for B_{12} conjugation include treatment and pre-activation of the 5'-OH group on B_{12} to generate an electrophilic intermediate (**1)**, which can be isolated prior to further modification by a variety of nucleophiles (Figure 4.4). Reaction with a glycine methyl ester followed by saponification yields a product with a carboxylic acid handle (**2**). Diamines such as 1,6 diaminohexane and 4,7,10-trioxa-1,13-tridecanediamine will react with (**1**), under dilute conditions, to yield products (**3-5**) with convenient terminal primary amine functionality.

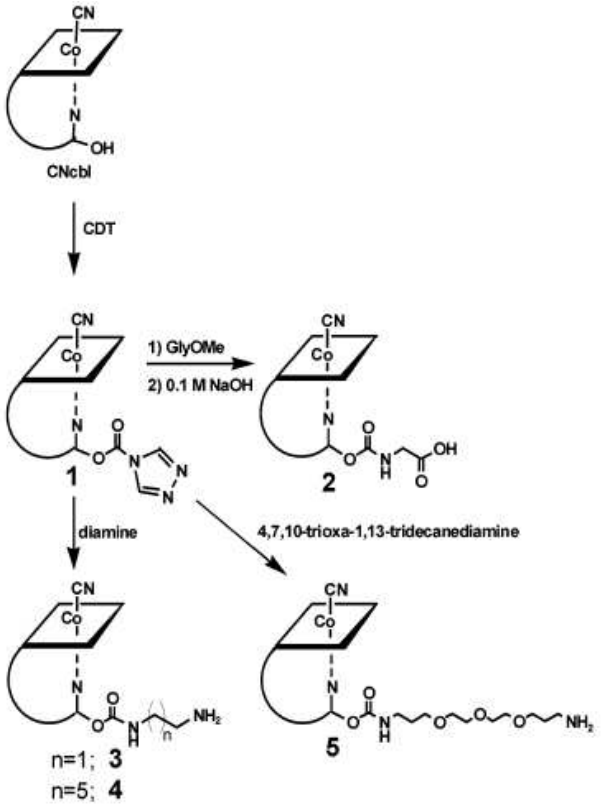

Figure 4. 4. A reaction scheme for deriving amino- and carboxyl- VB_{12} from cyanocobalamin-5'-OH modification [27].

To extend the utility of vitamin B_{12} derivatisation, fluorescent probes have been added to the 5' OH-ribose of vitamin B_{12}, as shown by Fedosov *et al*. [28] and in related work [29]. The declining application of radioactive ^{57}Co-labelled B_{12} on the grounds of safety has prompted investigation into the use of alternative methods for tracing B_{12} and its conjugates. The fluorescent conjugate of vitamin B_{12} (Figure 4.5) was synthesised through coupling 5- (and 6-) carboxyrhodamine succinimidyl ester to an amino derivative of B_{12} modified at the 5'-OH-ribose position.

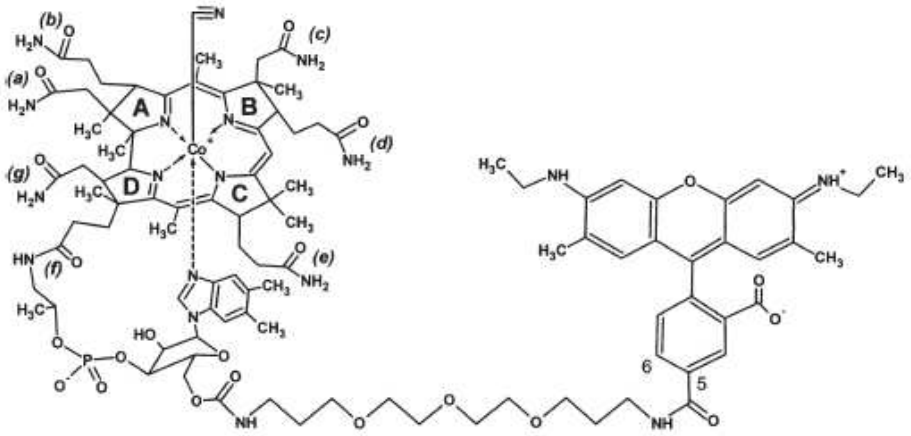

Figure 4. 5. Fluorescent conjugate of vitamin B_{12} [28].

Vitamin B_{12} can also be modified at the 5'-ribofuranosyl-OH position to yield a carboxylic acid handle in replacement of the aforementioned amino spacer. Such a procedure would involve reaction with glycine methyl ester followed by saponification [27]. This would permit conjugation to alternative nanoparticles or fluorescent dyes with reactive amine groups at their surface. This option of course widens the scope for application of B_{12} as a targeting moiety for the delivery of other components into or across cells or mucosal surfaces. Extensive uptake of vitamin B_{12} is considered to be a good marker of fast growing cancer cells. Imaging of tumours with the help of derivatives as detailed above, as well as targeted delivery of conjugated drugs is an exciting avenue for further B_{12}-related research.

The following list summarises reactions to functionalise B_{12} and derivatives [30]:

(i) Reaction of carboxy-VB_{12} with substituted amines

$$VB_{12}\text{-}COOH + NH_2\text{-}R \rightarrow VB_{12}\text{-}CONH\text{-}R + H_2O$$

(ii) Reaction of carboxy-VB_{12} with substituted phenols

$$VB_{12}\text{-}COOH + OH\text{-}Ph\text{-}R \rightarrow VB_{12}\text{-}CO\text{-}O\text{-}Ph\text{-}R + H_2O$$

(iii) Reaction of amino-VB_{12} with substituted carboxylates

$$VB_{12}\text{-}NH_2 + COOH\text{-}R \rightarrow VB_{12}\text{-}NHCO\text{-}R + H_2O$$

The work in this chapter describes the synthesis and characterisation of an amino-derivative of vitamin B_{12} which was activated at the 5'-hydroxyl group of the ribose moiety using 1,1'-carbonyldiimidazole (CDI). The resultant α-ω-aminohexylcarbamate B_{12} derivative was intended to allow reaction with carboxy-functional nanoparticles containing fluorescent dyes (as model carriers). In addition, previous studies have shown that the α-ω-aminohexylcarbamate B_{12} retains its binding activity for transcobalamin (II), haptocorrin, and IF [7, 31].The derivative prepared in this chapter was designed for transport studies of modified nanoparticles using *in vitro* cell models of the intestinal and bronchial epithelium *via* specific VB_{12} receptors found on the apical surface.

4.2 Methods

4.2.1 Synthesis of α-ω-aminohexylcarbamate vitamin B_{12}

1,1'-Carbonyldiimidazole (CDI, 260 mg, 0.32 mmol) was added to cyanocobalamin (1.0 g, 0.74 mmol), previously dissolved in anhydrous dimethyl-sulfoxide (12 ml). The mixture was stirred for 1.5 hrs at 30˚C. Dry 1,6-hexanediamine (314 mg, 2.7 mmol) was added and the mixture stirred at room temperature over 24 hrs. Moisture was removed from the reaction mixture through azeotropic distillation with toluene. The mixture was then poured into 30 ml ethyl acetate and left to stand. The mixture was transferred to glass vials and centrifuged using an MSE Centaur 2 at 14,000 rpm for 10 min. The supernatant was decanted and the residue sonicated for 5 min in acetone (50ml). The resultant supernatant was filtered and the solid washed with acetone. The crude product was purified by silica column chromatography (isopropanol 45%, *n*-butanol 30%, ammonia 4% and water 21%). Thin layer chromatography (TLC) was

carried out on pre-coated aluminium sheets with 0.2 mm silica gel F_{254} from Fluka (Sigma-Aldrich) (^{i}PrOH 30/*n*-BuOH 45/H_2O 21/NH_4OH 4/TEA 1 ml). Following TLC analysis, the relevant fractions were pooled and the solvent was removed using rotary evaporation. The remaining derivative in its solid form was flushed with N_2 before being stored at -20˚C for future use. All vitamin B_{12} and its analogues were treated as photo-sensitive. Reactions were therefore carried out in the dark and reagents and products were stored in aluminium foil.

4.2.2 Analytical purification and characterisation

Preparative high performance liquid chromatography (HPLC) of the product was carried out using a Waters Associates system using a Waters X-Bridge C18 column (100 x 19 mm). The vitamin B_{12} product was eluted with 100% water containing 10 mM ammonium formate and 0.1% (v/v) of ammonia solution (pH9.5, solvent A) and 95% acetonitrile (Fisher Chemical, HPLC gradient grade) with 5% water and 0.1% ammonia solution (in water) (solvent B), using a gradient system at 20 mL/min comprising linear gradients from 3% solvent B to 10% solvent B at 2 min, 35% solvent B at 11.5 min and 95% solvent B at 12 min. Purity (>95%) was determined using a Waters analytical HPLC system with a Waters 996 photodiode array detector at wavelengths 230-400 nm. NMR spectra of the product and starting material (cyanocobalamin) were obtained using a Bruker AV600 spectrometer equipped with a 5mm TXI (^{1}H, ^{13}C, ^{15}N) cryoprobe running TopSpin v2.1 in deutero-methanol (CD_3OD) solution. The method was adapted from McEwan *et al*. [26]. This part of the work was carried out by Ian Whitcombe and Adam Hold at UCB (Slough, Berkshire, UK). In addition, the ^{1}H-NMR data was interpreted with the assistance of Dr Francisco Fernández Trillo (University of Nottingham, UK).

4.3 Results & Discussion

4.3.1 Thin layer chromatography analysis

From the preparative silica column, 100 fractions of 12 ml were collected and all even number fractions (2-80 inclusive) were subjected to TLC analysis and compared against crude product and unmodified VB_{12} (cyanocobalamin) (Figure 4.6).

Separations proved difficult owing to slow migration behaviour, due to high solvent viscosity and the swelling of the silica during elution.

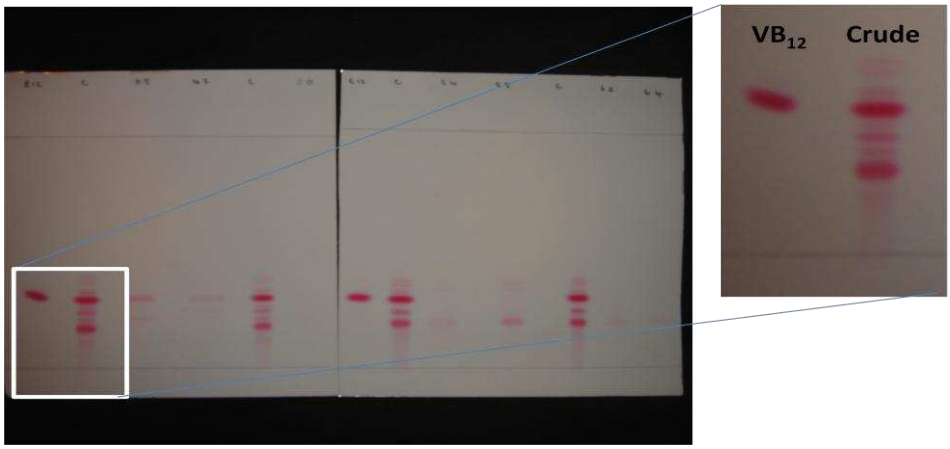

Figure 4. 6. TLC analysis comparisons of cyanocobalamin (VB_{12}) and crude product fractions.

(crude product fractions initially comprising multiple species, as shown by separation of a series of components with different Rf values). Fractions were collected until a single spot was obtained. Note: the product sourced from these fractions had a different Rf value to the starting material (VB_{12}).

In order to obtain better separations of the product material, the TLC eluent composition was altered slightly *via* the addition of more water. In addition, the TLC plate was pre-eluted in the eluent with the aim of neutralising the charges on the silica to aid eventual movement of the material. These changes in conditions were not effective in improving the separation. For optimised TLC eluent conditions, approximately 2 ml of methanol was added to each of the fractions prior to capillary spotting. Both crude product and B_{12} were dissolved in methanol for this experiment. In addition TEA (15% v/v) was added to the original eluent. These alterations resulted in a better separation, reduced spreading and faster migrations on the TLC plates. Fractions 54-64 inclusive were pooled on account of their migration behaviours on the TLC plate and their marked difference to Vitamin B_{12}.

Preliminary TLC analysis of the crude product revealed two distinct species according to their respective separations; one corresponding to vitamin B_{12} and another which had an R_f (retention factor) value of 0.11 (Figure 4.7), which agreed with the literature value quoted for the 1,6-diaminohexane (α-ω-aminohexylcarbamate) derivative of VB_{12} [26].

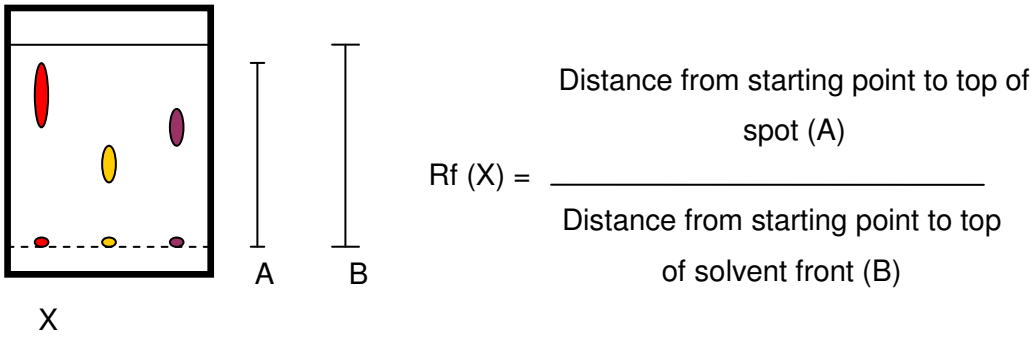

Figure 4. 7.Calculation of the retention factor value from TLC.

Following the same TLC procedure and using the same eluent conditions, a larger quantity of the crude product was separated via a capillary dragging spotting technique (Figure 4.8). This technique is commonly used to obtain small amounts of pure product from a crude mixture. The pure sample can be scraped from the plate using a scalpel blade - the silica can be removed *via* simple centrifugation to yield sufficient quantities of product for mass spectrometry analysis or associated analytical techniques.

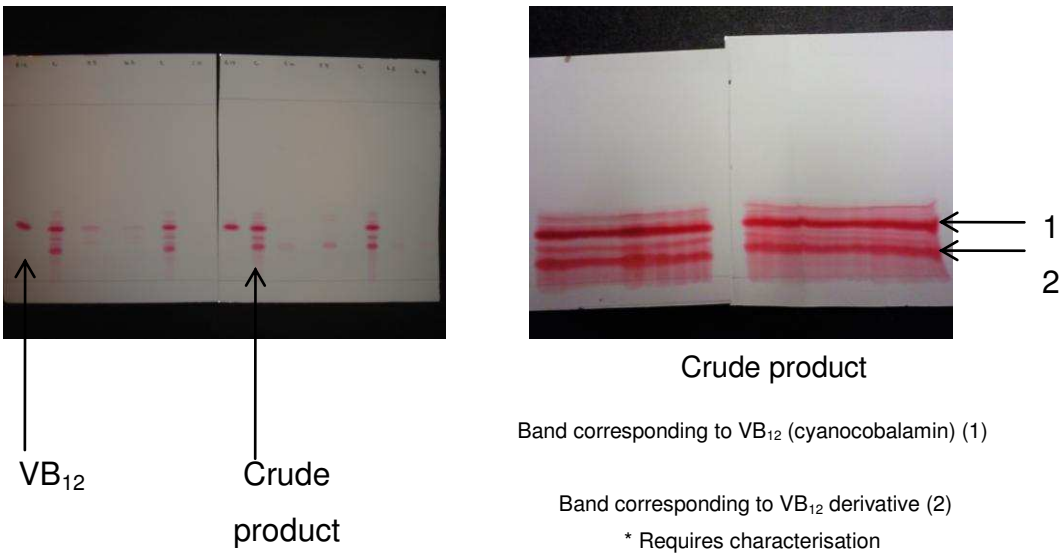

Figure 4. 8. Capillary dragging technique for mass spectrometry analysis.

4.3.2 HPLC purification and TOF-MS analysis

The purity (>95%) of the α-ω-aminohexylcarbamate derivative of B_{12} was confirmed by HPLC. Figure 4.9 shows liquid chromatographs of the product both before and after purification. The species of interest (i.e: pure α-ω-aminohexylcarbamate B_{12} derivative)

had a retention time of 2.53 min under the conditions used (see section 4.2.2). It is clearly apparent from the chromatographs that a high level of purity had been achieved, as depicted by a single clear peak at 2.53 min and a flat baseline (Figure 4.9, top), as compared with the crude material post silica-column (Figure 4.9, bottom), which comprised several peaks (of which the fraction of interest corresponded to the largest peak with a retention time of 2.54 min), and had a higher signal to noise ratio.

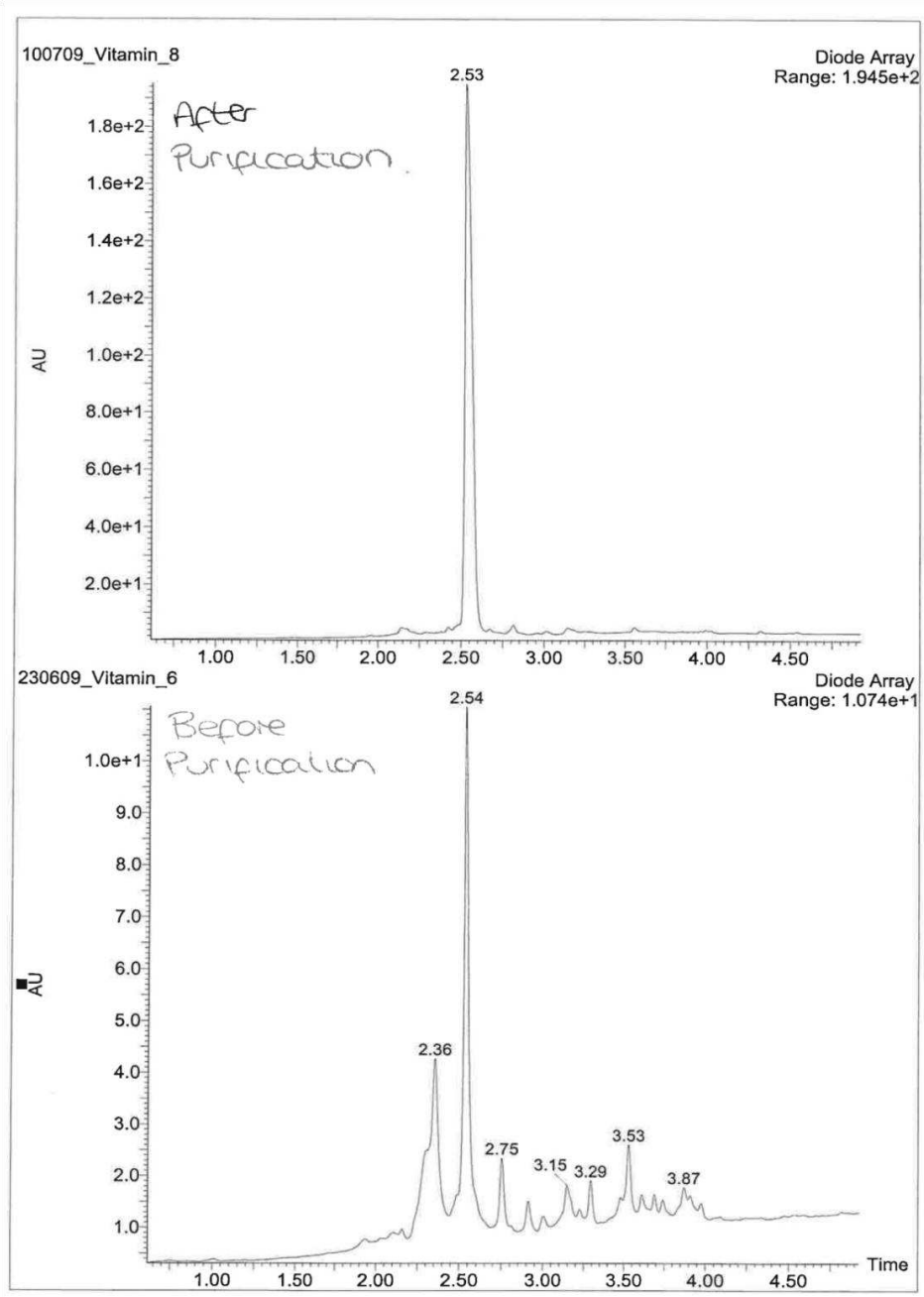

Figure 4. 9. Liquid chromatographs of crude (bottom; labelled 'before purification') and purified α-ω-aminohexylcarbamate vitamin B_{12} (top; labelled 'after purification').

TOF-MS analysis (Figure 4.10) revealed a peak (26% area) for 1500.39 m/z, appearing as doubly charged species at 750.19 $(M+2H)^{2+}$. Despite the later identification of peaks resembling product masses, the relative abundances were low. It is possible that fragments will vary in ionisation state depending on the matrix (protonation possible at the amino group as well as the linking phosphate).

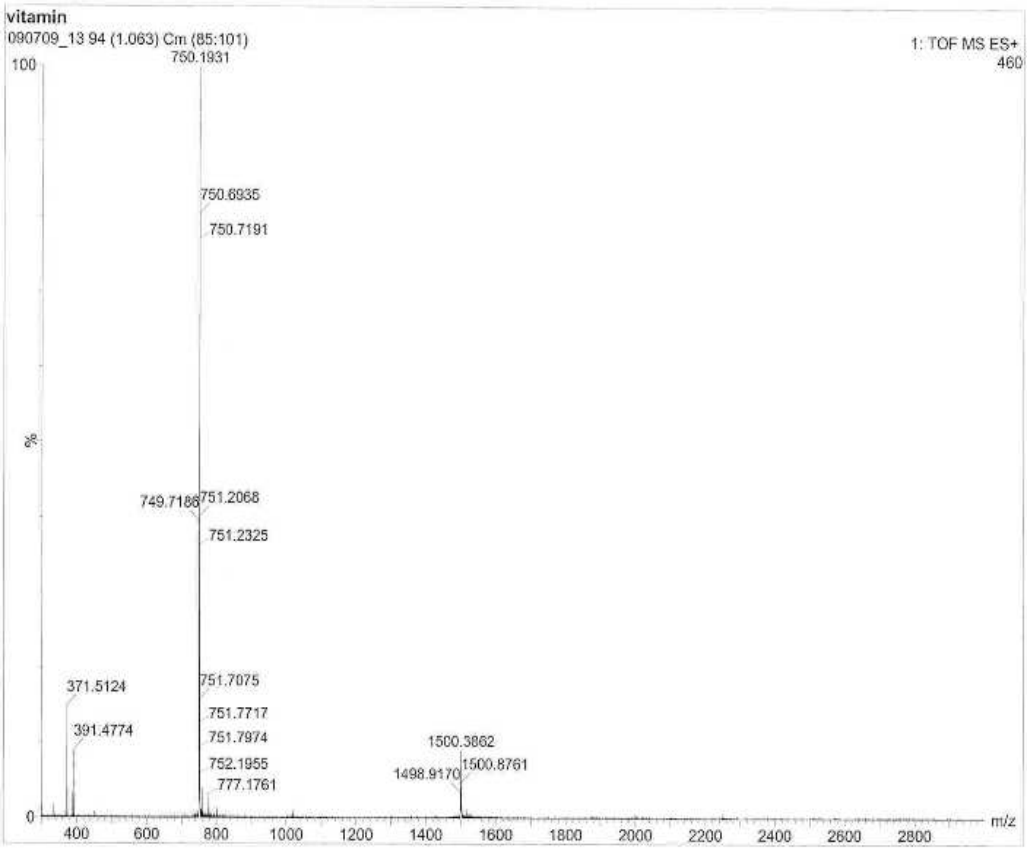

Figure 4. 10. TOF-MS of purified α-ω-aminohexylcarbamate vitamin B_{12}.

4.3.3 Characterisation of α-ω-aminohexylcarbamate VB_{12} derivative by ^{1}H-NMR

While NMR characterisation of the vitamin B_{12} derivative was of crucial importance to confirm identity and to assess purity, full peak assignment of the product was not necessary as the compound was not a new chemical entity. Comparison of the ^{1}H-NMR spectra obtained for the derivative with that of unmodified cyanocobalamin required particular attention to the assignment of peaks for the linker (hexanediamine) and any changes in coupling patterns on the ribose moiety resulting from modification of the ribofuranose 5'-hydroxyl moiety of B_{12}. Thus, the presence of these peaks in the product as absent in native B_{12} would give a good indication, when combined with MS

and HPLC analysis, that the desired compound, which has previously been reported [26, 27], was successfully synthesised. Careful inspection of the ^{1}H-NMR signals for the ribose ring revealed that its signals were significantly shifted after functionalisation, especially those closer to the 5' hydroxyl group. In addition, new resonances arising from the C6 linker (hexanediamine) could be observed (denoted by the letter **e**) (Figure 4.11). The signals arising from (**f**) and (**g**) on the hexanediamine linker remain hidden in this ^{1}H NMR spectrum. Therefore, accurate assignments of (**f**) and (**g**) required COSY experiments (see below).

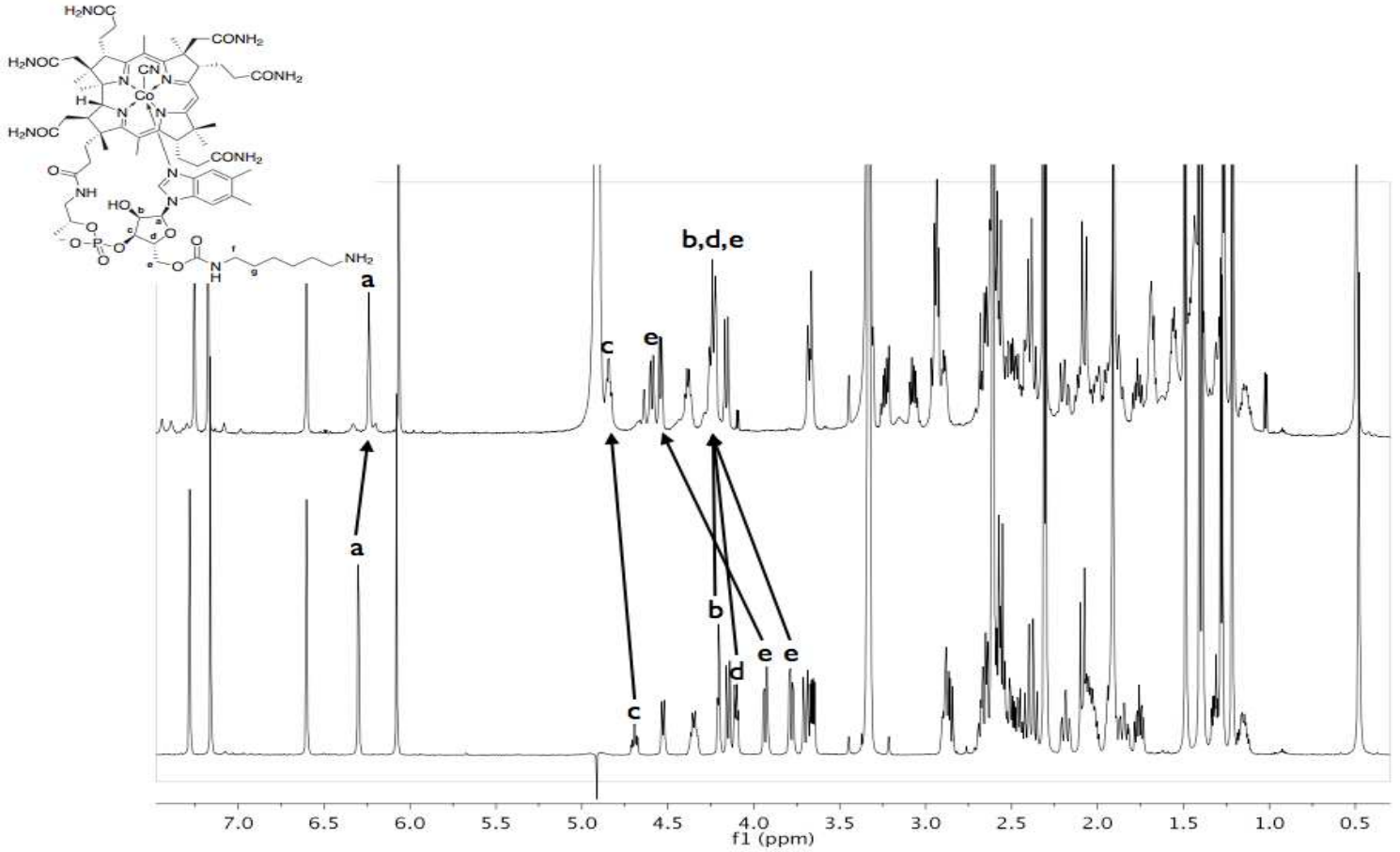

Figure 4. 11. ^{1}H-NMR (MeOD, 400 MHz) of α-ω-aminohexylcarbamate vitamin B_{12} (top) and cyanocobalamin (bottom).

Assignments of (f) and (g) were not possible at this stage of the analysis.

In order to assign more accurately the functional groups on the hexanediamine moiety of the VB_{12} derivative, two dimensional NMR spectroscopy experiments were carried out in addition to conventional NMR. Two dimensional homonuclear nuclear magnetic resonance experiments are recorded through *correlation spectroscopy* (COSY), of which several types include conventional correlation spectroscopy, *total correlation spectroscopy* (TOCSY) and *nuclear Overhauser effect spectroscopy* (NOESY) [32]. The COSY and TOCSY processes transfer magnetisation through the chemical bonds between adjacent protons. Because conventional COSY experiments are only capable of transferring magnetisation between protons on adjacent atoms (*i.e.* an alpha proton transfers magnetisation to the beta protons, the beta protons transfer to the alpha and gamma protons, if any are present, then the gamma proton transfers to the beta and delta protons, *etc*), TOCSY is often used in conjunction. Here, magnetisation is relayed through all protons on a portion of the molecule; thereby enabling a direct transfer among all the protons that are connected by adjacent atoms (*i.e.* the alpha and all other protons are able to relay magnetisation to the beta, gamma, delta and epsilon if they are connected by a continuous chain of protons).

TOCSY ^{1}H-NMR experiments were therefore used to selectively irradiate at specific proton positions to show adjacent coupling. The units of both axes represent chemical shifts. Following irradiation of a proton the ribose moiety of native cyanocobalamin (Figure 4.12 bottom, as depicted by the letter **a**), this signal is propagated to reveal adjacent coupling protons which can be assigned accordingly to each portion of the ribose ring (**b**, **c**, **d** and **e**). Comparison with the spectrum of the α-ω-aminohexylcarbamate derivative of vitamin B_{12}, i.e. the product (Figure 4.12, top), there is an apparent shift in field with a reduction in the number of signals, resulting from interference from the presence of the C6 linker. Despite a loss of propagation in the signal, making the assignment of (**f**) and (**g**) difficult, the comparison of the two very different spectra serves to show the marked presence of the C6 linker, giving confidence that successful derivatisation has taken place.

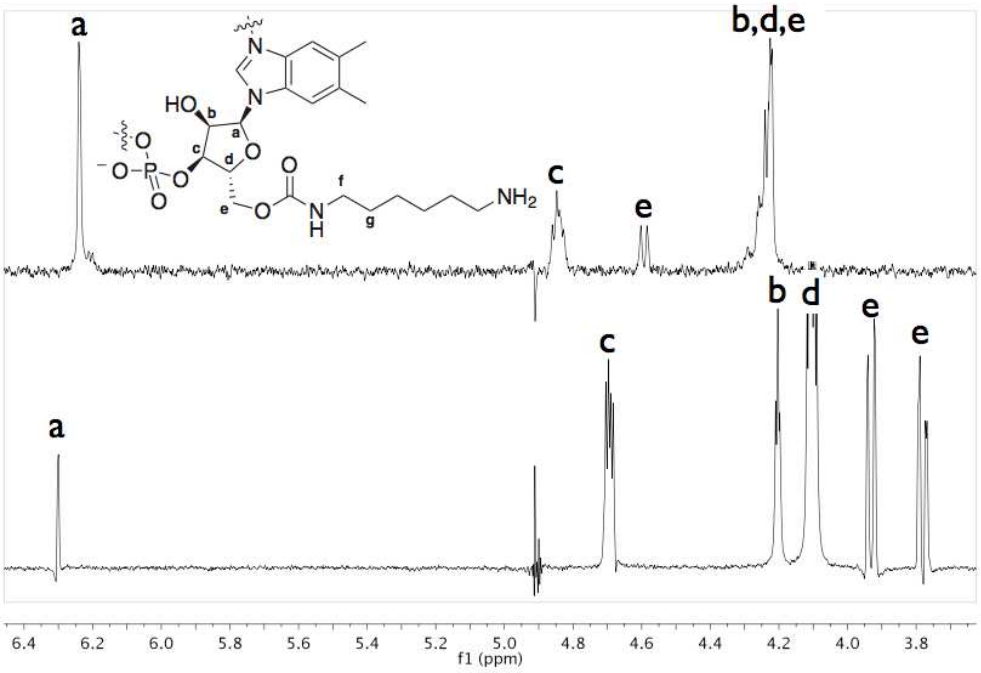

Figure 4. 12. 1D selective TOCSY 1H-NMR spectrum (MeOD, 600 MHz) of α-ω-aminohexylcarbamate vitamin B_{12} (irradiated at 6.24 ppm with 200 ms TOCSY mixing time) (top) and cyanocobalamin (irradiated 1t 4.7 ppm with 60 ms TOCSY mixing time (bottom).

Following irradiation of a proton the ribose moiety of native cyanocobalamin (bottom, as depicted by the letter a), this signal is propagated, to reveal adjacent coupling protons which can be assigned accordingly to each portion of the ribose ring (b, c, d and e).

COSY ^{1}H-NMR was used not only to cross-check previous assignments, but also to assign two new signals in the spectra for the derivative which were not found in the spectra for cyanocobalamin (starting material). And although these signals could be attributed to several regions on the molecule, ie: methyls at a chiral centre (Figure 4.13 blue/red arrows), it is likely that these arise from two key protons on the C6 linker itself (Figure 4.13, **f** and **g**), providing further evidence for identity of the α-ω-aminohexylcarbamate derivative of B_{12}. From this, a sound protocol for the amino-derivatisation of vitamin B_{12} with hexane-diamine and similar linkers such as 4,7,10-trioxa-1,13-tridecanediamine was verified.

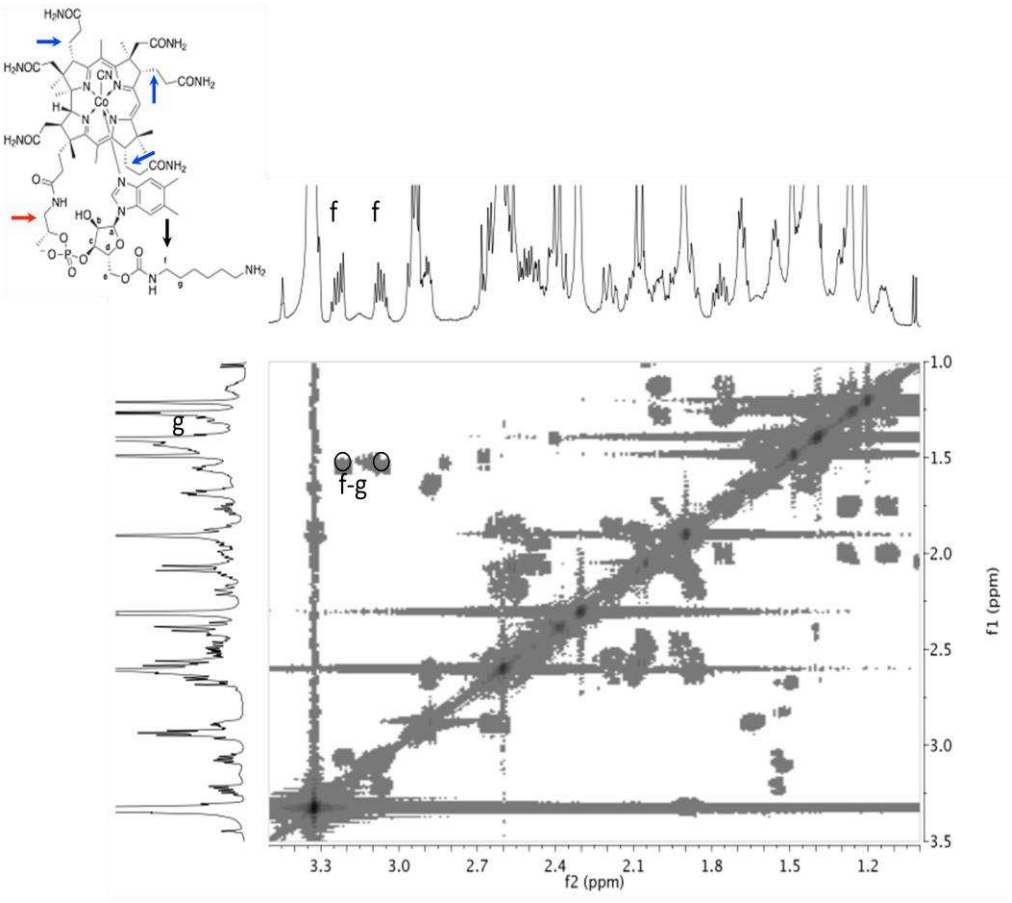

Figure 4. 13. COSY (MeOD, 300 MHz) of α-ω-aminohexylcarbamate vitamin B_{12} (2 scans per increment 2048 x 400 points).

4.3.4 Evaluation of analytical methods for B_{12} and B_{12}-conjugate/derivative characterisation

Further analytical methods available for the structural characterisation of vitamin B_{12} derivatives include spectrophotometry, chemiluminescence, atomic absorption spectrometry, electrochemical analysis, matrix-assisted laser desorption/ionisation (MALDI), time-of-flight mass spectrometry (TOF-MS) and high performance liquid chromatography (HPLC) amongst others [33]. The MS analysis of large molecules such as vitamin B_{12}/vitamin B_{12} analogues can be problematic owing to poor ionisation efficiency. The establishment of a sensitive high performance liquid chromatography-electrospray ionisation-mass spectrometry (HPLC-ESI-MS) method for B_{12} in food products was made possible through simple preparative processes and application of high cone voltages in a study carried out by Luo and co-workers (2006) [33].

Kinsel *et al*. [34] reported that the MALDI-TOF spectra of vitamin B_{12} resulted in low apparent abundances of the protonated molecule. Thus, obtaining sufficient sensitivity for detection remains a challenge from an analytical perspective. Despite the issues of low sensitivity and poor selectivity associated with structural determination of vitamin B_{12} and its derivatives, such quantitative data is necessary for future work as a means of confirming the precise identity of the synthesised material.

4.3.5 Evaluation of B_{12}-conjugate chemistry and uptake mechanisms

Initial studies focused on the design of uptake systems based on a simple covalent linkage to the modified B_{12} molecule [5, 17, 35]. However, it was soon evident that potential utility of such an uptake system was severely handicapped by the low absorption capacity (1 µg/dose in man); the difficulties in covalent attachment to B_{12} and exposure to proteolytic enzymes. With reference to the bioconjugation of B_{12} and the resulting biological efficacy of these systems, in one such study [3], the *in vitro* and *in vivo* potency of LHRH antagonists were found to be greatly reduced following direct conjugation to B_{12}, which the authors attributed to steric hindrance following the binding of the conjugate to the pituitary receptor for LHRH by the bulky B_{12} molecule being in close proximity to the peptide. In an attempt to overcome this problem, spacer groups attached by non-cleavable linkers were used to produce conjugates between the (2-aminoethyl) amido *e*VB_{12} and the ANTIDE analogues, thereby separating the bulky B_{12} group from the peptide. B_{12} conjugates formed with either, an anilido-(PA)/EGS-derived spacer, or a DSS-derived spacer, had an *in vitro* activity similar to that of the native peptide, suggesting that placing the B_{12} group at some distance from the ANTIDE restored the affinity of ANTIDE for its receptor. It was found that these conjugates had very low activities *in vivo*, possibly due to the removal of the conjugates from the circulation by the B_{12}-binding proteins (TCI and TCII). In order to minimise the possibility of steric hindrance produced by the presence of B_{12} in the conjugates, or reduced systemic bioavailability of the conjugates as a result of clearance by B_{12}-binding proteins, B_{12}-peptide conjugates were prepared using linkers which are potentially biodegradable *in vivo*. The disulphide-linked B_{12}-ANTIDE

conjugates were found to have a slightly reduced *in vitro* potency in comparison to ANTIDE or the anilido and EGS-linked B_{12}-ANTIDE conjugates. In contrast, the disulphide-linked conjugates showed a dramatic increase in their *in vivo* potencies when compared to the non-cleavable, extended spacer conjugates. A conjugate containing a spacer of similar length, including a non-cleavable thioether bond in place of the disulphide bond, showed greatly reduced *in vivo* activity, suggesting that the increased activity of the disulphide-linked conjugate was due its ability to be cleaved *in vivo*.

Russell-Jones and colleagues worked on amplifying the uptake capacity of the system by incorporating the therapeutic within biodegradable nanoparticles and then targeting them using B_{12} decoration on the surface [36]. To this end, a comparison study [26], tested the biological application of twelve biologically active ribose-5'-carbamate derivatives of vitamin B_{12}. The ribose-5'-hydroxyl group of vitamin B_{12} was activated through the use of 1,1'-carbonyldiimidazole (CDI), 1,1'-carbonyldi- (1,2,4-triazole) (CDT), or di(1-benzotriazolyl) carbonate (DBTC). Subsequent addition of an aminoalkane, diaminoalkane, or alkane diacid dihydrazide gave rise to vitamin B_{12} derivatives suitable for attachment to various proteins, peptides, or nanospheres to enable oral delivery utilising the vitamin B_{12} uptake system. The ribose-5'-carbamate derivatives were found to possess similar affinity for IF as that of the *e*-monocarboxylic acid of vitamin B_{12}. The affinity for HC was similar to cyanocobalamin or even greater for some of the smaller derivatives. Polystyrene nanoparticles derivatised with vitamin B_{12} 5'-carbamate adipic dihydrazide into Caco-2 cells showed significantly higher levels of transport of the particles, when compared to unmodified particles.

Chasalani *et al*. [13], evaluated the effect of cross-linking and the nature of the B_{12}-derivative on the biological effectiveness of B_{12}-conjugated dextran nanoparticles for delivery of insulin in animal models. In this study, amino alkyl B_{12} derivatives suitable for oral delivery were synthesised at the 5'-hydroxy ribose and *e*-propionamide sites *via* carbamate and ester/amide linkages, and were coupled to succinic acid modified

dextran nanoparticles of varied cross-linking. The vitamin B_{12} *e*-monoacid, which possesses ten-fold higher affinity for IF and for TCII compared to other isomers [37], was coupled with diamines. Low yields (19-20%) were obtained for both the amino ethyl *e*'VB_{12} and amino hexyl e'VB_{12} derivatives, compared to native B_{12}. Amino hexyl 5'O VB_{12} and amino dodecyl 5'O VB_{12} prepared in a related study were found to have 45-65% yields [38]. Despite the high yields (85-90%) obtained for additional acid derivatives such as 5'O succinoyl- and 5'O glutroyl $VB_{12,}$ the highly labile ester bond renders these derivatives inappropriate for drug delivery. Regarding the nanoparticle surface coverage by B_{12}, the binding of 5'O succinoyl- and 5'O glutroyl derivatives was also higher compared to the 5'O H and 5'O D derivatives (5.0 to 5.7 *Vs* 4.0 to 4.4% w/w particles). Thus, the results from this particular study revealed that B_{12} derivatives comprising an amide linkage and a long spacer were more efficacious in binding to nanoparticles compared with carbamate derivatives. Results from the *in vivo* studies showed that the hypoglycaemic action of the NP conjugates containing carbamate-linked B_{12} was higher compared to ester/amide linked VB_{12}. Moreover, the hypoglycaemic action was significantly higher with hexyl conjugates (initial phase) and the glutaroyl conjugates (secondary phase), compared to the control group. The authors postulated that the delayed action of the glutaroyl conjugates resulted from hydrolysis of the ester linkages in the gut and the cleaved ligand may compete for absorption with the NP's conjugate. Alternatively, they reasoned that the IF affinity for the glutaroyl derivative may be low. Overall, the authors affirmed that dextran NP conjugates comprising low levels of cross linking and coated with a carbamate derivative of B_{12} showed promise for the effective oral delivery of insulin in animal models.

4.4 Conclusion

In order to exploit the potential of the vitamin B_{12} transport system in the oral delivery of proteins, peptides and immunogens, the ligand itself requires manipulation to permit its attachment to the carrier system in question. Vitamin B_{12}, was therefore derivatised at the 5'-ribose position by an α,ω-aminohexylcarbamate group, as it has been suggested that these vitamin B_{12}- derivatives can maintain their binding affinity for IF

[26] and other B_{12}-binding proteins, while providing functionality to attach to carrier particles (Chapters 5-7). Furthermore, the carbamate link is stable under the acidic conditions of the stomach, [26] an absolute requirement for an intended oral delivery system. Selection of the α-ω-aminohexylcarbamate derivative of B_{12} was based on a sought compromise between its slightly reduced affinities for the B_{12} binding proteins (compared to the e-mono acid of VB_{12}); with provision of better synthetic yield, enhanced stability (without hydrolysable bonds) and reduced steric hindrance of nanoparticles on B_{12} by the presence of a six carbon linker. Activation of the 5'-hydroxyl group in the cyanocobalamin ribose ring with CDI followed by derivatisation with a slight excess of 1,6-hexanediamine proceeded successfully as shown by TLC analysis. Separated fractions from column chromatography were shown by ^{1}H-NMR and TOCSY and COSY experiments to contain the desired B_{12} derivative.

In a complementary procedure, the crude product was purified by HPLC and analysed by mass spectrometry. The spectrum obtained was consistent with ion fragments of the product although yields of the pure adduct were low. TOF-MS analysis revealed a peak (26% area) for 1500.39 m/z, appearing as doubly charged species at 750.19 $(M+2H)^{2+}$. Moreover, further smaller fragments were detected bearing closer resemblance to the expected molecular weight of the derivative (1498.61). The combined analyses gave sufficient indication of successful synthesis to allow exploration of the biological applications of this derivative following its conjugation to carboxylate PS nanoparticles.

4.5 References

1. Russell-Jones, G., *Utilisation of the natural mechanism for Vitamin B12 uptake for the oral delivery of Therapeutics.* Eur. J. Pharm. Biopharm., 1996. **42**(241).
2. Russell-Jones, G.J., *Oral delivery of therapeutic proteins and peptides by the vitamin B12 uptake system*. Peptide-based drug design: controlling transport and metabolism, ed. M.D. Taylor, and Amidon, G.L. 1995, Washington DC.: ACS.
3. Russell-Jones, G., Westwood, S.W., Farnworth, P.G., Findlay, J.K., and Burger H.G., *Synthesis of LHRH antagonists suitable for oral administration via the vitamin B12 uptake system.* Bioconjug. Chem., 1995. **6**: p. 34-42.
4. Habberfield, A.D., Jensen-Pippo, K, Ralph, L, Westwood, S.W and Russell-Jones, G.J., *Vitamin B12-mediated uptake of recombinant therapeutic proteins from the gut.* Int. J. Pharm., 1996. **145**: p. 1-8.
5. Russell-Jones, G.J., Westwood, S.W., Habberfield, A.D., *Vitamin B_{12}-mediated oral delivery systems for granulocyte-colony stimulating factor and erythropoietin.* Bioconjugate Chem., 1995. **6**: p. 459-465.
6. Wilson, S., Reinhard, K.S., Gao, X., *Drug delivery and targeting with vitamin B12 conjugates*. 2007, New York University: United States.
7. Pathare, P.M., Wilbur, D.S., Heusser, S., Quadros, E.V., McLoughlin, P., & Morgan, A.C., *Synthesis of cobalamin-biotin conjugates that vary in the position of cobalamin coupling. Evaluation of Cobalamin Derivative binding to Transcobalamin II.* Bioconjugate Chem., 1996. **7**: p. 217-232.
8. Hippe, E., E. Haber, and H. Olesen, *Nature of vitamin B 12 binding. II. Steric orientation of vitamin B 12 on binding and number of combining sites of human intrinsic factor and the transcobalamins.* Biochim Biophys Acta, 1971. **243**(1): p. 75-82.
9. Ahrenstedt, S.S. and J.I. Thorell, *The production of antibodies to vitamin B-12.* Clin Chim Acta, 1979. **95**(3): p. 419-23.
10. Habberfield, A.D., O. Kinstler, and C. Pitt, Patent US5574018: *Conjugates of vitamin B12 and proteins*. 1994.
11. Alsenz, J., Russell-Jones, G.J., Westwood, S., Levet-Trafit, B. & de Smidt, P.C., *Oral absorption of peptides through the cobalamin (Vitamin B12) Pathway in the Rat Intestine.* Pharm. Res., 2000. **17**(7): p. 825-832.
12. Petrus, A.K., et al., *Vitamin B12 as a carrier for the oral delivery of insulin.* ChemMedChem, 2007. **2**(12): p. 1717-21.
13. Chasalani, K.B., Russell-Jones, G.J., Jain, A.K., Diwan, P.V. & Jain, S.K., *Effective oral delivery of insulin in animal models using vitamin B12-coated dextran nanoparticles.* J Control Release, 2007. **122**: p. 141-150.
14. Clardy, S.M., et al., *Vitamin B12 in drug delivery: breaking through the barriers to a B12 bioconjugate pharmaceutical.* Expert Opin Drug Deliv, 2011. **8**(1): p. 127-40.
15. Jacobsen, D.W. and F.M. Huennekens, *Purification of B12-binding proteins using a photo dissociative affinity matrix.* Methods in Enzymology, 1986. **123**: p. 29-36.
16. Mathan, V.I., Babior, B.M., & Donaldson, R.M., *Kinetics of the attachment of intrinsic-factor-bound cobalamides to ileal receptors.* J. Clin. Invest., 1974. **54**: p. 598-608.
17. Habberfield, A.D., Jensen-Pippo, K., Ralph, L., Westwood, S.W., Russell-Jones, G.J., *Vitamin B_{12}-mediated uptake of erythropoietin and granulocyte colony stimulating factor in vitro and in vivo.* Int. J. Pharm., 1996. **145**: p. 1-8.
18. Wuerges, J., et al., *Vitamin B12 transport proteins: crystallographic analysis of beta-axial ligand substitutions in cobalamin bound to transcobalamin.* IUBMB Life, 2007. **59**(11): p. 722-9.
19. Wang, X., L. Wei, and L.P. Kotra, *Cyanocobalamin (vitamin B12) conjugates with enhanced solubility.* Bioorg Med Chem, 2007. **15**(4): p. 1780-7.

20. Alsenz, J., et al., *Oral absorption of peptides through the cobalamin (vitamin B12) pathway in the rat intestine.* Pharm Res, 2000. **17**(7): p. 825-32.
21. Ruiz-Sanchez, P., et al., *Syntheses and characterization of vitamin B12-Pt(II) conjugates and their adenosylation in an enzymatic assay.* J Biol Inorg Chem, 2008. **13**(3): p. 335-47.
22. Mathews, F.S., et al., *Crystal structure of human intrinsic factor: cobalamin complex at 2.6-A resolution.* Proc Natl Acad Sci U S A, 2007. **104**(44): p. 17311-6.
23. Wuerges, J., et al., *Structural basis for mammalian vitamin B12 transport by transcobalamin.* Proc Natl Acad Sci U S A, 2006. **103**(12): p. 4386-91.
24. Andersen, C.B., et al., *Structural basis for receptor recognition of vitamin-B(12)-intrinsic factor complexes.* Nature. **464**(7287): p. 445-8.
25. Kristiansen, M., et al., *Molecular dissection of the intrinsic factor-vitamin B12 receptor, cubilin, discloses regions important for membrane association and ligand binding.* J Biol Chem, 1999. **274**(29): p. 20540-4.
26. McEwan, J.F., H.S. Veitch, and G.J. Russell-Jones, *Synthesis and biological activity of ribose-5'-carbamate derivatives of vitamin B(12).* Bioconjug Chem, 1999. **10**(6): p. 1131-6.
27. Horton, R.A., Bagnato, J.D., Grissom, C.B., *Structural determination of 5'-OH α–Ribofuranoside Modified cobalamins via ^{13}C and DEPT NMR.* J. Org. Chem, 2003. **68**: p. 7108-7111.
28. Fedosov, S.N., Grissom, C.B., Fedosova, N.U., Moestrup, S.K., Nexo, E., Petersen, T.E., *Application of a fluorescent cobalamin analogue for analysis of the binding kinetics.* FEBS Journal, 2006. **273**: p. 4742-4753.
29. Grissom, C.B., West, F.G., McGreevy, J., Bentz, J.S., Cannon, M.J., *Fluorescent cobalamins and uses there of*. 2005, University of Utah research foundation, Salt Lake City, UT: US.
30. Russell-Jones, G.J., and Westwood, S.W., *Oral Delivery systems for microparticles*. 2000, Biotech Australia Pty, LTD.
31. Castle, W.B., *Cobalamin: Biochemistry and Pathophysiology*, ed. B.M. Babior. 1975, New York: John Wiley & Sons.
32. Wuthrich, K., *Protein structure determination in solution by NMR spectroscopy.* J Biol Chem, 1990. **265**(36): p. 22059-62.
33. Luo, X., et al., *HPLC-ESI-MS of vitamin B_{12} in food products and in multivitamins-multimineral tablets.* Analytica Chimica Acta, 2006. **562**: p. 185-189.
34. Kinsel, G.R., L.M. Preston, and D.H. Russell, *Fragmentation of vitamin B_{12} during 337nm Matrix-assisted Laser Desorption Ionisation.* Biol. Mass Spectrom., 1994. **23**: p. 205-211.
35. Russell-Jones, G.J., de Aizpurua, H.J., *Vitamin B_{12}: a novel carrier for orally presented antigens.* Proc. Int. Symp. Control. Release Bioact. Mater., 1988. **15**: p. 142-143.
36. Russell-Jones, G.J., Arthur, L., Walker, H., *Vitamin B_{12}-mediated transport of nanoparticles across caco-2 cells.* Int. J. Pharm., 1999. **179**(247-255).
37. Kolhouse, J.F. and R.H. Allen, *Absorption plasma transport, and cellular retention of cobalamin analogues in the rabbit: evidence for the existence of multiple mechanisms that prevent the absorption and tissue dissemination of naturally occurring cobalamin analogues.* J. Clin. Invest., 1977. **60**: p. 1381–1392.
38. Chasalani, K.B., Russell-Jones, G.J., Yandrapu, S.K., Diwan, P.V., Jain, S.K. , *A novel vitamin B12 nanosphere conjugate carrier system for peroral delivery of insulin.* Journal of Controlled Release, 2007. **117**: p. 421-429.

Chapter 5: Epithelial transport of nanoparticles: pathway switching through bioconjugation

5.1 Introduction

Synthetic drug carriers that exploit natural cellular transport pathways are highly desirable for diagnostic and therapeutic applications [1, 2]. Of particular interest are nanoparticulate carriers that resemble viruses in their ability to target and be internalised by cells, but which are not infective or toxic. Features of viruses important in their cellular trafficking are their size (50-150 nm range) and their functional surface ligands, especially for cellular and sub-cellular receptors. It is not surprising therefore that many synthetic drug delivery systems for intracellular delivery have been based on virus-inspired designs [3, 4]. These typically involve a therapeutic compound incorporated into a nanoscale carrier 'core', which is coated with ligand(s) aimed to specifically guide the carrier towards a particular intracellular pathway, enabling delivery of the incorporated therapeutic to a desired intracellular location [5]. However, the conjugated-carrier may not adopt the assumed ligand-directed pathway, as demonstrated by a recent landmark paper [6], which indicated that some trafficking pathways can be perturbed by synthetic nanoparticles in ways that differ from the transport activated by the ligand functionality alone.

In this chapter, the work set out to probe whether a ligand-mediated pathway, well-characterised for transport of molecules into and through the epithelial cells of the gut, could be exploited by model nanoparticle drug carriers for effective systemic delivery of biotherapeutics *via* mucosal surfaces. Vitamin B_{12} was selected as the ligand, as its intestinal uptake has already been considered for oral delivery of biotherapeutics [7-10]. Previous attempts to deliver biotherapeutics directly conjugated to vitamin B_{12} resulted in loss of therapeutic activity due to digestion of the labile biotherapeutic in the gastrointestinal tract [11, 12]. More recently, vitamin B_{12}-conjugated nanoparticulate carriers have been evaluated in order to incorporate and protect the biotherapeutic [10, 13] (as discussed in Chapter 4).

Importantly however, the use of B_{12}-conjugated nanocarriers to deliver biotherapeutics across the intestinal surface assumes that the B_{12}-nanoparticles traverse the epithelium in a manner that follows the soluble vitamin B_{12} pathway (Chapter 1, section 1.5.2.3), *i.e.* the attached nanoparticle does not perturb the transport pathway. This assumes cellular internalisation of the entire cubilin receptor-intrinsic factor-B_{12}-nanoparticle complex bound to megalin *via* clathrin-coated vesicles (Figure 5.1) [14, 15], followed by an endosomal stage where the cubilin and megalin receptors dissociate from the complex and recycle to the epithelial cell surface. The remaining intrinsic factor (IF)-B_{12}-nanoparticle complex would then be transported to the lysosome where, in the case of soluble B_{12}, IF protein is degraded to release free B_{12} [16]. The vitamin B_{12}-nanoparticles would then be transported out of the lysosome by an as yet unidentified mechanism, as B_{12} is assumed to do [17]. Of key significance is that, at the start of this study, the mechanism of cellular internalisation and intracellular trafficking of B_{12}-conjugated nanoparticles had not been documented.

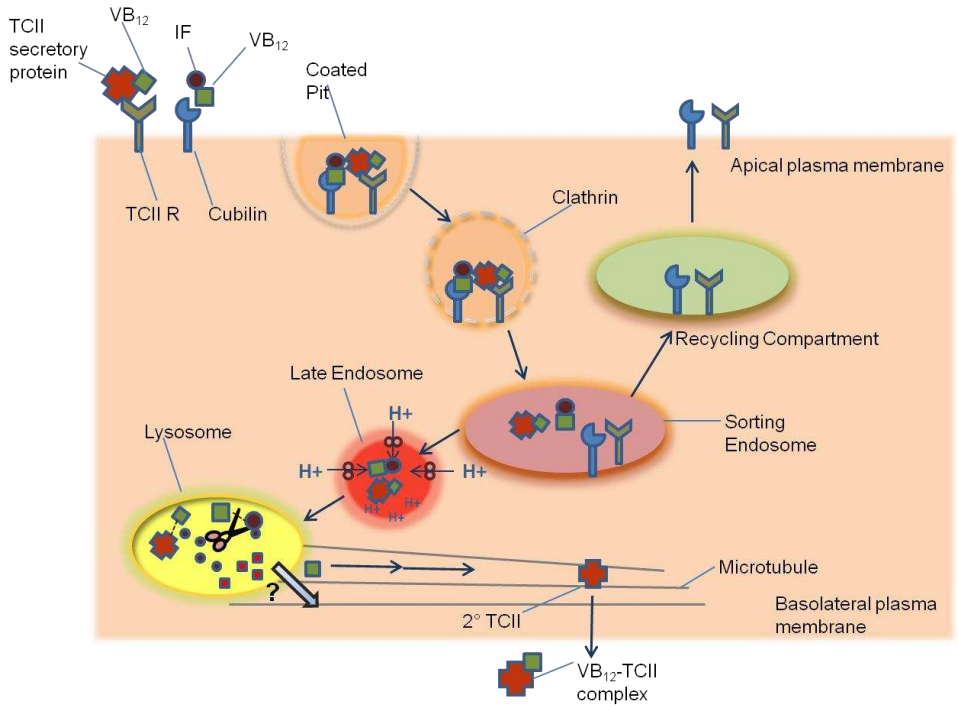

Figure 5. 1. Schematic representation of VB_{12}-cellular internalisation and trafficking, *in vivo*.

Note that for the sake of simplicity, megalin was in this instance, not depicted in the figure.

The principal aim of this work, therefore, was to probe the mechanisms of entry and transport across the cells of nanoparticles conjugated to vitamin B_{12}, and so demonstrate a model system that might have wider implications for delivery of therapeutic and/or diagnostic nanoparticles in general [18-20]. The model carrier was prepared from functionalised polystyrene (PS) nanoparticles spanning the 50-200 nm size range, covering viral dimensions as well as sizes reported optimal for endocytotic processes [21]. In order to display vitamin B_{12} as a ligand on the nanoparticle surface free from steric hindrance, an α-ω-aminohexylcarbamate derivative of B_{12} was prepared (Chapter 4) and conjugated to carboxylated PS nanoparticles by standard carbodiimide chemistries. For the cell studies, a cell culture model of the intestinal epithelium was utilised; the Caco-2 (human intestinal) cell line when cultured on permeable membrane supports, is the most extensively used model for vitamin B_{12}-mediated drug delivery [8, 22, 23]. These cell cultures exhibit unidirectional transport of vitamin B_{12} in the apical-to-basolateral direction [8], and also in an IF dependent and IF-independent fashion. The latter is likely due to the expression of the Transcobalamin II receptor (responsible for the internalisation of transcobalamin II *in vivo*) on their apical surface [24]. The suitability of the Caco-2 cell culture as an epithelial model was verified by confirming the expression of cubilin receptor (a prerequisite for a functioning vitamin B_{12} transport pathway, see chapter 3) as well as the presence of functioning caveolae and clathrin mediated endocytic pathways.

The purpose of this work was to assess the cellular uptake, transport and intracellular trafficking behaviours of B_{12}-conjugated nanoparticles in Caco-2 monolayers. In this respect, transport studies were conducted in the presence of chemical inhibitors of clathrin and caveolae-mediated endocytosis. Furthermore, lysosomal markers were used to identify the sub-cellular localisation of these nanoparticles. Importantly, comparisons of the pathways for cell uptake and transport were made between B_{12}-bearing nanoparticles and their unmodified counterparts, in addition to the soluble vitamin B_{12} ligand. Overall, this study aimed to assess whether the attachment of nanoscale carriers to natural ligands can alter their cellular trafficking behaviour in a way that can be exploited for the delivery of biotherapeutics.

5.2 Methods

5.2.1 Preparation and characterisation of the α-ω-aminohexylcarbamate derivative of vitamin B_{12}

The chemical synthesis and characterisation of the VB_{12} α-ω-aminohexylcarbamate derivative was described in chapter 4 (sections 4.2.1 and 4.2.2).

5.2.2 Preparation of vitamin B_{12}-conjugated nanoparticles

Fluorescent carboxylate Yellow Orange nanoparticles (YO, fluorescence spectrum equivalent to rhodamine, PolySciences Inc) of 50 nm, 100 nm and 200 nm (1 ml of 2.69, 2.6 and 2.63% aqueous suspension, respectively) were modified with the α-ω aminohexylcarbamate vitamin B_{12} derivative (10 mg) by activation with 1-ethyl-3-[3-Dimethylaminopropyl]carbodiimide (EDAC), in the presence of N-hydroxy-succinimide (NHS). The reaction was left to proceed for 5 hrs followed by incubation with glycine (100 mg/ml) in 50 mM carbonate buffer, pH 9.5. The nanoparticles were dialysed extensively against distilled water over 24 hrs, with the water exchanged at regular intervals.

5.2.3 B_{12}-conjugated nanoparticle characterisation

The mean diameter of both B_{12}-conjugated nanoparticles and 'unmodified' nanoparticles (50, 100 and 200 nm nominal diameter) was determined by Dynamic Light Scattering (DLS) using a Viskotec 802 system. The nanoparticles (all 400 µg/ml), suspended in HBSS at pH 7.4 (to replicate the conditions in which the nanoparticles were applied to cells) were then analysed using the default programme setting, wherein the optimal intensity count was 300 k counts and the temperature was 25°C. Omnisize software was used to calculate the particle size. The experimental values obtained were then exported and plotted in Microsoft Excel. The zeta potential of the nanoparticles (suspended in HBSS, pH 7.4) was measured using a Zetasizer ZS (Malvern Instruments, UK). The reported value represents the mean of 3 measurements.

Fluorescence emission spectra of both vitamin B_{12}-conjugated and unmodified nanoparticle suspensions in HBSS (400 µg/ml) were recorded on a Cary Eclipse fluorimeter (λ_{ex} = 529 nm). The unmodified nanoparticle suspensions were titrated with increasing volumes of soluble cyanocobalamin (present in nanoparticle suspensions in order to prevent dilution of nanoparticles upon titration). 200 µg of vitamin B_{12} was added to 500 µl of 400 µg/ml nanoparticle suspensions. This was then used to titrate the unmodified nanoparticles, with the suspension added to unmodified nanoparticles in steps of 5-20 µl. Spectra were recorded after each addition and calibration curves were generated based on percent weight vitamin B_{12} against fluorescence intensity. The concentration of carboxyl groups on unmodified YO-NP was calculated by potentiometric titration. Experiments were conducted with unmodified nanoparticles (50, 100, 200 nm), using a Fisher brand® Hydrus 600 pH meter and a Thermo fisher orion 911 pH electrode at room temperature (23 ℃). Unmodified nanoparticles were diluted 1:5 using distilled water obtained from an ELGA purification system (resistivity 15 M.Ω.cm). The pH of the nanoparticle suspensions was lowered to 1.70 using 1M HCl. Stepwise additions of 0.1M NaOH were made until neutral pH was attained. The concentration of carboxyl groups was calculated from the difference between the number of moles of HCl originally added and those of NaOH used for neutralisation. The density of the carboxylic acids on the surface (d_a) expressed in number per nm^2 was calculated using the equation below:

$$d_a = \frac{mol_a \times N_A}{NP \times SA}$$

Where:

- mol_a is the calculated moles of acid
- N_A is Avogadro's number
- NP is the number of particles (calculated from the density provided by the manufacturer and corrected for dilution).
- SA is the surface area of the particle expressed in nm^2.

5.2.4 Cell Culture

The protocols for routine culture of Caco-2 cells are described in Chapter 2 (sections 2.1 and 2.2).

5.2.5 Cellular uptake and transport studies of B_{12}-conjugated nanoparticles

Culture medium was removed from filter-cultured Caco-2 cells and replaced with Hank's Balanced Salt Solution (HBSS), buffered with 2-[4-(2-hydroxyethyl)piperazin-1-yl]ethanesulfonic acid (HEPES, 20mM) and cell monolayers incubated for 45 min. Unmodified YO nanoparticles (50, 100, 200nm) and vitamin B_{12}-conjugated nanoparticles were suspended in HBSS/HEPES to achieve a final concentration of 400 µg/ml. 3 µg of recombinant human intrinsic factor (rHUIF, Autogen Bioclear Ltd) was added per 1 ml of 400 µg/ml suspension of B_{12}-conjugated nanoparticles. This amounted to 5.6, 45.1 and 360.9 molecules of IF *per* one nanoparticle for 50, 100 and 200 nm nanoparticles, respectively. The solution was incubated at 37˚C prior to their application to cells. Following a routine assessment of TEER (as described in chapter 2, section 2.2.2), nanoparticle suspensions (0.5 ml) were applied to the apical chamber of triplicate wells and the Caco-2 cultures incubated at 37˚C over 3 hrs. At 30 minute sampling intervals, 100 µl was removed from the basolateral side and analysed for fluorescence. Sample volumes were replaced with 100 µl of HEPES/HBSS to maintain a constant basal volume. Internalised fluorescence (indicating nanoparticle uptake) was determined by cell lysis using 0.2% Triton X-100 (Fluka) (10 min incubation). Cell uptake of nanoparticles was quantified by fluorescence (Dynex, microplate reader, 529 nm/546 nm) using calibration curves. The effect of a 'competitor' on receptor-mediated uptake of nanoparticles was assessed in the presence of excess cyanocobalamin (500 µg per 0.5 ml of vitamin B_{12}-conjugated nanoparticles). Soluble vitamin B_{12} transport studies were conducted in a similar manner to nanoparticle transport experiments, but instead of fluorescence detection, vitamin B_{12} was quantified by UV absorbance (350 nm, Beckman Coultier DU 800 UV spectrophotometer).

5.2.6 Immunostaining for clathrin and caveolin-1

Immunostaining for clathrin and caveolin-1 in Caco-2 monolayers was conducted in the manner described in Chapter 2, section 2.2.5.5.

5.2.7 mRNA expression of Caveolin-1

mRNA was isolated from filter-cultured Caco-2 cells on day 7, day 14 and day 21 of transwell® culture using the method described in section 2.2.6.1.1. cDNA was synthesised using the protocol described in section 2.2.6.1.2. A conventional PCR was performed on the PTC-200 Thermal Cycler to amplify the cDNA which was then visualised using gel electrophoresis (section 2.2.6.2). The expected size of the amplified cDNA fragment was 361bp (see section 2.2.6.2.1 for primer details).

5.2.8 Lysosomal cell trafficking studies

Caco-2 cells were cultured as polarised monolayers in the manner described previously (chapter 2, section 2.2.1). Lysotracker™ Green DND-26 (Invitrogen) was diluted (according to the manufacturer's instructions) in HBSS and nanoparticles (unmodified and vitamin B_{12}-conjugated) were suspended in this solution to achieve a final incubation concentration of 250 µg/ml. The lysotracker-containing nanoparticle suspensions (0.5 ml) were applied to the apical side of the cell monolayers and incubated at 37˚C for 2 hrs. The IF-B_{12}-nanoparticle composites were prepared as described above. For anti-LAMP 1 immunostaining studies, nanoparticles (unmodified and B_{12}-conjugated) were applied (in HEPES-buffered HBSS) to the apical side and the cells incubated at 37°C over 2 hrs. The reader is referred to Chapter 2, section 2.2.5.3 for further experimental details of sample preparation for confocal microscopy.

5.2.9 Clathrin and caveolae inhibition studies

Caco-2 cell monolayers were treated with inhibitors of specific endocytic pathways, genistein (200 µM), filipin (5 µg/ml) or chlorpromazine (10 µg/ml), dissolved in HBSS/HEPES for 1hr at 37°C prior to the addition of nanoparticles [25]. Unmodified and vitamin B_{12}-conjugated nanoparticles (in the presence of IF) were applied suspended in HBSS/HEPES (400 µg/ml) containing one of the above inhibitors and incubated for 3 hrs. At 30-min sampling intervals, 100 µl samples were removed from

the basolateral side for fluorescence determination in order to quantify the transport of the nanoparticles (as described in section 5.2.5). At the final time point, nanoparticle internalisation was determined by cell lysis also described in section 5.2.5. For the potassium depletion study, conducted to perturb clathrin-mediated endocytosis [25, 26], Caco-2 cells were washed once with potassium free buffer (pH 7.4), containing 140 mM NaCl (BDH, Analar®), 20 mM HEPES, 1 mM $CaCl_2$, 1 mM $MgCl_2$ and 1 mg/ml D-glucose (GIBCO™), followed by a wash with a hypotonic buffer (potassium free buffer diluted 1:1 with water). The cells were then washed again twice with potassium free buffer. Control wells were treated with buffer (pH 7.4), containing 140 mM NaCl, 20 mM HEPES, 1 mM $CaCl_2$, 1 mM $MgCl_2$, 1 mg/ml D-glucose and 10 mM KCl. Vitamin B_{12}-conjugated nanoparticles were incubated with the cells in potassium free or potassium containing buffer as indicated. Subsequently, nanoparticle uptake and transport was determined by fluorescence. As a control for clathrin-mediated uptake [25], FITC-transferrin (Autogen Bioclear, LTD) (dissolved in HBSS to a final incubation concentration of 100 µg/ml), was applied to the apical chambers in the presence or absence of chlorpromazine (10 µg/ml), a specific inhibitor of clathrin-mediated endocytosis. In addition, native cyanocobalamin (vitamin B_{12}), in the presence of IF was also applied in conjunction with the same inhibitor, to confirm the route of internalisation of the soluble ligand and cell uptake and transport was determined via UV-absorbance at 350 nm. To assess the specificity of filipin as an inhibitor of caveolae-mediated uptake [27, 28], transport of Alexa Fluor 488-labelled cholera toxin subunit B (Invitrogen, applied at 5 µg/ml) was determined following its application with or without filipin (5 µg/ml).

Importantly, in order to verify that there were no adverse of toxic effects on cell monolayer by treatment with these agents, TEER reversibility measurements were carried out in a separate series of experiments. Cell monolayers were incubated with chlorpromazine (1.25-10 µg/ml), filipin (1.25-5 µg/ml), K+ depleting medium and Genistein (at a fixed concentration of 200 µM) and TEER was measured every 30 min over 3 hours in HEPES/HBSS in the presence of the inhibitors. In addition TEER measurements were recorded in culture medium before incubation with the inhibitor

and 24 hours after incubation to assess for permanent damage to the cell monolayer (note: after 3 hours, the chemical agents were removed and culture medium replaced).

5.3 Results & Discussion

5.3.1 Characterisation and conjugation of α-ω-aminohexylcarbamate vitamin B_{12} to functionalised nanoparticles

Fluorescent YO PS nanoparticles were selected for surface modification with the α-ω-aminohexylcarbamate vitamin B_{12} derivative. These nanoparticles not only have surface carboxylic acid groups, permitting attachment of derivatised vitamin B_{12} but also contain a rhodamine-like fluorophore, allowing easy quantitation. In order to functionalise the surface of YO nanoparticles, vitamin B_{12} was amino derivatised using a 5'-ribose carbamate linkage (Chapter 4), as it has been suggested that these vitamin B_{12}-carbamate derivatives provide an increased yield and affinity towards intrinsic factor [29]. Furthermore, the carbamate should be stable under the acidic conditions of the stomach [29], an absolute requirement for oral delivery. Therefore, the 5'-hydroxyl group in cyanocobalamin's ribose ring was activated with CDI to be immediately derivatised with a slight excess of 1,6-hexanediamine (Figure 5.2a). Successful derivatisation of cyanocobalamin was confirmed by means of NMR, MS and HPLC (see Chapter 4, section 4.3). The synthesised α-ω-aminohexylcarbamate-vitamin B_{12} derivative was reacted with carboxylated functionalised YO polystyrene nanoparticles in the presence of 1-ethyl-3-[3-dimethylaminopropyl]carbodiimide (EDAC) and N-hydroxy-succinimide (NHS) and purified by dialysis to yield the desired vitamin B_{12}-conjugated nanoparticles (Figure 5.2c).

In addition, it was observed that the fluorescence intensity of nanoparticles decreased following the conjugation process. This fluorescence quenching property of vitamin B_{12} has been previously reported [30, 31]. It was therefore decided to attempt to exploit this phenomenon in order to establish the presence of vitamin B_{12} on the surface of nanoparticles. Based on this fluorescence quenching effect, the comparison of fluorescence intensity of the vitamin B_{12}-conjugated to that of unmodified YO

nanoparticles showed a markedly lower fluorescence for the nanoparticles with surface conjugated vitamin B_{12} (Figure 5.2d and further details provided in section 5.3.3).

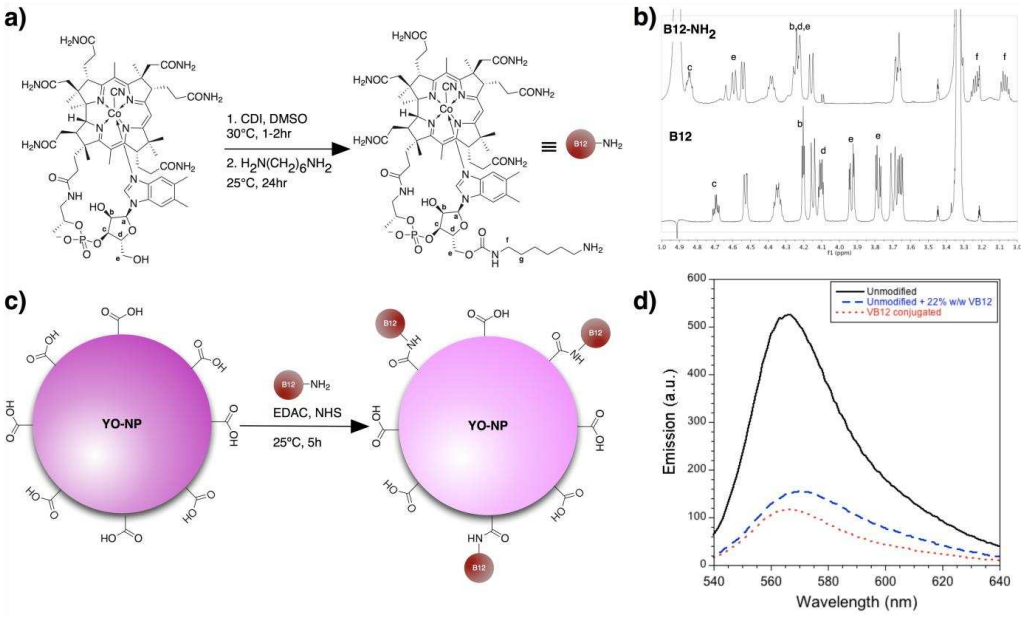

Figure 5. 2. Synthesis and characterisation of α-ω-aminohexylcarbamate-vitamin B_{12}

a) Reaction scheme for synthesis of α-ω-aminohexylcarbamate-vitamin B_{12} b) ^{1}H-NMR (expanded region) of purified cyanocobalamin and α-ω-aminohexylcarbamate-vitamin B_{12}, c) Schematic of the conjugation of α-ω-aminohexylcarbamate-vitamin B_{12} to fluorescent YO nanoparticles, d) Comparison of the fluorescent spectra of YO (50 nm) nanoparticles; and in the presence of free vitamin B_{12} (unmodified + 22% w/w VB_{12}) and vitamin B_{12}-conjugated YO (50 nm) nanoparticles.

5.3.2 B_{12}-conjugated nanoparticle characterisation

To confirm that following conjugation, nanoparticle size distribution did not significantly change, or that aggregation did not occur to a significant extent, particle size distribution was assessed *via* dynamic light scattering (Figure 5.3 and table 5.3c). The results indicate that the diameters determined experimentally are slightly smaller than the nominal diameters provided by the manufacturer (Polysciences, Inc): 42 nm, ~80 nm and ~140 nm for 50, 100 and 200 nm sized unmodified nanoparticles respectively. Data demonstrates the somewhat increased hydrodynamic diameter of the B_{12}-conjugated nanoparticles relative to their unmodified counterparts with an increase in their respective particle size to 78 nm, 200 nm and 280 nm, for B_{12}-conjugated nanoparticles of nominal 50, 100 and 200 nm size, respectively, which is indicative of a degree of nanoparticle aggregation. However, the increased particle size remained

within the accepted limits for cellular internalisation by endocytosis [25]. For ease of data comparison between B_{12}-conjugated and unmodified nanoparticles, B_{12}-conjugated nanoparticles of 50, 100 and 200 nm are hereafter referred to as their initial 'pre-conjugated' nominal diameter. B_{12} conjugation to nanoparticles was also indicated by a change in nanoparticle surface charge (zeta potential) post conjugation. The data overall demonstrates that unmodified nanoparticles of all sizes display a higher negative surface potential than their B_{12}-conjugated analogues (Figure 5.3d), due to surface charge shielding by B_{12} on the surface of the conjugated nanoparticles.

a)

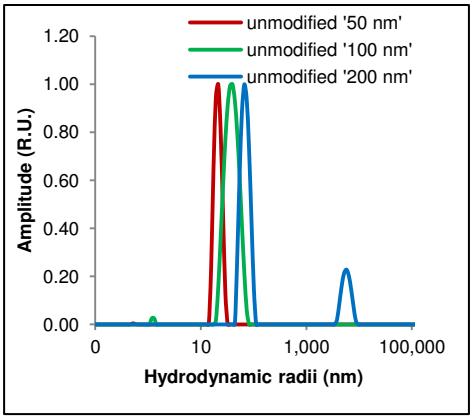

b)

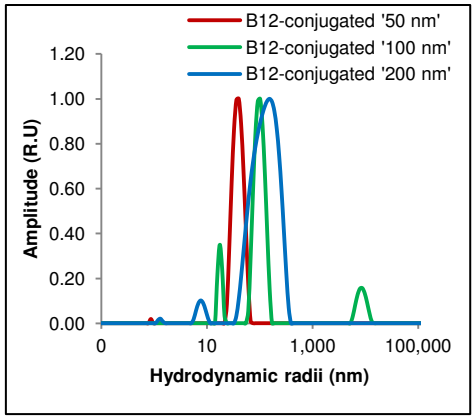

c)

Sample	Peak	% Area	Rh (nm)	% RSD
NP50	1 2	99.3 0.7	21.22 2.41e+6	15.5 16.9
NP100	1 2	0.6 99.4	1.24 39.95	5.2 28.6
NP200	1 2	81.5 18.5	69.86 5798.35	18.5 18.4
B_{12}-conjugated (50 nm)	1 2	0.3 99.7	0.86 39.32	0.0 22.1
B_{12}-conjugated (100 nm)	1 2 3	11.4 79.4 9.2	17.64 100.06 7990.49	8.7 21.4 14.6
B_{12}-conjugated (200 nm)	1 2	3.0 97.0	7.73 139.84	15.8 48.9

d)

	Unmodified nanoparticles (50 nm)	B_{12}-conjugated (50 nm)	Unmodified nanoparticles (100 nm)	B_{12}-conjugated (100 nm)	Unmodified nanoparticles (200 nm)	B_{12}-conjugated (200 nm)
Zeta Potential (mV)	-34.6	-26.3	-32.1	-27.8	-33.1	-27.4
Zeta deviation (mV)	0.06	1.67	0.61	0.64	0.17	2.55

Figure 5. 3. Size and surface characterisation of B_{12}-conjugated nanoparticles.

DLS measurements for a) unmodified polystyrene Polysciences nanoparticles and b) B_{12}-conjugated PS nanoparticles, c) a tabulated summary of DLS data showing Rh (hydrodynamic radii, nm), % occupied by peak and % relative standard deviation (RSD), d) Zeta potential of unconjugated and vitamin B_{12}-conjugated nanoparticles. The data represent a mean of 10 measurements for DLS. Measurements were recorded at 25°C in Hank's Balanced Salt Solution (HBSS, biological solution in which nanoparticles were applied to the cells).

5.3.3 Quantitative analysis of B_{12} attachment

In order to obtain quantitative information on nanoparticle surface coverage by $B_{12,}$ an option to quantify ligand loading would be to analyse the remaining ligand in the supernatants/dialysates after particle purification, as conducted by Chalasani *et al.* [13]. However, this method offers uncertainties as to the efficiency of ligand recovery during washing steps/dialysis. Other options open to consideration were analytical techniques based on NMR, UV/Vis and infra-red spectrophotometry. Experimentally,

all of these techniques display limitations. Nuclear magnetic resonance techniques require swelling of the polystyrene nanoparticles prior to analysis of molecular B_{12}. Even then, the presence of B_{12} peaks would be masked by the signals generated from the polystyrene.

It was therefore opted to explore the fluorescence quenching properties of vitamin B_{12} [30], as indicated in Figure 5.2d and Figure 5.4, not only to confirm successful conjugation, but to attempt to quantify the amount of B_{12}-ligand attached to the surface of the nanoparticles. When the unmodified nanoparticles were exposed to free vitamin B_{12} in solution; this produced a decrease in nanoparticle-associated fluorescence intensity as the amount of free vitamin B_{12} was increased (Figure 5.4a), but was restored after removal of free vitamin B_{12} by dialysis (Figure 5.4d). On the contrary, for vitamin B_{12} conjugated nanoparticles the fluorescence intensity did not increase following dialysis (Figure 5.4d). Taken together, this data confirms successful B_{12} conjugation to the nanoparticles. To quantify B_{12} attachment, emission of YO-polystyrene nanoparticles was measured in the presence of increasing amounts of B_{12} (shown for 50 nm nanoparticles in Figure 5.4a) and the maximal emission peaks plotted as a function of the weight percentage of free B_{12} added (Figure 5.4a). Fitting this data to an exponential decay model (Figure 5.4b) ($R^2 \geq 0.997$) allowed determination of the weight percentage of B_{12} in B_{12}-conjugated particles. This way, B_{12} loading for 50, 100 and 200 nm nanoparticles was estimated to be 24%, 28% and 20% w/w, respectively. However, these values are above those calculated for shoulder-to-shoulder conjugation and thus this data cannot be used to accurately quantify the level of B_{12} on the particle surface. This is because the fluorescence quenching effect of free vitamin B_{12} would be expected to differ somewhat to that of B_{12} covalently bound to nanoparticles. In fact, a red shift in fluorescence was observed for the YO nanoparticles in the presence of free B_{12}, that was not detected in PS nanoparticles with B_{12} covalently bound to their surfaces (Figure 5.4c). This could be explained by the dependence of quenching effect on diffusion and the distance between the two species [32], a scenario where covalently immobilised B_{12} will be different to free B_{12}.

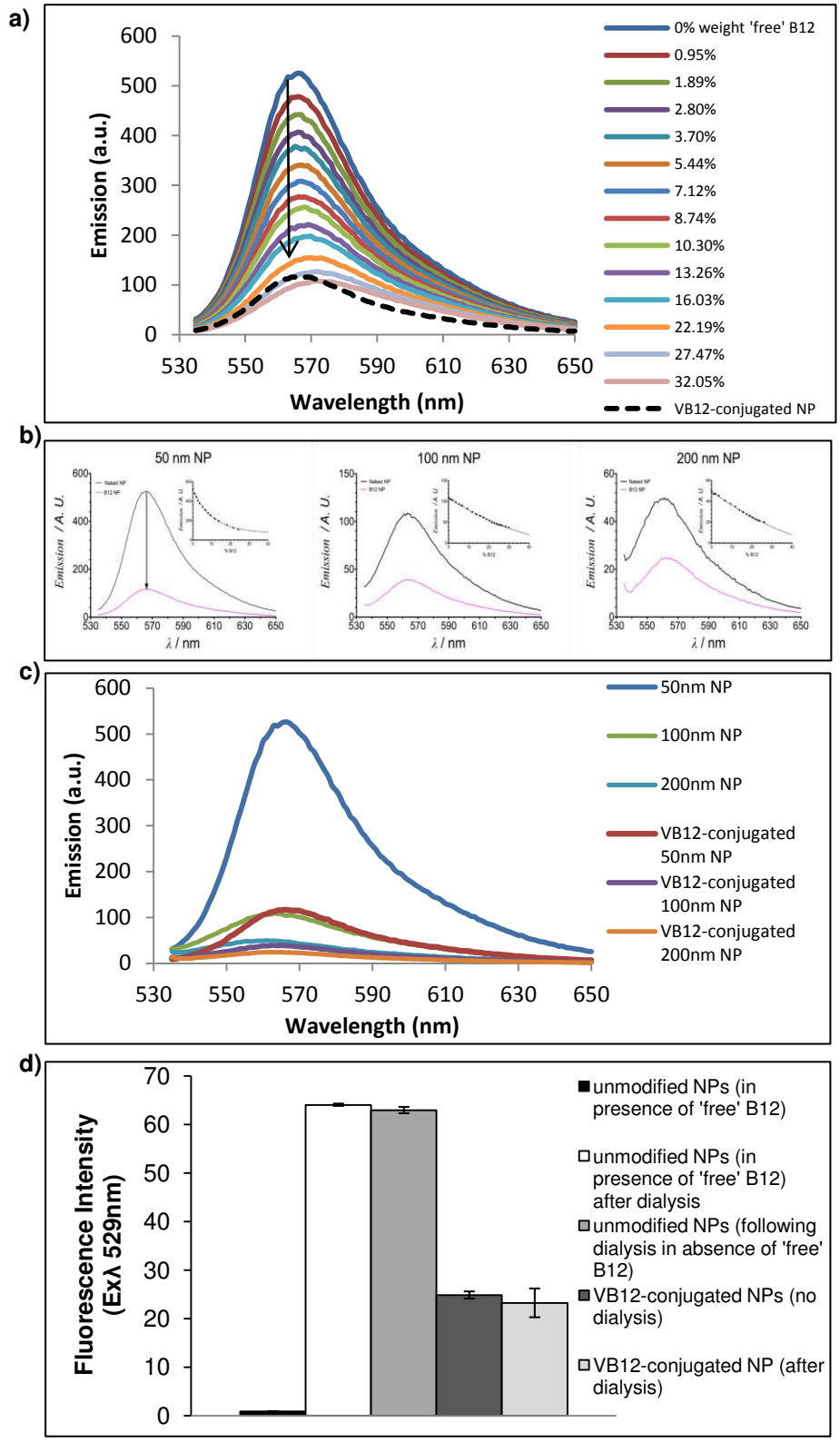

Figure 5. 4. Fluorescence characterisation of YO Polysciences, Inc. nanoparticles.

a) Wavelength scan (530-650 nm) of 50 nm unmodified nanoparticles with increasing percentage amounts (w/w) of soluble B_{12} and of B_{12}-conjugated nanoparticles (shown in black) b) Exponential decay model ($R^2 \geq 0.997$) for determination of the weight percentage of B_{12} in B_{12}-conjugated particles (Data was fitted using Prism5 v 5.0 from GraphPad Software, Inc, using an in built model) c) Wavelength scan showing unmodified nanoparticles and B_{12}-conjugated nanoparticles for 50, 100 and 200 nm particle sizes. d) Dialysis experiment showing restored fluorescence intensity of unmodified nanoparticles following removal of free B_{12} and comparison with B_{12}-conjugated nanoparticles.

Theoretically, the maximum shoulder-to-shoulder conjugation of B_{12} to nanoparticles (whereby B_{12} covers nanoparticle surface completely) yields a loading of 6.6%, 3.4% and 1.7% (w/w) for 50 nm, 100 nm and 200 nm nanoparticles (or 0.25 groups per nm^2 for all three particle sizes), respectively, assuming 4 nm^2 for vitamin B_{12} ligand (as modelled from the chemical structure of vitamin B_{12}). On the other hand, the extent of B_{12} loading on nanoparticle surface depends on the number of functional carboxylic acid groups available. To investigate this, potentiometric titration experiments were conducted with unmodified nanoparticles. From this data (Figure 5.5) the density of carboxyl groups on the nanoparticles was calculated, obtaining values of 2.23, 8.86 and 20.8 groups *per* nm^2 of 50 nm, 100 nm and 200 nm particles, respectively.

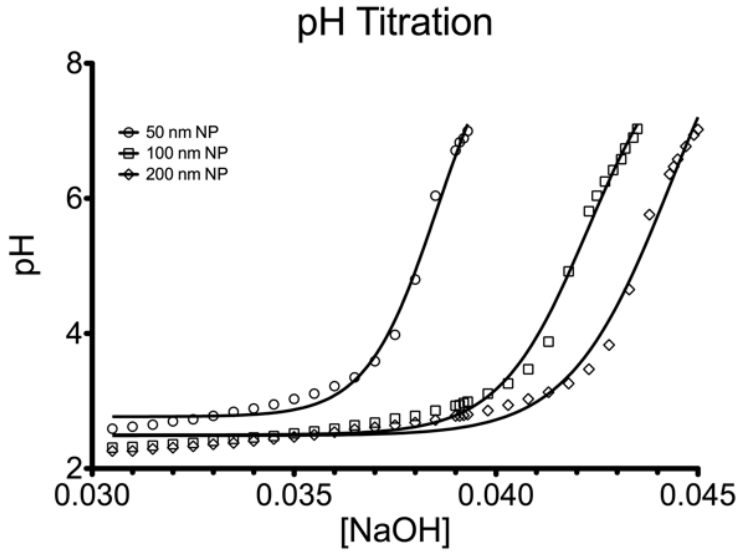

Figure 5. 5. Potentiometric titration of unmodified YO carboxy polystyrene nanoparticles (50, 100, 200 nm) with 0.05M NaOH.

Although it was not possible to confirm this data with the manufacturer (Polysciences, Inc), this high level of acidic functional groups *per* nanoparticle area, also documented for Polysciences nanoparticles in other works [33], actually exceeds the number of groups required for shoulder-to-shoulder conjugation of B_{12} (considering the approximate 4 nm^2 area of B_{12}). Therefore, the high density of the surface acid groups on the nanoparticle surface (for all sizes) indicates that the level of B_{12} conjugation to nanoparticles is not limited by the availability of acidic groups, but by the conjugation efficiency. 'Shoulder-to-shoulder' conjugation would require 1.85 mg B_{12} for 50 nm,

0.92 mg for 100 nm and 0.46 mg for 200 nm nanoparticle suspensions used (with equal volumes of nanoparticle suspensions used in each conjugation reaction), whilst an excess of 10 mg of B_{12} was employed. As it is not expected that the conjugation efficiency would be greatly affected by the size of nanoparticles, and with excess of both charged groups and vitamin B_{12} derivative for shoulder-to-shoulder conjugation, one would expect similar surface conjugation *per* surface area on the three different sized nanoparticles, hence the spatial distribution of vitamin B_{12} ligand is likely to be similar for all nanoparticle sizes. The ligand surface density has been shown to play an important role in cellular interaction and uptake; however a significant effect is seen at the lower levels of surface modification with a plateau after which there is no further effect of increasing ligand density on nanoparticle uptake [34-38]. Taken together, this suggests that the ligand distribution on the nanoparticle surface, and their presentation to the cells, would be similar (assuming a statistical distribution), hence minimising any biological effects relating to ligand surface coverage.

5.3.4 Cell uptake and transport of vitamin B_{12}-conjugated nanoparticles

Cell uptake studies (Figure 5.6a) demonstrated that internalisation of 50 nm vitamin B_{12}-conjugated nanoparticles occurred to a significantly greater extent (28 $\mu g/cm^2$ of cell monolayer area over the 3 hr experiment) as compared to unmodified nanoparticles of the same size (1.5 $\mu g/cm^2$ *per* cell monolayer). This demonstrates that conjugation of vitamin B_{12} to nanoparticles enhances their endocytosis. It should be noted that although intrinsic factor (IF) binds to cyanocobalamin in a 1:1 molar ratio [39], the amount of IF (1.5 µg) added to the cell monolayers in combination with the B_{12}-conjugated nanoparticles is likely to be significantly lower than the amount of particle-conjugated vitamin B_{12}. However, considering its notably larger molecular mass (55000 Da *versus* 1497 Da for α-ω-aminohexylcarbamate-vitamin B_{12}), one IF molecule is expected to occupy a significantly larger area on the nanoparticle surface. Furthermore, cell uptake of the nanoparticle-bound vitamin B_{12}-IF is likely to result from binding of one such complex to the cell surface cubilin receptor, as reported for soluble B_{12}-IF [40]. The amount of IF added to the nanoparticle systems (expressed as the number of molecules) exceeded the number of particles for all the particle sizes

employed, with approximately 6, 45 and 361 molecules of IF *per* particle for 50, 100 and 200 nm nanoparticles, respectively. Provided that IF localisation on the nanoparticle surface is a random event (based on random vitamin B_{12} functionalisation of nanoparticles), and with multiple molecules of IF on the nanoparticle surface, nanoparticles are 'statistically likely' to approach the cell surface receptors in the 'correct position'.

The competitive inhibition study demonstrated that cellular uptake of vitamin B_{12}-conjugated nanoparticles was significantly inhibited by the presence of excess free vitamin B_{12}, from 28 µg/cm^2 to 1.7 µg/cm^2 (Figure 5.6a). Regarding transcellular transport of nanoparticles, the experiments (Figure 5.6b) demonstrate an increased translocation of B_{12}-conjugated nanoparticles relative to the unmodified counterparts, with the level of transport amounting to 7.3 µg/cm^2 and 1.3 µg/cm^2 in a 3 hr experiment, respectively. The transport of B_{12}-conjugated nanoparticles was reduced in the competitive experiment with free B_{12} to 1.3 µg/cm^2. 500 µg of cyanocobalamin per 0.5 ml of B_{12}-conjugated nanoparticles was considered a sufficient excess considering the maximum theoretical (shoulder-to-shoulder) conjugation of 6.6% w/w which equates to 13.2 µg of conjugated B_{12} per 0.5 ml of 50 nm nanoparticles). The suppression of cell uptake and transport of B_{12}-conjugated nanoparticles by excess of free vitamin B_{12} (Figures 5.6a and b), implies that these processes are indeed dependent on binding of the conjugated ligand (with IF) to vitamin B_{12}-receptor (cubilin). It should be noted that data on nanoparticle transport across the cell monolayers probably underestimates the transport capacity of vitamin B_{12}-conjugated nanoparticles, due to the previously reported hindered translocation of the nanoparticles through the pores in the filters used to culture the cells [8, 41].

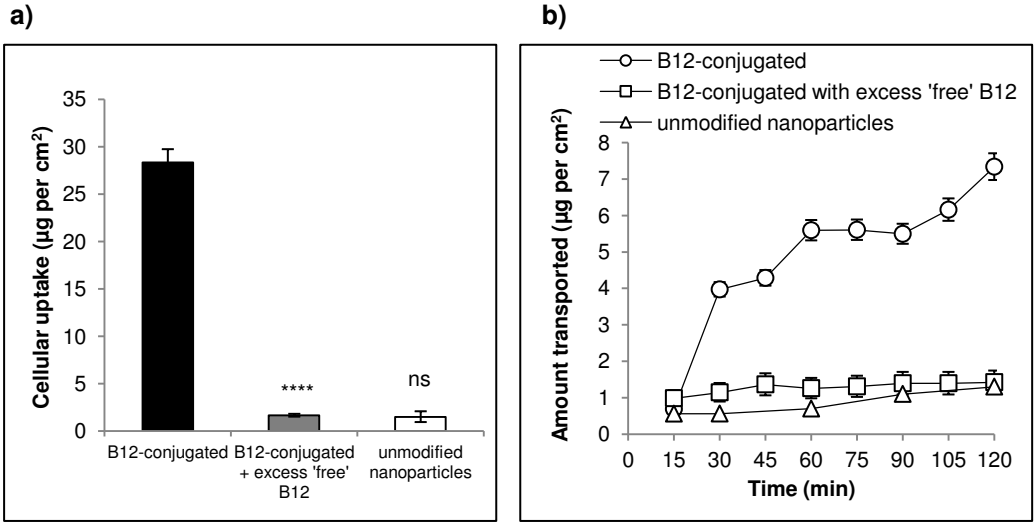

Figure 5. 6. Cell uptake and transport of unmodified and vitamin B_{12}-conjugated nanoparticles in Caco-2 monolayers.

a) cell uptake b) transport of B_{12}-conjugated nanoparticles per se or in competition experiment with excess free vitamin B_{12} in solution, compared with unmodified nanoparticles. 50 nm YO fluorescent nanoparticles were used and the experiments conducted in the presence of intrinsic factor (IF) in all cases. Data represents the mean ± SD (n=3).Statistical comparison (ANOVA) performed between 'B12-conjugated' and B12-conjugated + excess free B12' and 'B12-conjugated + excess free B12' and 'unmodified nanoparticles', where **** denotes p>0.0001 and 'ns' denotes 'not signficant'

5.3.5 Effect of nanoparticle size on cell uptake and transport of vitamin B_{12}-conjugated nanoparticles

There have been numerous studies assessing the impact of particle size on uptake by epithelial cells *in vitro,* [42, 43] but rather fewer studies [8, 44] have been conducted with systems where ligand-modified nanoparticles of specific size ranges were utilised to target particular epithelial transport pathways. Ligand B_{12} modified nanoparticles of three different (nominal) sizes (50, 100 and 200 nm polystyrene lattices with narrow size distribution) were therefore created, encompassing the generally accepted size range for endocytosis in epithelial cells and cellular uptake, as well as translocation across, the polarised cell monolayers was studied (Figure 5.7). Data was calculated and analysed in terms of *mass* of nanoparticles (important from drug delivery perspective). However, further analysis of the *number* of nanoparticles internalised and transported by the cells (important for understanding the number of events occurring) was conducted. The data together highlights the influence of particle size on both of these parameters.

In terms of *mass* of nanoparticles, vitamin B_{12}-conjugation promoted greater (statistically significant) internalisation of nanoparticles of 50 and 100 nm, compared to unmodified nanoparticles (Figure 5.7a), with the level of internalisation of 39 µg/cell layer for 100 nm (conjugated), in comparison to 32 µg/cell layer for 50 nm nanoparticles (unmodified). Cell uptake of B_{12}-conjugated nanoparticles of 200 nm (approximately 8 µg/cell layer) was, however, similar to the unmodified nanoparticles of the same size (approximately 6 µg/cell layer) (Figure 5.7a). Considering the same data in terms of *number* of uptake events occurring, it is apparent that 50 nm B_{12}-conjugated nanoparticles were taken up by the cells in the greatest number ($4.7x10^{11}$/cell layer), followed by 100 nm B_{12}-conjugated nanoparticles ($7.1x10^{10}$), followed by 200 nm B_{12}-conjugated nanoparticles ($1.7x10^{9}$). The observed trend follows an approximate 6.6-fold decrease in the *number* of internalised nanoparticles from 50 to 100 nm and a 40.9-fold reduction from 100 to 200 nm.

The transport of vitamin B_{12}-conjugated nanoparticles across the cell monolayers (Figure 5.7b) mirrored the general trends in cell uptake (Figure 5.7a). As nanoparticle size increased from 50 to 100 nm, the *mass* of nanoparticles that translocated across the cells during the experiment increased from 5.8 µg to 14 µg respectively, but was reduced to 1.4 µg for 200 nm nanoparticles. Considering the *number* of nanoparticles transported across the cell monolayers, there was a decrease from $8.5x10^{10}$ to $2.6x10^{10}$ to $3.2x10^{8}$ as nanoparticle size increased from 50 nm to 100 nm to 200 nm, respectively, indicating a 3.3-fold reduction in transport when nanoparticle diameter increased from 50 to 100 nm and 81.1-fold reduction for the size increase from 100 to 200 nm. Expressing the *number* of transported nanoparticles as a ratio of internalised nanoparticles, indicates that 50 nm and 200 nm nanoparticles were in fact least efficiently translocated, with 1 in 5.5 of internalized nanoparticles traversing into the basal medium in both cases, whereas 1 in 2.8 of internalised 100 nm nanoparticles translocated across the cell monolayer. However a potential underestimation due to issues of nanoparticles diffusion though pores of the supporting membrane, as mentioned above, should be taken into account, particularly as particle size increases.

Of importance for transmucosal delivery of biologicals, is the maximum amount of translocation of the therapeutic from the luminal to the basal side of the epithelium, which is dependent on both maximal therapeutic loading capacity and a high number of receptor-governed events. This data indicates that a nominal particle size of 100 nm would yield optimal delivery capacities for a vitamin B_{12}-mediated drug delivery system.

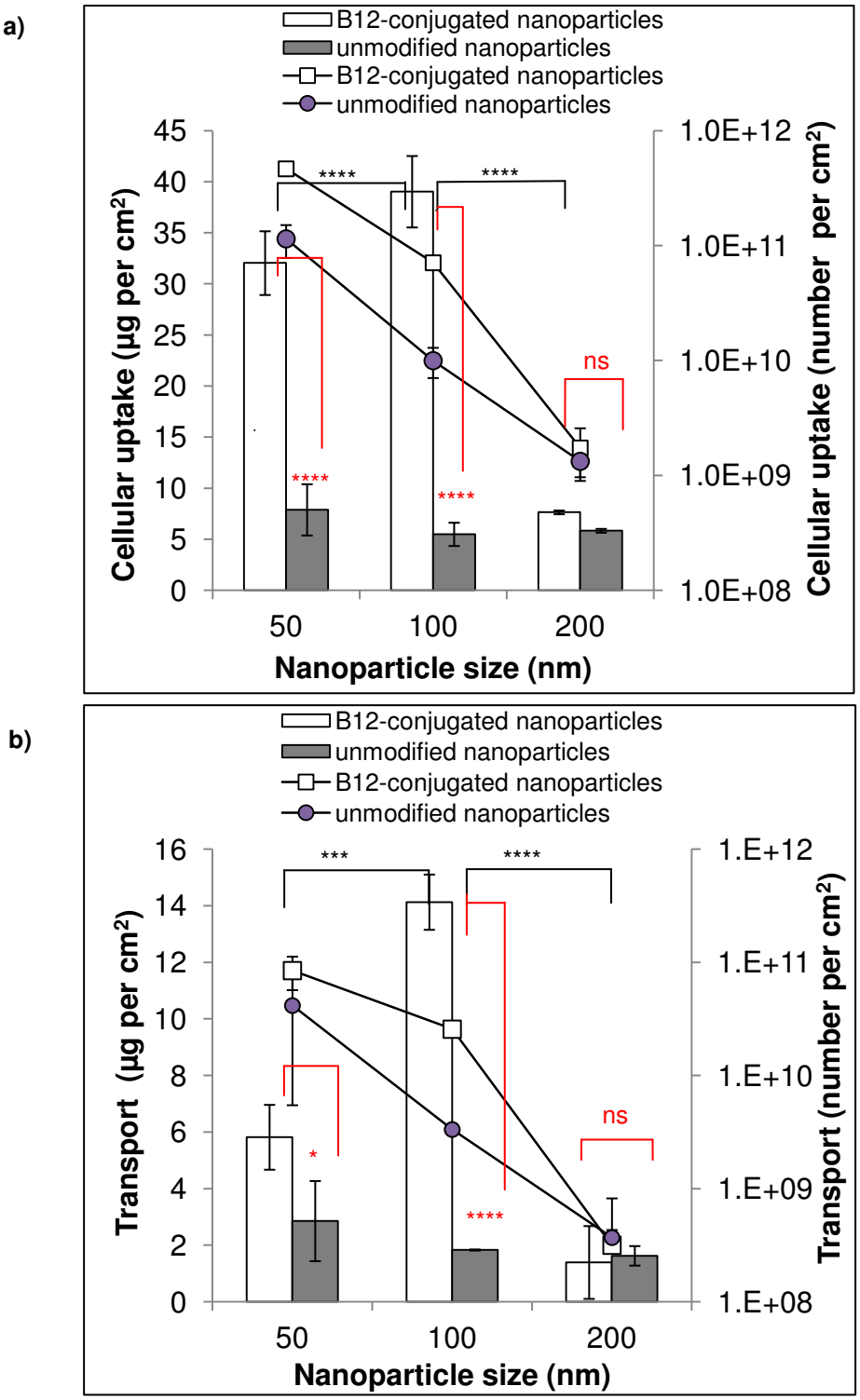

Figure 5. 7. Effect of particle size on cell uptake and transport of vitamin B_{12}-conjugated nanoparticles in Caco-2 monolayers.

a) Cell uptake and b) transport across the cell monolayers. Vitamin B_{12}-conjugated nanoparticles of 50nm, 100nm and 200nm were used and nanoparticles were quantified in terms of mass (per surface area of the cell monolayer) and number. Bars denote nanoparticle amount (primary axis), whereas lines represent nanoparticle number (secondary Yaxis). Data represents the mean ± SD (n=3). Statistical comparison between *amount* data related to the uptake and transport of B_{12}-conjugated nanoparticles (100 nm *vs* 50 nm and 200 nm *vs* 100 nm shown in black) and B_{12}-conjugated nanoparticles *vs*. unmodified nanoparticles of the same nominal size (shown in red).

5.3.6 Cell uptake and trafficking of vitamin B_{12}-conjugated nanoparticles

In the mechanism of soluble vitamin B_{12} absorption across the epithelium *in vivo,* the IF-B_{12} complex is believed to traffic into the lysosome, where IF protein is degraded to release B_{12} [17]. From the perspective of transmucosal delivery of biologicals, this would mean that the internalised carrier and the incorporated biologic are reaching the highly degradative lysosomal compartment, seriously undermining their delivery potentials. A series of studies were conducted to establish whether the vitamin B_{12}-conjugated nanoparticles also reach the lysosomal compartment following cell internalisation. The rationale for Lysotracker™ staining and LAMP1 immunostaining was discussed in Chapter 2 (section 2.2.5.3). These studies were conducted on 50 nm (B_{12}-conjugated and unmodified) nanoparticles, as this particle size is amenable to all the different cellular internalisation pathways possible. Control experiments in the absence of nanoparticles established that the Lysotracker™ probe is undetectable (Figure 5.8a) and that LAMP1 is only observed at a very low level (Figure 5.8b), both indicating that the lysosomal compartment is only 'active' when endocytosis occurs. When unmodified nanoparticles were applied to the cells, the images indicate their co-localisation with the Lysotracker™ marker (Figure 5.8c), suggesting the presence of unmodified nanoparticles in the lysosomal compartments. This in turn indicates that the intracellular trafficking of unmodified nanoparticles largely follows the 'degradative route' reaching lysosomes. Furthermore, staining for LAMP1 after cell incubation with unmodified nanoparticles shows intensive punctate staining of this lysosomal protein within the cytosol (Figure 5.8d), suggesting the presence of lysosomal structures.

Following cell layer incubation with vitamin B_{12}-conjugated nanoparticles (Figure 5.8e), lysosomal compartments were not detected by the Lysotracker™ probe, while LAMP1 staining revealed protein distribution that was diffuse throughout the cytoplasm of the cells (Figure 5.8f) rather than clustered as punctate regions, as in the case with unmodified nanoparticles (Figure 5.8d).

Taken together, this data indicates that the unmodified nanoparticles are trafficked to the lysosomes, but the B_{12}-conjugated nanoparticles circumnavigate lysosomal compartmentalisation.

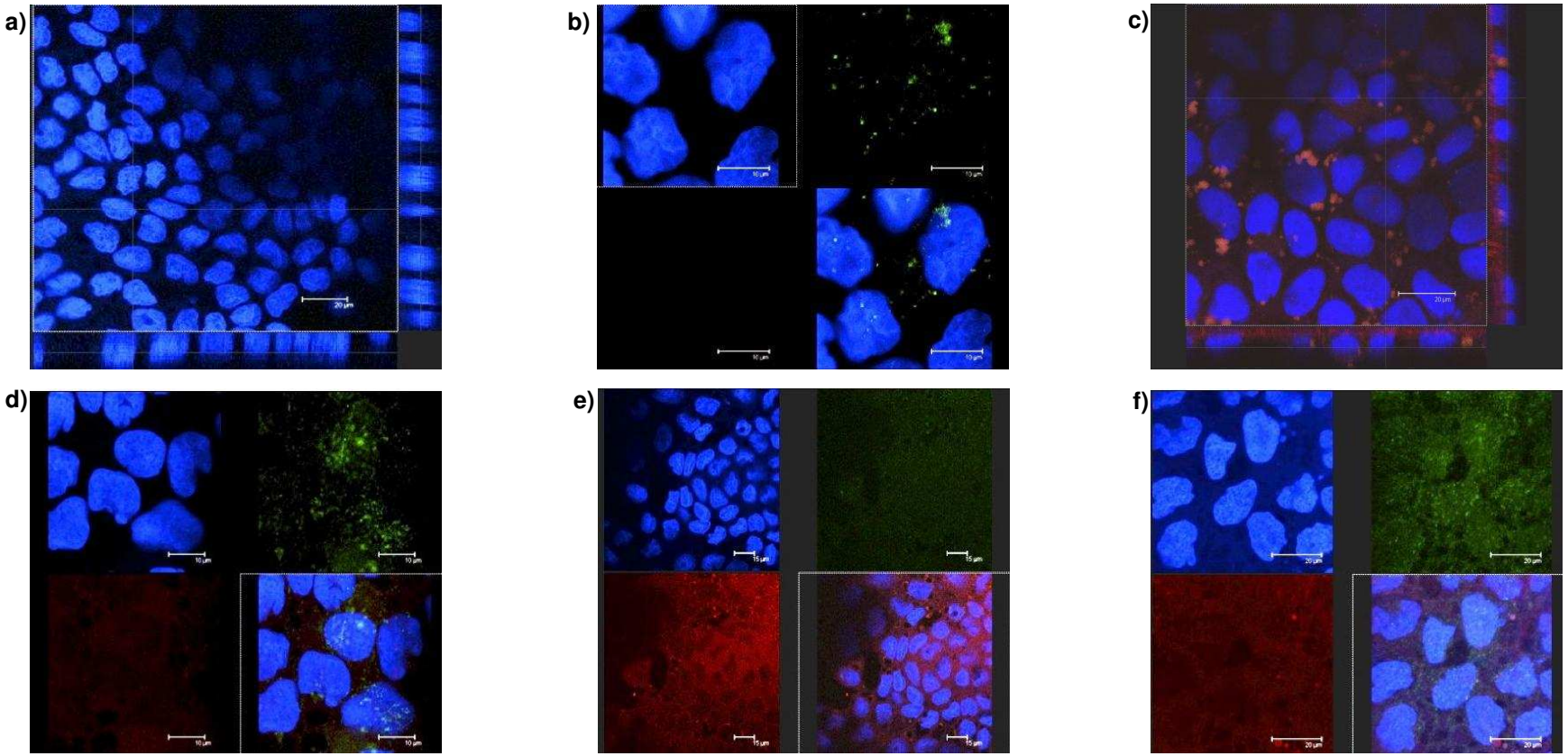

Figure 5. 8. Characterisation of Caco-2 cell layer uptake of 50 nm vitamin B_{12}-conjugated nanoparticles by confocal microscopy.

a) Cell staining with Lysotracker Green DND-26 in the absence of nanoparticles b) immunostaining for lysosomal associated-membrane protein 1 (LAMP1) in the absence of nanoparticles, c) Co-localisation of unmodified nanoparticles with lysosomal compartments, d) Immunostaining for LAMP1 protein following cell incubation with unmodified nanoparticles, e) Staining with Lysotracker Green DND-26 after cell incubation with vitamin B_{12}-conjugated nanoparticles (red), f) Immunostaining for LAMP1 following exposure of cells to vitamin B_{12}-conjugated nanoparticles. Lysotracker Green DND-26 excitation 504, emission 511 nm; YO nanoparticle excitation 529, emission 546 nm.

Furthermore, a series of control Lysotracker™ experiments were conducted to ensure that the imaged pattern (in Figure 5.8) did not result from fluorophore cross emission. The reader is referred to Chapter 2, section 2.2.5.3 (Table 2.1) for further experimental details. In experiment A (Figure 5.9, sub-figures Ai-iii), cells were incubated with both YO nanoparticles and unlabelled non-fluorescent nanoparticles and imaged under the settings for Lysotracker™. The generated green signal has a weak intensity (Aii), showing that cross emission between the YO nanoparticle fluorescence and the green Lysotracker™ fluorescence is minimal. In a separate experiment, where cells were stained with the Lysotracker™ probe in the absence of YO nanoparticles, but in the presence of unlabelled non-fluorescent nanoparticles (Figure 5.9B) the sample was imaged under the YO nanoparticle emission settings. In this case, a weak red signal was observed (Bii), confirming minimal red-green cross-emission. The presence of the unlabelled nanoparticles in the latter experiment was important; as the Lysotracker™ probe was not detected in the absence of nanoparticles following HBSS-induced serum starve (Figure 5.8a).

In a similar series of experiments (C-E in Figure 5.9 and in Table 2.1, Chapter 2), cells were treated with the YO nanoparticles and imaged under the Lysotracker™ settings (while Lysotracker™ staining was omitted). Under these conditions, a green signal was not observed (Figure 5.9Cii). Conversely, applying the Lysotracker™ probe (in the absence of the YO nanoparticles) and imaging the cells under the YO nanoparticle settings does not result in a significant red signal (Figure 5.9Dii). Lastly, cells imaged with unlabelled (non-fluorescent) nanoparticles under the Lysotracker™ settings (Table 2.1, experiment E, Figure 5.9Eii) displayed a similar punctate staining pattern to cells imaged with unmodified YO fluorescent nanoparticles (Figure 5.8c), which serves to verify that the pattern seen is not a result of cross-emission between the YO fluorophore and the Lysotracker™ fluorophore in the other sequential scan overlay experiments (Figure 5.8). Furthermore, it concludes the point that the Lysotracker™ probe is only detectable in the presence of nanoparticles. Taken together, these control experiments confirm that the Lysotracker-nanoparticle co-localisation data

shown in Figure 5.8 results from true fluorescence from both species as opposed to experimental artefact from cross-emission between the fluorophores.

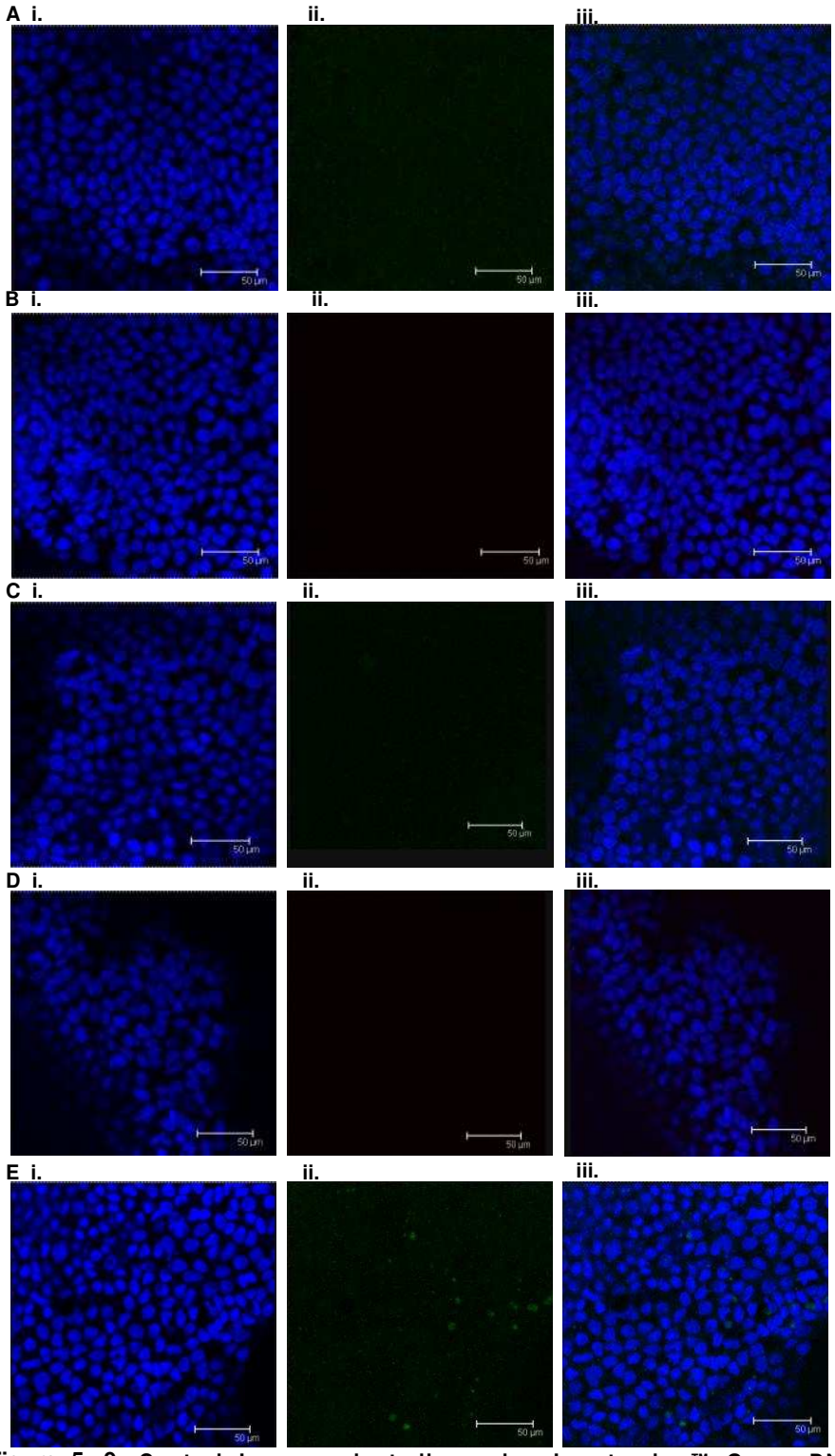

Figure 5. 9. Control Lysosomal studies using Lysotracker™ Green DND-26 with unmodified nanoparticles (50 nm) in Caco-2 monolayers.

A) Cells treated with both unlabelled (non-fluorescent) 50 nm nanoparticles and YO fluorescent 50 nm nanoparticles and imaged under Lysotracker™ settings: i) blue channel (Hoechst stain) for cell nuclei; ii) green channel, iii) overlay image of blue and green channels. B) Cells treated with unlabelled nanoparticles and the Lysotracker™ probe and imaged under YO nanoparticle settings: i) blue channel (Hoechst stain) for cell nuclei; ii) red channel, iii) overlay image of blue and red channels. C) Cells treated with YO 50 nm nanoparticles and imaged under Lysotracker™ settings: i) blue channel (Hoechst stain) for cell nuclei, ii) green channel, iii) overlay image of blue and green channels. D) Cells treated with the Lysotracker™ probe and imaged under YO nanoparticle settings: i) blue channel (Hoechst stain) for cell nuclei, ii) red channel, iii) overlay image of blue and red channels. E) Cells treated with unlabelled (non-fluorescent) 50 nm nanoparticles and Lysotracker™ probe and imaged under Lysotracker™ settings: i) blue channel (Hoechst stain) for cell nuclei, ii) green channel, iii) overlay image of blue and green channels.

In summary, the cell uptake and trafficking data suggests that surface decoration of nanoparticles with vitamin B_{12} has a profound effect on intracellular trafficking, giving rise to lysosomal bypass – a phenomenon that has not been demonstrated to occur in the process of cell uptake of soluble vitamin B_{12}. Adoption of an intracellular pathway that is different to both soluble vitamin B_{12} and unmodified nanoparticles, indicates a switch in intracellular trafficking of the B_{12} ligand, as a direct consequence of its attachment to a nanoparticle surface.

5.3.7 Cubilin, caveolin-1 and clathrin expression in Caco-2 cells

In order to further investigate the internalisation and cellular trafficking of B_{12}-conjugated nanoparticles, it was initially confirmed that the Caco-2 cultures employed in this study as a model of the intestinal epithelium express the appropriate structural components implicated in the vitamin B_{12} uptake and transport pathway (Figure 5.1). In Chapter 3 (section 3.3.4), the data demonstrated an abundant expression of the vitamin B_{12} cell surface receptor, cubilin (and also gene and protein expression of TCII receptor and the TCII carrier protein, respectively). The expression of cubilin is relevant to the ligand-receptor binding stage of endocytosis, while other components of the cell machinery are responsible for subsequent trafficking of vitamin B_{12}. Further work was therefore conducted to determine whether Caco-2 cultures express relevant components of specific endocytic pathways. This includes the presence of essential components of clathrin-coated pits, implicated in the internalisation of the soluble B_{12}-IF complex, as well as caveolae, another possible route for material internalisation by cells. Caco-2 cell monolayers immunostained for clathrin, the protein responsible for the formation of clathrin 'coated-pits', clearly show the presence of fluorescence indicative of clathrin expression (Figure 5.10 ai), in contrast to the control experiment (Figure 5.10 aii).

Unlike clathrin expression, there are contradictory reports regarding the presence of caveolin-1 in Caco-2 cells and the resulting ability of Caco-2 cells to internalise material *via* caveolae-like domains [27, 45-47]. Expression of caveolin-1 protein in

cells is generally considered sufficient and necessary to drive the formation of morphologically identifiable caveolae [48-50], and immunostaining of Caco-2 monolayers (Figure 5.9 bi) revealed its clear expression and presence at cell-cell boundaries. It should be noted that cellular permeabilisation (with Triton X-100) in this experiment was necessary, based on the generally accepted view that both the NH_2- and the COOH- termini of caveolin-1 face the cytoplasm and that no portion of the protein is extracellular [51, 52]. The lack of fluorescence in the control overlay image rules out experimental artifacts possibly resulting from non-specific antibody binding (Figure 5.10 bii). The data hence indicate that Caco-2 monolayers are capable of undertaking both, clathrin and caveolin-mediated endocytosis.

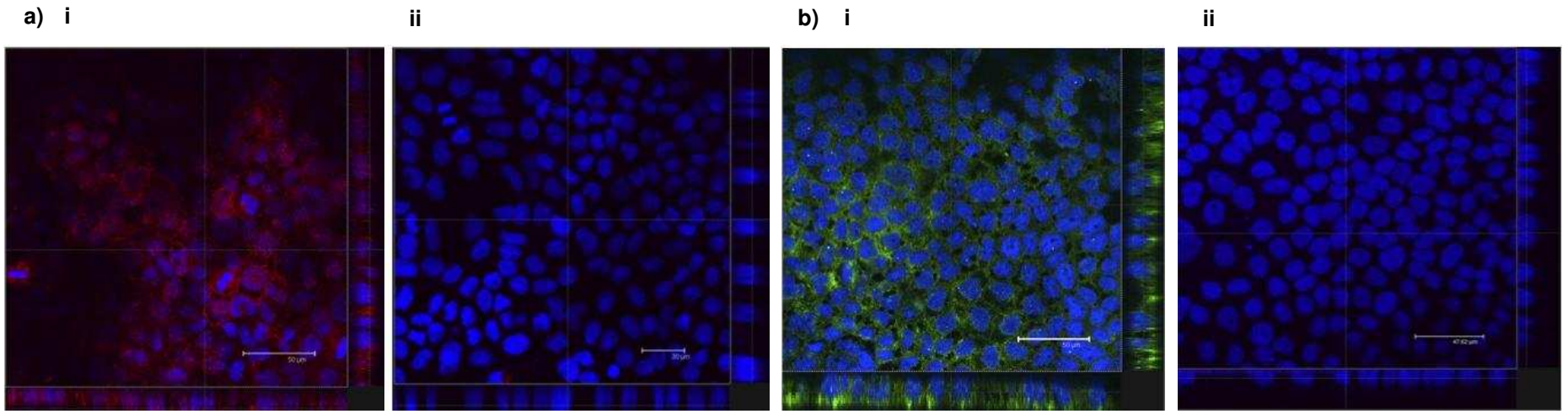

Figure 5. 10. Expression of select endocytic components by immunohistochemistry in Caco-2 monolayer model.

a) i. Expression of caveolin-1, shown by treating cells with anti-human caveolin 1 H-97, followed by goat, anti-rabbit IgG-Rhodamine, and ii. Control monolayer, incubated with goat, anti-rabbit IgG-Rhodamine only. b) i. Expression of clathrin, as demonstrated by cell incubation with rabbit anti-clathrin primary antibody and goat, anti-rabbit IgG-FITC, and ii. Control monolayer treated with the secondary, goat, anti-rabbit IgG-FITC only. Cell nuclei were labelled with Hoechst 33342 (blue) in all cases.

5.3.8 mRNA expression of Caveolin-1 in Caco-2 monolayers

Further to immunostaining (section 5.3.7) which revealed expression of the caveolin-1 protein in Caco-2 cells, the presence of caveolin-1 in differentiated Caco-2 cell cultures was confirmed at mRNA level. Figure 5.11 shows caveolin-1 mRNA expression on day 7, 14 and 21 of Transwell® culture, with an amplified cDNA product of 362bp. These results (both immunostaining and PCR) are in agreement with published data from Mayor *et al*. [53], who demonstrated expression of caveolin in Caco-2 cells using immunofluorescence techniques and Field *et al*. [47] who found expression of caveolin-1 at the mRNA level. In contrast to these findings, Mirre *et al*. [54] and Vogel *et al*. [55] failed to detect expression of caveolin-1 at either mRNA or protein level. These conflicting findings are likely to be a result of variability among Caco-2 cell lines and the heterogeneity of protein expression from the same Caco-2 cell clone [47, 56, 57].

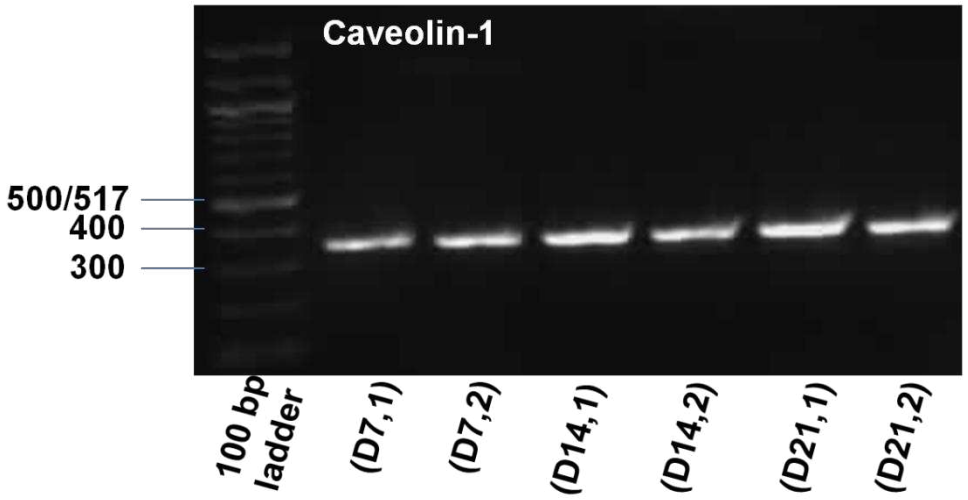

Figure 5. 11. mRNA expression of caveolin-1 in Caco-2 cell monolayers on day 7 (D7), day 14 (D14) and day 21 (D21) of culture.

5.3.9 Cellular trafficking of free vitamin B_{12}

The cell trafficking pathway of native, soluble vitamin B_{12} *in vivo* is well established, as discussed in section 5.1. As a starting point to decipher the uptake and intracellular trafficking pathways of B_{12}-conjugated nanoparticles, it was aimed to confirm the previously documented cell uptake and transport mechanism of vitamin B_{12}-IF. To this

end, the effect of clathrin and caveolae inhibitors on cell uptake and transport of vitamin B_{12} (cyanocobalamin), in the presence of IF, was assessed.

The cell trafficking inhibitors used in this study, namely chlorpromazine and filipin, have been used extensively as specific inhibitors of clathrin- and caveolae-mediated endocytosis, respectively [25, 27, 58]. The pathway-inhibiting effects of chlorpromazine and filipin in Caco-2 layers were confirmed by testing the uptake and transport of pathway-selective ligands, transferrin [59, 60] and cholera toxin B-subunit [27, 58] (section 5.3.10). The results revealed that vitamin B_{12} internalisation (Figure 5.12a) and transport (Figure 5.12b) were sensitive to the effects of chlorpromazine, with a 4-fold decrease in both uptake into and transport across the cells. Vitamin B_{12} trafficking, on the other hand, remained largely unaffected by the action of caveolae inhibitor, filipin. This data, therefore, agrees with the previous reports that vitamin B_{12} (in the presence of IF) exploits the clathrin-mediated route in the process of internalisation in Caco-2 cells. However, it must be noted that other vitamin B_{12} transport pathways are operating in conjunction with the IF-mediated pathway (as discussed in Chapter 6).

In the above experiments, vitamin B_{12} was applied at a high (non-physiological) concentration as these studies were designed not to assess its permeation capacity by the intestinal epithelium but to investigate the cellular trafficking pathway of vitamin B_{12} and to enable quantitation by UV absorbance, as opposed to detection by radio-labelling.

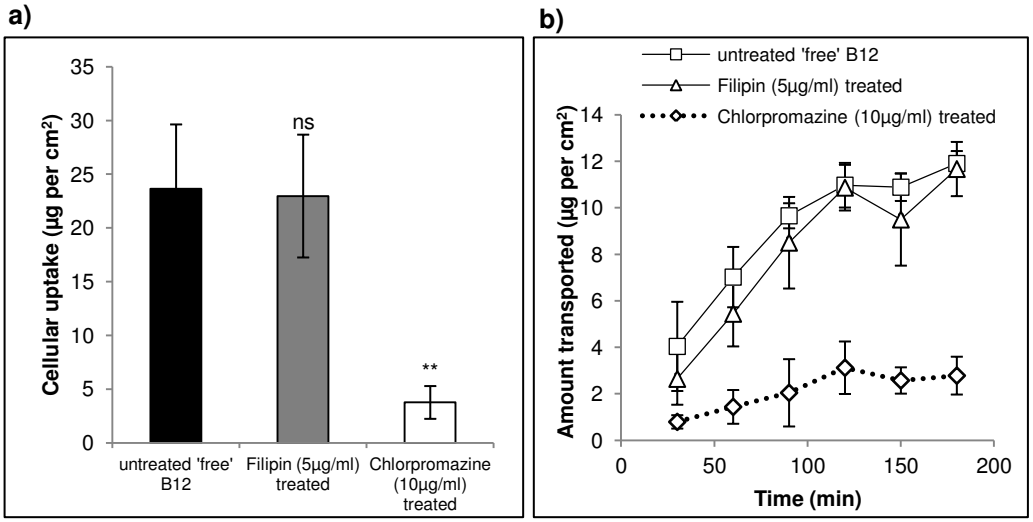

Figure 5. 12. Effect of endocytic pathway-specific inhibitors on cell uptake and transport of soluble vitamin B_{12}.

a) Effect of chlorpromazine and filipin on cell uptake of vitamin B_{12}, b) Effect of chlorpromazine and filipin on transport of vitamin B_{12} across Caco-2 monolayers. Vitamin B_{12} was applied in combination with IF and quantified by UVAbs (350nm). Data represents the mean ± SD (n=3). Statistical comparison with the preceding data set; 'ns' = non significant and ** denotes $p<0.01$.

5.3.10 Cell trafficking of vitamin B_{12}-conjugated nanoparticles

Earlier experiments (Figure 5.6) showed that vitamin B_{12}-conjugated nanoparticles are both internalised and transported across the Caco-2 cell monolayers in a notably more efficient manner than unmodified nanoparticles. Data also provided evidence of involvement of the vitamin B_{12} transport pathway in cell uptake and transport of vitamin B_{12}-bearing nanoparticles (Figure 5.6). Whilst the biological pathway of free (i.e. non-particle immobilised) vitamin B_{12} is well established, the cell trafficking routes of vitamin B_{12}-conjugated nanoparticles have not been demonstrated, despite their investigation and suggested use for oral delivery of biologicals [10, 13]. It was therefore sought to establish this by assessing the effect of inhibitors of specific cell entry pathways on the uptake and transport of vitamin B_{12}-conjugated nanoparticles. In addition to using chlorpromazine and filipin, the clathrin- or caveolae-mediated pathways were also inhibited, by the way of potassium depletion and the use of genistein, respectively. Previous studies have shown that depletion of intracellular potassium inhibits clathrin-mediated endocytosis [25, 61], whilst genistein, a known

inhibitor of the tyrosine kinases involved in caveolae-mediated endocytosis [62, 63], was used to suppress caveolae-mediated pathways.

The data shows that cell uptake of vitamin B_{12}-conjugated nanoparticles was unaffected by chlorpromazine treatment, which produced a statistically insignificant reduction in the extent of nanoparticle uptake (Figure 5.13a). Considering the effect of chlorpromazine on nanoparticle transport across the cells (Figure 5.13b), although an inhibitory effect on the level of transport was seen in the initial phase of the experiment (the first two hours), the amount of vitamin B_{12}-conjugated nanoparticles transported to the basolateral side (across the cell layers) at 3hrs measurement point reached the values seen in untreated cells. It is not entirely clear why an initial inhibitory effect on transport was apparent, though it may have resulted from chlorpromazine interference with cytoskeletal function and consequent decreased transport of material towards the basolateral membrane [64, 65]. These trends therefore suggest that cell uptake and transport of vitamin B_{12}-conjugated nanoparticles was largely unaffected by the inhibition of clathrin. To confirm this, the cell uptake and transport behaviours of B_{12}-bearing nanoparticles were determined using an alternative clathrin pathway inhibiting approach. The data from experiments conducted in potassium-depleted medium (Figure 5.13c) indicated no effect on cell uptake of vitamin B_{12}-conjugated nanoparticles, as there was no significant difference between the level of cell uptake in potassium-deprived conditions and controls (potassium supplemented medium). A lack of inhibitory effect was also seen in transport experiments, where the absence of potassium did not affect the extent of B_{12}-conjugated nanoparticle transport across the Caco-2 cell monolayers (Figure 5.13d). It must be noted however that in the latter experiment, the extent of nanoparticle transport for both potassium depleted and control conditions were markedly lower (by more than 2-fold) compared to the previous studies, which were conducted in HBSS buffer, suggesting that the overall nanoparticle transport partially depends on the type of cell medium. Overall, inhibition of the clathrin endocytic pathway in two different ways did not suppress the cell uptake or transport of vitamin B_{12}-conjugated nanoparticles, therefore excluding a role of this

pathway in the uptake and cellular transport of this ligand-bearing nanoparticulate system.

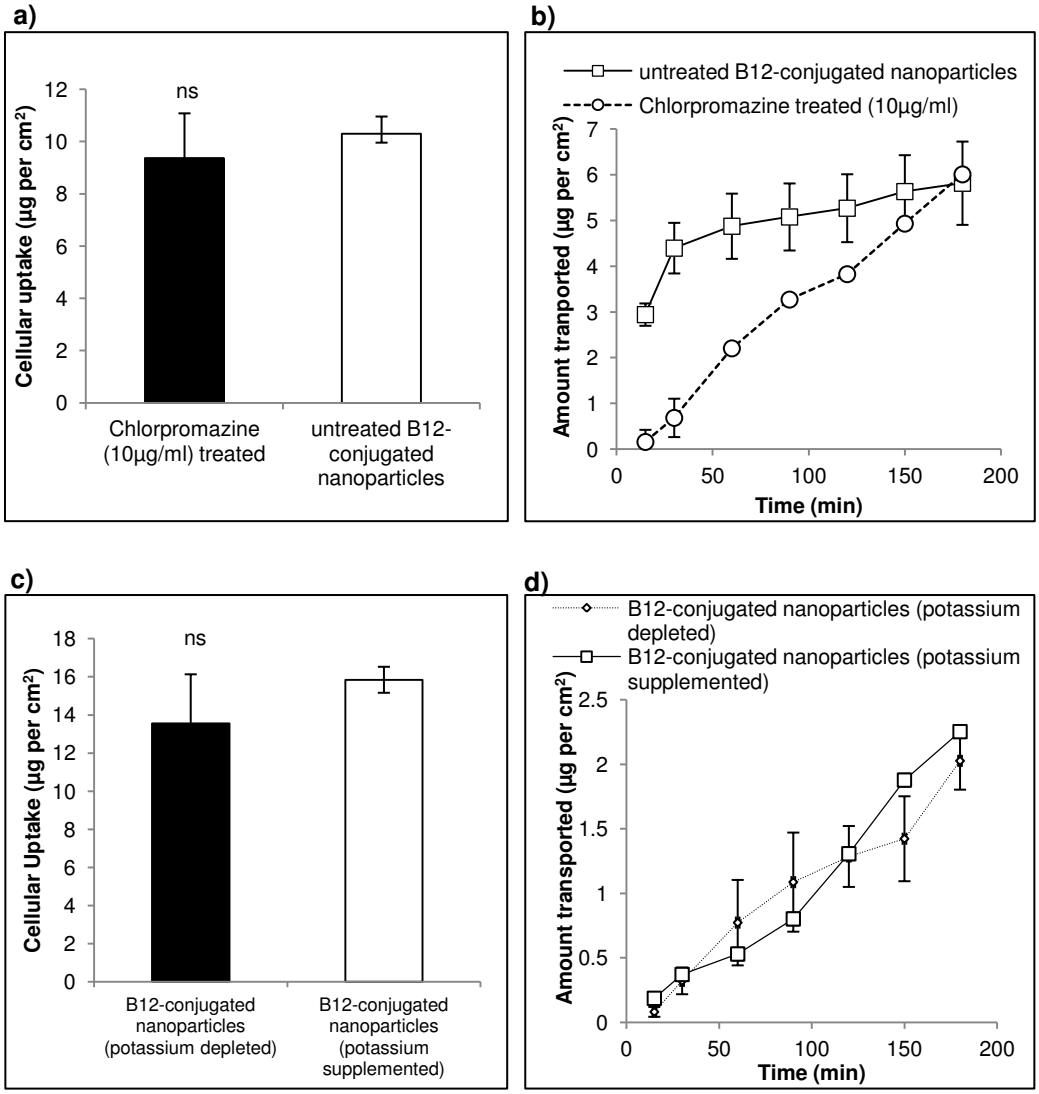

Figure 5. 13. Effect of clathrin inhibition on cell uptake and transport of vitamin B_{12}-conjugated nanoparticles.

a) Effect of chlorpromazine on cell uptake and b) transport of nanoparticles. c) Effect of potassium depletion on cell uptake and d) transport of nanoparticles. Cell uptake and transport studies were conducted with B_{12}-conjugated nanoparticles of 50nm nominal diameter and in the presence of IF. Data represents the mean ± SD (n=3).

Following the demonstration that the clathrin pathway is not involved in cell processes responsible for trafficking vitamin B_{12}-conjugated nanoparticles, the subsequent focus was on determining whether inhibiting the caveolae-dependent pathway would exhibit any effect. Indeed, treatment by filipin gave rise to a pronounced reduction of cell

uptake of vitamin B_{12}-conjugated nanoparticles by approximately 5-fold (Figure 5.14a). The effect is mirrored in the data depicting the transport of vitamin B_{12}-linked nanoparticles in the presence of the same agent (Figure 5.14b), where the transport of nanoparticles was suppressed by nearly 6-fold (1.2 µg *vs* 5.8 µg at 3hrs measurement point for filipin treated and control cells, respectively). It should be noted that, for the purpose of comparison, the data for the control experiment depicting transport of B_{12}-conjugated nanoparticles across untreated cells, presented in Figure 5.14b, was also used in the clathrin inhibition experiment (Figure 5.13b). As in the case of the clathrin inhibition studies, the definitive role of caveolae in the internalisation and transport of vitamin B_{12}-conjugated nanoparticles was confirmed by employing a second inhibitory agent specific to the caveolae endocytic pathway. In the presence of this agent, genistein, cell uptake of vitamin B_{12}-conjugated nanoparticles was significantly reduced (5-fold, Figure 5.14c). The effect was largely reproduced in the transport experiment (Figure 5.14d), where genistein dramatically suppressed the transport of vitamin B_{12}-bearing nanoparticles across Caco-2 monolayers, with the extent of inhibition amounting to 29-fold at the 3hr measurement point.

Taken together, the data from inhibition of specific endocytic pathways suggests that the caveolae-mediated route is predominantly implicated in the cell uptake and transport of this vitamin B_{12}-conjugated nanosystem. The fact that soluble vitamin B_{12} (complexed with IF) trafficking is mediated by clathrin, whilst vitamin B_{12}-bearing nanoparticles exploit caveolae-mediated route(s), is interesting.

The 'switch' in cell entry and intracellular trafficking pathway could result from the nature of nanoparticle-bound vitamin B_{12} ligand interaction with its receptor (cubilin) being different to free vitamin B_{12}. The close proximity of multiple nanoparticle-immobilised ligands may result in multivalent binding (simultaneous interaction of multiple ligands with multiple receptors) of nanoparticle-associated vitamin B_{12}-IF complexes to cubilin. It is possible that this 'unnatural' vitamin B_{12} ligand-cubilin interaction may trigger a cell uptake and intracellular trafficking mechanism that is entirely different to that of free vitamin B_{12}. Indeed, the profound effect of ligand presentation on the cell uptake pathway was recently shown in a study from our group

by Moradi *et al*. [38]. In this work the effect of nanoparticle-bound ligand distribution on cellular internalisation was explored using folate-decorated nanoparticles. The results indicated that both the ligand density and 'clustering' (i.e. presentation of the ligand as 'patches' on nanoparticle surface) on the nanoparticle surface play a profound role in the biological mechanism of nanoparticle internalisation.

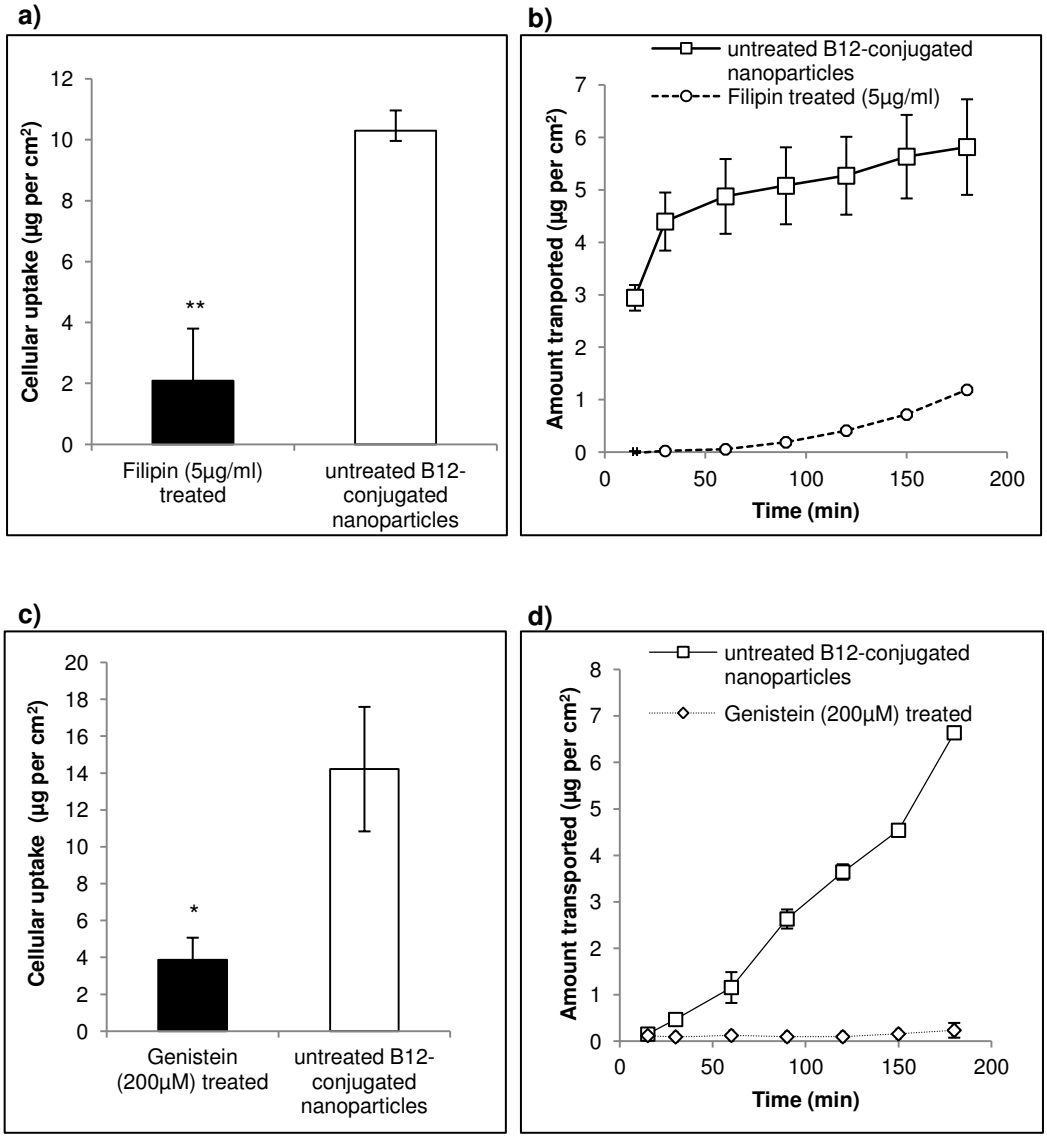

Figure 5. 14. Effect of caveolae inhibition on the uptake and transport of vitamin B_{12}-conjugated nanoparticles.

Effect of filipin on a) cell uptake and b) transport of nanoparticles, Effect of genistein on c) cell uptake and d) transport of nanoparticles. 50nm vitamin B_{12}-conjugated nanoparticles were applied in combination with IF. Data represents the mean ± SD (n=3).

The specificity of chlorpromazine and filipin inhibitors was determined by testing their effect on cell uptake and transport of pathway-selective ligands. These ligands included transferrin [59, 60] and cholera toxin B-subunit [27, 58], which are known to

internalise preferentially either by clathrin- or by caveolae-mediated endocytosis, respectively. In the presence of chlorpromazine (10 µg/ml), internalisation of FITC-transferrin was inhibited by approximately 9-fold (Figure 5.15a) and transport reduced 8-fold (Figure 5.15b). When incubated in combination with filipin (5 µg/ml), cell internalisation (Figure 5.15c) and transport (Figure 5.15d) of cholera-toxin B subunit was reduced by 2.5-fold. These studies thus revealed that at the concentrations used in this work, both chlorpromazine and filipin were effectively inhibiting clathrin- and caveolae-mediated pathways, respectively, in Caco-2 cells.

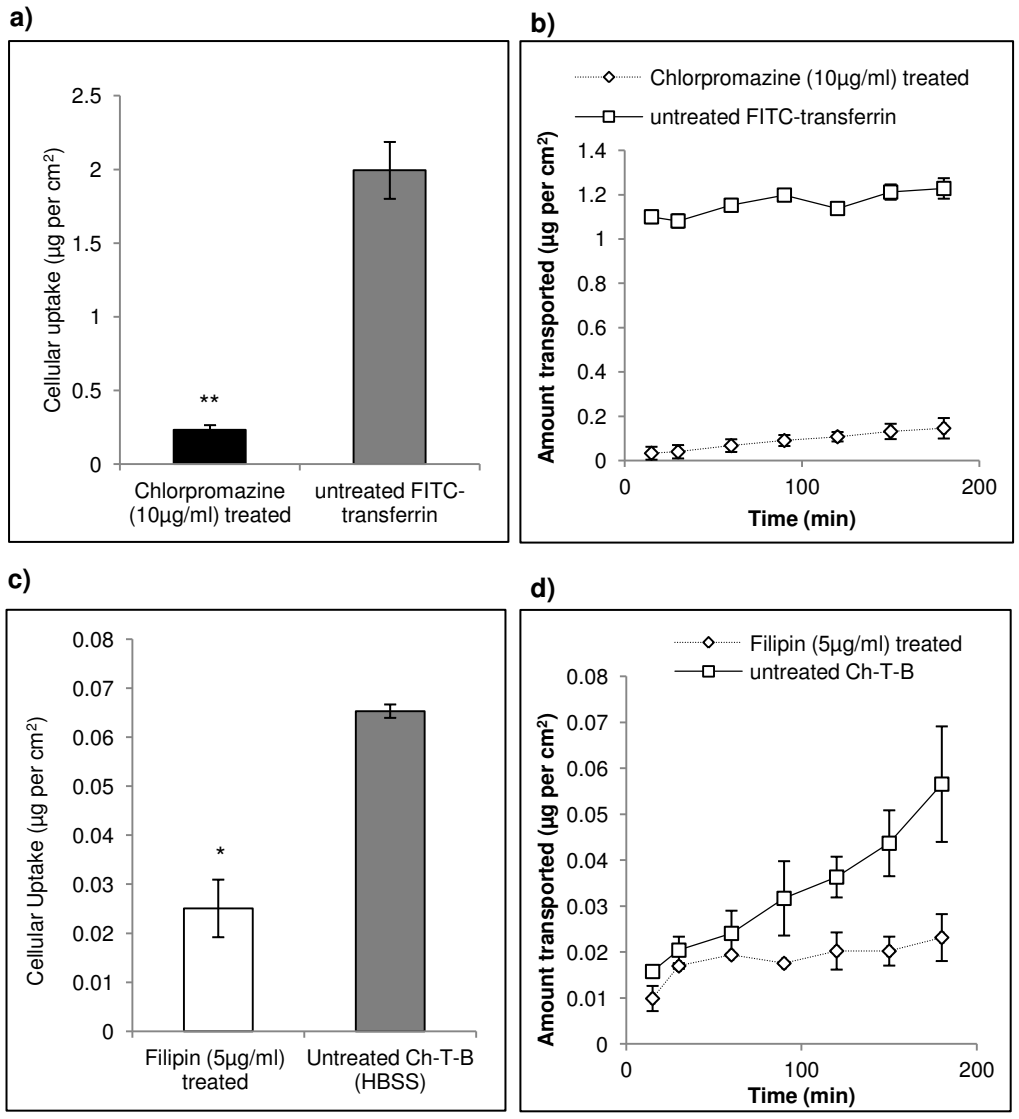

Figure 5. 15. Inhibition of cell uptake (a) and transport (b) of FITC-transferrin and Cholera-toxin B subunit (c, d) by chlorpromazine (10 µg/ml) and filipin (5 µg/ml). Data represents the mean ± SD (n=3).

TEER studies conducted during and following incubation with chlorpromazine, filipin, genistein and K+ depleting medium revealed no apparent adverse effects on the cell monolayers (Figure 5.16). Specifically, incubation with chlorpromazine over a concentration range of 1.25-10 µg/ml for 3 hours (5.16a), resulted in an initial drop in TEER over the first 30 min, followed by a steady recovery over 2.5 hours. This initial decrease in TEER is common following replacement of extracellular medium and results from cell acclimatisation to the change of conditions. Importantly, there was no concentration-dependent TEER response to chlorpromazine, with no difference in monolayers incubated with 1.25 µg/ml chlorpromazine and those incubated with the highest concentration (10 µg/ml). Furthermore, TEER reversibility, as measured following incubation and subsequent removal of chlorpromazine resulted in complete TEER recovery after 24 hours, regardless of the concentration used (Figure 5.16b). The dose-dependent TEER profile with filipin (1.25-5 µg/ml) revealed an apparent increase in TEER following the zero minute time point, with an eventual plateau after 1 hour incubation (Figure 5.16c). Although the reasons for TEER increase are not clear, the data shows that there was no apparent concentration-dependent long term TEER decrease, suggesting that within this concentration range, filipin did not cause any cell toxicity. The TEER reversibility experiment showed that after 24 hours, TEER was restored to levels similar to the baseline value (Figure 5.16d). For genistein, the TEER was measured at a single concentration of genistein (200 µM) as these were optimised conditions for the inhibition experiments (Figure 5.16e). After an initial drop between 0 and 30 min, the resistance remained constant over the 3 hour period (~500 Ωcm^2). TEER measurements taken at the 24 hour time point (Figure 5.16f) in supplemented medium revealed that although complete baseline recovery was not achieved, values >1000 Ωcm^2 indicated that at this concentration, genistein had caused no significant adverse effects to the cell monolayers. As mentioned previously, cell incubation in a potassium depleted medium altered the transport profile considerably. This too was reflected in the TEER profile (Figure 5.16e) as initial readings (at t=0), were ~450 Ωcm^2, suggesting that the cells were sensitive to the change. However, despite an initial further drop in TEER to >200 Ωcm^2 after 150 min,

a slight TEER recovery was noticed. Similarly, although TEER recovery was poor after 24 hours (~600 Ωcm^2, Figure 5.16f), the incremental rise following replacement in cell culture medium, was significant (as TEER had increased to greater than the baseline value in potassium depleted medium), indicating that although these conditions were not optimal for long-term cell incubation, the adverse effects were reversible.

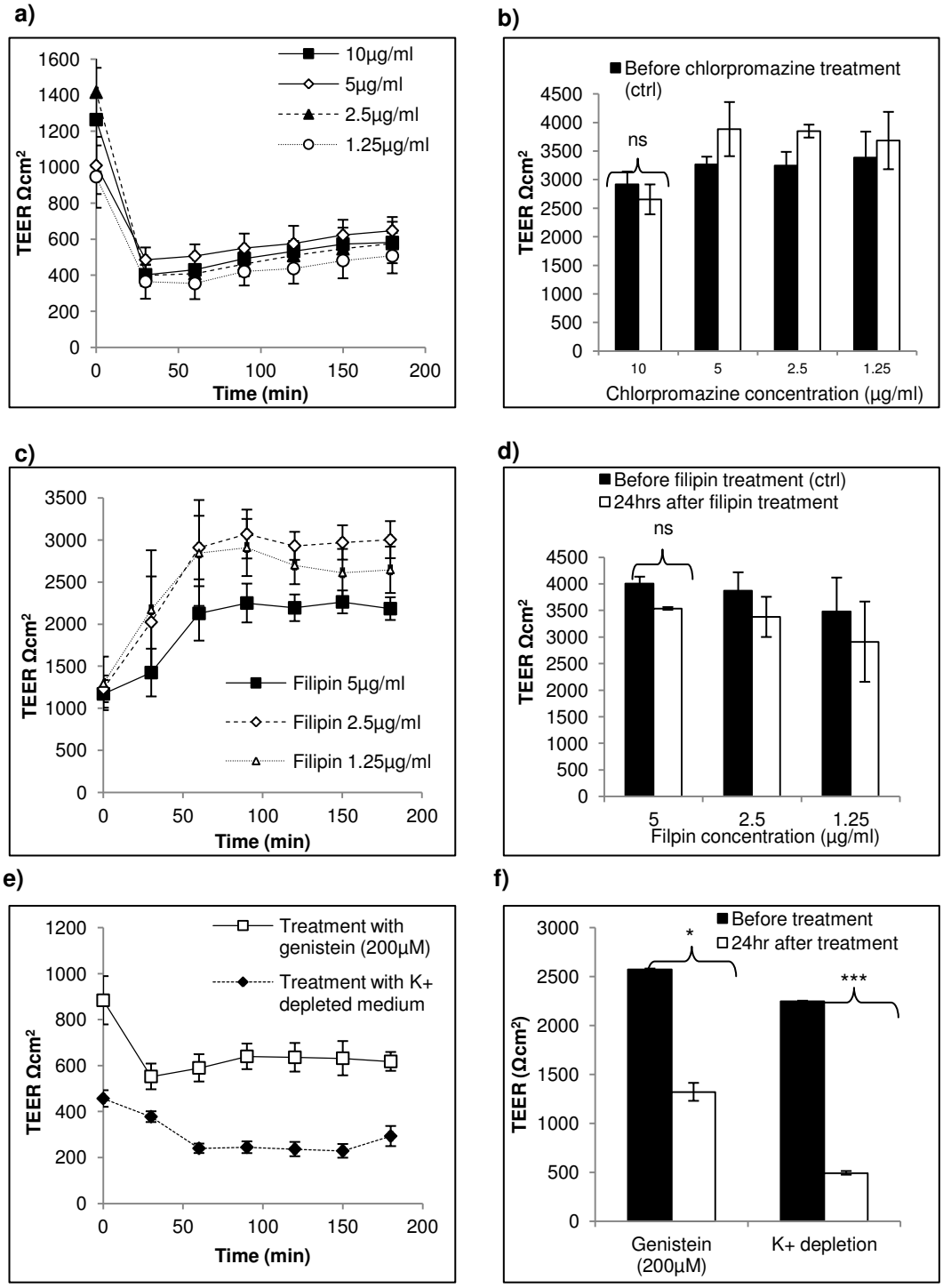

Figure 5. 16. Measurement of TEER on Caco-2 monolayers after treatment with inhibitors of clathrin and caveolae-mediated endocytosis.

a) treatment with chlorpromazine (1.25-10µg/ml) with TEER measurements over 3 hours, b) TEER recovery after 24 hr following treatment with chlorpromazine, c) treatment with filipin (1.25-5µg/ml) with TEER measurements over 3 hours, d) TEER recovery after 24 hr following treatment with filipin, e) treatment with genistein (200µM) and potassium depleted medium with TEER measurements over 3 hours, f) TEER recovery after 24 hr following treatment with genistein and after incubation of cells in a potassium depleted medium.

Having established that vitamin B_{12}-conjugated nanoparticles exploit a different cell trafficking pathway to soluble vitamin B_{12}, the next experimental step sought to determine whether this phenomenon was intrinsically due to nanoparticles. Inhibition of either clathrin or caveolae trafficking pathways, with chlorpromazine and filipin, respectively, did not demonstrate any remarkable effect on the uptake and transport of unmodified nonoparticles (of 50 nm in diameter as used throughout the study), suggesting a dominance of alternative (i.e. non-clathrin and non-caveolae) cell trafficking routes in their cell uptake and transport (Figure 5.17 a and b, respectively).

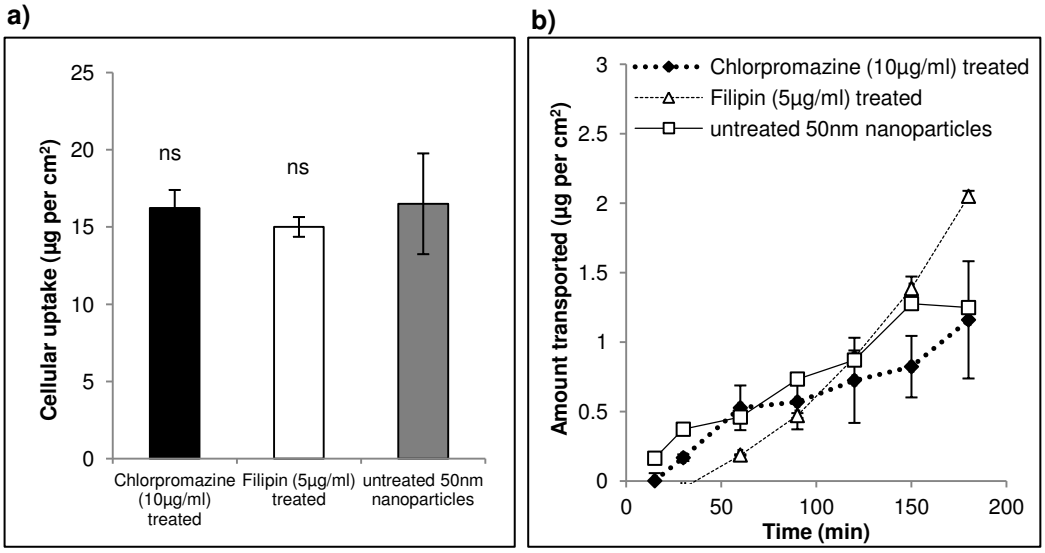

Figure 5. 17. Inhibition of a) cell uptake and b) transport of unmodified 50 nm PS nanoparticles by chlorpromazine (10 µg/ml) and filipin (5 µg/ml).

Data represents the mean ± SD (n=3).'ns' = non significant.

Literature reports on the cell uptake pathways of unmodified polystyrene nanoparticles are rather inconsistent. A study by Dausend *et al*. [66] demonstrated no inhibitory effect by chlorpromazine on the uptake of 120 nm negatively charged polystyrene nanoparticles by HeLa cells. On the other hand, dos Santos *et al*. [67] showed that chlorpromazine inhibited the internalisation of (carboxylated polystyrene) nanoparticles, with the extent of inhibition depending on the particle size (greater for 200 nm, as compared to smaller 40 nm sized nanoparticles). The authors also reported that genistein exerted minimal effect on the internalisation of 40 nm nanoparticles in 3 independent cell lines, which is in agreement with the data for 50 nm particles in this thesis (Figure 5.17). Work by Rejman *et al*. [21] also investigated the uptake pathway of similar systems, namely negatively charged polystyrene

nanoparticles, with sizes between 50 and 1000 nm in B16 cells (mouse melanoma cell line). The authors reported that treatment with inhibitors of caveolae-mediated endocytosis (filpin and genistein) did not affect the uptake of nanoparticles <200 nm in size, but inhibition with chlorpromazine treatment and potassium depletion elicited a greater effect for these particles (with the inhibitory effect diminishing as the size of the particle increased). The published work on the biological pathways of particle uptake hence suggests that both particle size and the cell line(s) employed in the study greatly influence the route of nanoparticle internalisation. A comparison between this thesis and the literature is hence problematic for unmodified nanoparticles and in the case of B_{12}-conjugated particles the comparison is not possible at all considering that the cell uptake mechanisms for B_{12}-decorated particle systems have not been reported. The data on the uptake of B_{12}-conjugated particles by intestinal Caco-2 cells reported here indicate that the involvement of the caveolar route is specific to the B_{12}-conjugate nanosystem (and not unmodified nanoparticles), where surface decoration of particles with vitamin B_{12} ligand is presumably essential for the shift in biological pathway of cell entry and intracellular transport.

5.4 Conclusions

The work detailed in this chapter demonstrated that surface-conjugation of vitamin B_{12} ligand to nanoparticles results in an unexpected intracellular trafficking behaviour in epithelial cell layers, with a 'switch' to a non-degradative caveolae pathway – a finding that may have important implications for oral delivery of nanoscale therapeutics and diagnostics. Although in the process of vitamin B_{12} uptake *in vivo,* lysosomal function is essential to degrade the associated IF [17], further studies are necessary to ascertain whether vitamin B_{12}-conjugated nanoparticles retain IF on exit from the cells and if so, what are the consequences in a therapeutic context. However, the ligand decoration effects observed in epithelial cell cultures on the intracellular trafficking of B_{12}-conjugated PS nanoparticles is, to the best of our knowledge, a previously unreported example of controlled pathway switching in this way. These findings may

provide significant new insights and chemical ‘design rules’ for nanoparticulate systems, which could enable their practical use in delivery of therapeutic and diagnostic macromolecules across the intestinal epithelium.

5.5 References

1. Algar, W.R., et al., *The Controlled Display of Biomolecules on Nanoparticles: A Challenge Suited to Bioorthogonal Chemistry.* Bioconjugate Chemistry, 2011. **22**(5): p. 825-858.
2. Gao, W., J.M. Chan, and O.C. Farokhzad, *pH-Responsive Nanoparticles for Drug Delivery.* Molecular Pharmaceutics, 2010. **7**(6): p. 1913-1920.
3. Yan, Y., et al., *Toward Therapeutic Delivery with Layer-by-Layer Engineered Particles.* Acs Nano, 2011. **5**(6): p. 4252-4257.
4. Zhang, X., et al., *Transfection ability and intracellular DNA pathway of nanostructured gene-delivery systems.* Nano Letters, 2008. **8**(8): p. 2432-2436.
5. Ghosh, P., et al., *Intracellular Delivery of a Membrane-Impermeable Enzyme in Active Form Using Functionalized Gold Nanoparticles.* Journal of the American Chemical Society, 2010. **132**(8): p. 2642-2645.
6. Tekle, C., et al., *Cellular trafficking of quantum dot-ligand bioconjugates and their induction of changes in normal routing of unconjugated ligands.* Nano Letters, 2008. **8**(7): p. 1858-1865.
7. Russell-Jones, G.J., *Oral delivery of therapeutic proteins and peptides by the vitamin B12 uptake system*. Peptide-based drug design: controlling transport and metabolism, ed. M.D.Taylor.and G.L. Amidon. 1995, ACS, Washington DC. 181-198.
8. Russell-Jones, G.J., L. Arthur, and H. Walker, *Vitamin B12-mediated transport of nanoparticles across Caco-2 cells.* Int J Pharm, 1999. **179**(2): p. 247-55.
9. Chalasani, K.B., et al., *Vitamin B12-biodegradable micro particulate conjugate carrier systems for peroral delivery of drugs, therapeutic peptides/proteins and vaccines*. 2002: US patent.
10. Chalasani, K.B., et al., *Effective oral delivery of insulin in animal models using vitamin B12-coated dextran nanoparticles.* J Control Release, 2007. **122**(2): p. 141-50.
11. Swaan, P.W., *Recent advances in intestinal macromolecular drug delivery via receptor-mediated transport pathways.* Pharm Res, 1998. **15**(6): p. 826-34.
12. Russell-Jones, G.J., et al., *Synthesis of LHRH antagonists suitable for oral administration via the vitamin B12 uptake system.* Bioconjug Chem, 1995. **6**(1): p. 34-42.
13. Chalasani, K.B., et al., *A novel vitamin B12-nanosphere conjugate carrier system for peroral delivery of insulin.* J Control Release, 2007. **117**(3): p. 421-9.
14. Moestrup, S.K., et al., *Megalin-mediated endocytosis of transcobalamin-vitamin-B12 complexes suggests a role of the receptor in vitamin-B12 homeostasis.* Proc Natl Acad Sci U S A, 1996. **93**(16): p. 8612-7.
15. Christensen, E.I. and H. Birn, *Megalin and cubilin: multifunctional endocytic receptors.* Nat Rev Mol Cell Biol, 2002. **3**(4): p. 256-66.
16. Gordon, M.M., et al., *Cathepsin L mediates intracellular ileal digestion of gastric intrinsic factor.* Am J Physiol, 1995. **268**(1 Pt 1): p. G33-40.
17. Tuma, P.L. and A.L. Hubbard, *Transcytosis: crossing cellular barriers.* Physiol Rev, 2003. **83**(3): p. 871-932.
18. Krpetic, Z., et al., *Negotiation of Intracellular Membrane Barriers by TAT-Modified Gold Nanoparticles.* Acs Nano, 2011. **5**(6): p. 5195-5201.
19. Nativo, P., I.A. Prior, and M. Brust, *Uptake and intracellular fate of surface-modified gold nanoparticles.* Acs Nano, 2008. **2**(8): p. 1639-1644.
20. De Jong, W.H., et al., *Particle size-dependent organ distribution of gold nanoparticles after intravenous administration.* Biomaterials, 2008. **29**(12): p. 1912-1919.
21. Rejman, J., et al., *Size-dependent internalization of particles via the pathways of clathrin- and caveolae-mediated endocytosis.* The Biochemical journal, 2004. **377**(Pt 1): p. 159-69.
22. Dix, C.J., et al., *The transport of vitamin B12 through polarized monolayers of Caco-2 cells.* Gastroenterology, 1990. **98**(5 Pt 1): p. 1272-9.

23. Dan, N. and D.F. Cutler, *Transcytosis and processing of Intrinsic factor-Cobalamin in Caco-2 cells.* The Journal of biological chemistry, 1994. **269**(29): p. 18849-18855.
24. Bose, S., et al., *Bipolar functional expression of transcobalamin II receptor in human intestinal epithelial Caco-2 cells.* J Biol Chem, 1997. **272**(6): p. 3538-43.
25. Rejman, J., et al., *Size-dependent internalization of particles via the pathways of clathrin- and caveolae-mediated endocytosis.* Biochem J, 2004. **377**(Pt 1): p. 159-69.
26. Zuhorn, I.S., R. Kalicharan, and D. Hoekstra, *Lipoplex-mediated transfection of mammalian cells occurs through the cholesterol-dependent clathrin-mediated pathway of endocytosis.* J Biol Chem, 2002. **277**(20): p. 18021-8.
27. Orlandi, P.A. and P.H. Fishman, *Filipin-dependent inhibition of cholera toxin: evidence for toxin internalization and activation through caveolae-like domains.* J Cell Biol, 1998. **141**(4): p. 905-15.
28. Lencer, W.I., T.R. Hirst, and R.K. Holmes, *Membrane traffic and the cellular uptake of cholera toxin.* Biochim Biophys Acta, 1999. **1450**(3): p. 177-90.
29. McEwan, J.F., H.S. Veitch, and G.J. Russell-Jones, *Synthesis and biological activity of ribose-5'-carbamate derivatives of vitamin B(12).* Bioconjug Chem, 1999. **10**(6): p. 1131-6.
30. Sun, J., X. Zhu, and M. Wu, *Hydroxypropyl-beta-cyclodextrin enhanced determination for the Vitamin B12 by fluorescence quenching method.* Journal of fluorescence, 2007. **17**(3): p. 265-70.
31. Xu, H., et al., *Fluorescence resonance energy transfer between acridine orange and rhodamine 6G and its analytical application for vitamin B12 with flow-injection laser-induced fluorescence detection.* Talanta, 2008. **77**(1): p. 176-81.
32. Valeur, B., *Molecular Fluorescence: Principles and Applications*. 2002: Wiley VCH 402.
33. Ahn, J.S., et al., *Self-assembled particle monolayers on polyelectrolyte multilayers: particle size effects on formation, structure, and optical properties.* Colloids and Surfaces A: Physicochem. Eng. Aspects 2005. **259**: p. 45-53.
34. Gu, F., et al., *Precise engineering of targeted nanoparticles by using self-assembled biointegrated block copolymers.* Proc Natl Acad Sci U S A, 2008. **105**(7): p. 2586-91.
35. Dawson, G.F. and G.W. Halbert, *The in vitro cell association of invasin coated polylactide-co-glycolide nanoparticles.* Pharm Res, 2000. **17**(11): p. 1420-5.
36. Oyewumi, M.O. and R.J. Mumper, *Influence of formulation parameters on gadolinium entrapment and tumor cell uptake using folate-coated nanoparticles.* Int J Pharm, 2003. **251**(1-2): p. 85-97.
37. Saeed, A.O., et al., *Modular construction of multifunctional bioresponsive cell-targeted nanoparticles for gene delivery.* Bioconjug Chem. **22**(2): p. 156-68.
38. Moradi, E., et al., *Ligand density and clustering effects on endocytosis of folate modified nanoparticles.* RSC Adv., 2012. **2**: p. 3025-3033.
39. Hippe, E., E. Haber, and H. Olesen, *Nature of vitamin B 12 binding. II. Steric orientation of vitamin B 12 on binding and number of combining sites of human intrinsic factor and the transcobalamins.* Biochim Biophys Acta, 1971. **243**(1): p. 75-82.
40. Kozyraki, R., et al., *The human intrinsic factor-vitamin B12 receptor, cubilin: molecular characterization and chromosomal mapping of the gene to 10p within the autosomal recessive megaloblastic anemia (MGA1) region.* Blood, 1998. **91**(10): p. 3593-600.
41. Jones, S.A., et al., *The Influence Of Nanoparticle Charge And Hydrophobicity Upon Translocation Across Respiratory Epithelial Cell Layers*, in *DDL*. 2008: Edinburgh, UK.
42. Harush-Frenkel, O., et al., *Targeting of nanoparticles to the clathrin-mediated endocytic pathway.* Biochem Biophys Res Commun, 2007. **353**(1): p. 26-32.
43. Qaddoumi, M.G., et al., *The characteristics and mechanisms of uptake of PLGA nanoparticles in rabbit conjunctival epithelial cell layers.* Pharm Res, 2004. **21**(4): p. 641-8.

44. Russell-Jones, G.J., H. Veitch, and L. Arthur, *Lectin-mediated transport of nanoparticles across Caco-2 and OK cells.* International journal of pharmaceutics, 1999. **190**(2): p. 165-74.
45. Ullrich, N., et al., *Stimulation by caveolin-1 of the hypotonicity-induced release of taurine and ATP at basolateral, but not apical, membrane of Caco-2 cells.* Am J Physiol Cell Physiol, 2006. **290**(5): p. C1287-96.
46. Patlolla, J.M., et al., *Overexpression of caveolin-1 in experimental colon adenocarcinomas and human colon cancer cell lines.* Oncol Rep, 2004. **11**(5): p. 957-63.
47. Field, F.J., et al., *Caveolin is present in intestinal cells: role in cholesterol trafficking?* J Lipid Res, 1998. **39**(10): p. 1938-50.
48. Cohen, A.W., Hnasko, R., Schubert, W., Lisanti, M.P., *Role of Caveolae and Caveolins in Health and Disease.* Physiol Rev, 2004. **84**: p. 1341-1379.
49. Li, S., et al., *Baculovirus-based expression of mammalian caveolin in Sf21 insect cells. A model system for the biochemical and morphological study of caveolae biogenesis.* J Biol Chem, 1996. **271**(45): p. 28647-54.
50. Razani, B., et al., *Caveolin-1-deficient mice are lean, resistant to diet-induced obesity, and show hypertriglyceridemia with adipocyte abnormalities.* J Biol Chem, 2002. **277**(10): p. 8635-47.
51. Dupree, P., et al., *Caveolae and sorting in the trans-Golgi network of epithelial cells.* EMBO J, 1993. **12**(4): p. 1597-605.
52. Sargiacomo, M., et al., *Oligomeric structure of caveolin: implications for caveolae membrane organization.* Proc Natl Acad Sci U S A, 1995. **92**(20): p. 9407-11.
53. Mayor, S., K.G. Rothberg, and F.R. Maxfield, *Sequestration of GPI-anchored proteins in caveolae triggered by cross-linking.* Science, 1994. **264**: p. 1948-1951.
54. Mirre, C., et al., *Detergent-resistant membrane microdomains from Caco-2 cells do not contain caveolin.* Am J Physiol, 1996. **271**(3 Pt 1): p. C887-94.
55. Vogel, U., K. Sandvig, and B. van Deurs, *Expression of caveolin-1 and polarized formation of invaginated caveolae in Caco-2 and MDCK II cells.* J Cell Sci, 1998. **111 (Pt 6)**: p. 825-32.
56. Vachon, P.H. and J.F. Beaulieu, *Transient mosaic patterns of morphological and functional differentiation in the Caco-2 cell line.* Gastroenterology, 1992. **103**(2): p. 414-23.
57. Giannoni, F., F.J. Field, and N.O. Davidson, *An improved reverse transcription polymerase chain reaction method to study apolipoprotein gene expression in Caco-2 cells.* J. Lipid. Res., 1994. **35**: p. 340-350.
58. Schnitzer, J.E., et al., *Filipin-sensitive caveolae-mediated transport in endothelium: reduced transcytosis, scavenger endocytosis, and capillary permeability of select macromolecules.* J Cell Biol, 1994. **127**(5): p. 1217-32.
59. Motley, A., et al., *Clathrin-mediated endocytosis in AP-2-depleted cells.* J Cell Biol, 2003. **162**(5): p. 909-18.
60. Lakadamyali, M., M.J. Rust, and X. Zhuang, *Ligands for clathrin-mediated endocytosis are differentially sorted into distinct populations of early endosomes.* Cell, 2006. **124**(5): p. 997-1009.
61. Larkin, J.M., et al., *Depletion of intracellular potassium arrests coated pit formation and receptor-mediated endocytosis in fibroblasts.* Cell, 1983. **33**(1): p. 273-85.
62. van der Aa, M.A., et al., *Cellular uptake of cationic polymer-DNA complexes via caveolae plays a pivotal role in gene transfection in COS-7 cells.* Pharm Res, 2007. **24**(8): p. 1590-8.
63. Parton, R.G., B. Joggerst, and K. Simons, *Regulated internalization of caveolae.* J Cell Biol, 1994. **127**(5): p. 1199-215.
64. Mentzel, S., et al., *In vivo antibody-mediated modulation of aminopeptidase A in mouse proximal tubular epithelial cells.* The journal of histochemistry and cytochemistry : official journal of the Histochemistry Society, 1999. **47**(7): p. 871-80.

65. Wells, A., et al., *Shaping up for shipping out: PLCgamma signaling of morphology changes in EGF-stimulated fibroblast migration.* Cell motility and the cytoskeleton, 1999. **44**(4): p. 227-33.
66. Dausend, J., et al., *Uptake mechanism of oppositely charged fluorescent nanoparticles in HeLa cells.* Macromol Biosci, 2008. **8**(12): p. 1135-43.
67. dos Santos, T., et al., *Effects of transport inhibitors on the cellular uptake of carboxylated polystyrene nanoparticles in different cell lines.* PLoS One. **6**(9): p. e24438.

Chapter 6: The role of intrinsic factor on cellular trafficking of vitamin B_{12}-conjugated nanoparticles

6.1 Introduction

The clear involvement of intrinsic factor (IF) in the intestinal absorption of vitamin B_{12}, together with the associated molecular mechanism, has been depicted in earlier sections of this thesis (Chapters 1, 4 &5). The trafficking (binding, internalisation and transcytosis) of soluble vitamin B_{12}, has been shown to be an IF-dependent phenomenon in several cell lines [1-8]. However, studies have also demonstrated the transport of vitamin B_{12} across epithelial cells in the absence of IF [9, 10]. This transport is thought to occur either paracellularly [11] (indeed with a molecular weight of 1356 Da, the paracellular route is expected to contribute to overall transport of vitamin B_{12}), as has been suggested for other subtypes within the vitamin B family (thiamin, riboflavin and pyridoxine) [12] or due to the complexation of vitamin B_{12} with apically localised-TCII, followed by recognition and endocytosis by the TCII-receptor (Chapter 1, section 1.5.2.3).

Whether the presence of IF is a crucial parameter influencing the uptake and transport of B_{12}-bearing nanoparticles is not clear. Similarly to soluble vitamin B_{12}, routes other than the cubilin-mediated pathway (which binds to the IF-vitamin B_{12} complex) could contribute to the uptake and transport of vitamin B_{12}-conjugated nanoparticles. This chapter details work conducted to consider the role of IF on the uptake and transport of B_{12}-conjugated nanoparticles in Caco-2 cells. The effect of IF on the trafficking pathways of B_{12}-nanoparticles was determined to establish whether IF dictates the cell trafficking of B_{12}-bearing nanoparticles.

6.2 Methods

6.2.1 Effect of IF on cell uptake and transport of B_{12}-conjugated nanoparticles

The chemical synthesis and characterisation of the vitamin B_{12} α-ω-aminohexylcarbamate derivative is described in Chapter 4 (sections 4.2.1 and 4.2.2). Methods for the preparation and characterisation of the B_{12}-conjugated nanoparticles are described in Chapter 5, sections 5.5.2-5.2.3.

For the cell uptake and transport studies, culture medium was removed from filter-cultured Caco-2 cells and replaced with HEPES (20mM) buffered HBSS and cell monolayers were incubated for 45 min. Unmodified YO nanoparticles and vitamin B_{12}-conjugated nanoparticles (50, 100, 200 nm) were suspended in HBSS/HEPES to achieve a final concentration of 400 µg/ml. B_{12}-conjugated nanoparticles were applied to the cells in the presence or absence of IF. Regarding the former, 3 µg of recombinant human IF (rHUIF, Autogen Bioclear Ltd) was added per 1 ml of 400 µg/ml suspension of B_{12}-conjugated nanoparticles (as discussed in Chapter 5, sections 5.2.5 and 5.3.4) and the solution was incubated at 37˚C prior to application to cells. Following TEER measurement (as described in chapter 2, section 2.2.2), nanoparticle suspensions (0.5ml) were applied to the apical chamber of triplicate wells and the Caco-2 cultures incubated at 37˚C over 3 hrs. At 30 minute sampling intervals, 100 µl was removed from the basolateral side and analysed for fluorescence. Sample volumes were replaced with 100 µl of HEPES/HBSS to maintain the same basal volume. Internalised fluorescence (signifying nanoparticle uptake) was determined following cell lysis using 0.2% v/v Triton X-100 (Fluka) (10 min incubation). Cell uptake of nanoparticles was quantified by fluorescence (Dynex, microplate reader, 529 nm/546 nm) using calibration curves (as in Chapter 5, section 5.2.5).

6.2.2 Effect of IF on cell uptake and transport of soluble B_{12}

In addition to nanoparticle studies, the effect of IF on cell uptake and transport was also determined for soluble vitamin B_{12}. Vitamin B_{12} (cyanocobalamin, 1 mg/ml) was applied (0.5 ml) to the Caco-2 cell monolayers (in HEPES-buffered HBSS, with or without IF (rHUIF), which was used at 3 µg/ml. It must be noted that application of IF

at a 1:1 molar ratio to vitamin B_{12} was not feasible due to the high applied concentration of vitamin B_{12}. Soluble vitamin B_{12} uptake and transport studies were analysed in a similar manner to the nanoparticle transport experiments, but instead vitamin B_{12} was quantified by UV absorbance (350 nm, Beckman Coultier DU 800 UV spectrophotometer), using a pre-constructed calibration curve. In addition, soluble B_{12} transport studies were conducted using different applied amounts (5 µg, 50 µg and 500 µg) at 37 ℃ and 4 ℃. These were carried out to determine whether soluble vitamin B_{12} transport is saturable and to assess the contribution of the paracellular (passive transport) route to overall transepithelial translocation of soluble B_{12}.

6.2.3 Effect of IF on cell uptake and transport pathways of B_{12}-conjugated nanoparticles

B_{12}-conjugated nanoparticles of 50 nm in size were applied to Caco-2 cell monolayers as a 400 µg/ml suspension (in HEPES:HBSS buffer), with or without IF (as in section 6.2.1) and in combination with inhibitors of clathrin and caveolae endocytosis. Caco-2 cell monolayers were treated with filipin (5 µg/ml) or chlorpromazine (10 µg/ml), diluted in HBSS/HEPES buffer for 1hr at 37℃ prior to the addition of nanoparticles (as detailed in Chapter 5, section 5.2.9). Vitamin B_{12}-conjugated nanoparticles (in either the presence or absence of IF) were applied suspended in HBSS/HEPES buffer (400 µg/ml) containing one of the above inhibitors at the appropriate concentration and incubated for 3 hrs. At 30 min sampling intervals, 100 µl samples were removed from the basolateral side for fluorescence determination in order to quantify the transport of the nanoparticles. At the final time point, nanoparticle internalisation was determined by cell lysis as described in Chapter 5, section 5.2.5.

6.3 Results and Discussion

6.3.1 Effect of IF on cell uptake and transport of B_{12}-conjugated nanoparticles

Assuming that B_{12}-conjugated nanoparticles cross the epithelial barrier in the manner mirroring that of soluble vitamin B_{12}, would suggest that the entire cubilin receptor-IF-B_{12}-nanoparticle complex would be internalised bound to megalin and *via* clathrin-coated vesicles [13, 14]. However, in chapter 5, it was shown clearly that the

trafficking of B_{12}-conjugated nanoparticles (in the presence of IF) in Caco-2 cells occurs in a way that is different to both soluble vitamin B_{12} and unmodified nanoparticles, hence further studies were needed to ascertain whether IF itself is important for the cell uptake and transport of B_{12}-bearing nanoparticles. Furthermore, there is evidence of transport of soluble vitamin B_{12} across epithelial cells in IF-free conditions [9, 10], which may arise from non-cubilin mediated pathways, such as through the paracellular route and *via* the TCII receptor.

Initial work in this chapter investigated whether the presence of IF influences the level of cell uptake of B_{12}-conjugated nanoparticles. In this regard, Figure 6.1a compares cellular internalisation of B_{12}-conjugated nanoparticles (50, 100 nm and 200 nm nominal diameter) in Caco-2 cells in the presence or absence of IF. The data shows that the effect of IF on the cell uptake of B_{12}-conjugated nanoparticles appears to be dependent on the nanoparticle size. Specifically, there was a 2.5-fold lower level of cell internalisation for 50 nm nanoparticles in the absence of IF (13 µg *per* cell layer *vs.* 32 µg in the presence of IF). However for the larger nanoparticles of 100 nm and 200 nm, a reduction in cell uptake in IF-free conditions was not statistically significant compared to conditions with added IF.

Regarding the apical-to-basolateral transport of B_{12}-conjugated nanoparticles between 30 min and 3 hrs (Figure 6.1b) for the 100 nm system, the rate of transport across the cell monolayers was higher in the presence of IF (as indicated by a higher slope gradient of 0.0318, compared to 0.022 in IF-free conditions, which amounts to a 1.45-fold increase), while the rate of transport for 50 nm B_{12}-conjugated nanoparticles during this period was not significantly affected by the presence of IF (gradients of 0.098 and 0.095 in the presence and absence of IF, respectively). For 200 nm B_{12}-conjugated nanoparticles, the presence of IF appeared to somewhat enhance the rate of transport (1.3-fold increase, indicated by in the change in slope gradient from 0.066 to 0.086).

In terms of comparison of transport rate in IF-free conditions for different particle sizes, 50 nm B_{12}-conjugated nanoparticles were transported at a lower rate compared to 100 nm sized counterparts, with 200 nm B_{12}-conjugated nanoparticles exhibiting the lowest rate of transport. This mirrors the trend observed for IF-supplemented conditions.

It is however important to note that the rate of transport appears to be at its highest during the first 30 minutes of the experiment (no intermediate measurements were made between 0 and 30 minutes), as shown by a large increment in transport amount from 0 minutes to 30 minutes. This pattern, shown in Figure 6.1b, may be expected for a receptor-mediated system, whereby following ligand application, receptors are rapidly occupied, leading to a net loss of receptors at the apical cell surface before they are able to recycle back to engage with more ligand [15]. During this time, ligands bound to the receptors move through a series of endocytic vesicles. This results in a flux of transported cargo 'all at once.' Continued exposure of the cells to the vitamin B_{12} ligand-bound nanoparticles then results in a sustained, but considerably slower rate of uptake and transport. Similar observations were reported by Paulos *et al.* [16] on the ligand binding and kinetics of folate receptor recycling.

IF elicited a more notable effect on the cumulative *amount* of B_{12}-conjugated nanoparticles transported over the three hour experiment for both 50 nm and 100 nm sized nanoparticles. This effect was more prominent for the transport of 50 nm B_{12}-conjugated nanoparticles, where IF enhanced the overall transport from 3.05 µg to 5.81 µg per cell layer, while for 100 nm sized B_{12}-nanoparticles, transported amounts reached 10.14 µg per cell layer in the absence of IF compared with 14.1 µg in the presence of IF. Addition of IF to 200 nm B_{12}-conjugated nanoparticles did not appear to significantly affect the overall amount transported (1.39 µg *versus* 1.34 µg in IF-containing and IF-absent conditions, respectively).

Overall, this data suggests that in the absence of IF, B_{12}-conjugated nanoparticles are still internalised and transported across intestinal Caco-2 monolayers, but the level of

this trafficking is of a reduced capacity compared to that occurring by cells in the presence of IF. Interestingly, in some instances (e.g. for 100 nm B_{12}-conjugated nanoparticles) IF appears to influence the extent of nanoparticle transport (in terms of both rate and amount), but appears not to affect their uptake by the cells. The reason for this is presently unclear, but it may be related to an effect on intracellular events occurring post particle uptake.

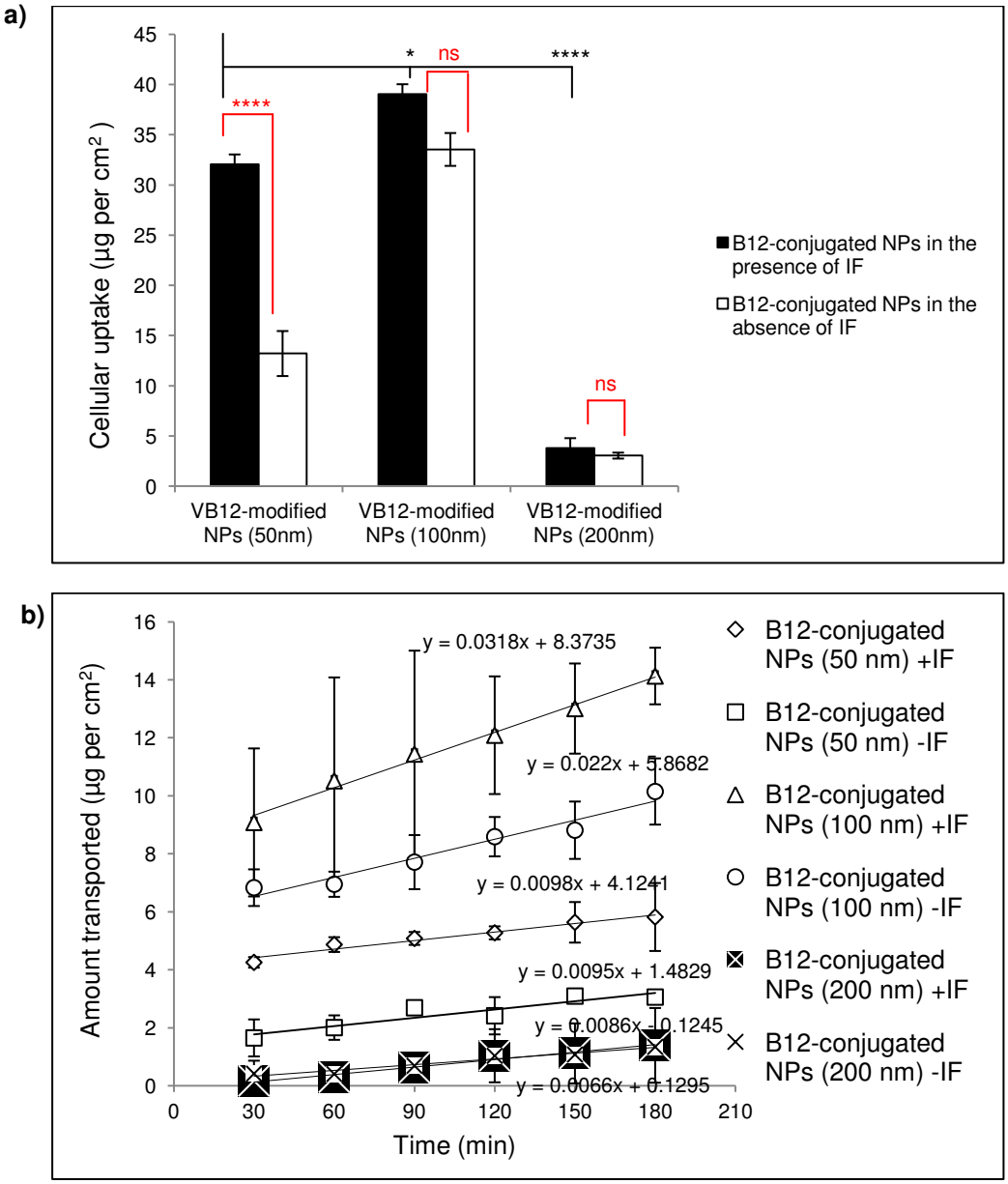

Figure 6. 1. Cell uptake and transport of B_{12}-conjugated nanoparticles in Caco-2 monolayers.

a) Cell uptake of B_{12}-conjugated nanoparticles of 50, 100 and 200 nm size in the presence and absence of intrinsic factor (IF), b) transport of B_{12}-conjugated nanoparticles of 50, 100 and 200 nm size in the presence and absence of IF. Data represents the mean ±SD (n=3). Data fitted with a linear trend line and the equation of the line is displayed for each data set.

Studies examining the role of IF on epithelial uptake and transport of B_{12}-bearing nanoparticles are rare. One such study investigated the effect of IF on the uptake and transport of vitamin B_{12}-conjugated nanoparticles of the same nominal size as those employed in this work (i.e. 50 nm, 100 nm and 200 nm) [10]. The authors reported that the addition of IF enhanced the uptake of vitamin B_{12}-bearing nanoparticles by only a small degree (likely to be statistically insignificant, though the authors did not provide a statistical comparison) and did not affect the level of transport – a trend that was apparent for all three particle sizes tested. This finding prompted the authors of the study to conclude that Caco-2 cells are able to internalise and transport B_{12}-nanoparticles in both an IF-independent and IF-dependent manner, without further explanation for the discrete role of IF on their system.

It must be noted that in the present study, the uptake and transport of B_{12}-conjugated nanoparticles in the absence of IF occurs to a notably greater extent compared to unmodified nanoparticles (Chapter 5, Figure 5.8). This would suggest that an additional, IF-independent vitamin-B_{12} pathway is operating in Caco-2 cells, which is in agreement with work by Russell-Jones *et al*. [10]. At this stage, one can only speculate that this secondary pathway is occurring *via* the TCII receptor. The expression of this receptor has previously been found in both the basolateral and apical membranes of Caco-2 cells in an apparent ratio of 6:1 and TCII was shown to mediate vitamin B_{12} endocytosis from both directions with a capacity proportionate to the extent of expression on basolateral and apical membranes [17]. The expression of the both TCII and the TCII receptor is also shown in this thesis (Chapter 3, sections 3.3.4.1 and 3.3.4.2, respectively).

The apical pathway for TCII-B_{12} endocytosis also appears to be functional in intact rat intestine [9]. Importantly however, the relevance of this pathway *in vivo* is not clear, as the presence of TCII carrier protein (a crucial component for the functioning of this pathway) in the intestinal lumen has not been demonstrated. Furthermore, patients with IF or cubilin defects, develop vitamin B_{12} deficiency [17, 18], highlighting that the TCII pathway may not be important for physiological absorption of vitamin B_{12} in man.

6.3.2 Effect of IF on cell uptake and transport of soluble B_{12}

Following studies that assessed the role of IF on cell internalisation and transport of B_{12}-conjugated nanoparticles, further experiments were conducted to establish whether IF contributes to the cell uptake and transport of soluble vitamin B_{12}. Data comparing the uptake of soluble vitamin B_{12} in culture conditions with added IF and those without IF (Figure 6.2a) shows a larger extent of uptake (2.3-fold higher) in the presence of IF. The data depicting the transport of soluble vitamin B_{12} across the cell layer in IF-containing or IF-free medium (Figure 6.2b), on the other hand, illustrates that the effect of IF on transport is not as apparent as its influence on the uptake. To this end, soluble vitamin B_{12} transported at a similar *rate* (amount transported over time) with or without IF. The cumulative amount of vitamin B_{12} transported across the cell monolayers in the experiment was somewhat higher when vitamin B_{12} was co-administered with IF in comparison to IF-free conditions, again dominated by the initial transport occurring between 0 and 30 minutes.

a)

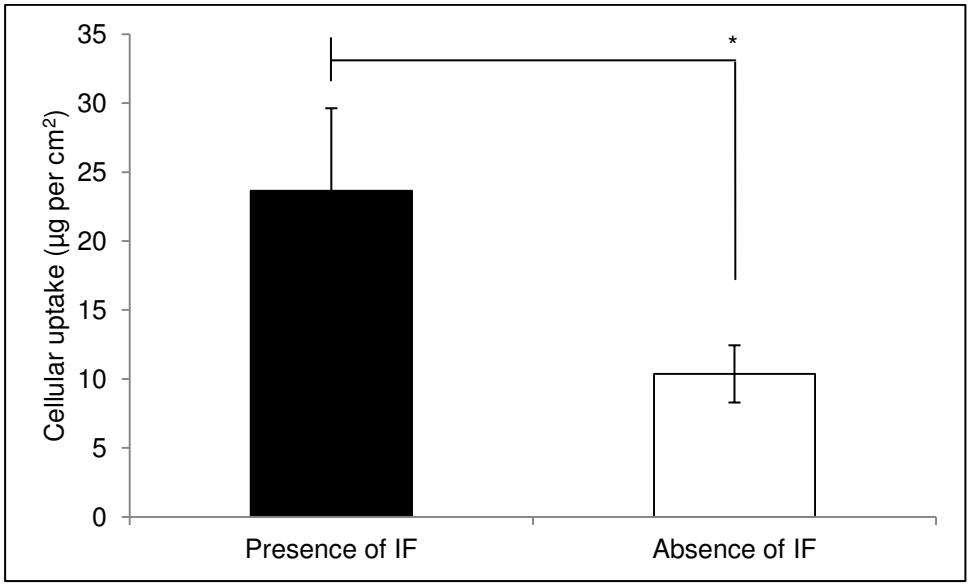

b)

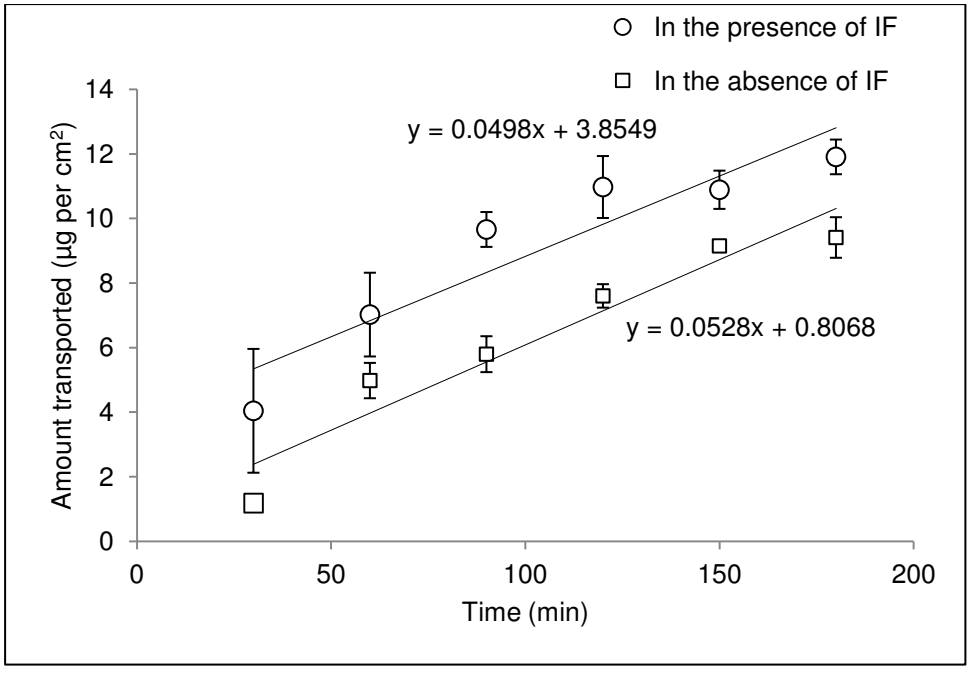

Figure 6. 2. Effect of intrinsic factor on the uptake and transport of soluble vitamin B_{12}.

Effect of IF on a) cell uptake and b) transport of nanoparticles, Soluble vitamin B_{12} (500 µg) was applied to the cell monolayers either in the presence or absence of IF. Data represents the mean ± SD (n=3).

It is rather difficult to compare our data on the role of IF on cell uptake and transport of (soluble) vitamin B_{12} with the literature. For example, in the aforementioned study by Russell-Jones and colleagues [10], the presence of IF was found to either inhibit or promote the uptake of soluble vitamin B_{12}, depending on cell passage number, whilst

transport was generally found to be facilitated by the presence of IF, although again, this was highly dependent on cell passage number, which adds complexity and makes the comparison between this work and studies by others (e.g. the publication by Russell-Jones *et al.* [10]) problematic. Furthermore, numerous studies [19-21] investigating vitamin B_{12} transport do not specify whether B_{12} was applied in combination with IF, making appropriate comparisons difficult.

An important difference between this work and some of the previous studies examining the uptake and trafficking of soluble vitamin B_{12} lies in the applied dose of vitamin B_{12}. The amount of vitamin B_{12} applied to Caco-2 monolayers in this work (500 µg per cell layer) were considerably higher compared to those used in some studies [22] where vitamin B_{12} was applied at more physiologically relevant amounts (e.g. 100 fmoles/well or 1.36 ng/well), while another study from the same group [10] fails to specify applied amounts of vitamin B_{12}. On the other hand, a group of studies from other authors have employed similar concentrations of soluble vitamin B_{12} to this work, with Sarti *et al*. [20] applying 50 µg/ml, Tronde *et al.* [21] using 10 µM (1.36 µg/ml) (both in Caco-2 monolayers) and Schanker *et al*. [11], measuring soluble vitamin B_{12} transport across rat lung following its application over a 100-fold range of concentrations from 0.01 to 1 mM, which was reported to be non-saturable. Non-saturable transport of soluble vitamin B_{12} across a 100-fold range of applied amounts (in the presence of IF) is also observed in the present work. The data in Figure 6.3 shows no plateau in the level of transport as the applied dose increased from 5 µg-500 µg at 37 ℃.

It should be noted that in the literature reports discussed above, the apparent permeability of soluble vitamin B_{12} across the mucosal models (i.e. Caco-2 cells or lung tissue) amounted to 1.8×10^{-7} cm/s [20], 1×10^{-7} cm/s [21] and 8×10^{-7} cm/s [11, 19], which are similar values to that reported in this chapter (7.54×10^{-7} cm/s, when expressing soluble vitamin B_{12} transport as an apparent permeability coefficient, calculated from Figure 6.2b according to the equation described in Chapter 2) and

indeed in other sections in this thesis. The conditions (higher than the physiological dose of soluble vitamin B_{12}) employed in this study were not used to predict the absorption capacity of the vitamin B_{12} by the intestinal epithelium; but to assess whether the additional effect of IF on cell uptake and transport of soluble vitamin B_{12} is similar to that seen for vitamin B_{12}–conjugated nanoparticles.

Figure 6.3 also depicts transport of soluble vitamin B_{12} across Caco-2 monolayers at 4 ℃ – conditions where energy-requiring cell processes are inhibited. The data indicates that in this scenario, the transport of soluble vitamin B_{12} across the cells is suppressed over all the applied concentrations.This data implies that at the concentration applied, a considerable proportion (up to 41%) of the transported soluble B_{12} traverses the Caco-2 monolayers passively, most likely through the paracellular corridor. This is perhaps not surprising considering the molecular weight of soluble vitamin B_{12} (1356 Da), as discussed in section 6.1.

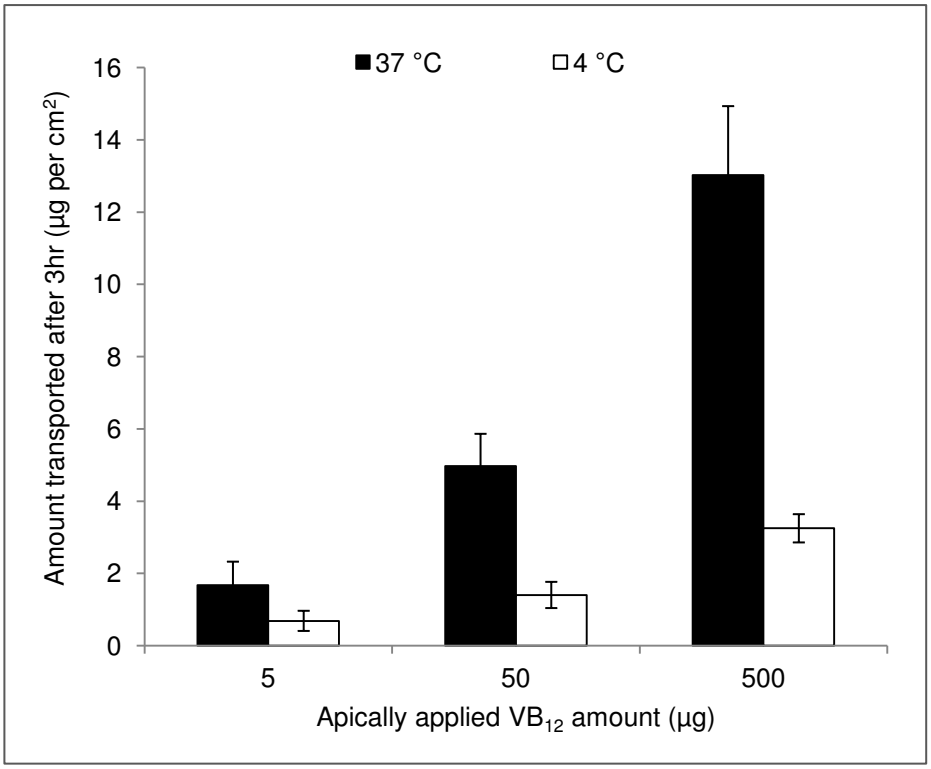

Figure 6. 3. Transport of soluble vitamin B_{12} (applied with IF in all cases) across Caco-2 cell monolayers, following different applied amounts (apically) at 37℃ and 4℃.

Data represents the mean ± SD (n=3).

6.3.3 Effect of IF on cell trafficking of soluble vitamin B_{12}

The role of clathrin-mediated uptake in cell trafficking pathway of native soluble vitamin B_{12} *in vivo* is well established [23]. The literature documented cell uptake and transport mechanisms of vitamin B_{12} in the presence of IF were confirmed in Chapter 5, where the results suggested that vitamin B_{12}-IF internalisation and transport were sensitive to the effects of chlorpromazine inhibition of the clathrin pathway, but remained insensitive to the effects of caveolae inhibition using filipin. Work presented in this section aimed to evaluate the cell uptake and trafficking of soluble vitamin B_{12} in the absence of IF.

In the presence of chlorpromazine, cell internalisation of soluble vitamin B_{12} in the absence of IF (Figure 6.4a) was inhibited by approximately 2.7-fold and reduced to a somewhat lower extent (~2.1-fold) in the presence of filipin (with a statistically significant more prominent effect by chlorpromazine). This suggests a role for both clathrin- and caveolae-mediated pathways in the process of cell trafficking of soluble B_{12} ligand in the absence of IF. Similarly, transport of B_{12} across Caco-2 cell monolayers was inhibited by both agents (Figure 6.4b), where the data revealed a 3.8-fold decrease following treatment by chlorpromazine, as compared to a 3.2-fold decrease in the presence of filipin. It is therefore likely that vitamin B_{12} trafficking in the absence of IF explores other cellular uptake and trafficking pathways, potentially implicating the role of the TCII receptor-mediated pathway.

In the current model of vitamin B_{12} trafficking, the TCII-B_{12} complex that is bound to the TCII-receptor is internalised *via* clathrin-coated pits, as in the case of the IF-B_{12} complex bound to cubilin [23]. In one experimental study [24], the TCII receptor was detected in the apically derived clathrin-coated vesicles and intermicrovillar clefts of the rat kidney, and although no further evidence was provided for its sub-cellular location within the intestine (or in Caco-2 cells), these findings nonetheless implicated a role for clathrin in the internalisation of the TCII receptor.

Contrary to literature reports [23, 24], the data presented in this section indicates that soluble B_{12} uptake in the absence of IF is dependent on both caveolae- and clathrin-

mediated endocytosis events. Therefore, unlike vitamin B_{12} uptake in the presence of IF (i.e. most likely in the form of the B_{12}-IF complex), which is governed by the clathrin pathway (as results suggested in Chapter 5, Figure 5.12), it appears that soluble vitamin B_{12} in the absence of IF may (also) exploit alternative routes, with one possibility being the TC-II receptor-mediated pathway.

The joint contribution of cellular pathways (i.e. both clathrin and caveolae) has also been implicated in the endocytosis of insulin [25]. Evidence indicates that in the endothelium, it can be endocytosed by both clathrin-coated and non-coated vesicular pathways [26, 27], consistent with the proposed idea that coated pits internalise insulin for degradative purposes and that in the endothelium, insulin can be internalised not only for degradation but for other purposes, such as transcytosis. Therefore, the association of receptors *either* within clathrin-coated pits *or* within caveolar structures *per se* does not necessarily limit them to adopting a single pathway when bound to ligand. Likewise and as partly demonstrated in Chapter 5, the highly complex cell trafficking pathways are not controlled by the ligand-receptor interaction alone and *in vitro* data may not necessarily reflect the *in vivo* situation (there may also be tissue-specific differences).

The finding therefore that soluble vitamin B_{12} uptake and transport in intestinal epithelial Caco-2 cells in the absence of IF utilise route(s) that do not follow those observed in the literature and do not display the same pattern of sensitivity to endocytosis inhibitors as the trafficking route in the presence of IF is therefore not entirely unexpected.

a)

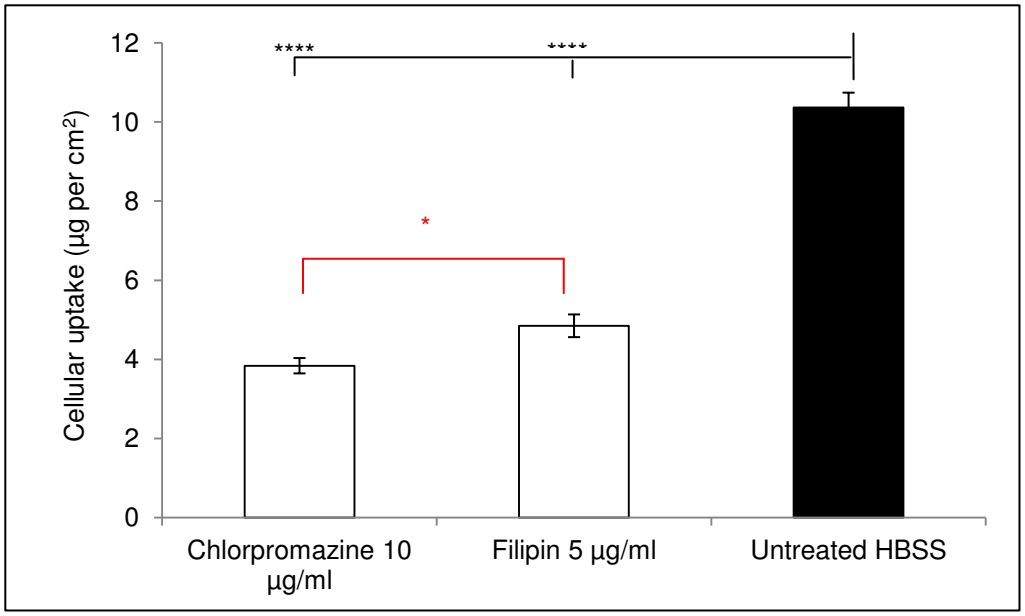

b)

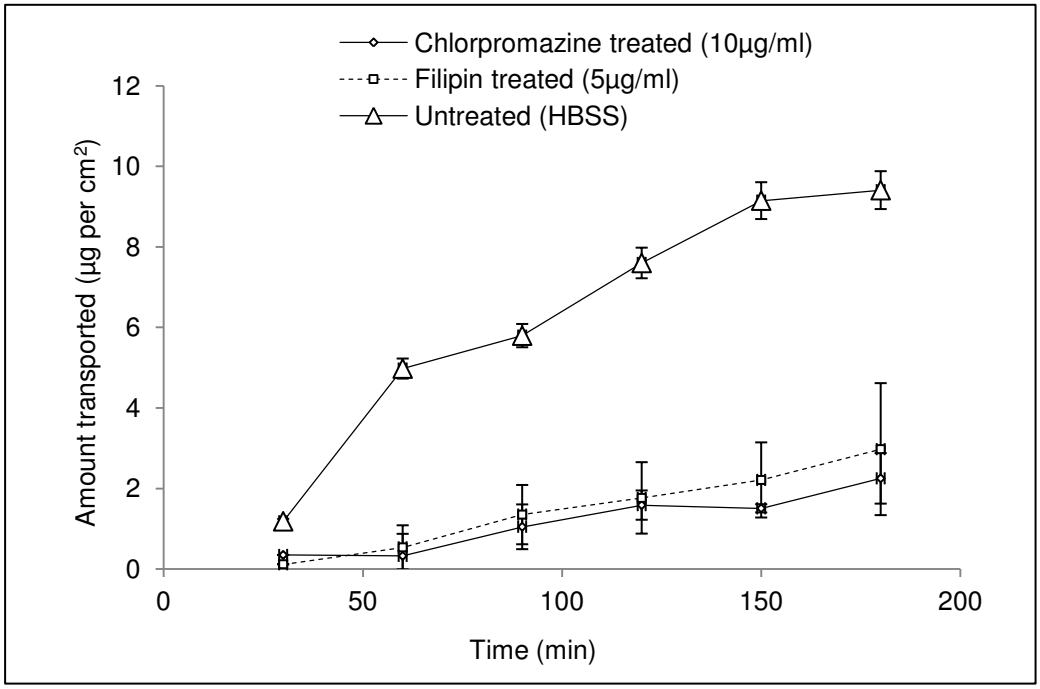

Figure 6. 4. Effect of endocytic pathway-specific inhibitors on cell uptake and transport of soluble vitamin B_{12} (applied at 1 mg/ml) in the absence of intrinsic factor.

a) Effect of chlorpromazine and filipin on cell uptake of vitamin B_{12}, and b) Effect of chlorpromazine and filipin on transport of vitamin B_{12} across Caco-2 monolayers. Vitamin B_{12} was applied in the absence of IF and quantified by UVAbs (350 nm). Data represents the mean ± SD (n=3).

In the studies examining the role of IF on the cell uptake and transport of soluble of vitamin B_{12} (Figures 6.2 and 6.3), together with the associated mechanisms, IF was

applied at a dose notably lower than a 1:1 molar ratio to vitamin B_{12} (with the latter applied at high doses). Importantly, the presence of IF is only essential for the cubilin-mediated pathway of vitamin B_{12} uptake and transport route. To this end, the overall cell uptake and transport of vitamin B_{12} is likely to occur through multiple pathways, including the TCII receptor and the paracellular route (which would contribute to transport rather than cell uptake), as shown in Figure 6.3.

6.3.4 Effect of IF on cell trafficking of B_{12}-conjugated nanoparticles

The cell internalisation route of vitamin B_{12}-conjugated nanoparticles (50 nm) under IF-free conditions was established using the pathway-specific cell trafficking inhibitors employed in the section above (and in Chapter 5). The concentrations of inhibitors employed to induce uptake inhibition without causing cell toxicity have been described elsewhere (Chapter 5, section 5.3.10). In addition, the uptake inhibition activity of these materials was tested on ligands known to internalise specifically *via* either clathrin- or caveolae-mediated routes (Chapter 5, Figure 5.15). Figure 6.5 reveals cell uptake and transport of B_{12}-conjugated nanoparticles in the presence of either chlorpromazine or filipin, and in the absence of IF (cell uptake data for B_{12}-conjugated nanoparticle uptake in the presence of IF, shown in Chapter 5, has been included for the purpose of comparison). Figure 6.5ai shows that in IF-free conditions, the cell uptake of B_{12}-conjugated nanoparticles is reduced 3.3-fold in the presence of chlorpromazine – a phenomenon that was not observed in the case of B_{12}-conjugated nanoparticles in the presence of IF (instead, chlorpromazine treatment exhibited no significant effect on particle internalisation amount). Filipin treatment somewhat inhibited the cellular uptake of B_{12}-conjugated nanoparticles in the absence of IF (approximately 1.4-fold reduction); this effect was less marked compared with B_{12}-conjugated nanoparticle uptake in the presence of IF (Figure 6.5aii).

Transport data in the absence of IF appears to follow a similar trend. Chlorpromazine treatment (Figure 6.5bi) resulted in a 1.8-fold reduction for B_{12}-conjugated nanoparticle transport, relative to the untreated control. Following filipin treatment B_{12}-conjugated nanoparticle transport across the cells (Figure 6.5bii) was inhibited during the initial

phase of the experiment (over 2 hr), but the amount of nanoparticles transported to the basolateral side at the 3 hr measurement point reached the values seen in the untreated cells. The reason for this apparent trend is not entirely clear as filipin, a known sterol-binding agent is shown to severely disrupt caveolae and caveolae-mediated endocytosis by way of removing cholesterol from the cell membranes causing vesicle flattening and disassembly [28, 29] , but it is also a used as a selective inhibitor for non-coated vesicular transcytosis [25], the effects of which are irreversible with time. To further investigate this phenomenon, uptake studies conducted at intermediate time points (between 0-3 hr) are required to determine whether filipin acts as an inhibitor in the early uptake phase. Indeed, if this proved to be the case, this may serve to account for the observed transport trends of B_{12}-conjugated nanoparticles and this “loss of effect” by filipin over time.

Overall, the data suggests that the transport of vitamin B_{12}-conjugated nanoparticles in the absence of IF was predominantly influenced by inhibition of the clathrin pathway. Although further studies using alternative inhibitors are needed to confirm these findings,this study suggests that IF plays an important additional role in dictating the internalisation and subsequent trafficking of both soluble vitamin B_{12} and B_{12}-conjugated nanoparticles. Under IF-free conditions, internalisation of vitamin B_{12} (or B_{12}-conjugated nanoparticles) by cubilin is not possible. The cubilin receptor needs to recognise and engage with the IF-B_{12} complex in order to trigger its endocytosis [30]. This infers the distinct involvement of a secondary receptor-mediated pathway. Thus it seems highly probable that the way in which B_{12}-conjugated nanoparticles are ‘processed’ by epithelial cells is governed by a different initial receptor-binding event (e.g. complexing to TCII and undergoing TCII receptor-mediated endocytosis) under IF-free conditions. Further mechanistic studies are needed in order to fully characterise this secondary (receptor-mediated) pathway and to delineate its involvement in the uptake and transport of B_{12}-conjugated nanoparticles. It must be noted that a comparison of our findings related to the role of IF on the trafficking of B_{12}-conjugated nanoparticles and existing literature is not possible due to the lack of such published studies.

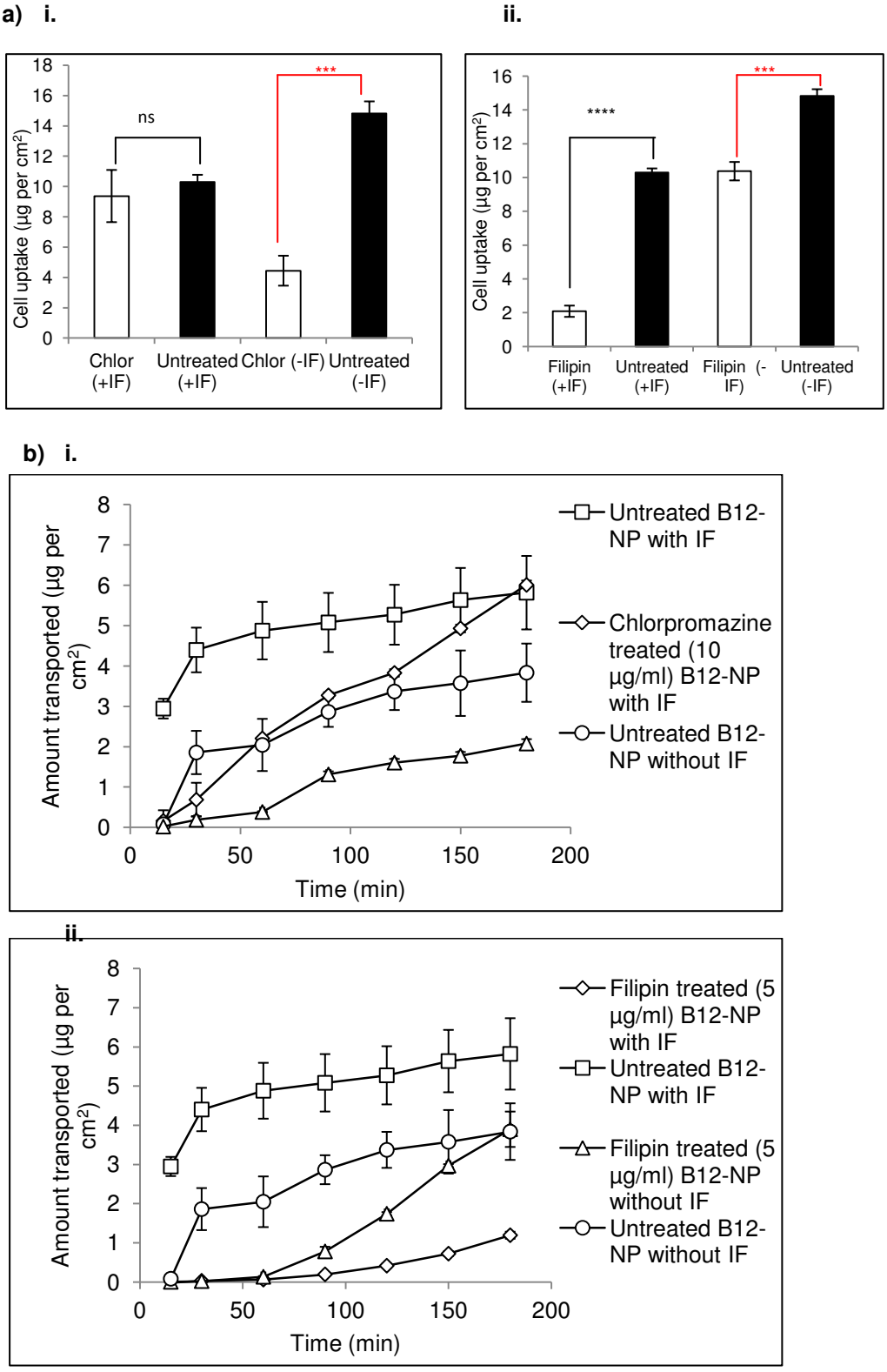

Figure 6. 5. Effect of clathrin and caveolae inhibition on cell uptake and transport of vitamin B_{12}-conjugated nanoparticles in the absence of IF.

a) Effect of chlorpromazine (i) and filipin (ii) on cell uptake of nanoparticles. Experiments where IF is added referred to as '+IF'. Experiments conducted in the absence of IF referred to as '-IF'. b) Effect of chlorpromazine (i) and filipin (ii) on the transport of nanoparticles. Cell uptake and transport studies were conducted with B_{12}-conjugated nanoparticles of 50nm diameter. Data represents the mean ± SD (n=3).

6.3.5 Cell trafficking summary of soluble B_{12} and B_{12}-conjugated nanoparticles in Caco-2 cells

The trafficking behaviours of soluble B_{12} and B_{12}-conjugated nanoparticles in intestinal Caco-2 monolayers, as suggested by data from experiments employing pharmacological inhibitors, are summarised in Table 6.1.

	Cell trafficking in Caco-2 cells occurring *via*		
	Clathrin	**Caveolae**	**Both**
Soluble B_{12} (with IF) see chapter 5	+	-	
Soluble B_{12} (without IF)			+
B_{12}-conjugated nanoparticles (50 nm, with IF) see chapter 5	-	+	
B_{12}-conjugated nanoparticles (50 nm, without IF)	+	(-)	(+)

Table 6. 1. Summary table showing observed cell trafficking behaviours of soluble B_{12} and B_{12}-conjugated nanoparticles (of 50 nm pre-conjugation diameter) across Caco-2 cells. '+' denotes positive involvement of pathway, '-' denotes no involvement of pathway. Brackets indicate some/minor involvement of pathway.

6.4 Conclusion

Previous reports have shown that IF adopts a crucial role in the internalisation of vitamin B_{12} through enabling recognition and internalisation *via* the cubilin receptor. In its absence, the B_{12} ligand is shuttled along a different pathway, likely involving recognition by TCII and subsequent internalisation *via* the TCII receptor.

In this chapter it was sought to determine whether IF is important for the cell uptake, transport and cell trafficking pathway of soluble vitamin B_{12} and B_{12}-conjugated nanoparticles in Caco-2 cells. Overall, the data suggests that in the absence of IF, B_{12}-conjugated nanoparticles are internalised and transported by cells to a lesser extent than when co-administered with IF, although the magnitude of this reduction was not substantial. The findings also demonstrate that soluble vitamin B_{12} trafficking (without IF) occurs *via* a different route to that used by vitamin B_{12}-IF (i.e. cubilin mediated).

Unlike B_{12}-nanoparticle uptake behaviours under IF-containing conditions, which were found to exploit a caveolae-mediated route, the cellular internalisation and transport of B_{12}-conjugated nanoparticles in the absence of IF were instead predominantly affected by inhibition of the clathrin pathway. As in the case of soluble VB_{12} trafficking, this further suggests the involvement of an uptake and trafficking route which is different to that in the presence of IF, indirectly implicating a role for the TCII receptor-mediated pathway in the endocytosis and transport of B_{12}-conjugated nanoparticles, a phenomenon which may be exploited in parallel to the conventional B_{12} pathway for vitamin B_{12}-mediated drug delivery.

6.5 References

1. Dix, C.J., et al., *The transport of vitamin B12 through polarized monolayers of Caco-2 cells.* Gastroenterology, 1990. **98**(5 Pt 1): p. 1272-9.
2. Wilson, G., et al., *Transport and permeability properties of human Caco-2 cells: an in vitro model of the intestinal epithelial barrier.* J. Control. Release, 1990. **11**: p. 25-40.
3. Ramanujam, K.S., S. Seetharam, and B. Seetharam, *Synthesis and secretion of cobalamin binding proteins by opossum kidney cells.* Biochem Biophys Res Commun, 1991. **179**(1): p. 543-50.
4. Hassan, I.F. and M. Mackay, *The transport of vitamin B12 across Caco-2 monolayers grown on permeable supports.* In Vitro Cell. Dev. Biol., 1992. **28**: p. 12.
5. Dan, N. and D.F. Cutler, *Transcytosis and processing of intrinsic factor-cobalamin in Caco-2 cells.* J Biol Chem, 1994. **269**(29): p. 18849-55.
6. Schohn, H., et al., *Synthesis and secretion of a cobalamin-binding protein by HT 29 cell line.* Biochem J, 1991. **280 (Pt 2)**: p. 427-30.
7. Gueant, J.L., et al., *Receptor-mediated endocytosis of the intrinsic factor-cobalamin complex in HT 29, a human colon carcinoma cell line.* FEBS Lett, 1992. **297**(3): p. 229-32.
8. Ramanujam, K.S., et al., *Expression of cobalamin transport proteins and cobalamin transcytosis by colon adenocarcinoma cells.* Am J Physiol, 1991. **260**(3 Pt 1): p. G416-22.
9. Bose, S., et al., *Bipolar functional expression of transcobalamin II receptor in human intestinal epithelial Caco-2 cells.* J Biol Chem, 1997. **272**(6): p. 3538-43.
10. Russell-Jones, G.J., L. Arthur, and H. Walker, *Vitamin B12-mediated transport of nanoparticles across Caco-2 cells.* Int J Pharm, 1999. **179**(2): p. 247-55.
11. Schanker, L.S. and J.A. Burton, *Absorption of heparin and cyanocobalamin from the rat lung.* Proc Soc Exp Biol Med, 1976. **152**(3): p. 377-80.
12. Zielinska-Dawidziak, M., et al., *Transport of high concentration of thiamin, riboflavin and pyridoxine across intestinal epithelial cells Caco-2.* J Nutr Sci Vitaminol (Tokyo), 2008. **54**(6): p. 423-9.
13. Moestrup, S.K., et al., *Megalin-mediated endocytosis of transcobalamin-vitamin-B12 complexes suggests a role of the receptor in vitamin-B12 homeostasis.* Proc Natl Acad Sci U S A, 1996. **93**(16): p. 8612-7.
14. Christensen, E.I. and H. Birn, *Megalin and cubilin: multifunctional endocytic receptors.* Nat Rev Mol Cell Biol, 2002. **3**(4): p. 256-66.
15. Lai, W.H., et al., *Ligand-mediated internalization, recycling, and downregulation of the epidermal growth factor receptor in vivo.* J Cell Biol, 1989. **109**(6 Pt 1): p. 2741-9.
16. Paulos, C.M., et al., *Ligand binding and kinetics of folate receptor recycling in vivo: impact on receptor-mediated drug delivery.* Mol Pharmacol, 2004. **66**(6): p. 1406-14.
17. Seetharam, B., *Receptor-mediated endocytosis of cobalamin (vitamin B12).* Annu Rev Nutr, 1999. **19**: p. 173-95.
18. Cooper, B.A. and D.S. Rosenblatt, *Inherited defects of vitamin B12 metabolism.* Annu Rev Nutr, 1987. **7**: p. 291-320.
19. Okumura, S., et al., *Evaluation of drug absorption after intrapulmonary administration using Xenopus pulmonary membranes: correlation with in vivo pulmonary absorption studies in rats.* Pharm Res, 1997. **14**(9): p. 1282-5.
20. Sarti, F., et al., *Poly(acrylic acid)-cysteine for oral vitamin B12 delivery.* Anal Biochem. **420**(1): p. 13-9.
21. Tronde, A., et al., *Pulmonary absorption rate and bioavailability of drugs in vivo in rats: structure-absorption relationships and physicochemical profiling of inhaled drugs.* J Pharm Sci, 2003. **92**(6): p. 1216-33.
22. Alsenz, J., et al., *Oral absorption of peptides through the cobalamin (vitamin B12) pathway in the rat intestine.* Pharm Res, 2000. **17**(7): p. 825-32.

23. Tuma, P.L. and A.L. Hubbard, *Transcytosis: crossing cellular barriers.* Physiol Rev, 2003. **83**(3): p. 871-932.
24. Bose, S., et al., *Regulation of expression of transcobalamin II receptor in the rat.* Biochem J, 1995. **310 (Pt 3)**: p. 923-9.
25. Schnitzer, J.E., et al., *Filipin-sensitive caveolae-mediated transport in endothelium: reduced transcytosis, scavenger endocytosis, and capillary permeability of select macromolecules.* J Cell Biol, 1994. **127**(5): p. 1217-32.
26. Roberts, R.L. and A. Sandra, *Receptor-mediated endocytosis of insulin by cultured endothelial cells.* Tissue Cell, 1992. **24**(5): p. 603-11.
27. King, G.L. and S.M. Johnson, *Receptor-mediated transport of insulin across endothelial cells.* Science, 1985. **227**(4694): p. 1583-6.
28. Rothberg, K.G., et al., *Cholesterol controls the clustering of the glycophospholipid-anchored membrane receptor for 5-methyltetrahydrofolate.* J Cell Biol, 1990. **111**(6 Pt 2): p. 2931-8.
29. Rothberg, K.G., et al., *Caveolin, a protein component of caveolae membrane coats.* Cell, 1992. **68**(4): p. 673-82.
30. Kozyraki, R., et al., *The human intrinsic factor-vitamin B12 receptor, cubilin: molecular characterization and chromosomal mapping of the gene to 10p within the autosomal recessive megaloblastic anemia (MGA1) region.* Blood, 1998. **91**(10): p. 3593-600.

Chapter 7: The vitamin B_{12} transport pathway in airway Calu-3 cells

7.1 Introduction

The receptor-mediated endocytosis pathway of B_{12} has shown potential for oral delivery of peptides and proteins [1-5], in addition to nanoparticulate carriers (conjugated to B_{12}), offering the possibility of enhanced drug delivery [4, 6]. Published work assessing the potential of the B_{12} pathway for delivery of protein therapeutics has focused on oral delivery, with studies being conducted either *in vivo* in rats [4] or *in vitro* using the intestinally-derived cell lines, Caco-2 [7, 8] and HT29 [9, 10]. In intestinal Caco-2 cells, the B_{12} pathway has been shown to transport nanoparticles, in addition to soluble protein therapeutics, modified with B_{12} [2]. This was covered in detail in chapter 5, where the previously unreported mechanism of cell internalisation and intracellular trafficking of B_{12}-conjugated nanoparticles, was explored.

This chapter describes work investigating whether the B_{12} endocytosis pathway is present and operates in bronchial Calu-3 cells. This objective is partly a result of earlier observations within our group, which showed that the Calu-3 cell line expresses folate receptors [11]. To the best of our knowledge, cubilin expression in epithelial cell lines originating from the airways has not previously been demonstrated and the B_{12} pathway not investigated. Initial experiments were conducted to determine whether Calu-3 cells express cubilin, the TCII receptor and the TCII carrier protein. This was followed by assessment of cell uptake and transcellular transport of B_{12}-conjugated nanoparticles and a delineation of the mechanisms involved, providing a comparison with the cell uptake and transport of B_{12}-bearing nanoparticles in Caco-2 cells.

7.2 Methods

7.2.1 Preparation of the α-ω-aminohexylcarbamate derivative of cyanocobalamin

Details on the chemical synthesis and characterisation of the α-ω-aminohexylcarbamate derivative of vitamin B_{12} are described in Chapter 4.

7.2.2 Preparation and surface characterisation of vitamin B_{12}-conjugated nanoparticles

Fluorescent carboxylate Yellow Orange (YO) nanoparticles of 50 nm and 100 nm (PolySciences Inc,) were modified with the α-ω aminohexylcarbamate vitamin B_{12} derivative by activation with 1-ethyl-3-[3-Dimethylaminopropyl]carbodiimide (EDAC), in the presence of N-hydroxy-succinimide (NHS). See Chapter 5 (5.2.2) for further experimental details. The presence of the B_{12} ligand on the surface of the nanoparticles was established using fluorescence quenching experiments (Chapter 5; section 5.2.3).

7.2.3 Cell Culture

The protocols for routine culture of Calu-3 cells are described in Chapter 2, section 2.2. Calu-3 cells were cultured for 21 days and under liquid-covered culture (LCC) conditions for all experiments detailed in this chapter. Culturing cells over the full 21 day period was considered important to ensure complete cell differentiation.

7.2.4 Barrier and morphological characterisation of Calu-3 cell layers

Calu-3 cells were cultured on filters following the methods detailed previously (section 2.2.1). TEER measurements were conducted (in the manner described in section 2.2.2) every 2 or 3 days, starting from day 2 to day 15-21 of culture. Calu-3 TEER profiling experiments were carried out by Dr Driton Vllasaliu (University of Nottingham).

The barrier capacity of polarised Calu-3 cell layers was confirmed by determining the permeability of FITC-dextrans (FD) of varying molar mass after 21 days in LCC culture. Culture medium of polarised cell layers was initially replaced with warmed (37 ℃) HBSS (transport medium) and cells were allowed to equilibrate for approximately 30 min. TEER measurements were taken to confirm cell layer intactness (refer to sections 2.2.2 and 2.2.3). HBSS was then removed from the apical side and replaced with FD solutions, comprising of FD4, FD10, FD20, FD40, FD70 or FD150 dissolved in HBSS (37 ℃) at 500 µg/ml. Cells were placed in the incubator at 37 ℃ in between

sampling intervals. FD permeability was determined as detailed in Chapter 2, section 2.2.3.

In a separate experiment, Calu-3 cells were imaged using SEM and TEM following 21-day culture on filters. Polarised Calu-3 cells were also stained for Zonula Occludens-1 (ZO-1) in the manner described in Chapter 2, section 2.2.5.

7.2.5 Immunohistochemical analysis of cubilin and TCII

Filter-cultured Calu-3 cells were selected for immunostaining experiments on day 21 of culture. The culture medium was replaced with HBSS and following a 45 min incubation period, TEER measurements were taken to ensure cell layer intactness. Cells were then fixed with 4% paraformaldehyde (in PBS) for 10 min. For TCII staining, cells were permeabilised with 0.2% (v/v) Triton X-100 for 10 min. Cells were then washed with PBS and incubated with 1% w/v BSA/PBS (for 1 hr). Antibodies to cubilin and TCII (cubilin H-300; Transcobalamin II H-260; both rabbit, anti-human; Santa Cruz Biotechnology, Inc.) were added to the cell samples diluted 1:50 in 1% BSA/PBS; cells were incubated for 30 min. Primary antibodies were then removed and cells washed 3 times with PBS, followed by incubation with the secondary antibody (goat, anti-rabbit IgG-rhodamine) diluted 1:100 (in 1% BSA/PBS) for another 30 min. A control experiment was conducted where polarised cells were incubated with the secondary antibody only. Following a final extensive washing step, the cell nuclei were stained with Hoechst 33342 (0.1 mg/ml) and the filter membranes excised from the inserts. Cells were mounted on glass slides using 1,4-diazabicyclo[2.2.2]octane (DABCO) (1%, diluted in 9:1 glycerol:PBS) and covered with glass cover slips. Confocal imaging was carried out using a Leica SP2 CLSM confocal microscope.

7.2.6 mRNA expression of cubilin and Transcobalamin II receptor

mRNA was isolated from filter-cultured Calu-3 cells on day 21 of culture on Transwell® inserts, using the method described in section 2.2.6.1.1. cDNA was synthesised using the protocol described in section 2.2.6.1.2. A conventional PCR was performed on the PTC-200 Thermal Cycler to amplify the cDNA, which was then visualised using gel electrophoresis (section 2.2.6.2). The expected size of the amplified cDNA fragments

was 602bp for cubilin and 343bp for CD320 (encoding Transcobalamin II receptor). The reader is referred to section 2.2.6.2.1 for primer details.

7.2.7 Immunostaining for clathrin and caveolin-1

Immunostaining for clathrin and caveolin-1 in polarised Calu-3 cells was carried out in a manner described previously (Chapter 2, section 2.2.5.5).

7.2.8 mRNA expression of caveolin-1

mRNA was isolated from polarised Calu-3 cells (cultured on Transwell® supports for 21 days using the method described in section 2.2.6.1.1). cDNA was synthesised using the protocol described in section 2.2.6.1.2. A conventional PCR was performed on the PTC-200 Thermal Cycler to amplify the cDNA, which was then visualised using gel electrophoresis (section 2.2.6.2). The expected size of the amplified cDNA fragment was 362bp (see section 2.2.6.2.1 for primer details).

7.2.9 Cellular uptake and transport of B_{12}-conjugated nanoparticles

Calu-3 cells were cultured on Transwell® supports over 21 days (as described in section 2.2). Culture medium was removed from the cells and replaced with Hank's Balanced Salt Solution (HBSS), buffered with 2-[4-(2-hydroxyethyl)piperazin-1-yl]ethanesulfonic acid (HEPES, 20mM) and cell monolayers incubated for 45 min. Unmodified YO nanoparticles (50 and 100 nm) and vitamin B_{12}-conjugated nanoparticles were suspended in HBSS/HEPES to achieve a final concentration of 400 µg/ml. Recombinant human intrinsic factor (rHUIF, Autogen Bioclear Ltd) was added (3 µg per 1 ml of 400 µg/ml nanoparticle suspension) and the solution was incubated at 37˚C prior to application to cells. Following a routine assessment of TEER (as described in chapter 2, section 2.2.2), nanoparticle suspensions (0.5 ml) were applied to the apical chamber of triplicate wells and the Calu-3 cultures incubated at 37˚C over 3 hrs. At 30 minute sampling intervals, 100 µl was removed from the basolateral side and analysed for fluorescence. Sample volumes were replaced with 100 µl of HEPES/HBSS to maintain sink conditions. Internalised fluorescence (indicating nanoparticle uptake) was determined by cell lysis using 0.2%

Triton X-100 (Fluka) (10 min incubation). Cell uptake of nanoparticles was quantified by fluorescence (Dynex, microplate reader, 529 nm/546 nm) using calibration curves. Soluble vitamin B_{12} transport studies were conducted as described in Chapter 5, section 5.2.5.

7.2.10 Lysosomal cell trafficking studies

Lysosomal cell trafficking studies using markers for lysosomes, Lysotracker™ Green DND-26 and anti-LAMP1 antibody, were carried out in the same manner as for Caco-2 cells, described in section 5.2.8.

7.2.11 Clathrin and caveolae inhibition studies

Cell trafficking inhibitory studies were conducted in the same way as for Caco-2 cells, detailed in section 5.2.9. Calu-3 cell layers (on day 21 of culture) were treated with inhibitors of specific endocytic pathways, filipin (5 µg/ml) or chlorpromazine (10 µg/ml), in HBSS/HEPES for 1 hr at 37°C prior to the addition of nanoparticles [12]. Unmodified and vitamin B_{12}-conjugated nanoparticles of 100 nm in diameter (400 µg/ml in HBSS/HEPES) in the presence or absence of IF were applied in combination with one of the above inhibitors for 3 hrs. It should be noted that 100 nm B_{12}-conjugated nanoparticles were used in the trafficking experiments in work described in this chapter (particle trafficking work in Caco-2 cells was conducted with 50 nm sized B_{12}-conjugated nanoparticles). Control experiments with known ligands for the clathrin- and caveolae-mediated pathways (FITC-transferrin at 100 µg/ml and cholera toxin-B-subunit at 5 µg/ml, respectively) were performed as described previously. In addition, native cyanocobalamin (vitamin B_{12}) in the presence of IF was also applied in conjunction with filipin or chlorpromazine to confirm the route of internalisation of the soluble ligand and quantified by UV-absorbance at 350 nm.

7.3 Results and Discussion

7.3.1 Characterisation of the α-ω-aminohexylcarbamate derivative of cyanocobalamin and vitamin B_{12}-conjugated nanoparticles

Characterisation of the α-ω-aminohexylcarbamate derivative of cyanocobalamin was described in Chapter 4, section 4.3. Likewise, characterisation of vitamin B_{12}-conjugated nanoparticles was detailed earlier (Chapter 5, sections 5.3.1-5.3.3).

7.3.2 Barrier and morphological characterisation of Calu-3 cell layers

In culture, the Calu-3 cell line produces features of differentiated, functional human airway epithelial cells [13], including the formation of the tight junctions [14-24]. The Calu-3 cell line as a model of the airways has demonstrated good *in vitro–in vivo* correlation in terms of drug permeation. This section shows data related to barrier and morphological characterisation of Calu-3 cells, cultured as polarised cell layers. Figure 7.1a depicts the development of TEER over time in culture. No significant increase in TEER was observed until day 7 of culture. Thereafter, TEER increased sharply, but subsequently reached a plateau after day 16 in culture. Immunostaining of polarised Calu-3 cells with an antibody to ZO-1 protein on day 21 (Figure 7.1b) revealed a typical distribution pattern of this protein as continuous 'belts' at cell-cell contacts. Figure 7.1c shows an SEM micrograph revealing closely packed cells, with distinct cell-cell boundaries and microvilli on the apical surface. The TEM micrograph (Figure 7.1d) highlights that Calu-3 cells also express a number of apically-located electron-translucent round granules of approximately 1 μm diameter, with some of these exhibiting an electron dense core. These resemble mucin granules of airway goblet cells in organisation and size [25], and their expression in Calu-3 cells has also been reported by other groups [13, 26, 27].

Finally, Figure 7.1e compares the permeability of FITC-dextrans of varying molecular mass across Calu-3 layers with Caco-2 cells. Apical-to-basolateral permeability decreased with increasing molecular mass of the solute (from 4 kDa to 150 kDa) in

Calu-3 cells, which is similar to the trend observed for Caco-2 cells. For example, the largest macromolecule, FD150 (150 kDa), exhibited a 34-fold lower permeability than the solute with the lowest molecular mass, FD4 (4 kDa). Comparing the permeability data in Calu-3 cell layers with that obtained in Caco-2 monolayers, it is clear that Calu-3 layers present a considerably greater barrier to the permeability of dextrans compared to Caco-2 monolayers. It is interesting to note that whilst the difference in permeability between FD4 and FD10 was not statistically significant in Caco-2 cells (Chapter 3, Figure 3.5), this difference in permeability in Calu-3 layers was notable (more than 2-fold). Furthermore, whilst FD4 exhibited a 5.3-fold higher permeability than FD40 in Calu-3 cells, this difference in Caco-2 cells amounted to only 2.5-fold. These observations hence indicate that the paracellular route in Caco-2 cells is able to accommodate the passage of macromolecular solutes of larger molar mass compared to Calu-3 cells. A detailed discussion related to the differences between Calu-3 and Caco-2 cell lines in terms of their morphology and barrier characteristics falls beyond the scope of this thesis and the reader is referred to a recent publication by our group [28].

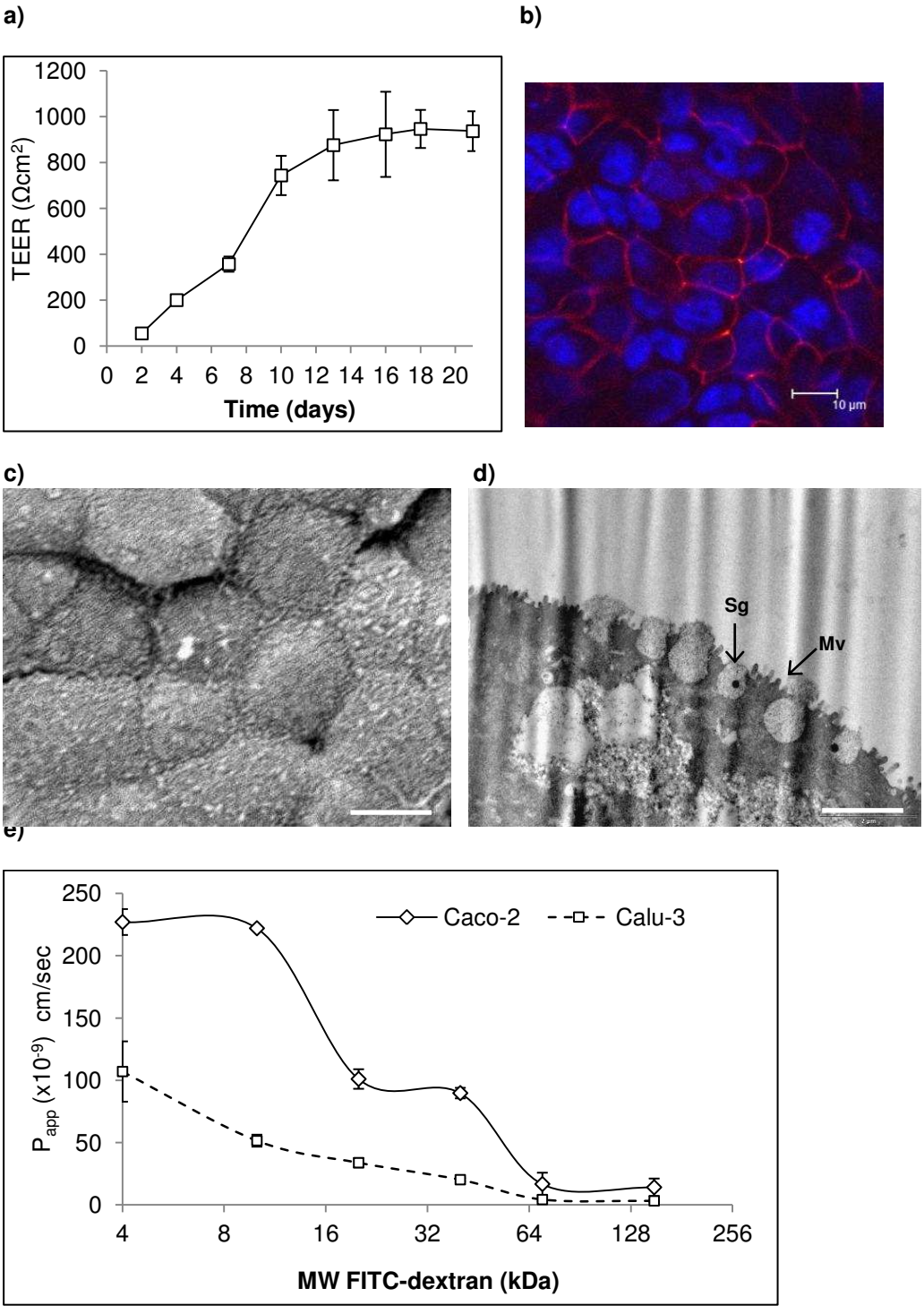

Figure 7. 1. Characterisation of Calu-3 cells, cultured on permeable supports as polarised cell layers.

a) TEER profile; expressed as the measured resistance per area (cm^2) of the cell layer. Background TEER due to the filter was subtracted from the reported values. Data presented as the mean ± SD (n=5). b) Staining for Zonula Occludens-1 (ZO-1) tight junction protein. Micrograph presented as an overlay image showing DAPI-labelled cell nuclei (blue) and ZO-1 distribution (red). c) SEM micrograph showing closely packed cells with microvilli (white line represents a scale bar of 10 µm). The observed cracks are artifacts resulting from sample processing for imaging. d) TEM micrograph showing a cell expressing microvilli (Mv) on the apical membrane and secretory granules (Sg). Scale bar=2 µm. e) Permeability of FITC-dextrans of approximate molecular weight of 4 kDa (FD4), 10 kDa (FD10), 20 kDa (FD20), 40kDa (FD40), 70 kDa (FD70) and 150 kDa (FD150) across Caco-2 and Calu-3 cell layers. Permeability expressed as apparent permeability coefficient (P_{app}), plotted against a logarithmic scale of the molecular weight of each FD. Data presented as the mean ± SD (n=4).

7.3.3 Immunohistochemical analysis of cubilin and TCII

Confocal micrographs of polarised Calu-3 cells, treated with the relevant antibodies reveal expression of cubilin (Figure 7.2a i). The control experiment, where the incubation step with the primary antibody was omitted, shows minimal fluorescence signal, excluding the possibility of non-specific antibody binding (Figure 7.2a ii).

In addition to confirming the presence of cubilin, further experiments were conducted to establish whether Calu-3 cells (cultured as polarised layers) express another relevant component of the vitamin B_{12} transport pathway. The role of transcobalamin II (TCII) in the transport of B_{12} was described earlier (Chapter 3, section 3.3.4.1). Immunostaining for this protein indicated its presence in Calu-3 cells (Figure 7.2b i). The pattern of fluorescence signal indicates a non-polar distribution of TCII (i.e. not confined to apical or basal side of the cells), consistent with its function of binding to vitamin B_{12} upon exit from the lysosomes for transport out of the cell. Again, the control experiment comprising cell treatment with the secondary antibody demonstrates absence of fluorescence signal (Figure 7.2b ii), indicating that the observed fluorescence is not due to non-specific binding of the secondary antibody. Immunostaining for TCII receptor – another component involved in the trafficking of vitamin B_{12} *in vivo* (internalisation in the absence of IF) – was not conducted due to the lack of commercially-available primary antibodies.

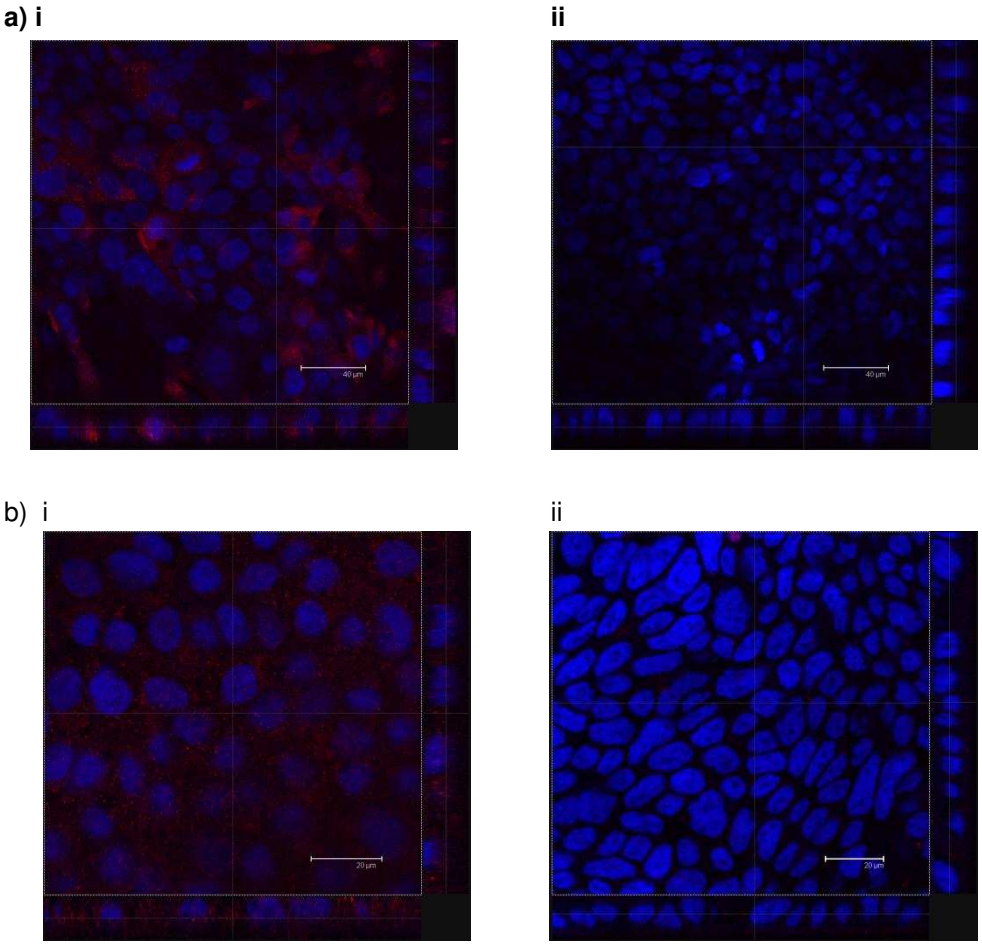

Figure 7. 2. Immunostaining for cubilin (VB_{12}-IF receptor) and transcobalamin II (TCII) in polarised Calu-3 cells.

a) Expression of cubilin receptor. i) Cells treated with anti-human cubilin H300 antibody, followed by goat, anti-rabbit IgG-Rhodamine. ii) Control experiment depicting cells treated only with the secondary antibody (goat, anti-rabbit IgG-Rhodamine). b) Expression of TCII. i) Cells treated with anti-human TCII H-260 antibody, followed by goat, anti-rabbit IgG-Rhodamine, ii) Control experiment where cells were treated with goat, anti-rabbit IgG-Rhodamine only. Blue=cell nuclei; Red=anti-rabbit IgG-Rhodamine.

7.3.4 mRNA expression of Cubilin and Transcobalamin II receptor

Calu-3 cells were also analysed for mRNA expression of cubilin and CD320 (encoding the transcobalamin II receptor). Total mRNA of Calu-3 cells was isolated following cell culture on filters under the conditions described earlier. Figure 7.3 reveals the expression of both cubilin (602 bp) and CD320 (343 bp) in Calu-3 cells. A secondary fragment (~260 bp) with weak intensity in addition to the band detected at 343 bp (for CD320) was noticed, apparent also in Caco-2 cell experiments (section 3.3.4.2).

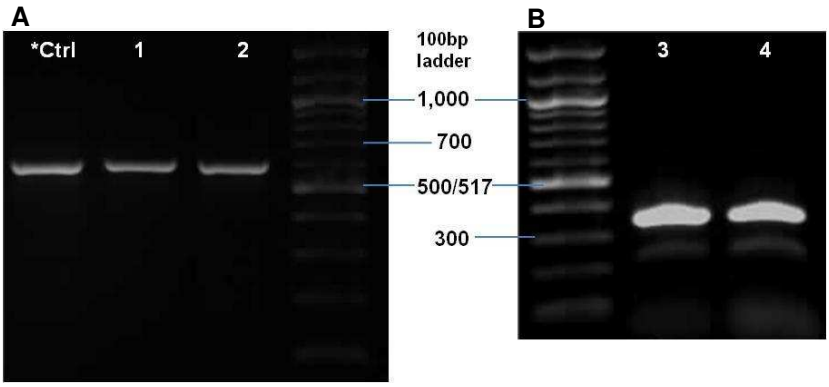

Figure 7. 3. mRNA expression of (A) cubilin (lanes 1 and 2) and (B) CD320 (TCII Receptor) in Calu-3 cells (lanes 3 and 4) on day 21 of culture.

*Ctrl denotes PCR product obtained from Caco-2 cell monolayer.

7.3.5 Clathrin and Caveolin-1 expression

Before attempting to unravel the biological mechanisms involved in the cellular trafficking of B_{12}-conjugated nanoparticles, it was first confirmed that the Calu-3 cells employed in this study as a model of the bronchial epithelium express the relevant components of relevant endocytic pathways. This includes the presence of essential constituents of clathrin 'coated pits', implicated in the internalisation of the soluble vitamin B_{12}-IF complex, as well as caveolae (a route found to be involved in the trafficking of B_{12}-conjugated nanoparticles in Caco-2 cells, Chapter 5). Immunostaining for clathrin, the protein responsible for the formation of clathrin coated pits, resulted in detection of fluorescence signal, indicative of clathrin expression (Figure 7.4a i), in contrast to the control experiment (Figure 7.4a ii). The expression of caveolin-1 protein in cells is essential for the formation of morphologically identifiable caveolae [29-31]. Immunostaining for this protein in Calu-3 cells (Figure 7.4b i) revealed its expression. (The absence of fluorescence in the control overlay image rules out experimental artefacts that may result from non-specific antibody binding, shown in Figure 7.4b ii.) The expression of these components was also demonstrated in a study conducted by Bradbury *et al*. [32], where the authors investigated the role of caveolae and clathrin-mediated pathways in the internalisation of cystic fibrosis transmembrane conductance regulator (CFTR) in Calu-3 cells. In a separate study, Moradi *et al*. [11] used inhibitors of clathrin and caveolae uptake pathways in the Calu-3 cell layer model

to delineate their respective roles in the internalisation of folate-decorated nanoparticles (showing that altering the density of the folate ligand on nanoparticle surface produces a change in the cell uptake pathway from predominantly clathrin to a predominantly caveolae-mediated route). Taken together, the data indicates that airway Calu-3 cells, cultured as polarised layers, express the relevant protein components that render them capable of undertaking both clathrin- and caveolin-mediated endocytosis, as in the case of intestinal Caco-2 cells.

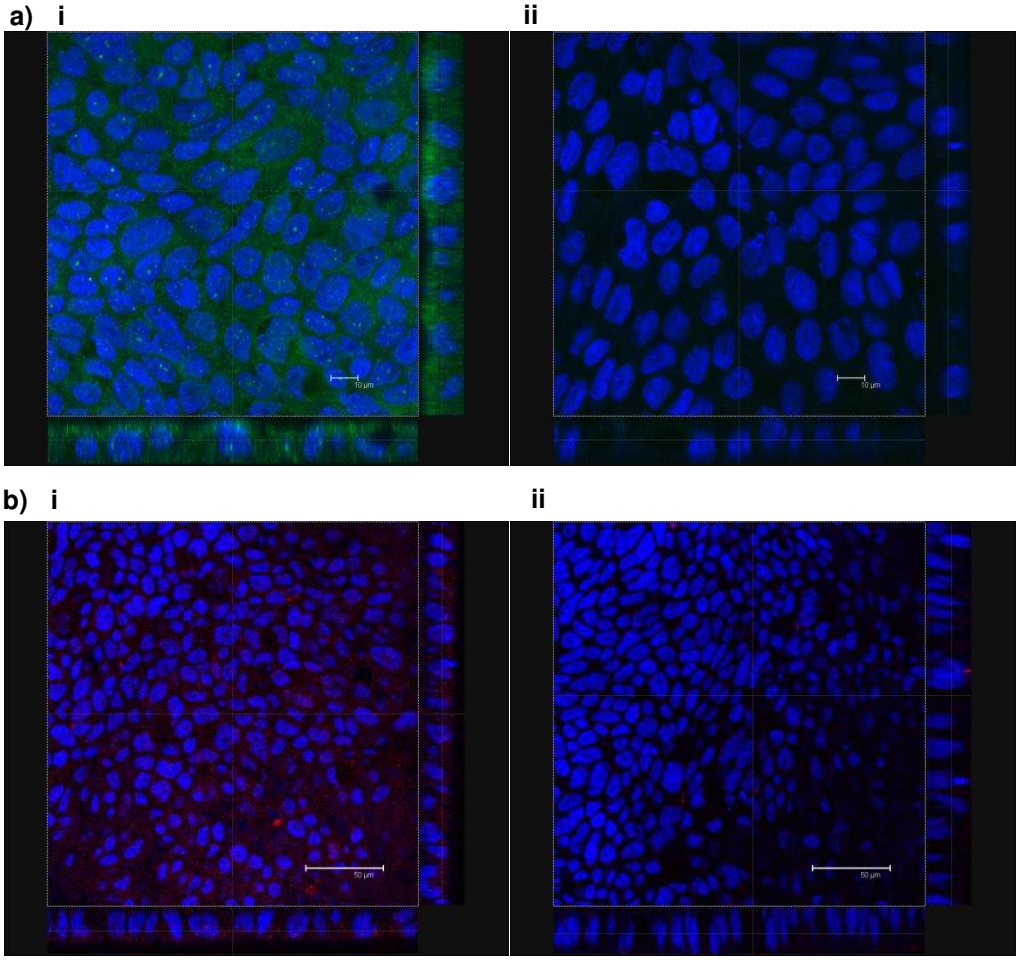

Figure 7. 4. Expression of select endocytic components by immunohistochemistry in polarised Calu-3 cells.

a) Staining for clathrin. i) Cells were incubated with rabbit, anti-human clathrin (primary) antibody and goat, anti-rabbit (secondary) IgG-FITC. ii) Control experiment where cells were treated with the secondary, goat, anti-rabbit IgG-FITC only. b) Staining for caveolin-1. i) Cells were treated with rabbit, anti-human caveolin 1 H-97, followed by goat, anti-rabbit IgG-Rhodamine. ii) Control experiment where cells were incubated with goat, anti-rabbit IgG-Rhodamine only. Cell nuclei (blue) were labelled with Hoechst 33342 in all cases. Immunostaining for all components was performed on day 21 of culture.

7.3.6 mRNA expression of caveolin-1

As mentioned earlier, caveolae are thought to be present in Calu-3 cells when cultured to form differentiated cell layers [11, 32, 33]. As cells lacking caveolin-1 do not form caveolae [34, 35], and heterologous expression of caveolin-1 induces the formation of caveolae in cells lacking these structures [36, 37], both immunohistochemical analysis (section 6.3.5) and mRNA expression (below) was used in this work to verify the existence of caveolin-1 and hence functioning caveolae in filter-cultured Calu-3 cells. Prior optimisation of the caveolin-1 PCR primers for work conducted with Caco-2 cDNA (Chapter 5, section 5.3.8) enabled assessment, using Calu-3 cDNA as a template. Figure 7.5 reveals data indicating caveolin-1 mRNA expression on day 21 of culture, with an amplified cDNA product of 362bp. The bright intensity of the bands (although not quantitative) serves to show that at the point when nanoparticle trafficking studies were conducted (i.e. on day 21 of culture), there is mRNA expression. Providing that downstream protein translation occurs, this in turn would drive the formation of functional caveolae in polarised airway Calu-3 cells, which may have implications for the uptake of B_{12}-conjugated nanoparticles (discussed later in this chapter), as also suggested for the uptake of poly(vinyl alcohol) nanoparticles in Calu-3 cells [33].

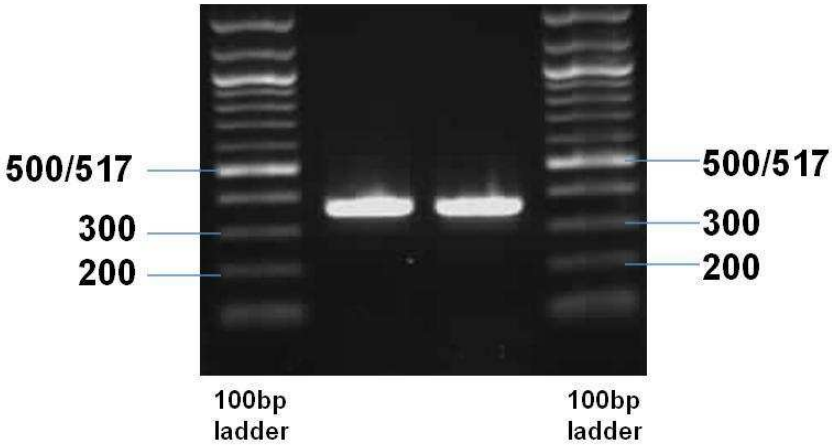

Figure 7. 5. mRNA expression of caveolin-1 on day 21 of filter-cultured Calu-3 cells (sample lanes 2 and 3, n=2).

7.3.7 Cell uptake and transport of B_{12}-conjugated nanoparticles

Figure 7.6a provides a comparison of cellular uptake of B_{12}-conjugated nanoparticles (of 50 nm and 100 nm nominal diameter) with unmodified nanoparticles in Calu-3 cells. It is clear from the figure that the amount of nanoparticles internalised by cells over the three-hour period was larger for B_{12}-conjugated nanoparticles, irrespective of their size, compared to unmodified nanoparticles (45 µg *versus* 31 µg, and 15 µg *versus* 8 µg for nanoparticles of 50 and 100 nm nominal diameter, respectively). B_{12}-conjugated nanoparticles of 50 nm were internalised to a greater extent than 100 nm B_{12}-conjugated nanoparticles (45 µg *versus* 15 µg). This finding is interesting as a similar study carried out in intestinal Caco-2 cells demonstrated the opposite phenomenon (Chapter 5, Figure 5.7a), where 100 nm B_{12}-conjugated nanoparticles were internalised in greater amount than the smaller 50 nm B_{12}-conjugated nanoparticles (39 µg *vs.* 32 µg, respectively).

Figure 7.6a also shows cell uptake of B_{12}-conjugated nanoparticles in the absence of IF. IF promoted a 1.25-fold increase in the uptake of B_{12}-conjugated 50 nm nanoparticles (45 µg *versus* 36 µg); for 100 nm B_{12}-conjugated nanoparticles, the difference in uptake in the presence of IF (15 µg) was not statistically significant compared to IF-free conditions (13 µg). Taking into account comparisons with Caco-2 cells (Chapter 6, Figure 6.1) – where IF promoted a 2.4-fold increase in the uptake of B_{12}-conjugated nanoparticles (50 nm diameter), but again elicited no statistically significant increase in the uptake of larger B_{12}-bearing particles – the role of IF seems ambiguous. However, a similar unremarkable effect of IF was also reported by Russell-Jones *et al*. [2], where IF induced only a modest effect on the uptake of B_{12}-modified polystyrene nanoparticles in Caco-2 cells. Furthermore, it seems that the influence of IF on the uptake of B_{12}-conjugated nanoparticles is restricted to smaller nanoparticles of <100 nm diameter in both cell lines. The largely unaffected uptake of B_{12}-conjugated nanoparticles in the absence of IF implies that an IF-independent pathway also operates in airway Calu-3 cells as in Caco-2 cells. This pathway may

involve the TCII receptor-mediated internalisation of B_{12}-conjugated nanoparticles bound to the TCII carrier protein, which has also been presumed by others [2, 38].

Transport of B_{12}-conjugated nanoparticles across Calu-3 cell layers was markedly greater than the unmodified counterparts for particles of both 50 and 100 nm (nominal) diameter (Figure 7.6b). To exemplify, whilst the cumulative amount transported within a 3-hour experiment reached 0.8 and 0.6 µg and for 50 and 100 nm particles, respectively, for B_{12}-conjugated nanoparticles the measured amounts were considerably higher, with transported levels amounting to 3.0 and 13.6 µg for 50 and 100 nm B_{12}-conjugated nanoparticles. The observation that B_{12}-modification of nanoparticles significantly influenced their cell uptake and transport behaviours in airway Calu-3 cells is important. These findings highlight the drug delivery potential of B_{12} bioconjugation, with regard to enhancing the mucosal transport of therapeutic nanocarriers in a different epithelial cell line (previous *in vitro* work demonstrating this potential was conducted solely in Caco-2 cells [2]). Moreover, the data demonstrates that it is potentially possible to exploit the vitamin B_{12} biological transport pathway for transmucosal delivery of nanomaterials across the airways, which has not been previously reported or suggested.

Comparing the transport of vitamin B_{12}-conjugated nanoparticles of different sizes across polarised Calu-3 cells, the data in Figure 7.6b shows a significantly greater transport for 100 nm, relative to 50 nm particles (13.6 µg *versus* 3.0 µg, respectively, in the presence of IF). This observation is interesting since it does not follow the trend of particle uptake data, where cell uptake was the most prominent for 50 nm B_{12}-conjugated nanoparticles. Consequently, only 7% of the internalised amount of 50 nm nanoparticles transported across the cell layers, compared with 88% for 100 nm B_{12}-conjugated nanoparticles. In the absence of IF, the extent of transport somewhat decreased, but followed a similar trend to nanoparticle transport in the presence of IF. Namely, the amounts of particles traversing the cell layers in a 3-hour experiment were 10.1 µg and 2.5 µg for 100 nm and 50 nm nanoparticles, respectively, equating

to a 1.17- and 1.34-fold reduction in cumulative transport, respectively, in the absence of IF. This observation is somewhat similar to the trend seen in Caco-2 cells (Chapter 6, section 6.3.1), where IF enhanced the cumulative amount of transport for both 50 nm and 100 nm B_{12}-conjugated nanoparticles.

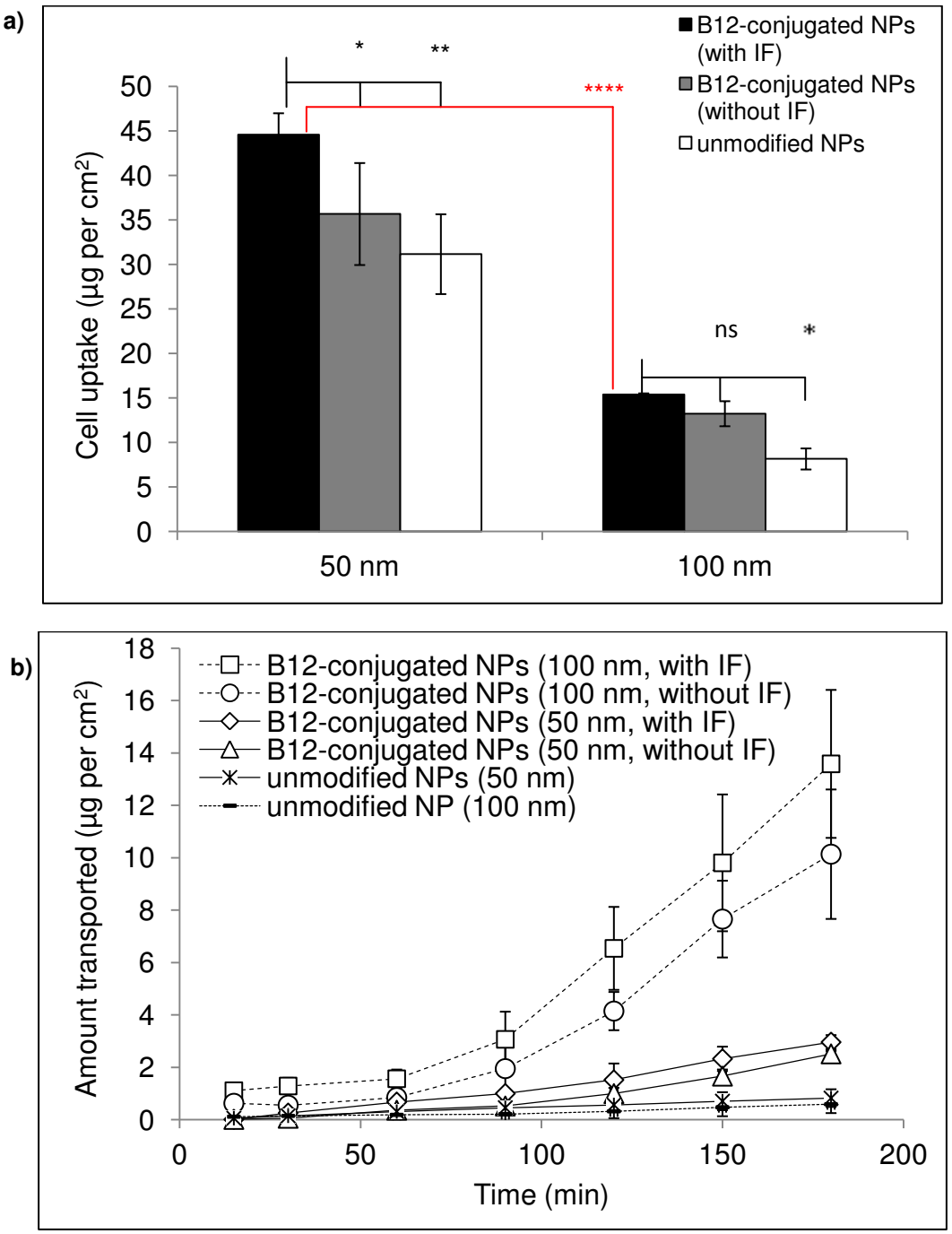

Figure 7. 6. Cell uptake and transport of B_{12}-conjugated nanoparticles in Calu-3 layers.

a) Cell uptake of B_{12}-conjugated nanoparticles (50 nm and 100 nm) in the presence and absence of intrinsic factor (IF) and unmodified NPs, b) transport of B_{12}-conjugated nanoparticles (50 and 100 nm) in the presence and absence of IF (3 µg recombinant human IF added per 1ml of nanoparticle suspension) and unmodified NPs. Data represents the mean ±SD (n=3). Statistical comparisons between B_{12}-conjugated NPs (in the presence of IF) of 50 vs. 100 nm (shown in red) and B_{12}-conjugated NPs (in presence of IF) vs. B_{12}-conjugated NPs in the absence of IF and unmodified NPs of 50 and 100 nm, respectively.

7.3.8 Cell trafficking of B_{12}-conjugated nanoparticles

As described in Chapter 5, in the process of cell trafficking of soluble vitamin B_{12} *in vivo,* the IF-B_{12} complex is believed to traffic into the lysosomes, where IF protein is degraded to release B_{12} [39]. From the perspective of trans-mucosal delivery of drug-loaded carriers, this would mean that the systems would localise into the highly degradative lysosomal compartment, thus undermining their drug delivery potential. Studies in Caco-2 cells revealed data suggesting that, unlike unmodified nanoparticles, B_{12}-conjugated nanoparticles may not localise into lysosomes (Chapter 5). Here it was sought to establish information regarding the cell uptake and intracellular processing of B_{12}-conjugated nanoparticles in relation to the involvement of lysosomes, in airway Calu-3 cells. Again, the Lysotracker™ probe [40] and immunostaining for lysosomal associated membrane protein (LAMP1) [41-43] were used as investigational tools allowing lysosomal staining.

Cells were initially treated with the Lysotracker™ probe and stained for LAMP1 in the absence of nanoparticles. This experiment revealed the presence of LAMP1 in cell samples (Figure 7.7a), inferring that lysosomes are permanent structures within the cell as would be expected for a major cellular organelle. Interestingly, the level of expression of LAMP1 in cells without nanoparticle application appears to be much higher in Calu-3 cells than that found in Caco-2 cells (Chapter 5, Figure 5.8). On the other hand, the fluorescence signal for the Lysotracker™ probe could not be detected in the absence of nanoparticles (Figure 7.7b). The group has observed this phenomenon in a number of cell lines and as Lysotracker™ is a fluorescent probe which accumulates in acidic compartments, this finding infers that the lysosomal compartment is only ‘active’ when endocytosis occurs. When unmodified nanoparticles were applied to the cells, the fluorescence signal for the lysosomal marker was clearly apparent (Figure 7.7c). Furthermore, the distribution pattern of this marker mirrored that of the nanoparticles. This co-localisation of the Lysotracker™ probe with the nanoparticles suggests the presence of unmodified nanoparticles in the

lysosomes. This in turn indicates that the intracellular trafficking of unmodified nanoparticles follows the 'degradative route', reaching lysosomes, as is consistent with findings in Caco-2 cells.

Data from LAMP1 staining experiments in Calu-3 cells showed a complex picture of fluorescence expression (Figure 7.7d). There were some similarities between the patterns of LAMP1 expression and unmodified nanoparticle co-localisation with the Lysotracker™, resulting in a composite picture showing some areas of segregation and some areas of co-localisation of label.

Following cell layer incubation with vitamin B_{12}-conjugated nanoparticles (50 nm nominal size), lysosomal compartments were not detected by the Lysotracker™ probe (Figure 7.7e), which is consistent with results found for Caco-2 cells. LAMP1 staining revealed diffuse cytosolic protein distribution (Figure 7.7f), similar to the control image (Figure 7.7a, cell sample in the absence of nanoparticles), but quite dissimilar from the distribution of the B_{12}-conjugated nanoparticles within the cell sample. Thus, there were few areas of co-localisation between the two labels, as revealed on the composite picture.

Drawing conclusions from the Lysotracker™ experiments, the results suggests that cell uptake and trafficking of B_{12}-conjugated nanoparticles in the airway Calu-3 cell line is similar to Caco-2 cells. Thus, it appears that the surface decoration of nanoparticles with vitamin B_{12} appears to affect their intracellular trafficking in Calu-3 cells. The possible avoidance of lysosomal trafficking by nanoparticles following B_{12}-conjugation – a phenomenon observed in both the intestinal and airway epithelial cell lines tested could indicate a cell line independent phenomenon.

The observations on LAMP1 as an indicator of lysosomal structures are much more difficult to interpret. As LAMP1 is a membrane marker, its use in distinguishing between intracellular organelles is much more dependent on effective segregation of membrane proteins between different but related organelles. Some groups have been

successful in using LAMP1 as a lysosomal marker in Calu-3 cells; for example, Bivas-Benita *et al*. [44] and Figueiredo *et al*. [45] reported cellular internalisation of PLGA-PEI nanoparticles of 200-230 nm (for gene delivery) and subsequent co-localisation of adsorbed rhodamine-labelled DNA with LAMP1, implying their endo-lysosomal fate. These examples all represent instances where an expected lysosomal accumulation has occurred and is equivalent to the data presented with the unmodified nanoparticles in this work. However, it is clear from the work in this thesis and from descriptions of the various intracellular pathways that there must be a number of inter-connecting membrane-bound intracellular trafficking compartments. There is however, no clear data in the literature on how the membranes and membrane proteins from these different compartments are trafficked. It must therefore be concluded that LAMP1 is a less useful marker for distinguishing these various membrane-bound vesicles.

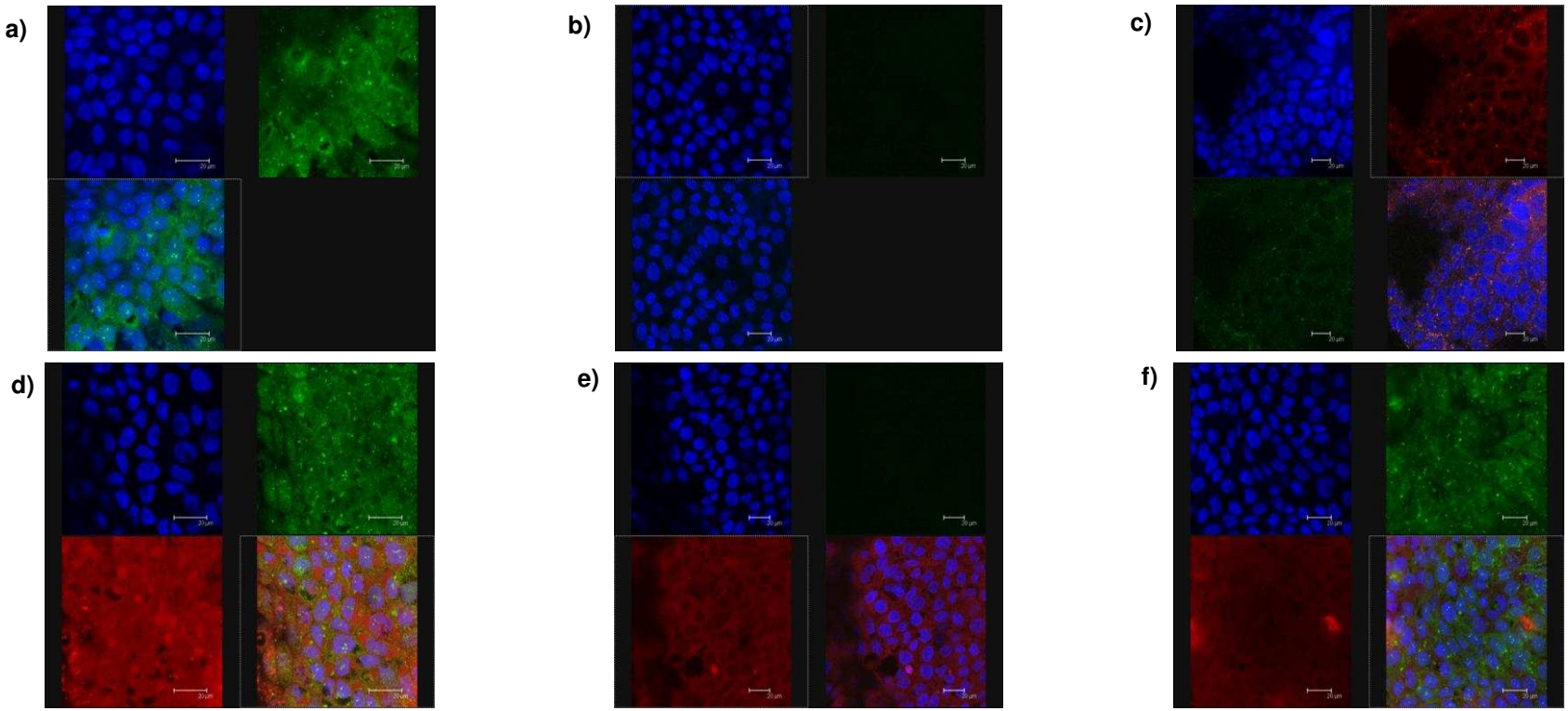

Figure 7. 7. Characterisation of Calu-3 cell layer uptake of vitamin B_{12}-conjugated nanoparticles (of 50 nm diameter) by confocal microscopy.

a) Confocal micrograph showing immunostaining for lysosomal associated-membrane protein 1 (LAMP1, green) in the absence of nanoparticles, b) Cell staining with Lysotracker Green DND-26 in the absence of nanoparticles, c) Co-localisation of unmodified nanoparticles (red) with Lysotracker Green DND-26 (green), d) Immunostaining for LAMP1 protein (green) following cell incubation with unmodified nanoparticles (red), e) Staining with Lysotracker Green DND-26 (green) after cell incubation with vitamin B_{12}-conjugated nanoparticles (red), f) Immunostaining for LAMP1 (green) following exposure of cells to vitamin B_{12}-conjugated nanoparticles (red). Lysotracker Green DND-26 excitation 504, emission 511 nm; YO nanoparticle excitation 529, emission 546nm; cell nuclei stained with Hoechst 33342.

7.3.9 Cellular trafficking of free vitamin B_{12}

The results shown in Chapter 5 (section 5.3.9) suggest that the cell uptake and transport of soluble vitamin B_{12} in Caco-2 cells is mediated *via* clathrin, which is consistent with literature reports [39]. This was suggested by the significant effects of a chemical inhibitor specific for this endocytic pathway, chlorpromazine. Work described in this section examined the mechanism of entry of soluble vitamin B_{12} in the bronchial cell line, Calu-3, by way of comparison.

The action of pathway specific cell trafficking inhibitors, chlorpromazine and filipin, in Calu-3 cells was initially confirmed by testing their effect on cell uptake and transport of pathway-selective ligands, transferrin [46, 47] and cholera toxin B-subunit [48, 49] (Figure 7.8a). Cell uptake of FITC-transferrin in the presence of chlorpromazine was inhibited by approximately 2-fold (Figure 7.8a i), which is a similar trend to work reported by Bradbury *et al*. [32], where the authors observed an approximate 4-fold reduction in the internalisation rate of ^{125}I-transferrin in the presence of chlorpromazine. On the other hand, filipin induced a dramatic, 21-fold decrease, in the cellular internalisation of cholera toxin B-subunit (Figure 7.8a ii). Transport experiments were also conducted for pathway-selective ligands and revealed notably low levels of transport in Calu-3 cells for both of these ligands, making analysis of any inhibitory effect in the presence of their respective endocytosis inhibitors problematic (the data is therefore not included in this thesis). However, cholera toxin B-subunit is known to be degraded intracellularly [50-52], whilst transferrin is in turn recycled with its receptor back to the apical domain *via* the recycling endosome [53]. Therefore, it is likely that the observed negligible transport of these ligands results from these phenomena. It is however, accepted that both transferrin and cholera toxin B-subunit are used as ligands to assess clathrin and caveolae-mediated *uptake* pathways [48, 54].

Vitamin B_{12} internalisation (Figure 7.8b i) and transport (Figure 7.8b ii) were markedly sensitive to the effects of chlorpromazine. Namely, cell uptake was inhibited by 19-

fold, whilst basolateral levels of soluble B_{12} reached a 12.8-fold lower amount at the terminal measurement point (3 hours) in the presence of chlorpromazine. Conversely, the uptake of soluble B_{12} by Calu-3 cells was only moderately inhibited by the action of filipin (1.3-fold decrease). Likewise, the effect of filipin on transport was notably less prominent than that of chlorpromazine, with an apparent larger influence on the rate at which transport took place rather than the final amount transported (12.7 and 14.9 µg in the presence and absence of filipin, respectively). The dramatic effect of chlorpromazine and the resulting inhibition of the clathrin pathway on the uptake of soluble vitamin B_{12} and the apparent lack of a significant influence by filipin as an inhibitor of caveolae-mediated pathway suggest that soluble vitamin B_{12} is internalised in Calu-3 cells predominantly *via* a clathrin-mediated route. The finding therefore complements the data with Caco-2 cells and previous reports based on *in vivo* studies [39, 55, 56] that vitamin B_{12} (in the presence of IF), predominantly exploits a clathrin-mediated route in the process of its internalisation in epithelial cells. However, contrary to findings in Caco-2 cells (under identical experimental conditions), where inhibition of caveolae-mediated endocytic route had no effect in the internalisation and transport of soluble vitamin B_{12}, the data suggests that in Calu-3 cells there might be some (albeit minor) involvement of the caveolae pathway in the process of trafficking of soluble vitamin B_{12}.

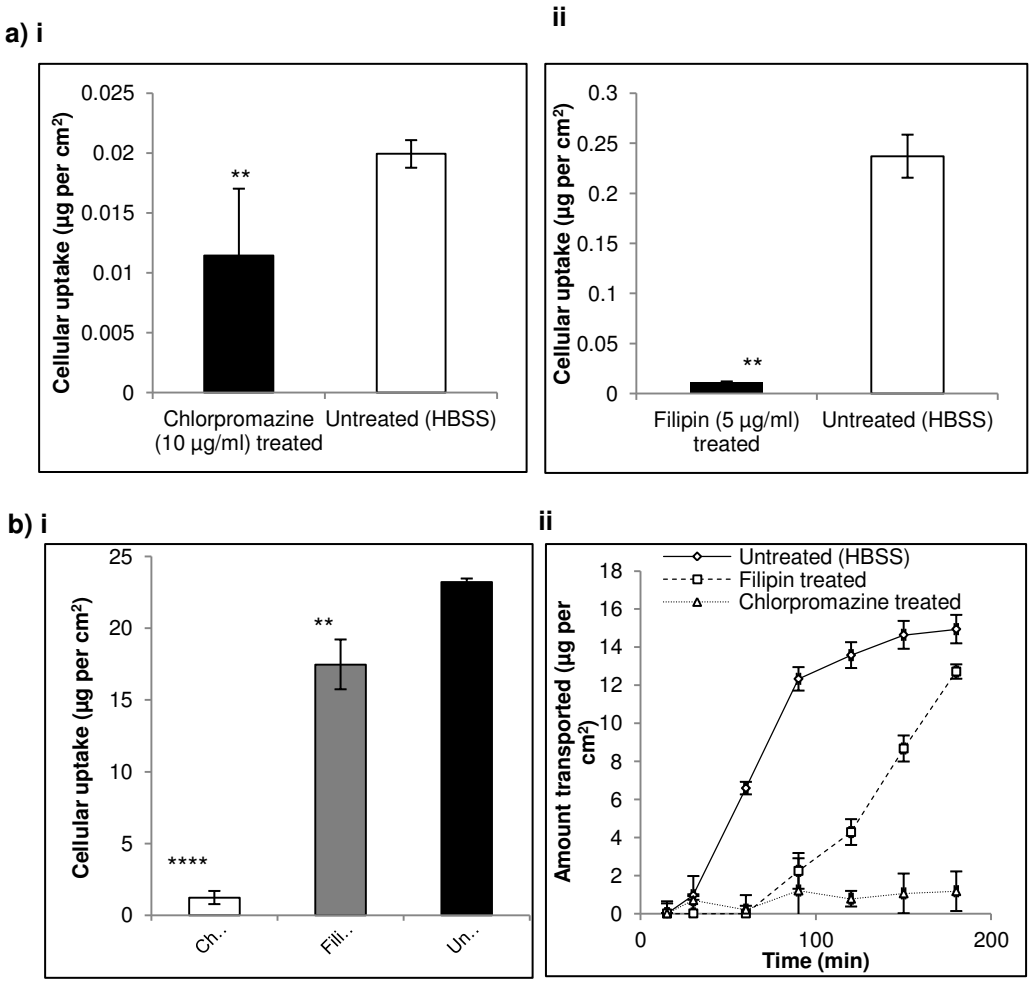

Figure 7. 8. Effect of endocytic pathway-specific inhibitors on cell uptake and transport of soluble vitamin B_{12} in Calu-3 cell layers.

ai) Effect of chlorpromazine on the cell uptake of FITC-transferrin in Calu-3 layers and ii) filipin on cell uptake of Cholera toxin B-subunit, and bi) Effect of chlorpromazine and filipin on cell uptake of vitamin B_{12} (statistical comparisons between chlorpromazine/filipin treated vs. untreated data), and ii) Effect of chlorpromazine and filipin on transport of vitamin B_{12} across Calu-3 layers. Vitamin B_{12} was applied in combination with IF and quantified by UVAbs (350 nm). Data represents the mean ± SD (n=3).

7.3.10 Cell trafficking of vitamin-B_{12} conjugated nanoparticles

Following the demonstration of cell trafficking of soluble vitamin B_{12}, by way of assessing sensitivity to pathway-specific inhibitors of endocytosis, the next set of experiments were directed towards determining the uptake pathway of B_{12}-conjugated nanoparticles (100 nm preconjugation diameter). Data showing the influence of cell treatment with chlorpromazine or filipin on internalisation of such particles by Calu-3 cells is shown in Figure (Figure 7.9a). Both agents were seen to affect the cell uptake of vitamin B_{12}-bearing nanoparticles, producing a statistically significant reduction in

the extent of particle uptake. Treatment with chlorpromazine induced a 3.4-fold decrease in nanoparticle internalisation, whereas with filipin a 2.1-fold reduction in the level of uptake was apparent.

Establishing the effect of clathrin and caveolae-mediated pathway inhibitors (chlorpromazine and filipin, respectively) on the apical-to-basolateral translocation of B_{12}-conjugated nanoparticles in Calu-3 cell layers, the data illustrates a dramatic effect for both agents. Following a 3-hour experimental period, cumulative amount of B_{12}-conjugated nanoparticles traversing the untreated cell layers reached ~17 µg. This level was 0.9 and 0.4 µg, in filipin and chlorpromazine treated cells, respectively (Figure 7.9b), highlighting a prominent effect.

These trends therefore suggest that cell uptake and transport of B_{12}-conjugated nanoparticles was dramatically affected by both clathrin and caveolae inhibition in Calu-3 cells. This phenomenon was not observed in Caco-2 cells, where B_{12}-conjugated nanoparticles (50 nm; in the presence of IF) were unaffected by treatment with two separate inhibitors of clathrin-mediated pathway, but their uptake and transport were notably sensitive to the effects of inhibitors of caveolae. At this stage, one can only speculate whether this is a consequence of a difference in cell uptake pathways between the two (intestinal and airway-originating) cell lines. Indeed, there is evidence for tissue-specific differences in endocytic mechanisms for a single ligand [57]. In one such example, albumin endocytosis (mediated by megalin) is reported to occur through a clathrin-dependent mechanism in most tissues [58-60]. However, in the choroid plexus a caveolae-dependent mechanism has been proposed [61]. In another example based on *in vitro* nanoparticle-based work, dos Santos *et al*. [62] reported variations in the effect of transport inhibitors (i.e. the different pathways involved) on the cellular uptake of carboxylated polystyrene nanoparticles in different human cell lines, namely in HeLa (cervical cancer), A549 (lung carcinoma) and 1321N1 (brain astrocytoma).

Thus, it may be possible that the mechanisms involved in vitamin B_{12} trafficking are somewhat different in the intestinal Caco-2 cell line and the airway-derived Calu-3 cell line. Another major factor that may account for some degree of difference in the pattern of cell uptake of vitamin B_{12}-conjugated nanoparticles is nanoparticle size, with 50 and 100 nm (nominal pre-conjugation diameter) particles used in Caco-2 and Calu-3 cells, respectively. The influence of particle size on endocytosis has been previously highlighted by several other groups [54, 62, 63], postulating that the particle size itself, with or without ligand can affect which endocytic pathways are involved.

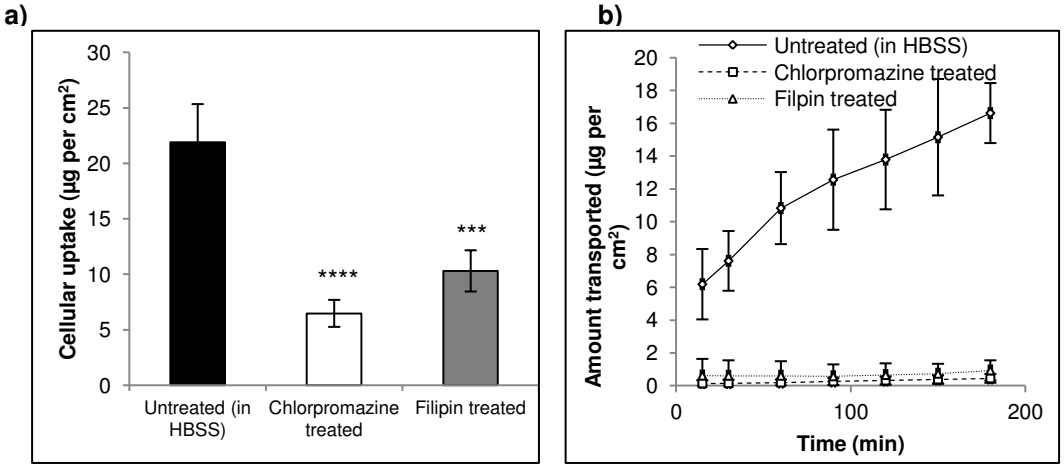

Figure 7. 9. Effect of endocytic pathway-specific inhibitors on cell uptake and transport of B_{12}-conjugated nanoparticles of 100 nm in Calu-3 cell layers.

a) Effect of chlorpromazine and filipin on the cell uptake of B_{12}-conjugated NPs in Calu-3 layers and b) Effect of chlorpromazine and filipin on transport of B_{12}-conjugated NPs across Calu-3 layers. Cell uptake and transport studies were conducted with B_{12}-conjugated nanoparticles of 100 nm diameter and in the presence of IF. Data represents the mean ± SD (n=4). Statistical comparisons between chlorpromazine/filipin treated vs. untreated data.

7.3.11 Cell trafficking summary of soluble B_{12} and B_{12}-conjugated nanoparticles in Calu-3 cells

The trafficking behaviours of soluble B_{12} and B_{12}-conjugated nanoparticles in Calu-3 layers, representing the airway epithelium, are summarised in Table 7.1. The summary data is based on findings from cell uptake and transport experiments in the presence of pharmacological inhibitors.

	Cell trafficking in Calu-3 cells occurring *via*		
	Clathrin	**Caveolae**	**Both**
Soluble B_{12} (with IF)	+	(-)	(+)
B_{12}-conjugated nanoparticles (100 nm, with IF)			+

Table 7. 1. Summary table showing observed cell trafficking behaviours of soluble B_{12} and B_{12}-conjugated nanoparticles (of 100 nm pre-conjugation diameter) across Calu-3 cells. '+' denotes positive involvement of pathway, '-' denotes no involvement of pathway. (Brackets) indicate some/minor involvement of pathway.

7.4 Conclusions

The work detailed in this chapter investigated the presence of the vitamin B_{12}-transport biological system in bronchial Calu-3 cells and its capacity to 'shuttle' B_{12}-bearing nanoparticles across these cells when cultured as polarised layers. Calu-3 cells were shown to express cubilin, the TCII receptor and the TCII carrier protein. B_{12}-conjugated nanoparticles internalised and traversed the Calu-3 cell layers considerably more efficiently than unmodified nanoparticles. Uptake and transport of B_{12}-conjugated nanoparticles was size-dependent and only modestly affected by the presence of IF. Confocal microscopy studies revealed that the cell uptake of B_{12}-conjugated nanoparticles (as well as unmodified counterparts) in the bronchial Calu-3 cell line follows a similar trend to uptake by intestinal Caco-2 cells, with the surface decoration of nanoparticles with B_{12} influencing intracellular distribution of nanoparticles. Data on the trafficking of soluble vitamin B_{12} (in the presence of IF) showed a predominantly clathrin-mediated route in the process of internalisation in Calu-3 cells (complementing findings in Caco-2 cells), with some indication of

caveolae involvement, hence suggesting an element of cross-talk between the two pathways in Calu-3 cells. Cell uptake and transport of vitamin B_{12}-conjugated nanoparticles was dramatically affected by both clathrin and caveolae inhibition in Calu-3 cells – an interesting finding that was not encountered in Caco-2 cells and thus warrants further investigation. Overall, the data shows that the components of the vitamin B_{12} trafficking machinery are expressed in airway Calu-3 cells and that vitamin B_{12}-conjugated nanoparticles traverse these cell layers. These previously unreported findings hence indicate that the vitamin B_{12} nanoparticle bioconjugation strategy shows potential for delivery of nanoparticulates across the airway mucosa, as well as the intestinal mucosa.

7.5 References

1. Russell-Jones, G.J., *Oral delivery of therapeutic proteins and peptides by the vitamin B12 uptake system*. Peptide-based drug design: controlling transport and metabolism, ed. M.D.T.a.G.L. Amidon. 1995, ACS, Washington DC. 181-198.
2. Russell-Jones, G.J., L. Arthur, and H. Walker, *Vitamin B12-mediated transport of nanoparticles across Caco-2 cells.* Int J Pharm, 1999. **179**(2): p. 247-55.
3. Chalasani, K.B., et al., *Vitamin B12-biodegradable micro particulate conjugate carrier systems for peroral delivery of drugs, therapeutic peptides/proteins and vaccines*. 2002: US patent.
4. Chalasani, K.B., et al., *Effective oral delivery of insulin in animal models using vitamin B12-coated dextran nanoparticles.* J Control Release, 2007. **122**(2): p. 141-50.
5. Russell-Jones, G.J., *Use of targeting agents to increase uptake and localization of drugs to the intestinal epithelium.* J Drug Target, 2004. **12**(2): p. 113-23.
6. Chalasani, K.B., et al., *A novel vitamin B12-nanosphere conjugate carrier system for peroral delivery of insulin.* J Control Release, 2007. **117**(3): p. 421-9.
7. Dix, C.J., et al., *The transport of vitamin B12 through polarized monolayers of Caco-2 cells.* Gastroenterology, 1990. **98**(5 Pt 1): p. 1272-9.
8. Ramanujam, K.S., et al., *Expression of cobalamin transport proteins and cobalamin transcytosis by colon adenocarcinoma cells.* Am J Physiol, 1991. **260**(3 Pt 1): p. G416-22.
9. Schohn, H., et al., *Synthesis and secretion of a cobalamin-binding protein by HT 29 cell line.* Biochem J, 1991. **280 (Pt 2)**: p. 427-30.
10. Gueant, J.L., et al., *Receptor-mediated endocytosis of the intrinsic factor-cobalamin complex in HT 29, a human colon carcinoma cell line.* FEBS Lett, 1992. **297**(3): p. 229-32.
11. Moradi, E., et al., *Ligand density and clustering effects on endocytosis of folate modified nanoparticles.* RSC Adv., 2012. **2**: p. 3025-3033.
12. Rejman, J., et al., *Size-dependent internalization of particles via the pathways of clathrin- and caveolae-mediated endocytosis.* Biochem J, 2004. **377**(Pt 1): p. 159-69.
13. Shen, B.Q., et al., *Calu-3: a human airway epithelial cell line that shows cAMP-dependent Cl- secretion.* Am J Physiol, 1994. **266**(5 Pt 1): p. L493-501.
14. Winton, H.L., et al., *Cell lines of pulmonary and non-pulmonary origin as tools to study the effects of house dust mite proteinases on the regulation of epithelial permeability.* Clin Exp Allergy, 1998. **28**(10): p. 1273-85.
15. Wan, H., et al., *Tight junction properties of the immortalized human bronchial epithelial cell lines Calu-3 and 16HBE14o.* Eur Respir J, 2000. **15**(6): p. 1058-68.
16. Cavet, M.E., M. West, and N.L. Simmons, *Transepithelial transport of the fluoroquinolone ciprofloxacin by human airway epithelial Calu-3 cells.* Antimicrob Agents Chemother, 1997. **41**(12): p. 2693-8.
17. Cooney, D., M. Kazantseva, and A.J. Hickey, *Development of a size-dependent aerosol deposition model utilising human airway epithelial cells for evaluating aerosol drug delivery.* Altern Lab Anim, 2004. **32**(6): p. 581-90.
18. Patel, J., et al., *Transport of HIV-protease inhibitors across 1 alpha,25di-hydroxy vitamin D3-treated Calu-3 cell monolayers: modulation of P-glycoprotein activity.* Pharm Res, 2002. **19**(11): p. 1696-703.
19. Pezron, I., et al., *Insulin aggregation and asymmetric transport across human bronchial epithelial cell monolayers (Calu-3).* J Pharm Sci, 2002. **91**(4): p. 1135-46.
20. Fiegel, J., et al., *Large porous particle impingement on lung epithelial cell monolayers--toward improved particle characterization in the lung*. Pharm Res, 2003. **20**(5): p. 788-96.

21. Ehrhardt, C., et al., *Drug absorption by the respiratory mucosa: cell culture models and particulate drug carriers.* J Aerosol Med, 2002. **15**(2): p. 131-9.
22. Mathia, N.R., et al., *Permeability characteristics of calu-3 human bronchial epithelial cells: in vitro-in vivo correlation to predict lung absorption in rats.* J Drug Target, 2002. **10**(1): p. 31-40.
23. Yang, T., et al., *Pulmonary delivery of low molecular weight heparins.* Pharm Res, 2004. **21**(11): p. 2009-16.
24. Trehin, R., et al., *Cellular uptake but low permeation of human calcitonin-derived cell penetrating peptides and Tat(47-57) through well-differentiated epithelial models.* Pharm Res, 2004. **21**(7): p. 1248-56.
25. Davis, C.W. and S.H. Randell, *Airway goblet and mucous cells: identical, similar, or different?* , in *Cilia and Mucus: from Development to Respiratory Defense*, S. M., Editor, Marcel Dekker. p. 195-210.
26. Grainger, C.I., et al., *Culture of Calu-3 cells at the air interface provides a representative model of the airway epithelial barrier.* Pharm Res, 2006. **23**(7): p. 1482-90.
27. Kreda, S.M., et al., *Coordinated release of nucleotides and mucin from human airway epithelial Calu-3 cells.* J Physiol, 2007. **584**(Pt 1): p. 245-59.
28. Vllasaliu, D., et al., *Barrier characteristics of epithelial cultures modelling the airway and intestinal mucosa: a comparison.* Biochem Biophys Res Commun, 2011. **415**(4): p. 579-85.
29. Cohen, A.W., Hnasko, R., Schubert, W., Lisanti, M.P., *Role of Caveolae and Caveolins in Health and Disease.* Physiol Rev, 2004. **84**: p. 1341-1379.
30. Li, S., et al., *Baculovirus-based expression of mammalian caveolin in Sf21 insect cells. A model system for the biochemical and morphological study of caveolae biogenesis.* J Biol Chem, 1996. **271**(45): p. 28647-54.
31. Razani, B., et al., *Caveolin-1-deficient mice are lean, resistant to diet-induced obesity, and show hypertriglyceridemia with adipocyte abnormalities.* J Biol Chem, 2002. **277**(10): p. 8635-47.
32. Bradbury, N.A., et al., *Characterization of the internalization pathways for the cystic fibrosis transmembrane conductance regulator.* Am J Physiol, 1999. **276**(4 Pt 1): p. L659-68.
33. Madlova, M., et al., *Poly(vinyl alcohol) nanoparticle stability in biological media and uptake in respiratory epithelial cell layers in vitro.* Eur J Pharm Biopharm, 2009. **72**(2): p. 437-43.
34. Duncan, M.J., J.S. Shin, and S.N. Abraham, *Microbial entry through caveolae: variations on a theme.* Cell Microbiol, 2002. **4**(12): p. 783-91.
35. Parton, R.G., *Caveolae and caveolins.* Curr Opin Cell Biol, 1996. **8**(4): p. 542-8.
36. Lipardi, C., et al., *Caveolin transfection results in caveolae formation but not apical sorting of glycosylphosphatidylinositol (GPI)-anchored proteins in epithelial cells.* J Cell Biol, 1998. **140**(3): p. 617-26.
37. Vogel, U., K. Sandvig, and B. van Deurs, *Expression of caveolin-1 and polarized formation of invaginated caveolae in Caco-2 and MDCK II cells.* J Cell Sci, 1998. **111 (Pt 6)**: p. 825-32.
38. Bose, S., et al., *Bipolar functional expression of transcobalamin II receptor in human intestinal epithelial Caco-2 cells.* J Biol Chem, 1997. **272**(6): p. 3538-43.
39. Tuma, P.L. and A.L. Hubbard, *Transcytosis: crossing cellular barriers.* Physiol Rev, 2003. **83**(3): p. 871-932.
40. Molecular Probes, M. *LysoTracker™ and LysoSensor™ Probes*. 1999 [cited.
41. Chen, J.W., et al., *Isolation and sequencing of a cDNA clone encoding lysosomal membrane glycoprotein mouse LAMP-1. Sequence similarity to proteins bearing onco-differentiation antigens.* J Biol Chem, 1988. **263**(18): p. 8754-8.
42. Granger, B.L., et al., *Characterization and cloning of lgp110, a lysosomal membrane glycoprotein from mouse and rat cells.* J Biol Chem, 1990. **265**(20): p. 12036-43.

43. Green, S.A., et al., *Kinetics of intracellular transport and sorting of lysosomal membrane and plasma membrane proteins.* J Cell Biol, 1987. **105**(3): p. 1227-40.
44. Bivas-Benita, M., et al., *PLGA-PEI nanoparticles for gene delivery to pulmonary epithelium.* Eur J Pharm Biopharm, 2004. **58**(1): p. 1-6.
45. Figueiredo, M. and R. Esenaliev, *PLGA nanoparticles for ultrasound-mediated gene delivery to solid tumors.* Journal of Drug Delivery, 2011. **2012**(Article ID 767839): p. 20.
46. Motley, A., et al., *Clathrin-mediated endocytosis in AP-2-depleted cells.* J Cell Biol, 2003. **162**(5): p. 909-18.
47. Lakadamyali, M., M.J. Rust, and X. Zhuang, *Ligands for clathrin-mediated endocytosis are differentially sorted into distinct populations of early endosomes.* Cell, 2006. **124**(5): p. 997-1009.
48. Orlandi, P.A. and P.H. Fishman, *Filipin-dependent inhibition of cholera toxin: evidence for toxin internalization and activation through caveolae-like domains.* J Cell Biol, 1998. **141**(4): p. 905-15.
49. Schnitzer, J.E., et al., *Filipin-sensitive caveolae-mediated transport in endothelium: reduced transcytosis, scavenger endocytosis, and capillary permeability of select macromolecules.* J Cell Biol, 1994. **127**(5): p. 1217-32.
50. Fishman, P.H., *Internalization and degradation of cholera toxin by cultured cells: relationship to toxin action.* J Cell Biol, 1982. **93**(3): p. 860-5.
51. Orlandi, P.A., P.K. Curran, and P.H. Fishman, *Brefeldin A blocks the response of cultured cells to cholera toxin. Implications for intracellular trafficking in toxin action.* J Biol Chem, 1993. **268**(16): p. 12010-6.
52. Orlandi, P.A. and P.H. Fishman, *Orientation of cholera toxin bound to target cells.* J Biol Chem, 1993. **268**(23): p. 17038-44.
53. Rojas, R. and G. Apodaca, *Immunoglobulin transport across polarized epithelial cells.* Nat Rev Mol Cell Biol, 2002. **3**(12): p. 944-55.
54. Rejman, J., et al., *Size-dependent internalization of particles via the pathways of clathrin- and caveolae-mediated endocytosis.* The Biochemical journal, 2004. **377**(Pt 1): p. 159-69.
55. Hammond, T.G. and P.J. Verroust, *Trafficking of apical proteins into clathrin-coated vesicles isolated from rat renal cortex.* Am J Physiol, 1994. **266**(4 Pt 2): p. F554-62.
56. Kozyraki, R., et al., *The intrinsic factor-vitamin B12 receptor, cubilin, is a high-affinity apolipoprotein A-I receptor facilitating endocytosis of high-density lipoprotein.* Nat Med, 1999. **5**(6): p. 656-61.
57. Bento-Abreu, A., et al., *Albumin endocytosis via megalin in astrocytes is caveola- and Dab-1 dependent and is required for the synthesis of the neurotrophic factor oleic acid.* J Neurochem, 2009. **111**(1): p. 49-60.
58. Christensen, E.I., et al., *Membrane receptors for endocytosis in the renal proximal tubule.* Int Rev Cytol, 1998. **180**: p. 237-84.
59. Gekle, M., *Renal tubule albumin transport.* Annu Rev Physiol, 2005. **67**: p. 573-94.
60. Lambot, N., et al., *Evidence for a clathrin-mediated recycling of albumin in human term placenta.* Biol Reprod, 2006. **75**(1): p. 90-7.
61. Carro, E., et al., *Choroid plexus megalin is involved in neuroprotection by serum insulin-like growth factor I.* J Neurosci, 2005. **25**(47): p. 10884-93.
62. dos Santos, T., et al., *Effects of transport inhibitors on the cellular uptake of carboxylated polystyrene nanoparticles in different cell lines.* PLoS One. **6**(9): p. e24438.
63. Dausend, J., et al., *Uptake mechanism of oppositely charged fluorescent nanoparticles in HeLa cells.* Macromol Biosci, 2008. **8**(12): p. 1135-43.

Chapter 8: Insulin nanocrystal formulations and their stabilisation by THPP

8.1 Introduction

Parenteral administration is currently the only clinically available route of insulin delivery. Alternative routes of administration (e.g. oral, nasal, rectal, pulmonary and ocular) have been extensively investigated [1]. Among them, the oral route is most convenient and most accepted by patients. However, the oral delivery of many therapeutic peptides and proteins like insulin remains an unresolved challenge because of their large size, hydrophilicity, and relative instability in the physiological environment [2]. Insulin is largely degraded by proteolytic enzymes in the gastrointestinal tract and is very poorly absorbed after oral administration [3, 4]. In order to protect it from biodegradation and to improve its intestinal absorption, insulin has been encapsulated in/or associated with polymeric biodegradable nanocapsules, nanospheres or microparticles associated or not, to surfactants or antiproteases [5-8], or otherwise coated with hydrophilic polymers such as chitosan [9-11]. Chitosan is a mucoadhesive, polycationic polymer known to facilitate drug absorption by localising drug concentration around absorptive cells [12], and prolonging drug residence time in the gut [13]. It is also an effective permeability enhancer because of its depolymerising action on cellular F-actin and the tight junction protein ZO-1 [9]. However, there are several limitations accompanying the aforementioned approaches for oral insulin formulations: carrier systems (ie: microparticles and nanospheres) slowly release insulin with small amounts being absorbed [14]. Furthermore, absorption only occurs in the small intestine and over a short time-frame which is not sufficient to achieve therapeutic doses of insulin. The drawbacks of penetration enhancers (surfactants and mucoadhesives) include: lack of specificity, allowing the content of the intestinal tract including toxins and pathogens to gain the same access to the bloodstream [15], and risk to mucous membranes by surfactants and damage of cell membrane by chelators. Surfactants can cause lysis of mucous membrane and may damage the lining of the gastrointestinal tract. Bioadhesive systems may be affected by the mucous turnover of

the gastrointestinal tract which varies based on the site of absorption. Moreover, directing a delivery system to a particular site of adhesion is yet to be achieved.

Therapeutic proteins like insulin, present many difficulties for drug delivery and formulation (Chapter 1, section 1.6). These macromolecules are quickly broken down and processed *in vivo* both in the gastrointestinal tract and by systemic regulatory systems. Therefore, they must be formulated to overcome physicochemical, chemical and biological instability during processing, storage and delivery [16]. Recently, the use of protein crystals in formulation design has been investigated [16-19]. Protein crystals could protect the integrity of the therapeutic agent in a lattice-type structure both prior to administration and post delivery. Protein crystals in their highly compact arrangement, may allow for sustained release of the therapeutic agent, which provides maximum drug loading and removes the need for repetitive dosing [16, 20].

In this chapter, work detailing the preparation of a heterogeneous population of nano- and micron-sized insulin crystals (by employing a modification of batch crystallisation protocols [17]) is described. Furthermore, the effects of THPP (β-[Tris(hydroxymethyl) phosphino] propionic acid) as a proof-of-concept crystal stabiliser were investigated. THPP is a water-soluble, trifunctional crosslinker that reacts with primary and secondary amines to produce covalent linkages in the form of P-CH_2-NH-R. Previous studies have employed THPP as a cross-linking agent to enhance the properties of elastin-like polypeptides (ELPs) for tissue engineering purposes [21, 22]. This work aimed to address the problem of colloidal instability of insulin in the absence of a stabilising crystallisation buffer by cross-linking the surface of newly formed crystals and then fine-tuning the extent of this cross-linking to produce stable nano-sized protein crystals and at the same time permitting the release of biologically active insulin with a slow release profile. The effects of THPP on crystal formation, stability, insulin release and bioactivity in mouse 3T3 fibroblasts were investigated. The potential toxicity of THPP itself was assessed using cell viability assays. The present work describes the design and characterisation of ‘stabilised’ micro- and nano-crystals which show promise for the development of a suitable oral delivery platform

for protein bioactives and laying the foundations for subsequent development of bioconjugated protein nanocrystals (i.e. surface decorated with vitamin B_{12}), which in turn would result in their improved mucosal absorption.

8.2 Methods

8.2.1 Preparation and stabilisation of insulin crystals

Hydrochloric acid (0.02M, 3 ml) was added to weighed aliquots of insulin powder and the mixture was swirled until the insulin had dissolved. To prepare the crystallisation buffer (previously optimised by the group), the following components were then added sequentially to produce a turbid solution: aqueous 12% w/v zinc chloride solution (24 µl), sodium chloride (0.36 g), sodium citrate solution (0.2M, 2 ml). The pH was adjusted to 6.25 with sodium hydroxide (0.1M). The solutions were then rotated on a centrifugal evaporator (Genevac® systems, Aqueous setting, 45℃) for 1.5 hrs until approximately half the solution had evaporated.

For experimental design 1, THPP solution (1 mg/ml) in corresponding insulin crystallisation buffer was prepared and added (immediately after the evaporation stage) in the following Insulin:THPP molar ratios: 3:2, 3:1, 6:1 and 12:1 to separate crystal preparations (n=2 for each) to achieve different extents of surface cross-linking. A control sample was prepared without THPP stabilisation. The samples were then placed in isopropanol and stored at -20℃ overnight. The following day, samples were transferred to 4℃ to counteract freeze-thaw shock and stored for up to two weeks for analysis.

For experimental design 2, insulin preparations were transferred to -20℃ overnight before THPP was added and incubated for a further 12-24 hr at 4℃. In both studies, the THPP-cross-linked Insulin preparations were extensively dialysed against distilled H_2O overnight and the distilled H_2O was replaced three or four times over the 24 hour period. A cellulose-ester membrane was used with a molecular weight cut-off of 25kDa.

8.2.2 Dynamic light scattering and disc centrifuge studies

For dynamic light scattering (DLS), samples were diluted 1:10 in their respective buffer and analysed using a Viscotek 802 system. The programme was run using the default mode, wherein the optimal intensity count was 300 k counts and the temperature was 25℃. Omnisize software was used to calculate the particle size data (which was set to an average of 10 readings per sample). Repeated measurements were carried out post-dialysis to assess the effects of THPP on crystal stabilisation.

Samples (with Insulin:THPP molar ratios of 3:1) were further analysed using centrifugal separation analysis. A sucrose gradient of 4-12% was built up on a CPS disc centrifuge (Analytik Ltd). The parameters were set for protein samples with a 1.24 g/ml density and a refractive index of 1.3. The instrument was calibrated before each run using 377 nm poly-(vinyl chloride) (PVC) particle standard followed by injection of sample (100 µl). This part of the work was conducted by Rosie Adsley (University of Nottingham).

8.2.3 Transmission Electron Microscopy (TEM)

100 HEX Copper mesh grids (TAAB) were coated with Formvar and carbon support film (3.05mm). Insulin solutions were subsequently diluted 10- to 100-fold, and aliquots (3.5 µl) were placed on the grids. After 30 seconds, two drops of 1% phosphotungstic acid (Sigma Aldrich) were then placed on the grid and left for 10–15 seconds. Excess water was removed with filter paper, and the grid was then left to air-dry for 30 minutes. Imaging was performed using an electron microscope (Tecnai BioTWIN, FEI) with an acceleration voltage of 100 kV and magnifications typically ranging from 1250-135000. The samples were prepared by Denise Christie (Advanced Microscopy Unit, University of Nottingham).

8.2.4 Insulin Release study

After dialysis to remove salt from the THPP-cross-linked insulin particle preparations (section 8.2.1), the amount of insulin retained was quantified using the commercially available BCA assay. This step was important as it enabled quantitation of the starting amount of insulin in each sample prior to the release experiment, thus enabling

eventual calculation of percent insulin release. Insulin standards (used to construct a calibration curve) were prepared in distilled H_2O (2M HCl was added drop wise to dissolve into solution). Both standard and sample (25 µl) were aliquotted into a 96 well plate and working BCA reagent (200 µl) was added (comprising BCA solution and 4% cupric sulphate in a 50:1 v/v ratio). The plate was incubated at 37°C for 30 min and the absorbance was measured at 562 nm on a Dynex MRX microtiter plate reader.

Each THPP-cross-linked insulin sample (1 ml) (of varying ratios of 3:2, 3:1, 6:1 and 12:1) was dialysed against 50 ml of 0.05M Trizma® base (pH adjusted to 7.4). A cellulose-ester membrane with a 100 kDa cut-off was used and the solutions were stirred continuously in a closed vessel using a magnetic stirrer. The samples (300 µl) were collected from the dialysate over a 48 hr duration over a series of intermediate time points. Sample volumes were replaced with fresh buffer (300 µl). Quantification of the amount of insulin released over the 48 hour period was carried out using high-performance liquid chromatography (HPLC) using an HP 1090 system. A Discovery® C18 (180 Å; 5 µm 250 x 4.6 mm) column (Supelco) in combination with a Discovery® C18 Supelguard pre-column was used. Two mobile phases were used: 0.1 % trifluoroacetic acid (TFA) in water and 0.1 % TFA in acetonitrile. The flow gradient was from 70 to 60% of the aqueous solution over 15 minutes and the flow rate was maintained at 1 ml/min. UV detection was at 215 and 275 nm and the insulin peak eluted at approximately 7 minutes.

8.2.5 THPP toxicity assays

Caco-2 (human intestinal) cells (passage 60) were seeded onto a 96-well plate at a density of 10,000 cells/cm^2. The cells were incubated overnight with supplemented EMEM media containing 10% foetal calf serum in an atmosphere of 5% CO_2 (37°C). The following day, the medium was replaced with HEPES:HBSS buffer (50 mM) and cells were left to equilibrate for 30 minutes. To the negative (positive, in the case of the LDH assay) control wells, Triton X-100 (0.2% v/v, 100 µl) was added (n=5) and fresh HEPES:HBSS was added to the positive (negative, in the case of the LDH assay) control wells. Varying concentrations of THPP (in HEPES:HBSS) were applied

to the sample wells (with five repeats per concentration) to achieve a final concentration range of 15.6-1000 µg/ml. The cells were incubated for 2-3hrs before the THPP solution was removed and the cells were washed three times with PBS. For the MTS assay, supplemented EMEM (100 µl) was added. CellTiter 96 ® Aqueous One solution MTS reagent (20 µl) was added to each well. The cells were incubated with the reagent for 3 hrs and the absorbance was measured at 490 nm on a Dynex MRX plate reader. For the LDH assay, 50 µl was removed from each well (including control wells) after incubation with THPP solution and aliquotted onto a new plate. Combined LDH assay reagents (100 µl) (LDH assay substrate solution, LDH assay cofactor preparation and LDH assay dye solution were mixed previously in equal volumes) were added to the samples and these were incubated for 30 min. The reaction was quenched with 1M HCl (15 µl). The absorbance was read at 490 nm on a Dynex MRX plate reader. The reader is referred to Chapter 2 (sections 2.2.4.2-2.2.4.3) for calculations of percent Relative Metabolic Activity and LDH release.

8.2.6 NIH 3T3 proliferation test for insulin bioactivity

Mouse NIH-3T3 fibroblasts (passage 45) were seeded onto a 96-well plate at a density of 10,000 cells/cm^2. They were incubated overnight in supplemented DMEM medium (containing 1% FCS) at an atmosphere of 5% CO_2 (37°C). A solution of insulin in 0.05M Trizma® base was prepared as a positive control and diluted to 100 nM in DMEM. Insulin samples which were collected from the HPLC release study (i.e. free insulin from the dialysate, again of varying THPP-cross-linked ratios) were all standardised to the same concentration (100 nM) using dilutions in DMEM medium and 100 µl was applied to the cells. Note, that the initial starting concentration of each insulin sample was determined from HPLC data. 0.2% Triton X-100 was applied (100 µl) to negative control wells and DMEM was also applied to reference control wells (n=6). The fibroblasts were incubated for 24 hrs with the insulin samples. The following day, the cells were washed three times with PBS and 100 µl of fresh supplemented DMEM medium was applied to the cells. The MTS reagent was added and the experiment followed as detailed in section 8.2.5 and Chapter 2 (section 2.2.4.2).

8.3 Results and Discussion

8.3.1 Stability of insulin crystals post-dialysis

The first task in this investigation was to establish and optimise a protocol for the development of insulin crystals of sub-micron range. This was achieved by carefully adjusting the ratio of components of the crystallisation buffer and experimenting with the centrifugal evaporation step until the conditions were optimised.

The second task was to investigate the use of THPP as proof-of-concept stabiliser for the newly formed insulin crystals, considered important to preserve the integrity of the small crystals following removal of the crystallisation buffer. To this end, varying the time of addition of THPP was one parameter investigated. In one experiment, THPP was added (in varying molar ratios) before the crystals were slow-frozen. In the complementary experiment, THPP (in varying molar ratios to insulin) was added after slow-freezing the crystals.

Particle size analysis was used to assess the effect that the timing of THPP addition has on the subsequent growth and stabilisation of the newly formed crystals. Figure 8.1 shows particle size distribution profiles for samples where THPP was added prior to placing insulin crystals in isopropanol at -20 ℃. The data indicate that after 24 hours of growth in sub zero temperatures, a heterogeneous population of Insulin particles had formed. Furthermore, the addition of THPP prior to slow-cooling did not reduce crystal formation but rather promoted it (i.e. produced size distributions of near optimal sub 500 nm range). Figure 8.1 (i), (ii), (iii), (iv) and (v) (pre-dialysis samples) show that regardless of THPP ratio, a range of different sized-insulin species are present. In all pre-dialysis samples, the predominant size range of the particles was found to be around 100-400 nm (occupying about 30-70% of the sample population), but both smaller species (~5-80 nm) and considerably larger particles (>20 µm in size) were also produced. The larger size particles were presumed to be insulin aggregates which had not undergone crystallisation. After extensive dialysis, the role of THPP became apparent. In the absence of THPP (Figure 8.1 post-dialysis (i)), it appeared that removal of salt promoted some destabilisation of the Insulin crystals and they

started to fall apart and then aggregate (this was also visually noticeable). Most of the sample area (59% of the population) had radii higher than $>10^5$ nm in size. Moreover, the proportion of crystals of a desirable size (<200 nm) had diminished. When compared directly with the data obtained prior to the dialysis procedure, a significant difference in both size and stability of the crystals was observed. Increasing the amount of THPP (decreasing the molar ratio of insulin to THPP) resulted in a substantial proportion of the population of Insulin crystals "surviving" and preserving resistance to destabilisation in the absence of their crystallisation buffer. For example, when the molar ratio of Insulin:THPP was 12:1 (Figure 8.1 post-dialysis (ii)), 78% of the sample had a mean radius of ~140nm and 14% was detected as 24 nm, compared with 8% which had formed aggregates. When the molar ratio was decreased to 6:1 (Figure 8.1 post-dialysis (iii)), 6% represented crystals with average mean radii of 9 µm and 9% was detected as aggregates. The remaining sample comprised a split population of crystals ~15-360 nm in size. When the molar ratio was decreased further to 3:1 (Figure 8.1 post-dialysis (iv)), no aggregates were detected and 43% of the population comprised a mean radius of ~40 nm, the remaining 57% of crystals were around 230 nm in size. A ratio of 3:2 (Figure 8.1 post-dialysis (v)) produced a largely homogenous population with an average size of 88 nm (95.5%).

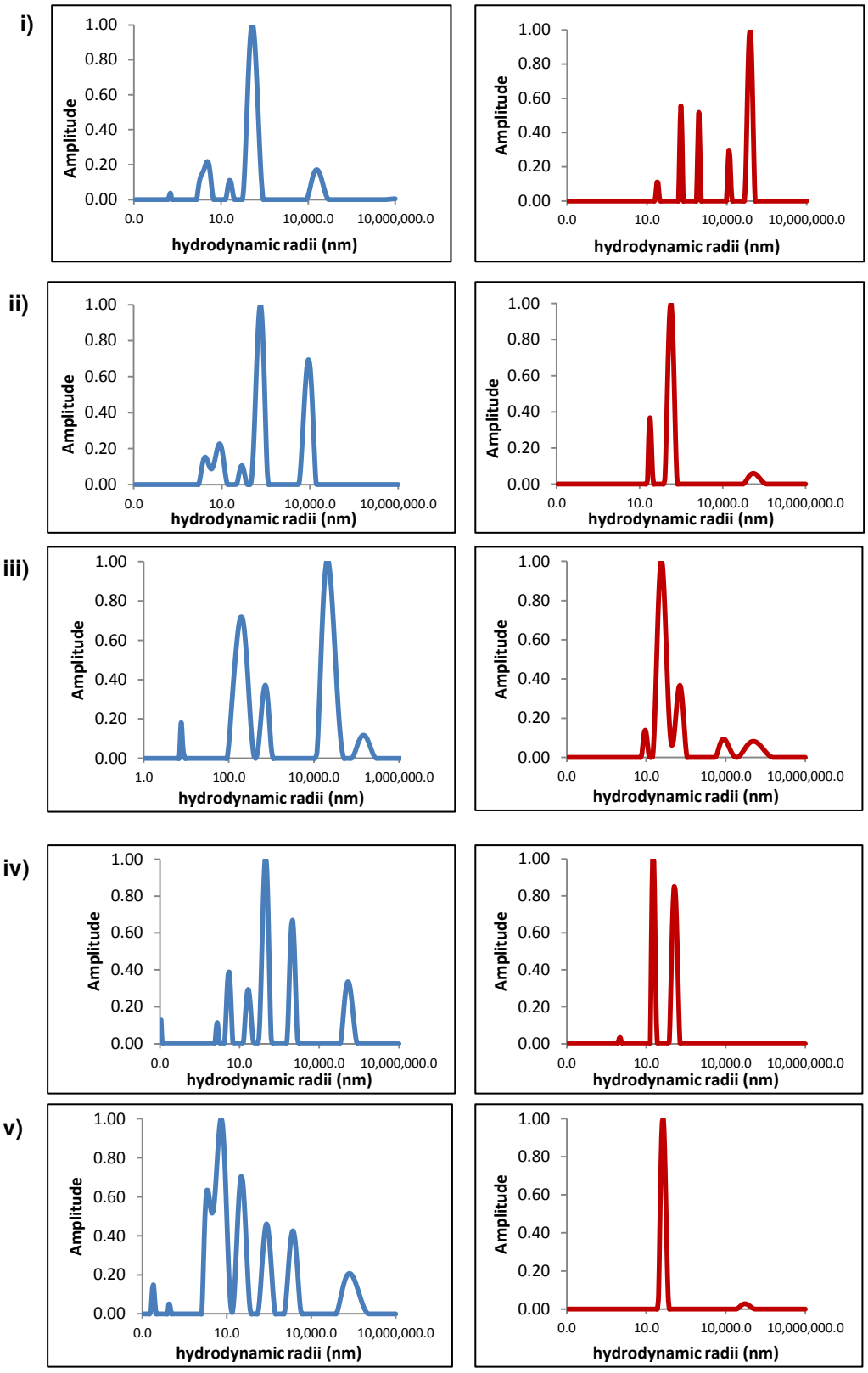

Figure 8. 1. Dynamic light scattering intensity distributions for experimental design 1 (the addition of THPP prior to freezing).

Pre-dialysis samples on left (blue), Post-dialysis samples on right (red) i) No THPP (ctrl), ii) 12:1 Insulin:THPP, iii) 6:1 Insulin:THPP, iv) 3:1 Insulin:THPP, v) 3:2 Insulin:THPP.

In the second experiment, THPP was added after the slow-freezing process and again, particle size analysis was conducted on the samples both pre- and post-dialysis (Figure 8.2). In drawing a comparison with the control (no THPP, Figure 8.2(i)) and samples prepared with THPP before freezing (Figure 8.1), the data revealed a different pattern. For 12:1, 6:1, 3:1 and 3:2 (Figure 8.2 pre-dialysis (ii), (iii), (iv) and (v) respectively) we postulate that the addition of THPP after freezing either had a detrimental effect on the stabilisation of the newly formed crystals or its absence prior to freezing actually hindered heterogeneous crystal growth. This is reflected by both the absence of smaller crystals and by the presence of large aggregates. For example for 12:1 (Figure 8.2 pre-dialysis (ii)), >59% of the population were greater than 950 nm in size and 17% presented an average mean radii of 66 nm. Furthermore, increasing the amount of THPP seemed to exacerbate the aggregation problem with 35% of the population exceeding 2 µm in size and the majority forming aggregates for 6:1 Insulin:THPP (Figure 8.2 pre-dialysis (iii)). Again, for 3:1 (Figure 8.2 pre-dialysis (iv)), 88% of the sample population formed aggregates (although these may well have been large crystals). A similar profile was observed for 3:2 samples with 16% bearing an average radius of ~770 nm and 65% representative of >4 µm. After these samples were dialysed, we observed a huge reduction in yield (data not shown) and a significant proportion of the Insulin had formed aggregates. Of note, however, in the presence of THPP, new species were detected in the sample after dialysis. For example, for both 3:1 and 3:2 samples (Figure 8.2 post-dialysis (iv), (v) respectively), a bimodal distribution was observed with crystals bearing a mean radius of ~15-30 nm and ~115-130 nm.

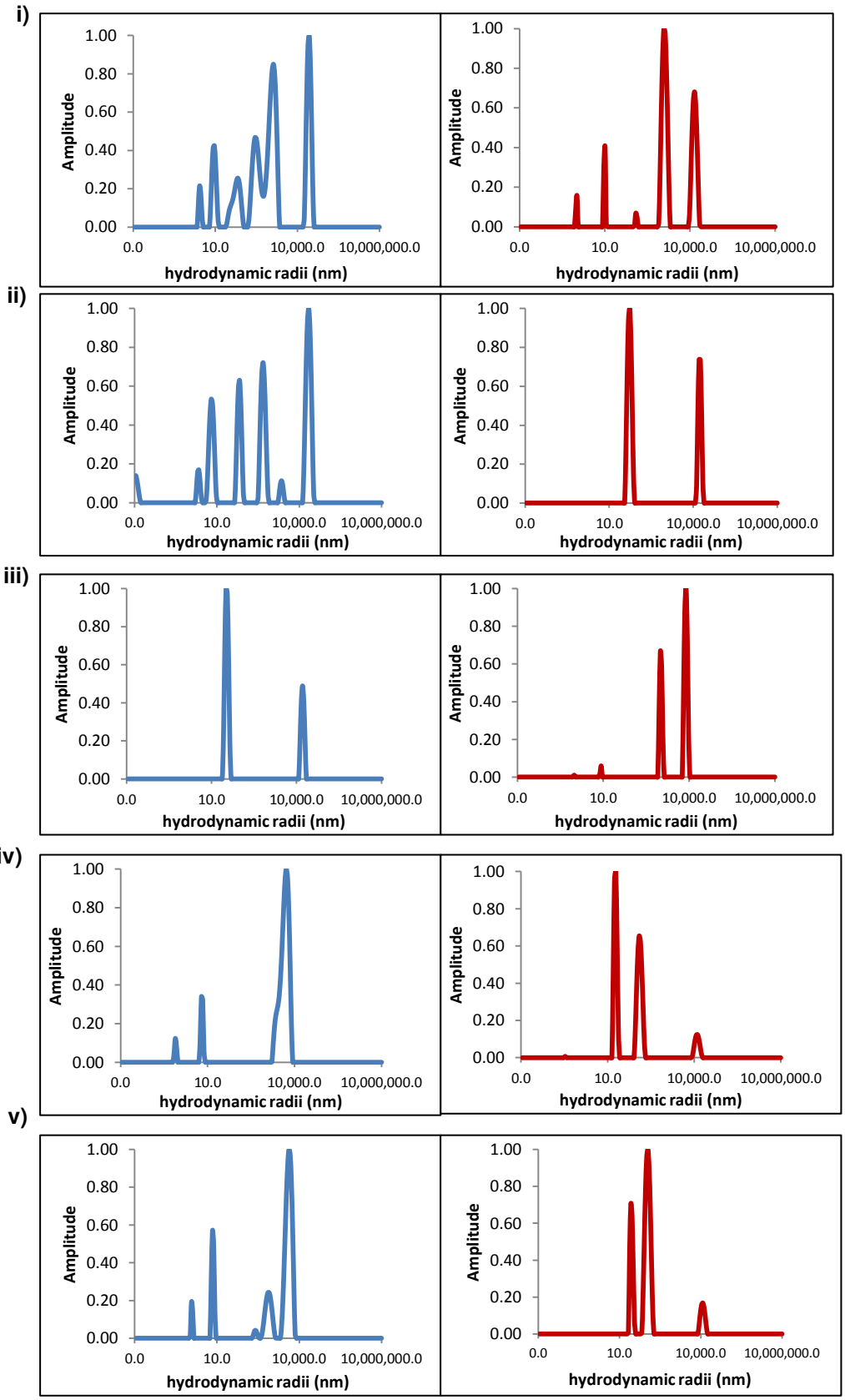

Figure 8. 2. Dynamic light scattering intensity distributions for experimental design 2 (the addition of THPP after freezing).

Pre-dialysis samples on left (blue), post-dialysis samples on right (red) - i) No THPP (ctrl), ii) 12:1 Insulin:THPP, iii) 6:1 Insulin:THPP, iv) 3:1 Insulin:THPP, v) 3:2 Insulin:THPP.

Figure 8.3 shows the visual differences between samples post-dialysis. This was so that we could observe changes to the opacity of the samples based on the timing of THPP addition. For the design 1 samples, as the amount of THPP was increased, the solutions became more transparent (A → J), with the exception of those samples that were subjected to experimental design 2 (THPP added after freezing). In direct comparison with its neighbouring solution (at the same Insulin:THPP ratio), samples where THPP was added before freezing appear clearer (Figure 8.3. C, E, G, I), than those where THPP was added after freezing (Figure 3. D, F, H, J), which appear opaque or cloudy. Furthermore, as the molar ratio of Insulin:THPP increases, this marked contrast, decreases. This suggests that when THPP is administered prior to freezing it either adds to the colloidal stability of the crystals or promotes the formation of smaller crystals, which in turn is responsible for the opague or 'blue-ish' appearance of the solution.

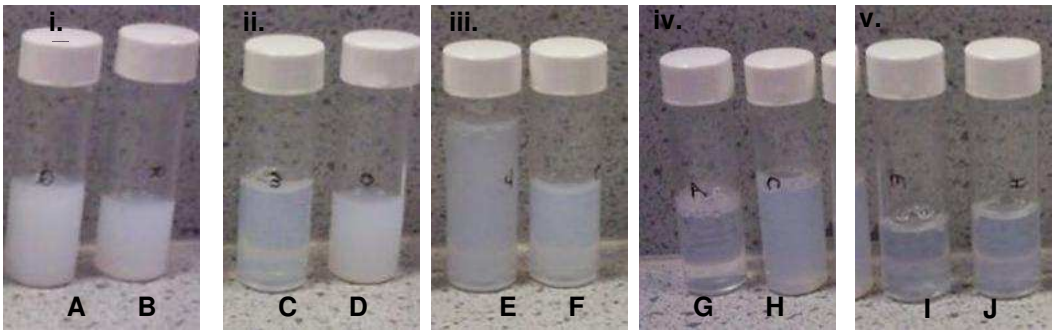

Figure 8. 3. Photograph showing visual appearance of Insulin samples post- dialysis.

The samples were paired according to Insulin:THPP ratio with experimental design 1 & 2 samples placed next to each other (ie: samples I & J correspond to 3:2 Insulin:THPP, experimental design 1 and 2 respectively). i.e. sample on left of each sub-figure prepared using experimental design 1, sample on right of each sub-figure prepared using experimental design 2: i) No THPP (ctrl), ii) 12:1 Insulin:THPP, iii) 6:1 Insulin:THPP, iv) 3:1 Insulin:THPP, v) 3:2 Insulin:THPP

8.3.2 Disc Centrifuge analysis

DLS analysis is poor at distinguishing between populations with similar sizes but these different populations of samples are however readily separated by centrifugation. CPS resolves very close multi-modal particle distributions and distinguishes small shifts in particle size. Rather than using a predictive algorithm, the disc centrifuge technique

physically separates nanoparticles before measurements are recorded. Disc centrifuge analysis was carried out on the samples. In this report, we show only a comparison of a single sample pre- and post-dialysis (3:1 Insulin:THPP from experimental design 1, see Figure 8.1 (iv)). Owing to the limitations of the technique, it was not possible to generate a complete size-range profile ranging from nanometers to micrometers. We therefore selected two different centrifugal speeds: the first was used to detect particles ranging from 0.01-0.4 microns and the second was used to detect particles in the 0.2-0.5 micron range. Therefore, large aggregates of Insulin were not detected using this method.

Disc centrifuge analysis revealed a bimodal distribution of insulin crystals both pre- and post-dialysis over a range of 0.01-5 µm (Figure 8.4). The dialysis procedure appeared to slightly reduce the nominal sizes of the smaller crystal populations. For example, the calculated median for the detected peak over the small size distribution was reduced from 0.032 µm to 0.020 µm (Figure 8.4 (i), (iii)). However, an asymmetric biomodal distribution of particle sizes was observed for the upper limit of detection (Figure 8.4, (iv)) with a median of 0.72 µm following dialysis.

Referring back to the DLS data for the same Insulin:THPP ratio (Figure 8.1 (iv)), approximately 60% of the pre-dialysis sample comprised crystals ranging from 3-190 nm in size of this 60%, 9.4% were 43 nm and 39% were 190 nm in size. This largely supports disc centrifuge data across this particular size range (Figure 8.4 (i)). However, DLS data reveals peaks corresponding to an intermediate size range (0.19<x>2 µm), which is not detected on the disc centrifuge. This could be as a result of aggregation of the sample over time, leading to a corresponding peak on CPS at 3.55 µm. Post-dialysis samples analysed on the CPS (Figure 8.4 (iii), (iv)) resemble more closely corresponding DLS samples (refer to Figure 8.1, (iv, post-dialysis)) with peaks on CPS giving a mean value of 0.046 µm and peaks on DLS giving a mean value of 0.036 µm. Similarly, a minimal peak on the CPS at ~0.3 µm corresponds with a peak on the DLS at ~0.24 µm. Again, aggregation of the sample is likely to precede peaks detected at 0.6 µm and 1 µm on the CPS (Figure 8.4 (iv)). DLS data analysis should be accompanied with an element of caution as the technique often fails to

identify multi-modal particle distributions with small differences in particle size. On the other hand, CPS analysis can be used to verify the existence of skewed particle distributions, which are separated according to mass. Therefore, the two techniques can be used in combination for more accurate particle-size determination. On the whole, DLS and CPS data are in close agreement particularly for particles sub-0.2 µm in size.

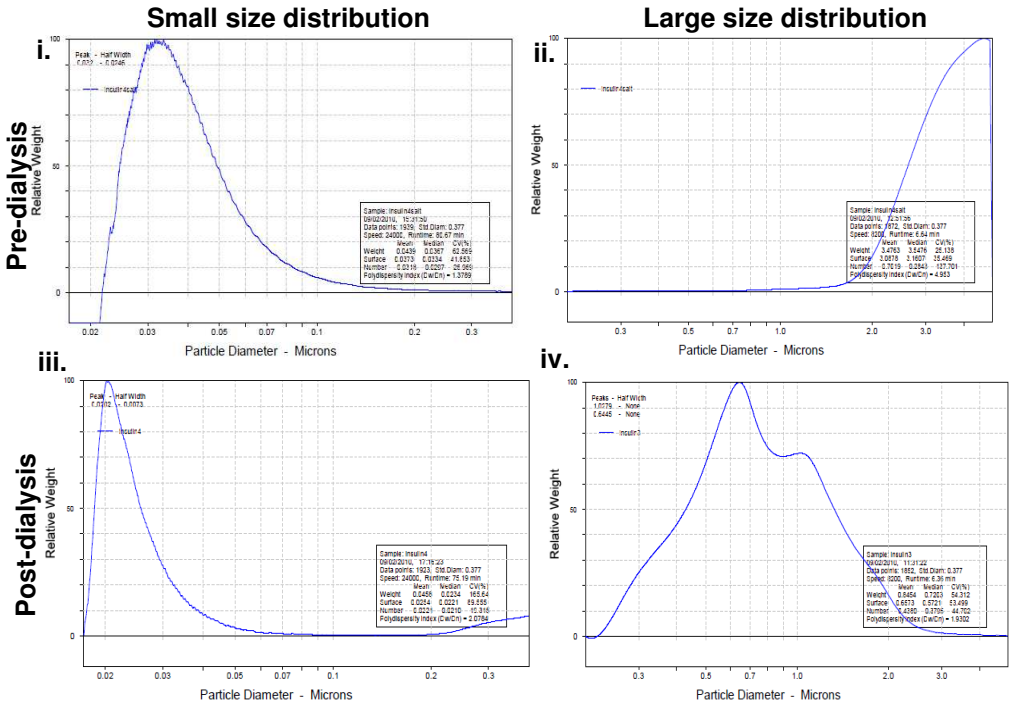

Figure 8. 4. Disc centrifuge analysis on 3:1 Insulin:THPP (experimental design 1).

i) pre-dialysis (in salt) 0.01-0.4 µm size distribution, ii) pre-dialysis (in salt) 0.2-5 µm size distribution, iii) post-dialysis (in water) 0.01-0.4 µm size distribution, iv) post-dialysis (in water) 0.2-5 µm size distribution.

8.3.3 Transmission Electron Microscopy (TEM)

Electron micrographs confirmed that a heterogeneous population of Insulin crystals exist. Furthermore these images reveal that larger crystals (>1 µm) adopt a hexagonal configuration (Figure 8.5 (ii)). Figure 8.5 (iii) shows a crystal cluster (each approximately 60 nm in size) and these show angular characteristics giving confidence that these are not ill-defined insulin aggregates. Interestingly, degradation of the crystals is also visible (Figure 8.5 (iv)) where whole hexagonal crystals appear to have broken into pieces. This could be as a result of the TEM preparation.

Nevertheless, this serves to show that the insulin in the samples is crystalline in nature and not a collection of different sized aggregates which cannot be deduced from either of the sizing methods used in this study.

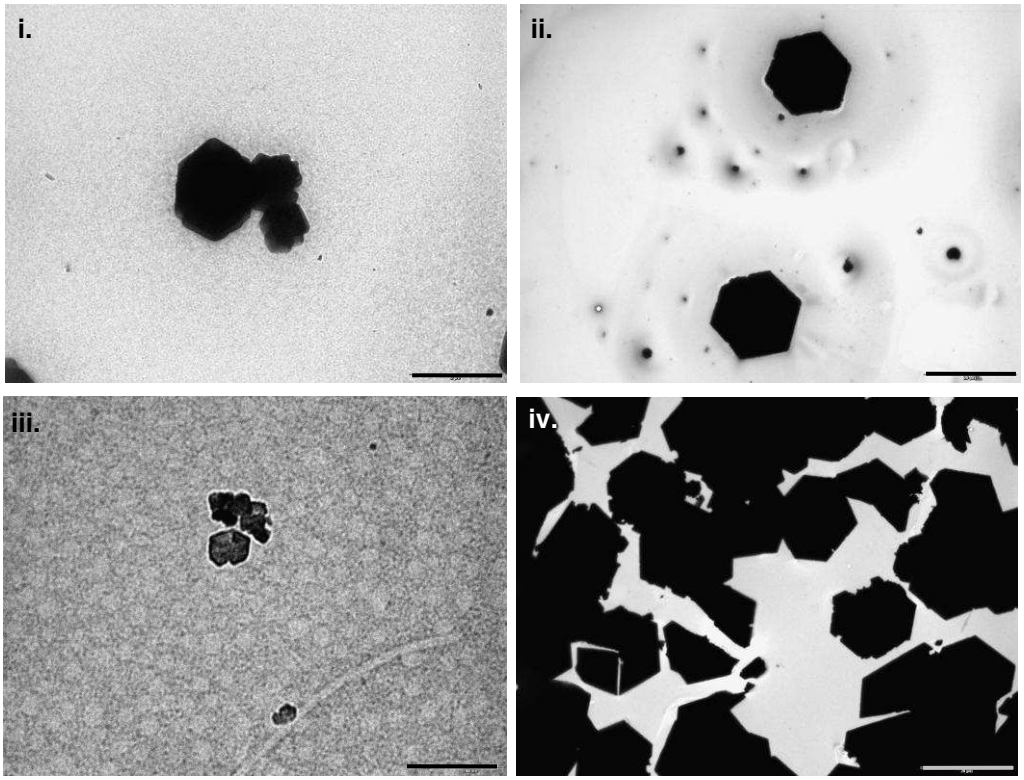

Figure 8. 5. Transmission electron microscopy images showing stabilised 3:1 Insulin:THPP crystals.

i) x11500 magnification, scale bar 2 µm, ii) x790 magnification, scale bar 20 µm, iii) x105000, scale bar 100 nm, iv) x790 magification, scale bar 20 µm.

8.3.4 THPP toxicity assays

Both MTS and LDH toxicity assays showed that regardless of the concentration used, THPP presented no significant toxicity towards Caco-2 cells as shown by the relevant comparisons with positive and negative controls (Figure 8.6). As shown on the graph, there was no apparent trend between an increase in THPP concentration and a decrease in the cell viability and at no concentration tested, is there a significant drop in the cell viability. These results are mirrored by the LDH data where low values indicate that the cell membrane integrity is preserved.

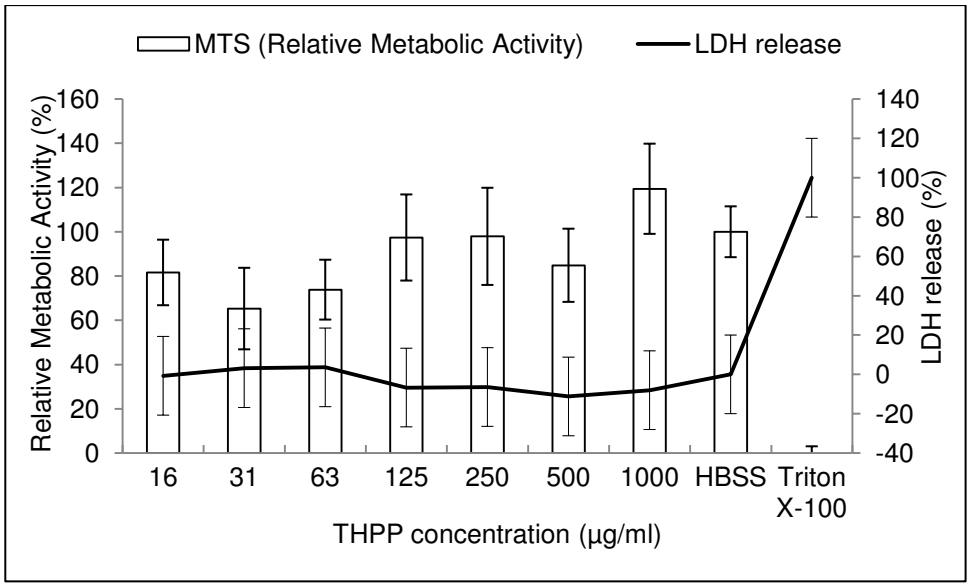

Figure 8. 6. Toxicity of THPP in Caco-2 cells.

Data showing mitochondrial activity (% cell viability) from MTS assay and Lactate dehydrogenase (LDH) assay showing % LDH release after two hours incubation with THPP at varying concentrations (16-1000µg/ml) relative to both Triton X-100 and HBSS controls. Data represents mean (n=6 ± SD).

8.3.5 Insulin release study

Release profiles from the Insulin:THPP cross-linked crystals prepared at different THPP:insulin ratios were compared (Figure 8.7). The data show highly variable release profiles which are seemingly dependent on the ratio of Insulin:THPP. The optimum ratio for release is illustrated by 3:1 Insulin:THPP crosslinked preparations, based on the highest percent released over time. After 3 hours, approximately 20% of insulin has been released. After 41 hours, the data reveals >80% release from the initial amount of cross-linked crystals dialysed. Furthermore, the release profile is fairly slow, which is desirable for protein bioactives with short half-lives.

Increasing the ratio of Insulin:THPP to 6:1 and 12:1 had a detrimental effect on the release properties. This might be attributed to destabilisation and precipitation of the insulin inside the dialysis tubing preventing subsequent release - likely a consequence of insufficient extents of THPP cross-linking. Furthermore, unlike the control sample (whereby insulin was dissolved at acidic pH), these samples were dialysed against 0.05M Trizma® base (and the pH was adjusted to pH 7.4.) This difference in pH

undoubtedly affects the solubility behaviour of insulin, as insulin has low solubility at neutral pH with solubilisation (1-10 mg/ml) only achieved under acidic conditions (pH 2-3) [23].

Preparations of 6:1 and 12:1 produced very similar release profiles with the total percent release not exceeding 50% of the initial amount. Interestingly, 3:2 Insulin:THPP also delivers a poor release profile (similar to 6:1 and 12:1). This could be as a result of extensive cross-linking of insulin at the surface preventing its release.

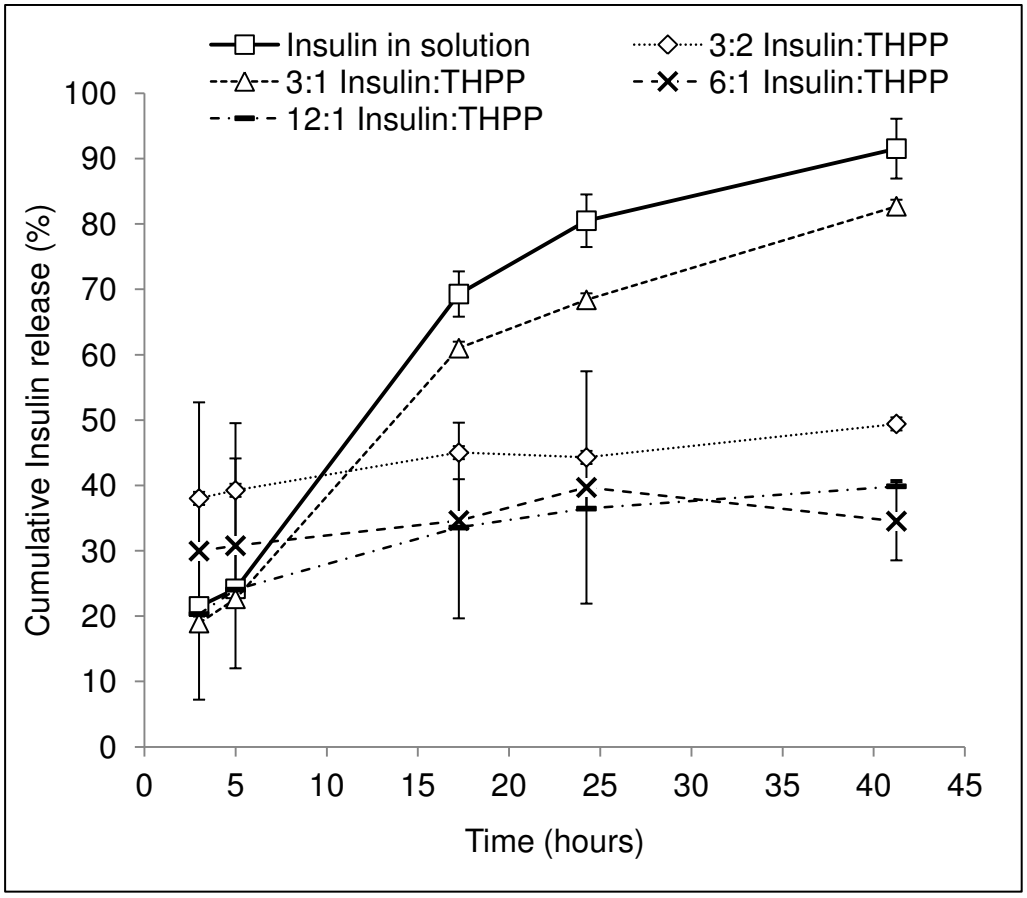

Figure 8. 7. Insulin release profile for descending cross-linking ratios of Insulin:THPP.

(n=2) (Insulin release measured using dialysis through 100kDa membrane). Insulin in solution dialysed and quantified by HPLC was used as the control (Ctrl) in this study.

8.3.6 In *vitro* bioactivity of insulin - NIH 3T3 proliferation assay

In this study, the MTS assay was used to measure the proliferative cellular response to Insulin (released from crystal preparations), as a marker of its bioactivity. Insulin is a well-known inducer of fibroblast and other cell-type proliferation *in vitro* and *in vivo* [24-26]. Growth induction by insulin is concentration dependent, therefore the effective

concentration at which insulin caused 3T3 proliferation was optimised initially. The amount of FCS supplemented in the medium was reduced 10-fold to detect the effects of exogenously added insulin. All samples were then standardised to the same concentration as the positive insulin control (insulin dissolved in cell growth medium) and applied to mouse 3T3 fibroblasts to assess whether the insulin released still retained its bioactivity after cross-linking with THPP and release from crystalline insulin. Insulin (100 nM) significantly increases metabolic activity compared to the DMEM control (Figure 8.8). This is suggestive of a proliferative response by the cells. Bioactivity of insulin released from cross-linked crystals, and applied to the cells at the same concentration as the control sample, shows a clear dependence on the extent of THPP cross-linking. For instance, insulin released from a 3:2 Insulin:THPP preparation, lost its ability to trigger fibroblast proliferation, relative to the DMEM medium. This might be attributed to a loss in the functionality of insulin through experimental processing or denaturation by cross-linking. Increasing the ratio to 3:1 and even 6:1 restores this activity with values close to the positive Insulin control. Furthermore, this study shows that minimal cross-linking of the surface of the Insulin crystals with THPP does not seem to affect insulin functionality and consequently, insulin-receptor interactions.

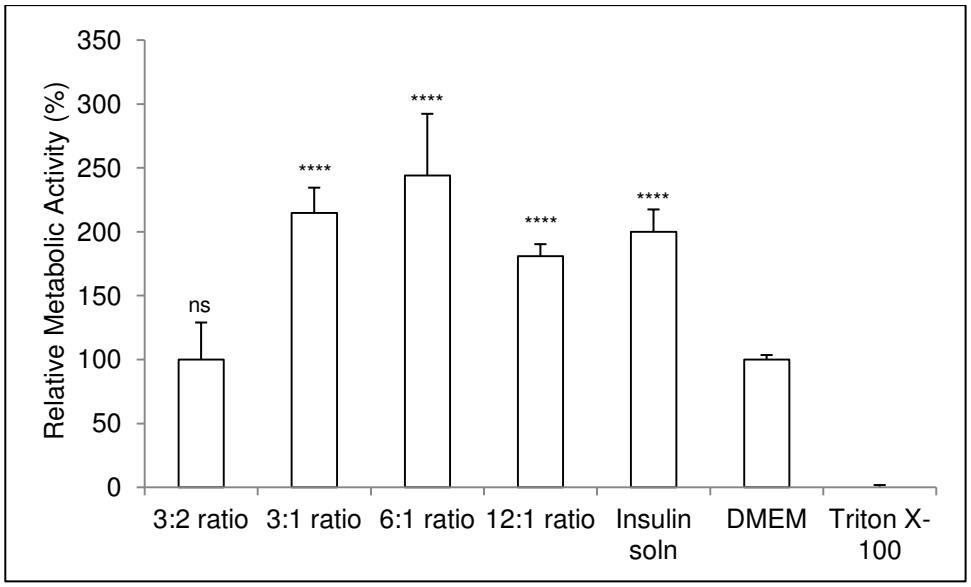

Figure 8. 8. NIH 3T3 proliferation assay by Insulin at varying ratios of THPP cross-linking.

Insulin dissolved in buffer (100nM) was used as a positive control. All insulin preparations (insulin release samples) were standardised to 100nM. Data represents mean (n=6 ± SD). Statistical comparisons with the DMEM control. 'ns' = not significant.

8.4 Conclusion

Nano-scale based protein formulations offer potential as stand-alone drug delivery systems and as such, have highly desirable drug delivery properties [27, 28]. Furthermore, protein nanocrystals can be fabricated to display functional ligands on their surface, enabling targeted therapy or enhanced absorption across the mucosal surfaces.

In this method-development study, a heterogeneous population of nano- and micron-sized insulin crystals were prepared using a variation of the batch crystallisation approach (the reader is referred to Chapter 1, section 1.6.2 for a more comprehensive review). To this end, the first objective was to establish and optimise a protocol for the development of insulin crystals of sub-micron range. The methods for preparation of insulin crystals using this approach are well-established [17]. However in addition, we incorporated a novel centrifugal evaporative step in order to obtain a supersaturated solution of insulin (Chapter 1, section 6.1.1, Figure 1.10) thereby initiating crystallisation. This was followed by a unique 'controlled' cooling method to yield well-

defined crystals ranging from 20 nm-3 μm in size as shown by light scattering and centrifugal separation techniques.

The next objective was to investigate THPP as a proof-of-concept stabiliser by partially cross-linking the surface of the crystals. It was sought to determine the optimal timing for addition of the stabilising agent, with respect to encouraging crystal growth and secondly; to establish the optimal extent of cross-linking allowing the eventual controlled release of biologically functional insulin. Interestingly, the timing of addition of THPP was important not only for the stabilisation of the crystals but also for their apparent formation. The studies revealed that adding THPP before slow-freezing the crystal preparations was beneficial for the colloidal stability of the forming crystals. Furthermore, an optimum ratio of 3:1 Insulin:THPP was demonstrated, in view of sufficient cross-linking to maintain stability of the crystals, but not too extensive in preventing release of biologically active insulin. In crystals, protein molecules adopt a highly symmetrical arrangement and their native confirmation is stabilised, [29] - it is thought that the THPP added preserves this ordered arrangement of molecules. *In vitro* toxicity assays revealed that THPP by itself is not harmful to cells, even at higher concentrations. However, further investigations, in particular immunological response studies, are needed in order to validate fully the use of this compound as a stabilising cross-linker. Of significant importance to pharmaceutical applications, the stabilised insulin crystals, were generally stable in the absence of their salt buffer, displayed a slow-release profile and the insulin released had retained its biological activity *in vitro*.

8.5 References

1. D.R. Owens, B. Zinman, and G. Bolli, *Alternative routes of insulin delivery.* Diabet. Med., 2003. **20**: p. 886–898.
2. Lee, V.H.L., Yamamoto, A., , *Penetration and enzymatic barriers to peptide and protein absorption.* Adv. Drug Deliv. Rev, 1990. **4**: p. 171–207
3. Rekha, M.R. and C.P. Sharma, *Synthesis and evaluation of lauryl succinyl chitosan particles towards oral insulin delivery and absorption.* J Control Release, 2009. **135**(2): p. 144-51.
4. Still, G., *Development of oral insulin: progress and current status.* Diabetes Metab Res Rev, 2002. **18**((Suppl 1)): p. S29-S37.
5. C. Damgé, P. Maincent, and N. Ubrich, *Oral delivery of insulin associated to polymeric nanoparticles in diabetic rats.* J. Control. Release, 2007. **117**: p. 163-170.
6. C. Damgé, M.A. C. Michel, and P. Couvreur, *New approach for oral administration of insulin with polyalkylcyanoacrylate nanocapsules as drug carrier.* Diabetes, 1988. **37**: p. 246-251.
7. C. Damgé, et al., *Poly(alkylcyanoacrylate) nanospheres for oral administration of insulin.* J. Pharm. Sci., 1997. **86**: p. 1403-1409.
8. M.A. Radwant and H.Y. Aboul-Enein, *The effect of oral absorption enhancers on the in vivo performance of insulin-loaded poly(ethylcyanoacrylate) nanospheres in diabetic rats*
J. Microencapsul., 2002. **19**: p. 225-235.
9. Z. Ma, T.M Lim, and L.-Y. Lim, *Pharmacological activity of peroral chitosan–insulin nanoparticles in diabetic rats.* International Journal of Pharmaceutics, 2005. **293**: p. 271-283.
10. Pan, Y., et al., *[Enhancement of gastrointestinal absorption of chitosan-coated insulin-loaded poly (lactic-co-glycolic acid) nanoparticles].* Yao Xue Xue Bao, 2003. **38**(6): p. 467-70.
11. Yu-Hsin Lin, et al., *Novel nanoparticles for oral insulin delivery via the paracellular pathway.* Nanotechnology, 2007. **18**: p. 1-11.
12. Lehr, C.M., Bouwstra, J.A., Schacht, E.H., Junginger, H.E., and *In vitro evaluation of mucoadhesive properties of chitosan and some other neutral polymers.* Int. J. Pharm., 1992. **78,**: p. 43–48.
13. Leung, S.H.S., Nagai, T., Machida, Y., and *Mucoadhesive dosage forms for peptide and protein drug delivery*. Peptide and Protein Drug Delivery., ed. V.H.L.E. Lee. 1991., New York,: Marcel Dekker,.
14. Gowthamarajan, K. and G.T. Kulkarni, *Oral Insulin - Fact or Fiction?* Resonance, 2003: p. 38-46.
15. Eaimtrakarn, S., Prasad, YVR., Ohno, T., *Absorption enhancing effect of Labrosol on the intestinal absorption of insulin in rats.* J. Drug. Target., 2002. **10**(3): p. 255-260.
16. Jen, A. and H.P. Merkle, *Diamonds in the rough: protein crystals from a formulation perspective.* Pharm Res, 2001. **18**(11): p. 1483-8.
17. Bromberg, L., J. Rashba-Step, and T. Scott, *Insulin particle formation in supersaturated aqueous solutions of poly(ethylene glycol).* Biophys J, 2005. **89**(5): p. 3424-33.
18. Shekunov, B.Y. and P. York, *Crystallization processes in pharmaceutical technology and drug delivery design.* Journal of Crystal Growth, 2000. **211**: p. 122-136.
19. Basu, S.K., et al., *Protein crystals for the delivery of biopharmaceuticals.* Expert Opinion on Biological Therapy, 2004. **4**(3): p. 301-317.
20. Putney, S.D. and P.A. Burke, *Improving protein therapeutics with sustained-release formulations.* Nat Biotechnol, 1998. **16**(2): p. 153-7.
21. Lim, D.W., et al., *Rapid cross-linking of elastin-like polypeptides with (hydroxymethyl)phosphines in aqueous solution.* Biomacromolecules, 2007. **8**(5): p. 1463-70.

22. Chow, D., et al., *Peptide-based Biopolymers in Biomedicine and Biotechnology.* Mater Sci Eng R Rep, 2008. **62**(4): p. 125-155.
23. Sigma-Aldrich. *Product information sheet for "Insulin from bovine pancreas"*. 2012 [cited 23/08/2012].
24. Svegliati-Baroni, G., et al., *Insulin and insulin-like growth factor-1 stimulate proliferation and type I collagen accumulation by human hepatic stellate cells: differential effects on signal transduction pathways.* Hepatology, 1999. **29**(6): p. 1743-51.
25. Monaco, S., et al., *Insulin stimulates fibroblast proliferation through calcium-calmodulin-dependent kinase II.* Cell Cycle, 2009. **8**(13): p. 2024-30.
26. She, Q.B., et al., *alpha(1)-antitrypsin can increase insulin-induced mitogenesis in various fibroblast and epithelial cell lines.* FEBS Lett, 2000. **473**(1): p. 33-6.
27. Algar, W.R., et al., *The controlled display of biomolecules on nanoparticles: a challenge suited to bioorthogonal chemistry.* Bioconjug Chem. **22**(5): p. 825-58.
28. Gao, W., J.M. Chan, and O.C. Farokhzad, *pH-Responsive nanoparticles for drug delivery.* Mol Pharm. **7**(6): p. 1913-20.
29. Shenoy, B., et al., *Stability of crystalline proteins.* Biotechnol Bioeng, 2001. **73**(5): p. 358-69.

Chapter 9: Summary & Future Directions

9.1 Final Summary

The field of biological therapeutics has recently taken off. However, this has not been followed by advances in development of novel delivery routes for this class of therapeutics. Perhaps frustratingly, the administration of biologics remains limited to the parenteral route. Exploiting the potential of the mucosal surfaces for non-invasive delivery of this class of drugs is made difficult by the physiological role of the mucosae, which is to restrict the movement of material from the external milieu into the systemic circulation.

Mucosally administered biologics such as protein drugs generally produce a low (predominantly clinically irrelevant) bioavailability. Drug delivery scientists have investigated a range of strategies to overcome the mucosal barrier in an attempt to improve the bioavailability of mucosally administered protein drugs. These have been reviewed in chapter 1. The ultimate goal being to develop a mucosal delivery strategy based on systems that exhibit no toxicity upon repeated administration, preserve the biological function of the therapeutic molecule, and achieve adequate bioavailability with minimal extra costs to the formulation (compared to parenteral systems) and which are amenable to different protein drugs.

This thesis has explored the potential of the vitamin B_{12} pathway, as one of the few known transepithelial biological transport pathways, for the systemic delivery of nanoparticles across the epithelium. It must be noted that proof-of-concept work demonstrating the potential of the vitamin B_{12} pathway to deliver nanoparticles (as drug carriers) across the intestinal epithelium (Caco-2 cells) has been previously published by other groups. This thesis therefore is predominantly focused on investigating the cell uptake and transport mechanisms involved in the process of nanoparticle delivery via the vitamin B_{12} pathway. The investigation was conducted *in vitro* using epithelial cell culture models (intestinal Caco-2 cells and bronchial Calu-3

cells) since these models allow control of experimental conditions, which is necessary for studying drug delivery-relevant biological mechanisms.

Initial work investigated the barrier property of Caco-2 cell monolayers and their suitability as a model for the vitamin B_{12} transport system (Chapter 3). To this end, work was conducted to determine mRNA expression, in addition to immunohistochemical analyses for the key proteins involved in the internalisation and transport of vitamin B_{12} *in vivo,* including the B_{12}-IF receptor, cubilin; the secondary receptor, transcobalamin II receptor (TCIIR), and the TCII carrier protein. The data confirmed that Caco-2 cells (as monolayers) express relevant components of the vitamin B_{12} transport system providing an adequate model to study drug delivery strategies exploiting the vitamin B_{12} trafficking pathway. Additionally, the Caco-2 cell line used in this work was also validated as an epithelial barrier suitable for the study of macromolecular absorption (by determining cell morphology and testing the permeability of model macromolecules). Following appropriate culture, Caco-2 cells formed polarised monolayers exhibiting TEER of >2000 $\Omega.cm^2$ and presented a barrier to the permeability of macromolecules (FITC-dextrans and insulin), with the magnitude of the barrier being proportional to the MW of the permeant. Furthermore, Caco-2 monolayers presented a significant barrier to the movement of nanoparticles. Considering their morphology, cells exhibited structural features that resemble the native epithelium, including the tight junctions and microvilli.

Subsequent work (Chapter 4-7) investigated the vitamin B_{12} transport pathway for the delivery of nanoparticulate carriers. The vitamin B_{12} ligand itself requires manipulation in the form of chemical modification to permit its attachment to the carrier system. Work detailed in chapter 4 describes the synthesis and characterisation of an amino-derivative of vitamin B_{12}, α-ω-aminohexylcarbamate B_{12}, which was activated at the 5'-hydroxyl group of the ribose moiety using 1,1'-carbonyldiimidazole (CDI). This was based on previous studies suggesting that the α-ω-aminohexylcarbamate B_{12} retains its binding affinity for transcobalamin (II), haptocorrin (HC) and intrinsic factor (IF).

Successful derivatisation of cyanocobalamin was confirmed by means of NMR, MS and HPLC. Inspection of the ^{1}H-NMR signals for the ribose ring revealed that its signals were significantly shifted after functionalisation, especially those closer to the 5' hydroxyl group. Furthermore, new signals arising from the C6 linker could be observed. The purity of the material was confirmed both by HPLC and MS, with the expected Mw 1497 observed. The resultant α-ω-aminohexylcarbamate VB_{12} derivative was reacted with fluorescently-labelled, carboxy-functionalised polystyrene nanoparticles in the presence of 1-ethyl-3-[3-dimethylaminopropyl]carbodiimide (EDAC) and N-hydroxy-succinimide (NHS), which following a purification step by dialysis,yielded the desired vitamin B_{12}-conjugated nanoparticles (Chapter 5).

For the cell studies described in Chapter 5, the suitability of the Caco-2 cell line as a model to study vitamin B_{12} epithelial transport pathway was verified not only by confirming the expression of cubilin receptor (and other essential components for B_{12} transport), but also by examining for the presence of functioning caveolae and clathrin mediated endocytic pathways. Further work demonstrated that vitamin B_{12}-conjugated nanoparticles were internalised and transported across the cells notably more efficiently compared to unmodified nanoparticles. Importantly, vitamin B_{12}-conjugated nanoparticles bypassed the lysosomal compartments, unlike unmodified nanoparticles. Cell internalisation and transport of vitamin B_{12}-conjugated nanoparticles remained largely unaffected by the inhibitors of clathrin-mediated endocytosis – the route governing vitamin B_{12}-IF internalisation *in vivo.* The cell internalisation and transport behaviour of B_{12}-nanoparticles was instead markedly impeded by specific inhibitors of caveolae-mediated endocytosis, demonstrating that vitamin B_{12} conjugated nanoparticles were trafficked by a different intracellular pathway to both free vitamin B_{12} as well as unmodified nanoparticles.

Work detailed in Chapter 6 set out to examine the role of intrinsic factor (IF) on the cellular uptake and transport of B_{12}-conjugated nanoparticles and on subsequent cell sorting processes in Caco-2 cells. Whether the presence of IF in the system is a crucial parameter influencing the uptake and transport of B_{12}-bearing nanoparticles was not clear prior to this work as, similarly to soluble vitamin B_{12}, routes other than

the cubilin-mediated pathway could contribute to the uptake and transport of B_{12}-conjugated nanoparticles. Experiments assessing the effect of IF on the trafficking pathways of B_{12}-nanoparticles were conducted to establish whether IF dictates the cell trafficking of B_{12}-bearing nanoparticles. Overall, the data suggests that in the absence of IF, B_{12}-conjugated nanoparticles are internalised and transported by cells to a lesser extent than when co-administered with IF, although the magnitude of this effect was not substantial. The findings also demonstrate that soluble vitamin B_{12} trafficking (without IF) occurs *via* a different route to that used by vitamin B_{12} in the presence of IF (i.e. cubilin mediated). Interestingly, while the uptake of vitamin B_{12}-nanoparticle in the presence of IF was found to exploit a caveolae-mediated route, cell internalisation and transport of B_{12}-conjugated nanoparticles in the absence of IF were predominantly affected by inhibition of the clathrin pathway. This suggests the involvement of a different cell uptake and trafficking route to that in the presence of IF, which implicates a role for the TCII receptor.

Work in Chapter 7 investigated the presence of the B_{12}-transport system and its potential role in the uptake and transport of B_{12}-bearing nanoparticles in polarised bronchial Calu-3 cells. This work is important as cubilin expression and the B_{12} transcytosis pathway in epithelial cell lines originating from the airways have not been previously reported. Initial experiments revealed cubilin, TCII receptor and TCII carrier protein expression in Calu-3 cells. Similarly to the findings in intestinal Caco-2 cells, B_{12}-conjugated nanoparticles were found to internalise and transport across the cell layers markedly more efficiently compared to unmodified nanoparticles. Calu-3 cells were also capable of internalising B_{12}-conjugated nanoparticles in an IF-dependent and IF-independent fashion, with particle size bearing a considerable effect on the extent of both uptake and transport. Lysosomal studies revealed that the cell uptake and trafficking of nanoparticles in the bronchial Calu-3 cell line mirrored the cell sorting processes found in Caco-2 cells, with the surface decoration of vitamin B_{12} playing a profound role on intracellular trafficking in both Caco-2 cells and in Calu-3 cells, giving rise to lysosomal bypass. Inhibitor studies complemented previous reports in Caco-2 cells (and the earlier findings in this thesis) that soluble vitamin B_{12} (in the presence of

IF) predominantly exploits a clathrin-mediated route in the process of internalisation in Calu-3 cells. However, contrary to findings in Caco-2 cells where caveolae played no role in the internalisation of vitamin B_{12}, the data suggested that to a degree, there could be an element of cross-talk between the two pathways in Calu-3 cells. The polystyrene nanoparticles employed in this work (Chapters 5-7) were merely used as 'model' therapeutic carriers to demonstrate whether transmucosal transport can be achieved following their conjugation to a biological ligand (vitamin B_{12}). The promising results obtained from *in vitro* work detailed in this thesis pave the way for further investigations *in vivo*, wherein the vitamin B_{12} ligand can be used to navigate 'real' therapeutic carriers across the epithelium. To this end, it was envisaged that the vitamin B_{12} transmucosal absorption strategy can perhaps, in the future be applied not only to nanocarriers but also protein therapeutics formulated in nano-sized entities, such as protein 'nanocrystal' formulations, which becomes the subject of the final chapter of this thesis.

Work in Chapter 8 was therefore conducted to investigate the formulation of a protein therapeutic as nanocrystals, with the view of exploring the potential of this carrier-free, nanoscale drug delivery strategy. Protein therapeutics formulated as nanoparticulates have highly desirable drug delivery properties. In this method development study, a heterogeneous population of nano- and micron-sized insulin crystals were prepared by a modification of the batch crystallisation approach. The first task in this investigation was to establish and optimise a protocol for the development of insulin crystals of sub-micron range. This was achieved by optimisation of the formulation conditions, including the ratio of components of the crystallisation buffer and the centrifugal evaporation step. Later, the effects of THPP (β-[Tris(hydroxymethyl) phosphino] propionic acid) as a proof-of-concept crystal stabiliser were investigated. The work aimed to address the problem of colloidal instability of insulin in the absence of the crystallisation buffer. The surface of formulated crystals was initially partially cross-linked with THPP, followed by optimisation of this cross-linking to produce stable nano- and micro-sized protein crystals that permit slow/controlled release profile of the

biologically active insulin. Importantly, *in vitro* cytotoxicity assays revealed that THPP is not harmful to cells and that THPP-stabilised insulin crystals were generally stable in the absence of their crystallisation buffer, displayed a slow-release profile and the released insulin had retained its biological activity *in vitro* (as determined by measuring its bioactivity in mouse 3T3 fibroblasts). Future optimisation of the formulation conditions to achieve protein crystals of desirable sizes (e.g. 50-200 nm range) and incorporation of suitable ligands, such as vitamin B_{12} in the system, has the potential to enhance mucosal delivery of protein-based therapeutics to therapeutically acceptable levels.

9.2 Future directions

Important factors for selecting a drug delivery method for commercial development generally includes market competition, patient convenience and compliance, requirement for local or topical delivery and systemic toxicity or other safety issues. However, with formulations of biological therapeutics such as proteins the delivery method has been dictated by the physicochemical properties of this class of therapeutics and the inability to overcome the mucosal barrier to achieve non-invasive delivery. Although researchers have actively worked to identify painless and non-invasive alternatives for administration of these drugs, ground-breaking advances are currently lacking. This is reflected by the fact that apart from a few peptide products (with a modest molecular weight) in the form of nasal sprays, commercially popular formulations of larger proteins and antibodies designed for oral or other mucosal delivery routes are virtually non-existent.

The mucosal barrier presents unique challenges for drug delivery scientists. Traditional approaches studied with the aim of overcoming this barrier for systemic delivery of biologics have mainly focused on the use of absorption enhancers or delivery systems that prolong the contact of the drug with the mucosal surface. These rather crude approaches are not without problems, as highlighted by the damaging effect of repeated application of some absorption enhancers such as surfactants. Exploiting the receptor-mediated cellular transport machinery for the purpose of

transmucosal drug delivery is potentially a more elegant approach. This strategy has recently received considerable attraction in the field of drug and gene delivery, with the potential of allowing targeted delivery. The use of drug carrier systems, such as nanoparticles, appended with ligands to target these receptors has opened new avenues for cellular or intra-cellular targeting. For the purpose of receptor-mediated delivery of macromolecular therapeutics across the mucosal surfaces, biological transport systems that transport cargo from the external environment (lumen) into the systemic circulation are of huge interest. Unfortunately not many such biological pathways are currently known and of the handful of identified systems, only some have demonstrated potential for mucosal drug delivery.

Current nanoparticle-mediated mucosal drug delivery research is restricted by an overall lack of understanding in the complex cell internalisation and cell sorting processes at the molecular level, which was the inspiration behind this work. The findings from this thesis overall demonstrated that surface-conjugation of vitamin B_{12} ligand to nanoparticles resulted in an unexpected intracellular trafficking behaviour in epithelial Caco-2 and Calu-3 cell layers, with a 'switch' to a non-degradative caveolae pathway, which is more desirable from a drug delivery perspective. This discovery is a previously unreported example of pathway switching via ligand decoration and may have important implications for non-invasive delivery of nanocarrier-associated therapeutic or diagnostic systems and diagnostics and warrants further investigation. The findings suggest that 'design rules' for nanoparticulate systems may exist, governing their cellular uptake processes and the resulting usefulness for drug delivery.

The vitamin B_{12} biological pathway is one of few epithelial biological transport systems which are being commercially exploited for the purpose of oral delivery of nanoscale drug carriers. This thesis confirms its potential in this area and adds important information in terms of the biological mechanisms. However, many questions remain unanswered about the use of nanoparticulate drug carriers for mucosal drug delivery in general. Therefore, any future advances in the area of nanoparticle-mediated mucosal protein delivery *via* the vitamin B_{12} pathway depends on future improvements

in our understanding relating to the long term safety concerns associated with the use of nanoparticles for mucosal drug delivery alongside parallel developments in 'targeted' protein nanocrystal formulations.